UNIVERSIDADE DE LISBOA

FACULDADE DE MEDICINA VETERINÁRIA

UNRAVELING THE REPLICATION PROCESS OF TOXOPLASMA GONDII THROUGH THE MOB1 PROTEIN

INÊS LOURENÇO DA SILVA DELGADO

Orientadores: Professora Doutora Sofia Bizarro Nolasco da Silva Narciso

Doutor José Alexandre da Costa Perdigão e Cameira Leitão

Tese especialmente elaborada para obtenção do grau de Doutor em Ciências Veterinárias na especialidade de de Ciências Biológicas e Biomédicas

2022

UNIVERSIDADE DE LISBOA

FACULDADE DE MEDICINA VETERINÁRIA

UNRAVELING THE REPLICATION PROCESS OF TOXOPLASMA GONDII THROUGH THE MOB1 PROTEIN

INÊS LOURENÇO DA SILVA DELGADO

Orientadores: Professora Doutora Sofia Bizarro Nolasco da Silva Narciso

Doutor José Alexandre da Costa Perdigão e Cameira Leitão

Tese especialmente elaborada para obtenção do grau de Doutor em Ciências Veterinárias na especialidade de de Ciências Biológicas e Biomédicas

Júri
Presidente: Professor Doutor Luis Filipe Lopes da Costa
Vogais:
- Professor Doutor Luis Miguel Ortega Mora
- Professora Doutora Ana Maria Luís Ramos Tomás
- Professor Doutor António José de Freitas Duarte
- Professora Doutora Sofia Bizarro Nolasco da Silva Narciso
- Doutora Sandra Isabel Conceição Antunes

2022

DECLARAÇÃO RELATIVA ÀS CONDIÇÕES DE REPRODUÇÃO DA TESE

Nome: Inês Lourenço da Silva Delgado

Título da Tese ou Dissertação: Unraveling the replication process of *Toxoplasma gondii* through the MOB1 protein

Ano de conclusão (indicar o da data da realização das provas públicas): 29 de Abril de 2022

Designação do curso de Mestrado ou de Doutoramento: Doutoramento em Ciências Veterinárias, especialidade de Ciências Biológicas e Biomédicas

Área científica em que melhor se enquadra (assinale uma):

☐ Clínica ☐ Produção Animal e Segurança Alimentar

☐ Morfologia e Função ☒ Sanidade Animal

Declaro sobre compromisso de honra que a tese ou dissertação agora entregue corresponde à que foi aprovada pelo júri constituído pela Faculdade de Medicina Veterinária da ULISBOA.

Declaro que concedo à Faculdade de Medicina Veterinária e aos seus agentes uma licença não-exclusiva para arquivar e tornar acessível, nomeadamente através do seu repositório institucional, nas condições abaixo indicadas, a minha tese ou dissertação, no todo ou em parte, em suporte digital.

Declaro que autorizo a Faculdade de Medicina Veterinária a arquivar mais de uma cópia da tese ou dissertação e a, sem alterar o seu conteúdo, converter o documento entregue, para qualquer formato de ficheiro, meio ou suporte, para efeitos de preservação e acesso.

Retenho todos os direitos de autor relativos à tese ou dissertação, e o direito de a usar em trabalhos futuros (como artigos ou livros).

Concordo que a minha tese ou dissertação seja colocada no repositório da Faculdade de Medicina Veterinária com o seguinte estatuto (assinale um):

1. ☒ Disponibilização imediata do conjunto do trabalho para acesso mundial;
2. ☐ Disponibilização do conjunto do trabalho para acesso exclusivo na Faculdade de Medicina Veterinária durante o período de ☐ 6 meses, ☐ 12 meses, sendo que após o tempo assinalado autorizo o acesso mundial*;

* Indique o motivo do embargo (OBRIGATÓRIO)

Nos exemplares das dissertações de mestrado ou teses de doutoramento entregues para a prestação de provas na Universidade e dos quais é obrigatoriamente enviado um exemplar para depósito na Biblioteca da Faculdade de Medicina Veterinária da Universidade de Lisboa deve constar uma das seguintes declarações (incluir apenas uma das três):

É AUTORIZADA A REPRODUÇÃO PARCIAL DESTA TESE/TRABALHO (indicar, caso tal seja necessário, nº máximo de páginas, ilustrações, gráficos, etc.) APENAS PARA EFEITOS DE INVESTIGAÇÃO, MEDIANTE DECLARAÇÃO ESCRITA DO INTERESSADO, QUE A TAL SE COMPROMETE.

Faculdade de Medicina Veterinária da Universidade de Lisboa, 29 de Abril de 2022

(indicar aqui a data da realização das provas públicas)

Assinatura: _____

"*The aim of argument, or of discussion, should not be victory, but progress*."

Pensées, Joseph Joubert (1848)

"The story so far: In the beginning, the Universe was created. This has made a lot of people very angry and been widely regarded as a bad move."

The Restaurant At The End Of The Universe, Douglas Adams (1980)

Agradecimentos/acknowledgments

Esta dissertação é o culminar de um trabalho que não teria sido possível sem muitas pessoas com as quais tive a sorte de me cruzar e sem diversas instituições que contribuiram para este projeto. Aproveito este momento muito especial para agradecer a todos os que me têm acompanhado e apoiado.

Agradeço ao CIISA - Centro de Investigação Interdisciplinar em Sanidade Animal e à FMV-UL - Faculdade de Medicina Veterinária da Universidade de Lisboa, nas pessoas do Professor Doutor Rui Caldeira, do Professor Doutor Luís Costa, do Professor Doutor António Duarte, Professor Doutor Luís Tavares e do Professor Doutor Carlos Fontes, por aceitarem acolher este projeto e por todo o apoio fornecido para a sua execução.

À Sofia Nolasco, minha orientadora, agradeço do fundo do coração por apostar em mim e por me abrir a porta para o mundo de *Toxoplasma*. Foi um percurso àrduo mas sempre com boa disposição. Agradeço todo o companheirismo e toda a disponibilidade, no laboratório e fora, assim como o empenho e força transmitidos. Ao Alexandre Leitão, meu co-orientador, agradeço por me receber no grupo e por todo o apoio. As conversas e os conselhos foram determinantes. A ambos agradeço os ensinamentos, a paciência e o apoio durante este percurso, assim como a inspiração e o incentivo para alcançar mais além. É muito bom chegar ao fim desta etapa convosco. Espero que venham mais.

À Helena Soares, a quem também devo a hipótese de trabalhar neste tema, agradeço a grande generosidade com o seu tempo e conhecimento assim como todo o apoio e todo o incentivo contagiante que deu para este trabalho.

Agradeço aos membros do TAHP/C4.11, que fizeram deste espaço mais do que um laboratório ou um gabinete. Tivemos os *labmeetings* mais longos mas também mais divertidos (que, ao passarem para o Zoom, mostraram cá em casa que me rio demais nas reuniões). Os almoços e lanches serão sempre lembrados com saudades, em particular dos chocolates. Ao Samuel Francisco, que desbravou muitos caminhos e que muito contribuiu para esta dissertação, sempre com os melhores conselhos gastronómicos. À Alexandra Tavares, com quem não me cheguei a cruzar no laboratório mas que ainda assim esteve sempre disponível para mergulhar nas memórias passadas e ajudar para além das expectativas. Ao Afonso Basto, que perdeu a minha chave do gabinete durante um ano, mostrando que nunca nada está perdido. Ao João Coelho, que tinha sempre uma ideia sábia para partilhar, nem que seja “isso é estúpido”. À Andreia Ferreira, à Mariana Domingues, à Mafalda Beleza e à Madalena Mendes, que contribuiram para este percurso da melhor maneira. Ao Eduardo Marcelino e à Helga Waap que contribuiram amavalmente para este trabalho com anticorpos. Em especial, à Sara

Zúquete e à Dulce Santos, que não se cansaram de gozar comigo ao longo destes anos. Espero que nunca se cansem. E que continuemos sempre na procura da nossa pessoa. À Catarina, e agora também à Teresa, por aguardarem pacientemente pelo dragão mágico. À Maria, pelo desenho que está agora na minha sala.

Agradeço a disponibilidade de todos os companheiros da FMV-UL pelas trocas de consumíveis, reagentes e sobretudo ideias, em particular à Margarida Simões, ao Gonçalo Frouco, ao Ferdinando Freitas, à Eva Cunha, ao David Ramilo, ao Marcos Santos, e à Sandra Aguiar, assim como o apoio indispensável da Idalina Camões, do Rui Vieira e da Ju Silva.

Ao Bruno Carmona, agradeço pela sua grande ajuda neste projeto. À Susana Araújo, agradeço a grande generosidade com conselhos e incentivo. À Ana Maria Munhoz e ao José Girão Bastos, agradeço o grande apoio na escrita desta dissertação.

Agradeço à plataforma de proteómica do I3S – Instituto de Investigação e Inovação em Saúde pelas análises e em particular ao Hugo Osório por toda a ajuda e todos os conselhos. Agrageço ao IGC – Instituto Gulbenkian de Ciência, pela oportunidade de usufruir das instalações de imagiologia (Advanced Imaging Lab, Imaging and Cytometry Unit).

Agradeço também a quem me acompanhou nos meus percursos anteriores, na FFUP – Faculdade de Farmácia da Universidade do Porto e no CIIMAR – Centro Interdisciplinar de Investigação Marinha e Ambiental, pois foram essenciais para eu chegar aqui.

Agradeço, de coração cheio de saudades, aos meus amigos e à minha família, a convencional e a unida e amigável. A vossa paciência, o apoio incansável, a confiança inexplicável e sobretudo a vossa capacidade admirável de me aturarem, com certeza um mistério que difícil de desvendar, deram-me alento nos piores e melhores momentos. Em especial, agradeço aos meus pais, Paula e Rui, à minha irmã, Joana, e ao meu namorado, Nuno. Vocês são o meu porto de abrigo e o grande motivo para eu estar a escrever isto. Não tenho palavras por isso faço uso das de Maya Angelou, *I sustain myself with the love of family*. À Saraby, à Nala, ao Hilário, ao Hulk e ao Pingo, sem vocês a família não estava completa.

This work could not have been accomplished without the support of several people to whom I would like to give my heartfelt acknowledgment. To the Toxo and Apicowplexa communities, for producing such excellent research and providing great platforms for exchange of knowledge. To Markus Meissner and his group, in particular Elena Jiménez-Ruiz, for providing us with knowledge, tools and advice that were indispensable for this work. To Andrew Hemphill, for sera, reagents, time, expertise and advice, but fundamentally chocolates, preferably Swiss-born. To Maria Francia, for the availability and guidance. To Ke Hu, Santosh

Nadipuram, Marc-Jan Gubbels, Boris Striepen, Carrie Brooks, and Érica Martins Duarte, for the kind supply of plasmids, antibodies and strains.

Funding

This work was funded by Fundação para a Ciência e Tecnologia (FCT) through the grant EXPL/CVT-EPI/1945/2013 and the doctoral scholarship SFRH/BD/95330/2013. Funding was also provided by CIISA - Centro de Investigação Interdisciplinar em Sanidade Animal, Faculdade de Medicina Veterinária, Universidade de Lisboa, through the research projects UID/CVT/00276/2013 and UID/CVT/00276/2019.

Desvendar o processo de replicação de *Toxoplasma gondii* através da proteína MOB1

Resumo

As proteínas da família *monospindle one binder* (MOB) são cinases adaptadoras de sinal altamente conservadas em eucariotas que são frequentemente essenciais para a sobrevivência das células e dos organismos. Historicamente, as proteínas MOB foram descritas como ativadoras de cinases que participam nas vias de sinalização *mitotic exit network/ septation initiation network* (MEN/SIN) que têm papéis centrais na regulação da citocinese, polaridade celular, proliferação celular e destino celular para controlar o crescimento e a regeneração dos órgãos. Nos metazoários, as proteínas MOB atuam como adaptadores centrais de sinal do módulo nuclear de cinases *mammalian sterile* 20 (MST) 1/2, *large tumor suppressor* (LATS) 1/2 e nuclear dbf2-related (NDR) 1/2 que fosforilam os co-ativadores transcricionais *Yes associated protein* (YAP)/ *WW domain containing transcription regulator 1* (TAZ), efetores da via de sinalização Hippo. Mais recentemente, as proteínas MOB mostraram também ter parceiros não-cinase e estar envolvidos na biologia dos cílios, indicando que a sua atividade e regulação é mais diversificada do que inicialmente foi admitido. Em particular, as proteínas MOB1 regulam o equilíbrio entre proliferação celular *versus* apoptose, a duplicação de centrossomas e a diferenciação celular em eucariotas multicelulares mas também a citocinese e a orientação do eixo de divisão em eucariotas unicelulares e multicelulares.

Toxoplasma gondii é um parasita intracelular obrigatório de grande importância veterinária e médica, afetando uma grande variedade de espécies animais e estando presente por todo o mundo. A sua distribuição e o facto de poder parasitar potencialmente todos os animais de sangue quente contribuíram para ser considerado o parasita de maior sucesso. Apesar de os seus hospedeiros geralmente não desenvolverem formas clínicas, *T. gondii* pode causar doença grave em hospedeiros imunocomprometidos e levar a aborto e malformações congénitas se a infeção é adquirida durante a gestação. *T. gondii* apresenta um ciclo de vida complexo, com uma fase assexuada e uma fase sexuada. Ao longo do seu ciclo de vida, é capaz de interconverter entre vários estádios celulares, nomeadamente entre os estádios de replicação rápida (taquizoítos) e os estádios de replicação lenta (bradizoítos) durante a fase assexuada, uma capacidade fundamental para o seu sucesso como parasita. Os bradizoítos produzem quistos tecidulares estabelecendo uma infeção crónica que permite a ocorrência de

recrudescência. A conversão entre estes estádios depende da regulação do ciclo celular do parasita e envolve diferenciação celular e regulação do processo de replicação.

T. gondii apresenta uma única proteína do tipo MOB. Esta proteína, designada MOB1, quando sobre expressa, leva a uma diminuição do ritmo de replicação do parasita. Adicionalmente, a transcrição do gene *Mob1* diminui fortemente após invasão da célula hospedeira, durante a fase de replicação ativa do parasita. Isso levou-nos a selecionar a proteína MOB1 como uma forte candidata a estar envolvida na regulação do processo de replicação de *T gondii*, o ponto de partida para o presente estudo.

Empregámos técnicas de genética reversa e tecnologia *clustered regularly interspaced short palindromic repeats* (CRISPR)/ CRISPR *associated endonuclease 9* (Cas9) para avaliar a função de MOB1 em *T. gondii*. Em contraste com o que foi observado em outros eucariotas unicelulares, como *Saccharomyces cerevisiae*, *Tetrahymena thermophila* e *Trypanosoma brucei*, a deleção do gene *Mob1* em *T. gondii* não levou a falhas de citocinese ou de progressão do ciclo celular durante o seu ciclo assexuado. Em vez disso, observámos um aumento no ritmo de replicação de taquizoítos, uma diminuição na regularidade do número de taquizoítos no interior dos vacúolos parasitóforos e uma perda significativa da sua capacidade de diferenciação do estádio de taquizoíto para o estádio de bradizoíto. Para além disso, a proteína MOB1 recombinante acumula-se numa linha média entre os núcleos das células filhas no final do processo de mitose sugerindo que a proteína MOB1 endógena pode estar envolvida no processo de divisão nuclear e/ou na saída de mitose e na entrada em citocinese. As proteínas miosina B/C, identificadas neste estudo como possíveis parceiras da proteína MOB1, apresentam uma localização semelhante à das proteínas recombinantes MOB1, sugerindo que a proteína MOB1 poderá estar associada a uma estrutura com base de actina/miosina envolvida no/s processo/s de mitose/citocinese.

Verificámos que o genoma de *T. gondii* codifica para outros potenciais membros de uma via de sinalização do tipo MEN/SIN/via Hippo, nomeadamente um cinase STE, duas cinases NDR, quatro proteínas 14-3-3 (co-efetoras da via Hippo), CDC14 e CRK2 (ambas proteínas efetoras de MEN/SIN). Notavelmente, os genes que codificam para as cinases NDR apresentam uma expressão semelhante à do gene *Mob1* ao longo do ciclo de vida de *T. gondii*, o que sugere uma funcionalidade coordenada entre a proteína MOB1 e as duas proteínas NDR.

Para elucidar a forma de atuar da proteína MOB1 em *T. gondii*, utilizámos um método de biotinilação de proximidade (BioID) e identificámos o interactoma da proteína MOB1 durante o estádio de taquizoíto. Esta análise detetou proteínas relacionadas com diversas categorias

funcionais, indicando um papel multivalente para a proteína MOB1. Detetámos várias proteínas que fazem parte do sistema ubiquitina-proteossoma indicando que a atividade da proteína MOB1 poderá ser regulada por este sistema. Outras categorias funcionais mais representadas no interactoma de MOB1 são proteínas relacionadas com o metabolismo celular, a síntese e o destino de proteínas, o transporte celular, o ciclo celular e o processamento de ácido desoxirribonucleico, a transcrição e a transdução de sinal. Identificámos ainda proteínas relacionadas com o sistema secretor e a estrutura celular. Contudo, muitas das proteínas detetadas não estão caracterizadas e, destas, a maioria pertence a grupos de proteínas restritos dos Apicomplexa e mesmo das coccídeas formadoras de quistos. As proteínas que compõem o interactoma da proteína MOB1 localizam-se sobretudo nas regiões do núcleo, membrana citoplasmática, citoplasma, retículo endoplasmático, complexo de Golgi, mitocôndria, apicoplasto, proteossoma e ribossomas. Estes dados apontam para uma proteína MOB1 que atua em vários domínios e que provavelmente tem uma função mais complexa do que apenas ativadora de cinase, uma propriedade já descrita em outros organismos eucariotas multicelulares. Os resultados da análise de sequências identificaram mais genes candidatos relacionados com as vias MEN/SIN, descritas em leveduras. Por outro lado, os fenótipos observados nos estudos de ganho e perda-de-função e os resultados dos estudos de interação por biotinilação de proximidade sugerem que *T. gondii* possa apresentar uma via de sinalição mais próxima funcionalmente da via Hippo, descrita em organismos multicelulares.

Também observámos que o *locus* do gene *Mob1* é transcrito a partir de ambas as cadeias genómicas e dá origem a ácidos ribonucleicos mensageiros com *splicing* alternativo. Os nossos resultados indicam que a proteína MOB1 é fortemente regulada ao longo do ciclo celular e ao longo do complexo ciclo de vida do parasita *T. gondii*, contribuindo para o controle da sua replicação e para a diferenciação entre os estádios de taquizoíto e de bradizoíto.

Este estudo contribui para uma visão diferente e trouxe a lume intervenientes chave da regulação do ciclo biológico de *T. gondii* e deu os primeiros passos para esclarecer a existência de uma hipotética via de sinalização do tipo MEN/SIN/Hippo neste parasita unicelular. Ao longo deste trabalho obtivemos várias estirpes transgénicas *T. gondii* de ganho e perda-de-função do gene *Mob1* e estabelecemos de metodologias envolvendo os sistemas CRISPR/Cas9 e BioID que serão exploradas em trabalhos futuros. Deste estudo, resultou ainda a identificação de um conjunto de proteínas potencialmente envolvidas na regulação da replicação, da regularidade do número de taquizoítos no interior dos vacúolos parasitóforos e/ou da conversão de estádios em *T. gondii.* Várias destas proteínas pertencem a famílias de proteínas características dos

Apicomplexa, constituindo este estudo um primeiro passo e uma base promissora para a caracterização de mecanismos moleculares próprios destes organismos.

Palavras-chave: *Toxoplasma gondii*, replicação, taquizoito, quisto de bradizoitos, proteína MOB1.

Unraveling the replication process of *Toxoplasma gondii* through the MOB1 protein

Abstract

MOB1 is a conserved protein that regulates cellular proliferation *versus* apoptosis, centrosome duplication and cellular differentiation in multicellular eukaryotes and also cytokinesis and division axis orientation in unicellular and multicellular eukaryotes. *Toxoplasma gondii*, an obligate intracellular parasite of veterinary and medical importance, presents one MOB1 protein. *T. gondii* interconverts between several cellular stages during its life cycle, namely between fast replicating tachyzoite and slow replicating bradyzoite stages during its asexual cycle, a key ability for its success as a parasite. Bradyzoites produce tissue cysts, establishing a chronic infection that enables recrudescence. Conversion is dependent on cell cycle regulation and involves cell differentiation and regulation of replication. This led us to select MOB1 as a strong candidate to be involved in the *Toxoplasma* replication process. We employed reverse genetics to assess the *Mob1* function in *T. gondii*. In opposition to what was observed in other unicellular eukaryotes, as *Tetrahymena* and *Trypanosoma*, *Mob1* knockout in *T. gondii* showed no cytokinesis impairment in its asexual cycle. Instead, we observed an increase in replication, a decrease in parasitophorous vacuole regularity and a significant loss in tachyzoite to bradyzoite conversion. Additionally, recombinant MOB1 accumulates in a midline between the daughter nuclei at the end of mitosis, suggesting MOB1 may be involved in this process. To elucidate how MOB1 acts in *T. gondii*, we employed a proximity biotinylation method and identified the MOB1 interactome. This analysis detected proteins related to several functional categories, indicating a multivalent role for MOB1 regulated by the ubiquitin-proteasome system. We also verified that the *Mob1* locus is transcribed from both genomic strands and gives rise to alternatively spliced variants. Our results indicate that MOB1 is tightly regulated along the cell cycle and along the life cycle of *T. gondii*, contributing to the control of replication and tachyzoite-bradyzoite differentiation.

Key-words: *Toxoplasma gondii*, replication, tachyzoite, bradyzoite cyst, MOB1 protein.

Table of contents

List of Figures

List of Tables

List of abbreviations and symbols

AGC	kinases related to PKA, PKG, and PKC
AMA1	apical membrane antigen 1
ANOVA	analysis of variance
AP1	clathrin adaptor protein 1 complex
APC/C	anaphase-promoting complex/cyclosome
ApiAP2	Apicomplexa Apetala-2
aPKC	atypical protein kinase C
APS	ammonium persulfate
ATG6	autophagy related 6 homolog
ATM	ataxia–telangiectasia-mutated
BECN1	beclin1
BFD1	bradyzoite-formation deficient 1 transcription factor
BMSC	bone marrow mesenchymal stem cell
bp	base pair
Bub2	budding uninhibited by benzimidazoles 2
C_term_Cas9	C-terminal Cas9
CAMK1	calcium/calmodulin dependent protein kinase 1
cAMP	cyclic adenosine monophosphate
cAMP	cyclic AMP
Cas	CRISPR associated endonuclease
CCDC124	coiled-coil domain containing protein 124
CDC	cell division cycle
CDK	cyclin-dependent kinase
cDNA	complimentary DNA
Cko	*Mob1* splitCas9 functional knockout
CNH	citron homology domain
Cre	Cre recombinase
Cre59	Cre fragment 1-59 aa
Cre60	Cre fragment 60-343 aa
CRISPR	clustered regularly interspaced short palindromic repeats
CRK	cyclin-dependent related kinase
CSN	constitutive photomorphogenesis 9 signalosome
CSN5	CSN subunit 5
DA	large (in Chinese)
DAPI	4′,6-diamidino-2-phenylindole
DEAD/DEAH	Asp-Glu-Ala-Asp/Asp-Glu-Ala-His
DHFR	dihydrofolate reductase
diCre	ku80::diCre
DMEM	Dulbecco's Modified Eagle Medium
dMGMOB1	dd-Myc-GFP-MOB1
DMSO	dimethyl sulfoxide

DNA	deoxyribonucleic acid
DSB	double stranded break
DYRK	dual specificity tyrosine (Y) phosphorylation regulated kinase
E1	ubiquitin-activating enzyme
E2	ubiquitin-conjugating enzyme
E3	ubiquitin-ligase enzyme
EDTA	ethylenediaminetetraacetic acid
eIF2	eukaryotic initiation factor-2
Eko	EGS *Mob1* knockout
ELMO	engulfment and cell motility
ER	endoplasmic reticulum
EuPaGDT	Eukaryotic Pathogen CRISPR sgRNA Design Tool
FAK	focal adhesion kinase
FB	FLAG-BirA
FBMOB1	FLAG-BirA-MOB1
FBS	fetal bovine serum
FDR	false discovery rate
FKBP	FK506 binding protein
FRB	FKBP rapamycin binding
GCK	germinal center kinase
gDNA	genomic DNA
Gid	glucose induced degradation deficient complex
GOI	gene of interest
GPCR	G-protein coupled receptor
GRA	dense granule protein
gRNA	protospacer or guide RNA
GSK	glycogen synthase kinases
GSko	*Mob1* gene-swap knockout
GST	glutathione S-transferase
GTPase	guanosine triphosphatase
HEPES	4-(2-hydroxyethyl)-1-piperazineethanesulfonic acid
HFF	human foreskin fibroblasts
HUCMSC	human umbilical cord mesenchymal stem cell
HX	hypoxanthine-xanthine-guanine phosphoribosyl transferase
iC	inducible *Mob1* splitCas9
iGSoe	inducible *Mob1* gene-swap overexpressing MOB1
IMC	inner membrane complex
indel	insertion or deletion
kb	kilobase pair
kDa	kiloDalton
KIBRA	kidney and brain protein
KO	knockout
LATS	large tumor supressor

Lgl	lethal-2-giant larvae
LIC	ligation independent cloning
loxP	locus of X-over P1
MAP	mitogen-activated protein kinases
Mats	Mob as tumor suppressor
MED	mediator of RNA polymerase II transcription subunit
mFMOB1	morn1-FLAG-MOB1
MIC	microne protein
Mko	ME49 *Mob1* knockout
MOB	monopolar spindle one binder
morn1	MORN1 promoter
MORN1	membrane occupation and recognition nexus 1
Mps1p	monopolar spindle one
mRNA	messenger RNA
MST	mammalian sterile 20
MTOC	microtubule organizing center
mTOR	mammalian target of rapamycin
N_term_Cas9	N-terminal Cas9
NAT	natural antisense transcript
ncRNA	non-coding RNA
NDR	nuclear dbf2-related
NF2	neurofibromin 2
NHEJ	non-homologous end joining
NLS	nuclear localization signal
ns	p-value not significant
PAGE	polyacrylamide gel electrophoresis
PBS	phosphate-buffered saline
PDAC	pancreatic ductal adenocarcinoma
Phos	phosphatase
PKAc	cAMP-dependent protein kinase (protein kinase A) catalytic subunit
PKAR	cAMP-dependent protein kinase regulatory subunit
PM	plasma membrane
PS	parental strain
PSMB1	proteasome subunit beta type 1
PSMB5	proteasome subunit beta type 5
PTM	post-translation modification
PV	parasitophorous vacuole
Rab GAP	Rab GTPase activating protein
Rab5	RAS-associated protein 5
RAD	DNA repair protein
RAM	regulation of Ace2 and morphogenesis
RAS	superfamily including RAS, RHO, RAB, RAN and ARF small GTPases
RH	RHΔHX

RING	really interesting new gene
RNA	ribonucleic acid
ROM	rhomboid protease
RON	rhoptry neck protein
ROP	rhoptry protein
RPN13	regulatory particle non-ATPase 13
rRNA	ribosomal RNA
SAG	surface antigen
SARAH	Salvador/Rassf/Hippo domain
SAV1	Salvador homolog 1
sCas9	splitCas9
SCF	Skp, Cullin, F-box
SDS	sodium dodecylsulphate
SE	standard error of the mean
Ser	serine
sgRNA	single guide RNA
SKP1	S-phase kinase-associated protein 1
SMC	structural maintenance of chromosomes
SNARE	soluble N-ethylmaleimide sensitive factor attachment protein receptor
ST	sense transcript
STRIPAK	striatin-interacting phosphatase and kinase
TAZ	WW domain containing transcription regulator 1 (alternative WWTR1)
TBC	Tre-2/Bub2/Cdc16
TBCB	tubulin cofactor B
TEAD	Transcriptional enhanced associate domain
TEMED	tetramethylethylenediamine
Thr	threonine
TIC	total ion chromatograms
TKL	tyrosine kinase-like
trRNA	transactivating RNA
Tub8	*Tub8* promoter
Tyr	tyrosine
U6	*U6* promoter
Ubi	ubiquitin family protein
ULK	unc-51-like kinase
UPS	ubiquitin-proteasome system
UTR	untranslated region
Wnt	wingless integrated
YAP	Yes associated protein
Yki	Yorkie
α	significance level

Chapter 1. Introduction

1.1. *Toxoplasma gondii*: a successful parasite

Toxoplasma gondii is frequently described as one of the most successful parasites due to its ubiquitous distribution and to the wide range of host species it is able to infect, with high prevalence rates around the world. The amenability of *T. gondii* to laboratory conservation and propagation, both *in vivo* and *in vitro*, and to genetic manipulation have made this parasite a widely used biological model for the study of conserved biological processes and biology of closely related parasites more challenging to manipulate in a laboratory setting (Jiménez-Ruiz et al. 2014).

T. gondii was initially observed in the tissues of the rodent *Ctenodactylus gundi by* Nicolle and Manceaux (1908) and in the tissues of a rabbit by Splendore (1908). At the time, the host *Ctenodactylus gundi was* erroneously identified as *Ctenodactylus gondi*, which resulted in the specific epithet of *T. gondii*. The name of the genus was given as a reference to the shape of the parasite, from the Greek *tóxon* meaning arc or bow and *plasma* meaning something molded (Nicolle and Manceaux 1909). *T. gondii* is an obligate intracellular parasite and is the causative agent of toxoplasmosis in humans and animals. *T. gondii* has a worldwide distribution infecting a vast variety of animals, but only a fraction develops disease (McLeod et al. 2014; Stelzer et al. 2019). Toxoplasmosis is usually acquired through accidental ingestion of either sporulated oocysts that are shed by the felid definitive host and found in food and water supplies, or through consumption of contaminated meat products containing tissue cysts. Rapidly dividing tachyzoites readily invade and replicate in many tissues and cell types, and, if not kept in check by the host's immune system, extensive proliferation causes acute disease and severe tissue pathology in multiple organs (Black and Boothroyd 2000). Thus, toxoplasmosis represents a considerable health risk mainly for immunocompromised individuals and for fetuses upon primary infection during pregnancy (Aguirre et al. 2019). Therapeutic and prophylactic options currently available are either insufficient or cause severe adverse side effects in both humans and animals (J.-L. Wang et al. 2019).

1.1.1. Toxoplasmosis: a prevalent and silent infection

Apicomplexan parasites are responsible for several diseases of great veterinary and medical relevance, including zoonotic diseases. The mosquito borne Hematozoan *Plasmodium* is the cause of malaria, a life-threatening disease with over 200 million cases estimated in 2019 ([WHO] 2020). The tick borne *Babesia* piroplasms cause hemolysis related disease and present zoonotic potential (Gray et al. 2010; Beugnet and Moreau 2015). *Cryptosporidium*, also a

zoonotic parasite, is a major cause of gastrointestinal disease in non-immunocompetent hosts (Tzipori and Ward 2002). Cyst forming Coccidia include the stenoxenous *Neospora caninum* and *Besnoitia besnoiti* that are major sources of economic loss in animal production (Reichel et al. 2013; Álvarez-García et al. 2014). *Toxoplasma* and *Sarcocystis* are also cyst-forming Coccidia but present much less host specificity with regards to the intermediate host. *T. gondii* is extreme in the variety of intermediate hosts it can infect, assumed to be all warm-blooded animals.

1.1.1.1. Epidemiology and transmission

Infection by *T. gondii* has been described in over 350 different host species, most of which inhabiting wild environments, including 31 felid species (Robert-Gangneux and Dardé 2012). The CDC estimates that over 60 million people present chronic toxoplasmosis in the United States and considers this infection as one of five neglected tropical diseases (Parise et al. 2014). In the European Union, only congenital toxoplasmosis is reported, with 208 cases reported in 2018 ([ECDC] 2021). However, only three countries have both mandatory screening programs of pregnant women and report screening data to the ECDC, with cases reported from 22 countries and France accounting for 72.6% of the cases. Therefore, the actual number of cases is likely higher than the reported. *T. gondii* seroprevalence varies widely among region. In humans, seroprevalences have been estimated at 8-76% among different countries (Flegr et al. 2014). Similar variations between very low and high seroprevalence rates have also been reported for various animal species around the world (Smith and Frenkel 1995; de Thoisy et al. 2003; Dabritz et al. 2008; Barros et al. 2018; Dubey, Murata, Cerqueira-Cézar, and Kwok 2020; Dubey, Murata, Cerqueira-Cézar, Kwok, et al. 2020; Dubey, Cerqueira-Cézar, et al. 2020). Felids, particularly wild species, tend to have high seroprevalence rates (Montazeri et al. 2020).

Infection can occur through horizontal and vertical transmission and can occur by three infective stages, sporozoites, bradyzoites, and tachyzoites. The parasite is able to bypass the definitive or the intermediate host during the course of its life cycle, adding further possibilities of perpetuating its cycle. The tachyzoite is not a resistance stage but plays an important role in *Toxoplasma* epidemiology if primary infection occurs during gestation, in which case there is a high probability of transmission to the fetus. Toxoplasmosis acquired through vertical transmission is of great importance in humans and in domestic animals, particularly in small ruminants (Dubey 2009; Robert-Gangneux and Dardé 2012; Dubey, Murata, Cerqueira-Cézar, and Kwok 2020). The sporozoites, enclosed in the sporulated oocyst, are resistance stages that remain viable and accumulate in the environment. This stage is strongly linked to the *T. gondii*

ubiquitous distribution and parasitic success (Shapiro et al. 2019). Oocyst ingestion explains infections by *T. gondii* in vegetarians and herbivore species, but this transmission route is not limited to these groups. A recent meta-analysis study reported a mean pooled prevalence of *T. gondii* oocysts in public environments of 16%, ranging from 8% to 23% in the sampled continents namely North America, Asia, South America and Europe (Maleki et al. 2021). Felids are able to shed millions of oocysts upon infection, acting as disseminators of the sporozoite infective stage. Risk factors for exposure to *T. gondii* in farm animals include presence of cats, but also rodents and birds, access to pastures, farm type and water quality (Moré et al. 2012; Guo et al. 2015; Shapiro et al. 2019). Direct contact with cats is not significantly associated with increased risk of exposure to *T. gondii* in humans (Robert-Gangneux and Dardé 2012). This is likely due to the short period of oocyst shedding after infection and to the fact that environmental sporulation is needed for the oocyst to become infectious, which takes one to five days. There is also evidence that, upon re-shedding, cats shed fewer total oocysts (Dubey and Frenkel 1974). Human infection caused by oocysts is associated to ingestion of shallow well water, uncooked vegetables, fruit and uncooked shellfish, and contact with soil (Kapperud et al. 1996; Cook et al. 2000; Berger et al. 2009; Jones et al. 2009; Robert-Gangneux and Dardé 2012). Ingestion of tissue cysts harboring bradyzoites is also an important route of transmission. Within the tissue cyst, bradyzoites are protected from the digestive proteolytic enzymes, thus are much likely to successfully infect a host through ingestion, compared to tachyzoites (Dubey 1998). Furthermore, tissues cysts harbor viable bradyzoites in the host's tissues indefinitely and are able to cause infection in definitive hosts but also in intermediate hosts, where new tissue cysts may develop. Therefore, tissue cysts enclosed bradyzoites consist of resistance stages in the host's tissues (Dubey 1998). Intermediate or definitive hosts are infected through carnivorism. Ingestion of undercooked meat has been consistently identified as a risk factor for exposure to *T. gondii* in humans (Kean et al. 1969; Kapperud et al. 1996; Cook et al. 2000; Jones et al. 2009). Furthermore, a study published in 1965 by Desmonts and colleagues demonstrated that *T. gondii* seroprevalence was associated to the ingestion of raw meat (Desmonts et al. 1965). The relative importance of *T. gondii* transmission through tissue cyst or oocyst ingestion in humans is still uncertain (Shapiro et al. 2019). However, the recent development of a western blot assay that detects specifically anti-*T. gondii* antibodies generated from oocyst infection may allow to differentiate between transmission routes (Hill et al. 2011). Solid organ transplantation is also recognized as a route of infection in humans, while raw milk may also transmit *T. gondii*, however these routes are not considered epidemiologically relevant (Ryning et al. 1979; Sacks et al. 1982; Fernàndez-Sabé et al. 2012; Dubey et al. 2014).

1.1.1.2. Infection and disease

Toxoplasmosis is frequently a silent infection, causing mild or no signs in immunocompetent hosts upon primary infection. Tachyzoite-bradyzoite conversion permits the formation of tissue cysts which remain viable in the host but do not cause disease, unless the host's immune system becomes compromised. Chronic toxoplasmosis is generally thought to not cause disease, being a concern mainly due to risk of recrudescence. However, evidence suggests that chronic infection is associated to a range of neuropsychiatric and behavioral disorders (Milne et al. 2020). Very rarely, severe clinical disease may occur upon primary infection of immunocompetent hosts (Montoya and Liesenfeld 2004; Dubey, Murata, Cerqueira-Cézar, and Kwok 2020). Most frequently, ocular toxoplasmosis was recorded in humans, but manifestations of generalized toxoplasmosis such as pneumonia, hepatitis and encephalitis have also been reported in humans and in other species (Montoya and Liesenfeld 2004; Calero-Berna and Gennari 2019). If primary toxoplasmosis occurs during pregnancy, transmission may occur to the fetus causing abortion or congenital infection possibly leading to severe generalized toxoplasmosis and death. Severe disease also occurs in immunocompromised hosts, mostly due to recrudescence of a chronic infection (Montoya and Liesenfeld 2004). Therapeutic options currently available fail to eliminate tissue cysts which may reactivate at a later stage of the host's life leading to recrudescence of acute toxoplasmosis, usually connected to a period of immune system compromise. A new compound, the tetrahydroquinolone JAG21, has recently been reported as a promising treatment for acute and chronic toxoplasmosis (McPhillie et al. 2020).

Primary infection was thought to protect felids from re-shedding of oocysts and intermediate hosts from disease and congenital transmission upon re-infection. However, several reports show that this is not always the case. Re-infection with a different *T. gondii* strain and factors related to host-specific biology seem to bypass this protection (Brandão et al. 2011; Lindsay and Dubey 2011; Zulpo et al. 2018). Although *T. gondii* is able to infect a great variety of animal species, susceptibility to infection and parasite resistance in tissues vary among species. Cattle are considered to be mostly resistant to clinical disease, including abortion and congenital infection, while also presenting low levels of tissues cysts in muscle tissues (Blaga et al. 2019; Dubey, Murata, Cerqueira-Cézar, Kwok, et al. 2020). Clinical toxoplasmosis is very rare in pigs, with occasional reproductive-related issues, and tissue cysts are more easily detected (Alves et al. 2019; Dubey, Cerqueira-Cézar, et al. 2020). An exception to the low rate of clinical toxoplasmosis has occurred in China where there have been several recent outbreaks. This is thought to be related to the genotypes most prevalent in this area,

namely genotypes ToxoDB #9 and #10 (Dubey, Cerqueira-Cézar, et al. 2020). Sheeps and goats are among the most affected domesticated species, with toxoplasmosis causing frequent reproductive issues and occasional disseminated disease in adults (Dubey 2009; Dubey, Murata, Cerqueira-Cézar, and Kwok 2020). Chickens are mostly resistant to clinical toxoplasmosis and frequently present high prevalence rates (Dubey 2010). As ground feeders, free range chickens can act as sentinels of environmental contamination with oocysts and are therefore useful for the study of *T. gondii* epidemiology (Dubey 2010). Marine mammals are frequently exposed to high levels of *T. gondii* oocysts due to land-to-sea transport, exhibiting clinical disease. This is thought to be associated with high levels of exposure to oocysts due to oocyst accumulation in marine ecosystems, where they remain viable for years (Shapiro et al. 2019).

1.1.2. An Apicomplexa parasite

T. gondii features the defining hallmarks of Apicomplexa namely an intracellular parasitic life style, an apical complex, a glideosome and an apicomplexan plastid termed apicoplast (Frénal, Dubremetz, et al. 2017; McFadden and Yeh 2017). Apicomplexa, Dinoflagellata and Ciliata include the majority of alveolates, unicellular eukaryotes that present very diverse life styles including phototrophy, predation, and intracellular parasitism (Walker et al. 2011). The Alveolata are named for its contiguous membranous vesicles or alveoli which are located immediately below the plasma membrane. While previous taxonomic classifications included Alveolata within the kingdom Protozoa, recent analyses taking advantage of technological progress in electron microscopy and gene sequencing have re-assigned Alveolata to the kingdom Chromista (Table 1). Cilliata and Dinoflagellata are mostly free-living or commensal organisms while Apicomplexa are obligatory intracellular parasites (Walker et al. 2011). Apicomplexa include the invertebrate parasites Gregarina, the blood parasites Hematozoa, the Coccidia, containing cyst-forming and non-cyst forming genera, and the more divergent and hard to classify Cryptosporidia (Šlapeta and Morin-Adeline 2011). Although Cryptosporidia were previously considered as part of Coccidia, phylogenetic analyses have shown that these parasites are more closely related to Gregarina (Šlapeta and Morin-Adeline 2011). Both Gregarina and Cryptosporidia have suffered loss of the apicoplast. It was initially thought that Hematozoa had largely lost the invasion-related structure conoid, however recent research showed that the conoid structures are conserved among all Apicomplexa clades and that the conoid is present throughout the life cycle of the hematozoan *Plasmodium berghei* (Koreny et al. 2021).

Table 1. Comparison of classical and updated taxonomic classifications of *Toxoplasma gondii*

Taxon	Classical classification	Updated classification
Kingdom	Protozoa	Chromista
Subkingdom	Dictyozoa	Harosa
Infrakingdom	Neozoa	Halvaria
Superphylum	Alveolata	Alveolata
Phylum	Apicomplexa	Myozoa
Infraphylum	Sporozoa	Apicomplexa
Superclass	Coccidia	Sporozoa
Class	Eucoccidea	Coccidiomorphea
Order	Eucoccidiorida	Eimeriida
Family	Sarcocystidae	Sarcocystidae
Genus	*Toxoplasma*	*Toxoplasma*
Species	*Toxoplasma gondii*	*Toxoplasma gondii*
References	Compilation of (Cavalier-Smith 1993; Cavalier-Smith 1998; Taylor et al. 2016)	Compilation of (Ruggiero et al. 2015; Rees et al. 2020)

1.1.3. Genetic diversity: one species, many strains

Several *T. gondii* strains have been isolated, which present genotypic and phenotypic differences. Strain nomenclature is not consensual, with designations of genotype, haplogroup, *Toxoplasma* Biological Resource Centre code, and conventional type designation being attributed according to the method used for characterization. Matches between the different designations are not always available. The initial characterization of the *T. gondii* population was based on samplings performed in Europe and North America. These identified a highly clonal population structure, grouped in three strain types designated types I, II, and III, with very low genetic divergence among types at DNA sequence level (Howe and Sibley 1995). These clonal lines emerged around 10^4 years ago, associated to an increased oral infectivity which allowed the bypass of sexual reproduction, and contemporary to agriculture expansion and to the domestication of the cat (Su et al. 2003). Conversely, *T. gondii* isolates from South America, Africa, and Asia are much more divergent. South America is particularly rich in divergent strains, with 88 genotypes having been isolated in Brazil alone (Khan et al. 2007; Pena et al. 2011). Evidence suggests that North and South American strains diverged from a common ancestor over 10^6 years ago (Khan et al. 2007). Type II strains predominate in Europe and North America while type III strains are less frequent but have a worldwide distribution (Robert-Gangneux and

Dardé 2012). Type I strains are the less abundant of the clonal lineages, being found mostly in Europe and America. Strains vary in virulence, which is frequently defined using the *T. gondii* mouse model. Type I strains (e.g. RH and GT1) are more virulent and present higher morbidity and mortality when infecting mice (Robert-Gangneux and Dardé 2012). This is coupled to lower rates of tissue cyst formation. South American strains frequently show type I strain-like virulence and tissue cyst formation ability, associated to lower potential for oral transmission which seems to be specific to the clonal lines (Fux et al. 2007). Type II strains (e.g. ME49 and Prugniaud) and type III strains (e.g. CTG and VEG) tend to be avirulent, presenting low morbidity and high rates of chronic infection with tissue cyst formation (Robert-Gangneux and Dardé 2012). Type III strains are slightly more virulent than type II strains. Evidence shows that clonal strains are more prevalent in human adapted environments while divergent strains are more prevalent in wild environments, suggesting separate anthropized and sylvatic cycles (Mercier et al. 2011; Khan et al. 2014).

1.1.4. One parasite, several specialized eukaryotic cells

1.1.4.1. Zoites, motile stages

During most of its life cycle, *T. gondii* exhibits a permanently polarized crescent shaped cell with an anterior-posterior axis, namely the motile or invasive zoite stages, namely merozoites, tachyzoites, bradyzoites, and sporozoites (Ferguson and Dubremetz 2014; Harding and Frischknecht 2020). These stages present 2 x 5-7 µm with a narrower anterior or apical pole and a more rounded posterior or basal pole (Robert-Gangneux and Dardé 2012; Ferguson and Dubremetz 2014). The *T. gondii* cells possess the universal eukaryotic organelles endoplasmic reticulum (ER), ribosomes, Golgi complex, ribosomes, one mitochondrion, centrosome, and nucleus (Robert-Gangneux and Dardé 2012). The nucleus is centrally located and presents a spherical shape with a shallow concavity directed towards the apical pole where the Golgi is located (Attias et al. 2020). The rough ER is continuous with the nuclear envelope (Ferguson and Dubremetz 2014). The single mitochondrion is long, with up to 10 µm in length folded inside the cell, and ramified (Melo et al. 2000). The centrosome is closely related to the nuclear membrane and is essential for cell division and organelle duplication (Striepen et al. 2000; Chen and Gubbels 2013). But *T. gondii* also present highly specialized structures, namely the apicoplast, the secretory organelles, the inner membrane complex (IMC), and the apical and basal complexes (Figure 1).

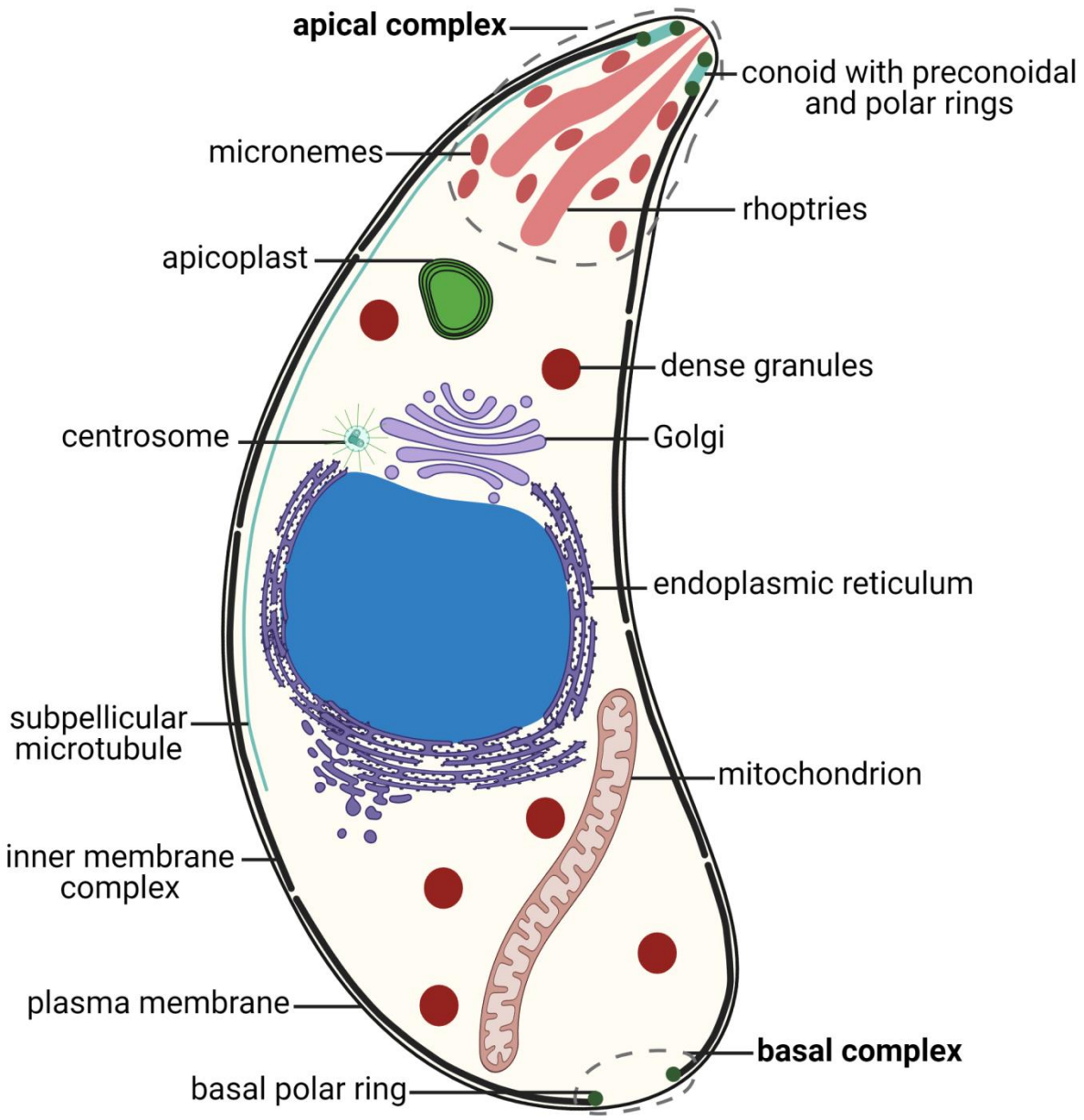

Figure 1. Morphology of the *Toxoplasma gondii* tachyzoite.

Schematic drawing of a transverse cut of a *T. gondii* tachyzoite where the main organelles and structures are represented. The apical and basal complexes are highlighted with grey interrupted lines. Created with BioRender.com.

The apicoplast, a plastid organelle resulting from secondary endosymbiosis of eukaryotic photosynthetic red algae that has lost its photosynthesis function but is an essential organelle (Brooks et al. 2010; Janouškovec et al. 2010; McFadden and Yeh 2017). The secretory system includes three secretory organelles: dense granules, rhoptries, and micronemes. Dense

granules are distributed throughout the cell while rhoptries and micronemes are located at the apical pole (Joiner and Roos 2002). The polarized subcellular localization of rhoptries and micronemes is connected to its roles in host cell attachment and invasion namely through the assembly of the moving junction, being a part of the highly specialized apical complex (Lebrun et al. 2014; Kato 2018). Besides the two secretory organelles, the apical complex is constituted by the conoid, a mesh of coiled microtubules limited at the top by the preconoidal rings and at the bottom by the inner polar ring, and two intraconoidal microtubules (Figure 2) (Dubey et al. 1998; Ferguson and Dubremetz 2014). The inner polar ring is a microtubule organizing center (MTOC) (Russell and Burns 1984; Nichols and Chiappino 1987; Morrissette and Sibley 2002). Although evidences suggest it is necessary for host cell invasion, the function of the conoid is not fully understood (Lebrun et al. 2014). The ability of the conoid to extend and retract, namely in extracellular zoites during the invasion process, suggests a mechanical role for this structure which is also involved in secretion (Hu et al. 2006; Katris et al. 2014). The subpellicular microtubules are a set of 22 spirally arranged microtubules that originate from the inner polar ring and extend to two thirds of the cell's length and support the pellicle through the cytosolic face of the IMC, conferring the cell's shape (Morrissette and Sibley 2002; Ferguson and Dubremetz 2014; Harding and Frischknecht 2020). The pellicle is a three layer structure highly specialized in the Apicomplexa. It is formed by the plasma membrane (PM) outer layer that encloses the parasite cell and the alveoli two inner layers that consist of flattened vesicles from the Golgi and ER arranged in longitudinal fused plates (Morrissette and Sibley 2002; Ferguson and Dubremetz 2014; Harding and Frischknecht 2020). The alveoli are supported by the subpellicular network, a stable mesh of intermediate filaments that run from the outer polar ring through the full length of the cell, responsible for the cell's mechanical stability (Mann and Beckers 2001). The intimately associated alveoli and subpellicular network are designated by the inner membrane complex (IMC) which is essential for parasite motility, host cell invasion and replication (Morrissette and Sibley 2002; Harding and Frischknecht 2020). Thus, the IMC forms a continuous double layered sheet that extends from the polar ring at the apical pole of the cell to the basal complex at the basal pole of the cell, forming two circular apertures at each end. At the basal pole, a basal complex is present including the basal polar ring, where the IMC terminates (Hu 2008). Several proteins have been characterized to be present in the basal complex (Morrissette and Sibley 2002; Harding and Frischknecht 2020). This includes proteins associated to the cytoskeleton and parasite replication, namely Myosin C, Centrin, Dynein and membrane occupation and recognition nexus 1 (MORN1) proteins (Figure 3) (Delbac et al. 2001; Hu et al. 2006; Gubbels et al. 2006; Heaslip et al. 2010). A 14-3-3 protein that belongs to

a conserved family of signaling proteins was also localized to the basal complex (Lorestani et al. 2012). MORN1 is present at the apical and basal rings but also in close proximity to the centrosome (Gubbels et al. 2006).

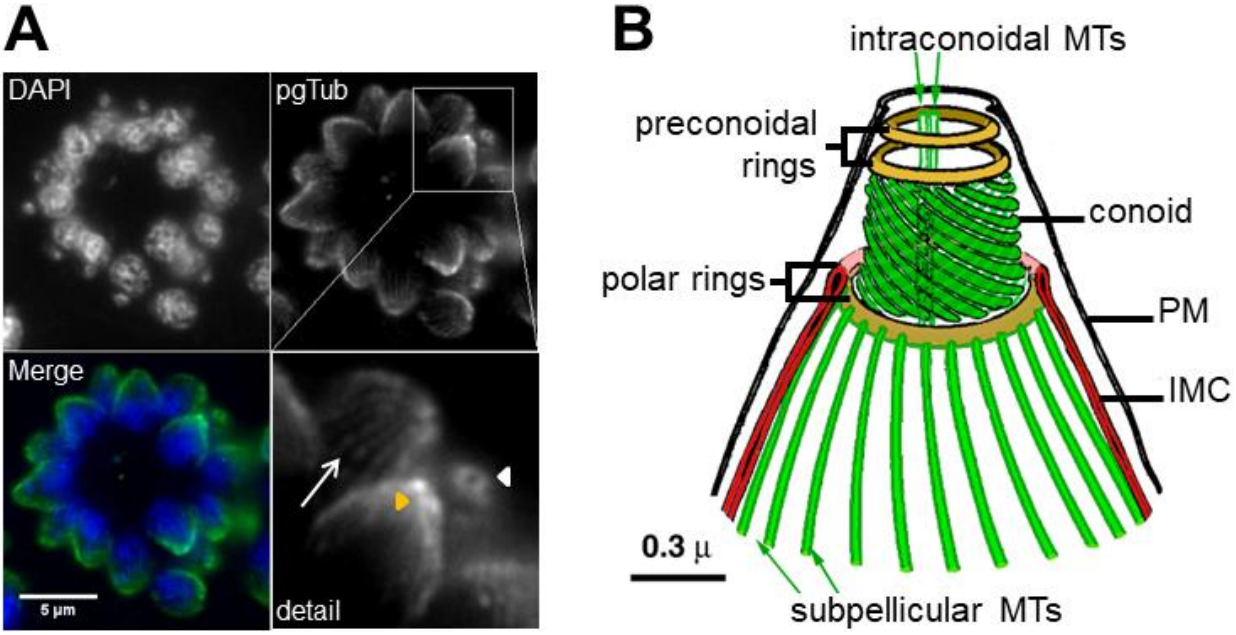

Figure 2. Tachyzoite apical cytoskeleton.

A) Immunofluorescence of intracellular tachyzoites where retracted conoids and subpellicular microtubules are visible. The tachyzoite apical structures are identified by polyglutamylated tubulin (pgTub), namely the conoid and attached rings (white arrowhead in top view, yellow arrowhead in side view), and the subpellicular microtubules (arrow), visible in the detail at the bottom right of the panel. DNA is stained with DAPI. The scale bar represents 5 µm. **B)** Diagram depicting the apical complex cytoskeletal structures with an extended conoid. The scale bar represents 0.3 µm (adapted from Hu et al. (2006), an open-access article distributed under the terms of the Creative Commons Attribution License which permits use of text and figures, provided the original work is cited). IMC – inner membrane complex; PM – plasma membrane; MTs – microtubules.

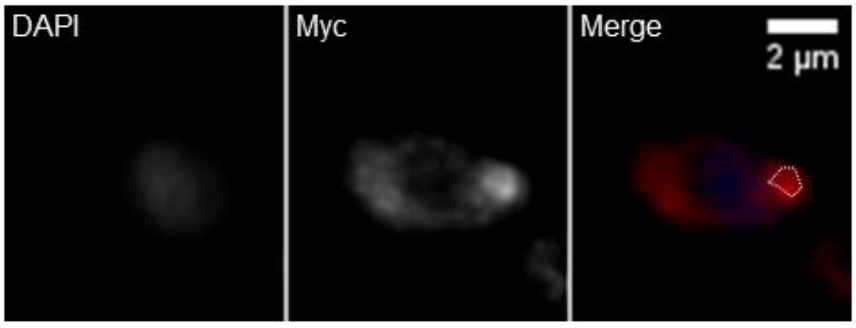

Figure 3. Tachyzoite basal polar ring.

Immunofluorescence of intracellular tachyzoites stably expressing a MORN1-Myc recombinant protein coupled to the MORN1 promoter region, pmorn. MORN1-Myc accumulates at the basal pole forming the basal polar ring

(highlighted by the white dotted line). The recombinant protein is stained with anti-Myc. DNA is stained with DAPI. The scale bar represents 2 µm. The *pmorn-Morn1-Myc-Cat* vector was a kind gift from Marc-Jan Gubbels (Biology Department of Biology, Boston College, USA).

The *T. gondii* zoite stages present slight differences in morphology, namely regarding the position of the nucleus and the number of micronemes. Tachyzoites and merozoites present a more central nucleus and fewer micronemes compared to bradyzoites and sporozoites that present a more basal nucleus and more numerous micronemes (Dubey et al. 1998; Ferguson and Dubremetz 2014). Lipid bodies are abundant in sporozoites, irregularly present in tachyzoites and absent in bradyzoites (Knoll et al. 2014). Bradyzoites are slimmer than tachyzoites, presenting solid rhoptries, which are labyrinthine in tachyzoites, and many amylopectin granules that are few or absent in tachyzoites (Dubey et al. 1998; Ferguson and Dubremetz 2014). Bradyzoites are also more resistant to proteolytic digestion than tachyzoites (Jacobs et al. 1960; Popiel et al. 1996; Dubey et al. 1998).

1.1.4.2. Non-motile and gamete stages

During its sexual development, *T. gondii* also develop non motile cells. First, merozoites divide frequently forming polyploid cell, schizonts, which later undergo individualization to form multiple merozoites (Attias et al. 2020). In order to produce gametes, *T. gondii* form non-motile gamonts: microgamonts and macrogamonts (Ferguson and Dubremetz 2014; Attias et al. 2020). Each microgamont can produce 15 to 30 mature microgametes, motile cells that present two flagella coupled to two basal bodies (MTOCs) and a mitochondrion at the flagellar base. The macrogamont is an oval cell that forms one mature macrogamete. Synthesis of the oocyst wall begins still in the macrogamont which possesses wall-forming bodies (Dubey et al. 1998; Ferguson and Dubremetz 2014; Attias et al. 2020). After fertilization, the unsporulated oocyst is formed with a single sporont. During sporulation, the sporont forms two sporocysts each containing four sporozoites, originating the sporulated oocyst (Dubey et al. 1998; Ferguson and Dubremetz 2014; Attias et al. 2020).

1.1.5. The complex *Toxoplasma gondii* life cycle: a path to success

T. gondii presents a facultative heteroxenous life cycle (Figure 4). Felids are the only animals capable of sustaining the sexual phase of the *T. gondii* life cycle, however all warm-blooded animals, including felids, can act as intermediate hosts. Transmission may occur

through three infective stages: bradyzoites, tachyzoites, and sporozoites. The parasite takes resistance forms in the tissues of intermediate hosts, tissue cysts, and in the environment, sporulated oocysts, increasing its chances for transmission. Furthermore, the three infective stages are able to produce infection in both definitive and intermediate hosts, being able to bypass the definitive host or the intermediate host. These features are fundamental for the global distribution and overall high seroprevalence that *T. gondii* presents.

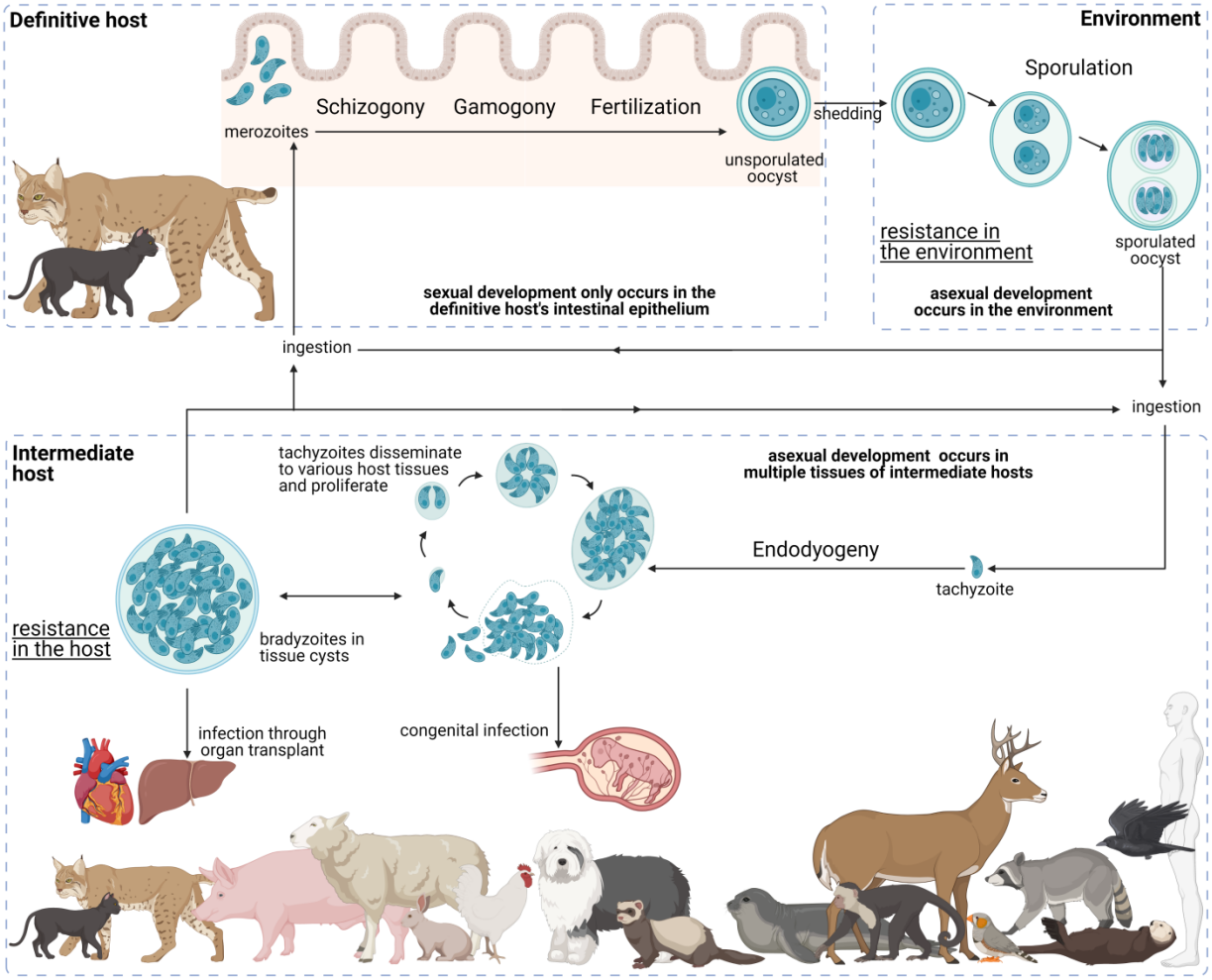

Figure 4. Life cycle of *Toxoplasma gondii*.

The *T. gondii* life cycle includes three main phases of development: in the definitive host, in the environment, and in the intermediate host (highlighted in grey interrupted lines). The various parasite stages and biological events are indicated relative to the development phase as well as how the different entities interplay. Created with BioRender.com.

1.1.5.1. Development in the definitive host

Only members of the Felidae family can sustain the *T. gondii* sexual phase. A recent study showed that this specificity is related to the absence of delta-6-desaturase intestinal activity in felids that results in high concentrations of linoleic acid in enterocytes (Di Genova et al. 2019). *T. gondii* sexual development was achieved in mice after reproduction of these conditions (Di Genova et al. 2019). Felids are fundamentally infected through carnivorism by the ingestion of *T. gondii* infected prey harboring tissue cysts. Although the definitive hosts are more readily infected through ingestion of tissues cysts harboring bradyzoites, infection in felids can occur through the three *T. gondii* infective stages, sporozoites, bradyzoites, or tachyzoites (Freyre et al. 1989; Dubey 2001; Dubey 2006). Upon digestion of the tissue cysts' wall by proteolytic enzymes, bradyzoites are released and able to infect the felid host. In the cat's gastrointestinal tract, the infective stages invade enterocytes and may differentiate to tachyzoites, which disseminate through the host body, or more frequently to merozoites, which remain in the felid gastrointestinal tract (Tomasina and Francia 2020). Here, merozoites initiate the sexual cycle with multiple rounds of asexual expansion in enterocytes (Dubey and Frenkel 1972; Dubey et al. 1998). This expansion occurs through endodyogeny, endopolygeny, or schizogony, depending on the merozoite/schizont stage (Dubey and Frenkel 1972; Dubey et al. 1998; Speer and Dubey 2005; Tomasina and Francia 2020). In endodyogeny, organelle replication is immediately followed by division and daughter cell budding (Francia and Striepen 2014). Schizogony is characterized by multiple rounds of nuclear replication and division followed by a final step of merozoite individualization (Francia and Striepen 2014). In endopolygeny, a form of schizogony, one merozoite first undergoes a series of nucleus, mitochondrion, and apicoplast replication without division followed by merozoite individualization that starts with formation of the IMC and apical complex (Ferguson and Dubremetz 2014). Merozoite egress from one enterocyte to invade a new enterocyte characterizes the development of a new generation of merozoites. Five types of *T. gondii* schizonts designated A to E occur successively and are considered morphologically different, with various generations per type (Dubey and Frenkel 1972; Dubey et al. 1998). No clear trigger has been identified, but it is believed that schizonts type D and E originate gametocytes, which are preferentially located in the ileum, whereas schizonts are distributed through jejunum, ileum, and occasionally colon (Dubey and Frenkel 1972; Dubey et al. 1998; Speer and Dubey 2005; Tomasina and Francia 2020). It is thought that the flagellated microgametes reach the non-motile macrogametes to undergo fertilization with production of a diploid sporont (Dubey and Frenkel 1972; Ferguson and Dubremetz 2014). Felids can shed 10^7-10^9 oocysts for 4-13 days following a first infection

with *T. gondii* through tissue cyst ingestion (Dubey and Frenkel 1972; Dubey 1995; H. Fritz et al. 2012). However, microgamonts represent only 2-5% of gamonts produced in felids' enterocytes, yielding a low microgamete to macrogamete ratio (Ferguson 2002; Ferguson and Dubremetz 2014; Tomasina and Francia 2020). Furthermore, it is thought that the biflagellate microgamete must reach the macrogamete inside the enterocyte for fertilization as the oocyst wall is formed by the macrogamont. The complex route that has to be taken by the microgamete makes unlikely that fertilization is a very frequent event, which is inconsistent with the high number of oocyst shed by felids. This prompted the hypothesis of parthenogenesis also occurring in the development of oocysts (Ferguson 2002; Ferguson and Dubremetz 2014; Tomasina and Francia 2020).

1.1.5.2. Environmental development

Ovoid unsporulated oocysts, containing the diploid sporont, are shed in felids' feces. This occurs three to ten days after ingestion of bradyzoites but only 18 days after ingestion of oocysts (Dubey 1996; Dubey 2001). The longer prepatent period upon ingestion of sporozoites compared to bradyzoites by the felid host is consistent with sporozoites first differentiating to tachyzoites which, after dissemination through the felid host body, convert to merozoites in the enteric tract, instead of direct sporozoite to merozoite differentiation (Freyre et al. 1989). The sporont undergoes sporulation with three nuclear divisions, a meiosis followed by two mitoses, and formation of the sporocysts walls (Dubey et al. 2017; Freppel et al. 2019). Notably, staining of the nuclear material suggests absence of the nuclear envelope during meiosis (Dubey et al. 2017). This contrasts with the report of a closed mitosis with maintenance of nuclear envelope integrity during the whole cell cycle, a characteristic common to Apicomplexans (Francia and Striepen 2014). Sporulation is usually completed within one to seven days, depending on conditions as temperature and aeration (Dubey et al. 1998; Freppel et al. 2019; Tomasina and Francia 2020). The sporulated oocyst, with two sporocysts containing four sporozoites each, is infective and remains viable in the environment. Sporulated oocysts are extremely resistant both to disinfection techniques and to environmental conditions, remaining infective for up to years (Freppel et al. 2019). Once in the environment, oocysts go through sporulation becoming a source of infection to new hosts.

1.1.5.3. Development in the intermediate host

T. gondii infects a wide variety of species as intermediate hosts, which are believed to include all warm-blooded animals. Notably, the asexual phase of the *T. gondii* life cycle also occurs in the felids that can therefore act as both definitive and intermediate hosts. Intermediate hosts are readily infected through ingestion of sporulated oocysts, tissue cysts, and tachyzoites, although the latter stage presents limited epidemiologic importance (Dubey 2001; Dubey 2006). Upon infection of an intermediate host, *T. gondii* infective sporozoites and bradyzoites differentiate to the tachyzoite stage (Ferguson and Dubremetz 2014; Knoll et al. 2014). Tachyzoites replicate inside a parasitophorous vacuole (PV) by endodyogeny and proceed to a rapid asexual expansion and dissemination to the host's tissues through the circulatory system. *T. gondii* proliferate in virtually any nucleated cell type, therefore the parasite is able to invade and replicate in various animal tissues. Tachyzoites are able to differentiate to bradyzoites, a stage that replicates at a much slower rate, forming tissue cysts that may remain viable in the host for the course of its life (Ferguson and Dubremetz 2014; Knoll et al. 2014). Tachyzoites are responsible for parasite dissemination and acute infection, but this rapid proliferation is ultimately controlled in most immunocompetent hosts. On the other hand, bradyzoites inside tissue cysts are responsible for chronic infection without obvious clinical signs. Tachyzoite-bradyzoite interconversion is a key aspect of the *T. gondii* life cycle as it allows resistance in the intermediate host and recrudescence of active infection when the host's immune system is no longer able to control tachyzoite proliferation.

1.1.6. The *Toxoplasma gondii* lytic cycle: an efficient proliferation strategy

Tachyzoites divide rapidly inside the host cell and, after several rounds of replication, egress from the host cell and seek a new cell to invade. This is designated the lytic cycle, as tachyzoites cause lysis of the cells upon egress.

1.1.6.1. Gliding motility

Like other Coccidia, *Toxoplasma gondii* zoites do not present locomotion specific organelles such as flagella or cilia but are still able to seek host cell to invade. This is done through a cellular movement without shape deformation known as gliding motility, which includes three movement types: circular gliding, upright twirling and helical rotation (King 1988; Håkansson et al. 1999). Gliding is achieved from the interaction of the apical complex, the actin

cytoskeleton, myosin motor proteins, and associated proteins which form a glideosome (Dobrowolski and Sibley 1996; Dobrowolski et al. 1997; Meissner et al. 2002; Opitz and Soldati 2002; Brossier et al. 2003). Endocytosis is involved in retrograde motility (Gras et al. 2019). Gliding motility is essential not only for the parasite to reach a potential host cell but also to successfully invade it and posteriorly egress form it (Soldati and Meissner 2004).

1.1.6.2. Attachment and invasion

Tachyzoite attachment to a host cell depends on the actomyosin system and on expression of surface antigens (SAGs) and microneme proteins (MICs) (Mineo and Kasper 1994; Jacquet et al. 2001; Rabenau et al. 2001; Cérède et al. 2005; Whitelaw et al. 2017). Following committed attachment, the parasite invades the host cell through a moving junction, a hoop-like structure involving close host-parasite interaction, formed by the secretion of rhoptry neck proteins (RONs) and the MIC apical membrane antigen 1 (AMA1) (Alexander et al. 2005; Carruthers and Boothroyd 2007). As parasite invasion progresses, the moving junction migrates from the apical to the posterior pole actively eliminating selected surface proteins from both host and parasite plasma membranes, namely transmembrane proteins (Mordue et al. 1999; Charron and Sibley 2004). This process and the simultaneous active invasion generated by the glideosome give rise to an invagination of the host plasma membrane resulting in the new PV and its surrounding parasitophorous vacuole membrane (Mordue et al. 1999; Charron and Sibley 2004; Carruthers and Boothroyd 2007). The invasion process also involves rearrangement of the host microtubule cytoskeleton which is associated with the moving junction (Walker et al. 2008; Sweeney et al. 2010; Cardoso et al. 2014).

1.1.6.3. Establishment of the parasitophorous vacuole

Inside the host cell, the parasite establishes the PV by modification of the invaginated vacuole. Upon closure of the vacuole, there is secretion of dense granule proteins (GRAs) and formation of a tubulo-vesicular intravacuolar network (Sibley et al. 1995; Mercier et al. 2002). The parasite manipulates the host cell through interaction with microtubules and recruitment of several host organelles to its proximity, namely endoplasmic reticulum, mitochondria, centrosome, and Golgi apparatus (de Melo et al. 1992; Melo and De Souza 1997; Sinai et al. 1997; Melo et al. 2001; Sehgal et al. 2005; Coppens et al. 2006; Cardoso et al. 2014; Ferguson and Dubremetz 2014). *T. gondii* also scavenges key nutrients from the host cell to the PV, as sphingolipids and cholesterol, from internalized organelles such as endocytic organelles, lipid

droplets and Rab vesicles (Coppens et al. 2000; Coppens et al. 2006; Romano et al. 2013; Nolan et al. 2017; Romano et al. 2017). The PV created by the parasite allows its intracellular replication protected from the host cell as the vacuole does not fuse with host acidic lysosomes (Jones and Hirsch 1972; Carvalho and Melo 2006).

1.1.6.4. Proliferation through endodyogeny

T. gondii tachyzoites replicate inside the PV by endodyogeny, a mechanism of internal daughter budding that involves the formation of two complete daughter cells inside an intact and polarized mother cell in each round of replication. Tachyzoites replicate synchronously at a 2^n rate, where "n" equals the number replication rounds, with a predictable number of tachyzoites after each replication round until parasite egress (Ferguson and Dubremetz 2014; Francia and Striepen 2014). This contrasts with endopolygeny and schizogony replications which tend to be asynchronous and do not follow a geometric expansion (Francia and Striepen 2014). The *T. gondii* cell cycle consists of three phases, a protein synthesis and growth gap phase or G1, a DNA synthesis phase or S, and a mitosis phase or M (Radke et al. 2001). The second gap phase G2, usually present in the eukaryotic cell cycle, is very short or absent in *T. gondii* (Radke et al. 2001). The first events of replication are Golgi and centrosome duplication which occur in late G1 and early S phases, respectively (Sheffield and Melton 1968; Hu et al. 2002; Hartmann et al. 2006; Nishi et al. 2008; Anderson-White et al. 2012). The beginning of budding occurs in late S phase with *de novo* formation of the daughter apical complexes which will act as scaffolds during daughter cell assembly (Radke et al. 2001; Hu et al. 2006). The cytoskeleton grows from the apical pole to the basal pole, engulfing the daughter organelles, beginning with Golgi and centrosome, followed by apicoplast, nucleus, and endoplasmic reticulum (Figure 5) (Striepen et al. 2000; Hu et al. 2002). The mitochondrion is the last organelle to divide and be engulfed by the forming daughter cytoskeleton, while the secretory organelles are formed *de novo* (Sheffield and Melton 1968; Nishi et al. 2008). At the basal pole, the basal complex ensures proper daughter segregation with MORN1 forming a contractile ring at this subcellular localization (Figure 6) (Lorestani et al. 2012). Daughter cell cytoskeleton formation is therefore intimately connected to cytokinesis. At the end of daughter cell assembly, the mother cell's cytoskeleton is degraded and its plasma membrane is recycled to the daughter cells along with newly formed plasma membrane (Sheffield and Melton 1968; Anderson-White et al. 2012). Proliferating tachyzoites inside the same PV are frequently observed still attached in its basal pole by the residual body, a remnant of the mother cell cytoplasm. Mitosis occurs simultaneously with the final steps of daughter cell assembly, while the mother cell apical

complex persists until the end of endodyogeny (Ferguson and Dubremetz 2014). Nuclear division occurs by closed mitosis in which the nuclear envelope maintains its integrity throughout the process, an aspect common to Apicomplexa (Ferguson and Dubremetz 2014; Francia and Striepen 2014). *T. gondii* is haploid (1N) with its DNA organized in 14 chromosomes. During mitosis, chromatin shows reduced condensation and the nucleolus structure is stable (Gubbels et al. 2008). After DNA replication, the nucleus develops two apical protrusions in late S phase that correspond to the location of the spindles (Radke et al. 2001). The spindles are intranuclear and localized within a funnel like structure formed by the nuclear envelope, the centrocone, and link the centrosome to the centromeres (Francia et al. 2012). Centromeres are bundled and bound to the nuclear envelope in close proximity to the centrosome during most of the cell cycle, with the exception of the spindle microtubule interaction during DNA segregation (Figure 6) (Francia and Striepen 2014). Mitosis occurs shortly after centrocone formation, with the spindle microtubules migrating posteriorly into the nucleus and causing a U-shaped nucleus (Radke et al. 2001; Francia and Striepen 2014). Finally, the two nuclear lobes are segregated by fission (Francia and Striepen 2014). The time necessary for one replication round varies according to the strain type, mainly due to the duration of the G1 phase, with a reported five hours for type I versus nine hours for types II and III (Radke et al. 2001). Mitosis and cytokinesis are quick processes that take around 20 minutes each (Radke et al. 2001).

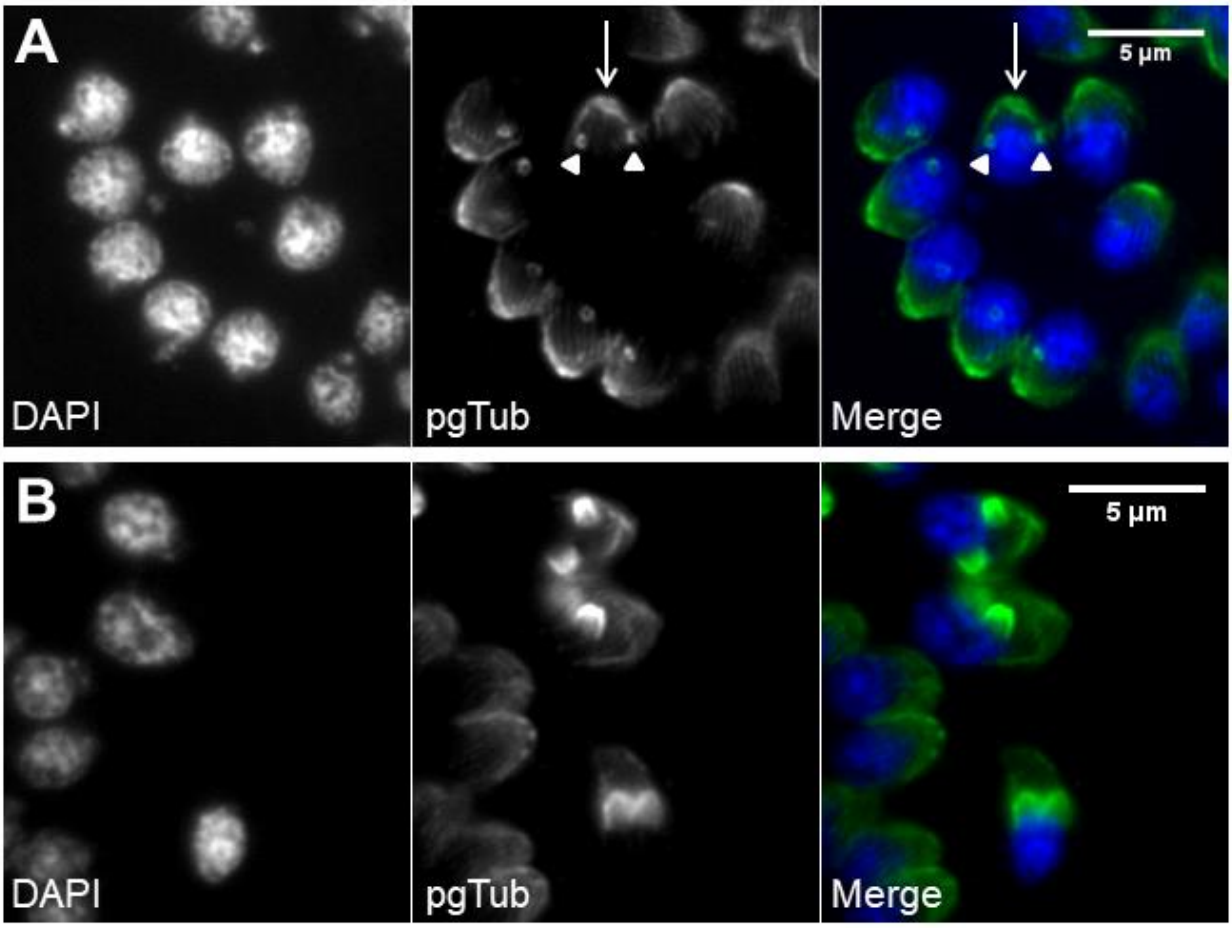

Figure 5. *De novo* formation of the cytoskeleton drives daughter cell assembly.

Immunofluorescence of intracellular tachyzoites in which the apical cytoskeleton is identified by polyglutamylated tubulin (pgTub) and DNA is stained with DAPI. **A)** Rosette with eight tachyzoites where the apical cytoskeleton is identified, namely the conoid and attached rings (white arrow), and subpellicular microtubules of the mother cells, but also the conoids of the forming daughter cells (white arrowheads). **B)** Three tachyzoites in the center show the forming daughter cell's apical cytoskeleton advancing towards the basal pole. The scale bars represents 5 µm.

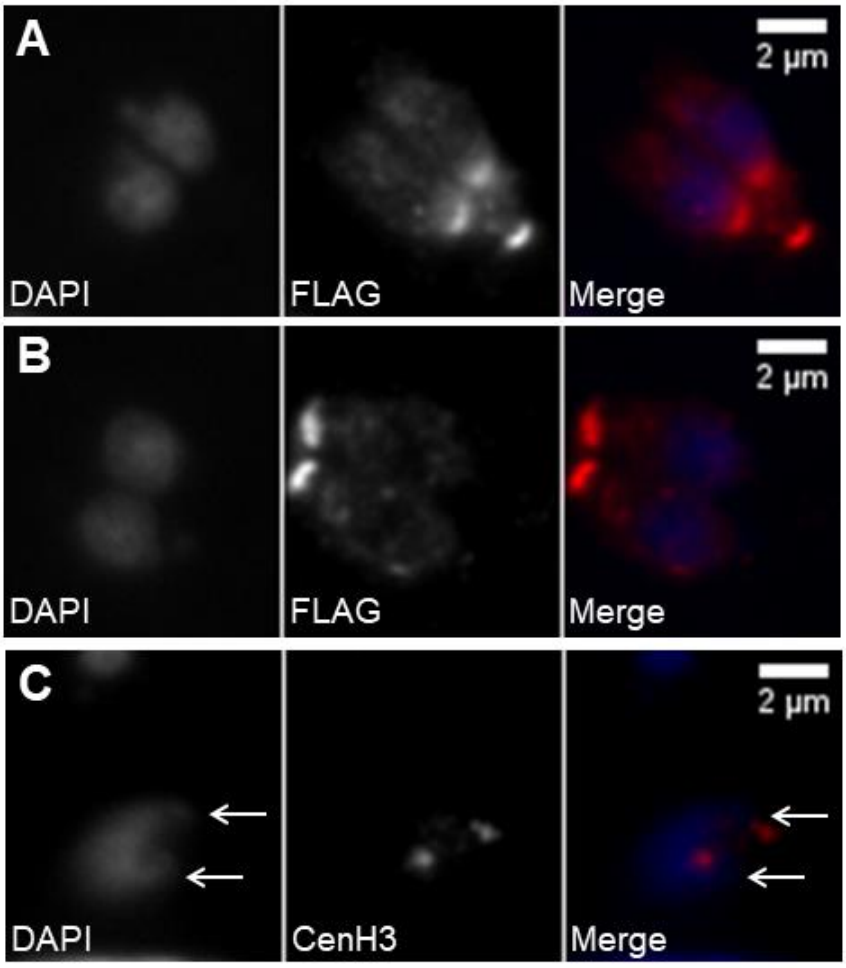

Figure 6. Daughter cell assembly involves DNA duplication and segregation.

A) and **B)** Immunofluorescence of intracellular tachyzoites stably expressing a FLAG-MORN1 recombinant protein coupled to the MORN1 promoter region. The recombinant protein is stained with anti-FLAG. DNA is stained with DAPI. The top panel (A) shows fully segregated DNA and the newly formed daughter cells' basal polar rings while the mother cell's basal polar ring is still present. The bottom panel (B) shows two fully mature, recently formed tachyzoites, each presenting one basal polar ring. **C)** Immunofluorescence of an intracellular tachyzoite that has suffered DNA duplication, marked by the presence of two centromeres. The nucleus shows two apical protrusions (white arrows), indicating the centrocones. The centromeres are identified by staining with anti-CenH3. DNA is stained with DAPI. The scale bars represents 2 µm.

1.1.6.5. Egress and repeat

Replication rounds ensue until depletion of the host cell, concluding with parasite egress. Egress is an active process that causes lysis of the host cell and enables tachyzoites to access new host cells to continue proliferation. Tachyzoite movement inside the PV signals imminent egress (Caldas et al. 2018). Successful egress is dependent on secretion of MICs and GRAs

that promote destabilization of the PV and host cell plasma membranes (Kafsack et al. 2009; Okada et al. 2013; Gras et al. 2017; LaFavers et al. 2017; Schultz and Carruthers 2018). Parasite motility is also essential not only to reach a new host cell but also to destabilize the membranes and successfully egress (Meissner et al. 2002; Frénal et al. 2014; Graindorge et al. 2016; Jacot et al. 2016). Phosphatidic acid is a signal for egress, acting through a guanylate cyclase (GC)-cGMP-protein kinase G (PKG)-inositol triphosphate (IP3) signaling pathway and promoting Ca^{2+} release, consequent activation of Ca^{2+}-dependent protein kinases (CDPKs) and micronemes activity (Bisio and Soldati-Favre 2019). Overall, Ca^{2+} is a major hub to trigger egress, having been extensively used to promote tachyzoite egress in cell culture (Endo et al. 1982; Lourido et al. 2012; Caldas et al. 2018). The succession of these processes (gliding motility, attachment, invasion, replication, and egress) enables tachyzoite expansion and proliferation throughout the host's tissues, causing cell lysis and tissue damages (Figure 7).

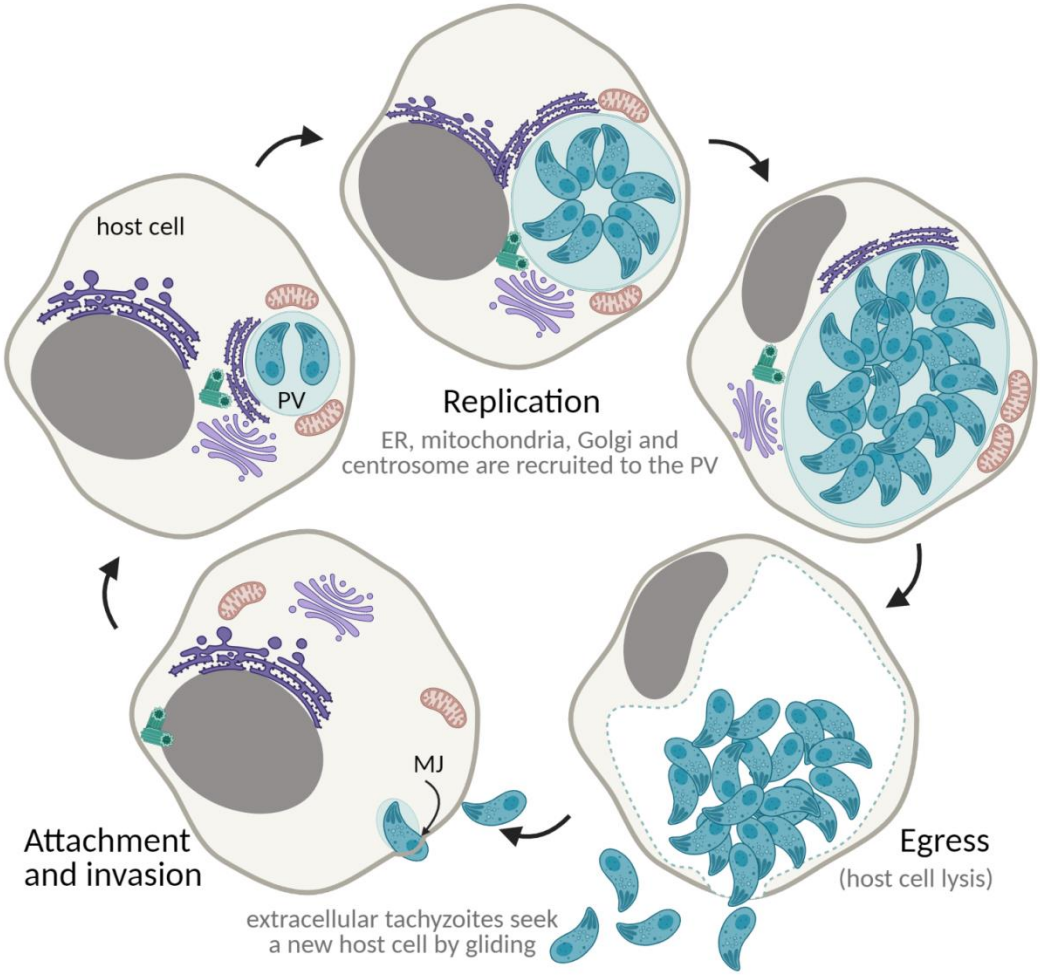

Figure 7. The lytic cycle.

ER – endoplasmic reticulum; PV – parasitophorous vacuole; MJ – moving junction. Created with BioRender.com.

1.1.7. The tissue cyst

Tachyzoites proceed to a rapid asexual expansion and dissemination to the host's tissues through the circulatory system, thanks to its ability to proliferate in virtually any nucleated cell type. Therefore, tachyzoite-bradyzoite conversion may also occur in any host tissue and can develop in any visceral organ. However, tissue cysts are most common in striated muscles (skeletal and cardiac muscle) and in nervous tissues (brain and eyes) (Dubey et al. 1998). *T. gondii* can interchange between the rapidly proliferating tachyzoite stage and the slowly replicating bradyzoite stage, which remains viable inside mature tissue cysts in a G0 cell cycle stage (Radke et al. 2003). Like tachyzoites, bradyzoites replicate by endodyogeny inside a PV, the tissue cyst (Figure 8) (Ferguson and Dubremetz 2014). The percentage of parasites actively replicating inside a tissue cyst lowers as the cyst matures, increasing in size and bradyzoite number (Ferguson and Dubremetz 2014). However, mature cyst size appears to not be solely dependent on bradyzoite number with tissue cysts presenting unexpected variability in parasite density (Watts et al. 2015). Furthermore, bradyzoites were shown to present active replication in levels not previously thought possible, as this stage was believed to remain fully quiescent (G0) inside the tissue cyst. Therefore, although the tissue cyst is a stable structure that allows the parasite to resist inside the intermediate host indefinitely, it is still an active structure with replicating parasites. This contrasts to the previous belief that bradyzoites were fully quiescent and non-replicating stages (Watts et al. 2015). Bradyzoite containing PVs (tissue cysts) present structural differences to tachyzoite containing PVs but both are intracellular structures, fully enclosed by the host cell membrane (Ferguson and Dubremetz 2014; Knoll et al. 2014). Early tissue cysts present a membrane with a very close fit and numerous invaginations with a shallow, irregular pattern presenting a ruffled appearance (Weiss and Kim 2000; Ferguson and Dubremetz 2014). The tubule-vesicular network, present in tachyzoite PVs, is absent in early tissue cysts which instead present an amorphous material in a thin layer (Ferguson and Dubremetz 2014). Mature tissue cysts present a thick wall, ranging 270-850 µm, with deep invaginations of the plasma membrane into the underlying granular material (Ferguson and Hutchison 1987; Ferguson and Dubremetz 2014). The tissue cyst wall is formed from the PV membrane and is rich in glycoproteins, binding the *Dolichos biflorus* agglutinin (DBA) and succinylated-wheat germ agglutinin lectins (Boothroyd et al. 1997). Although bradyzoite markers are detected early in immature tissue cysts, the bradyzoite specific structure is only observed three to four weeks after tissue cyst formation (Ferguson and Dubremetz 2014)

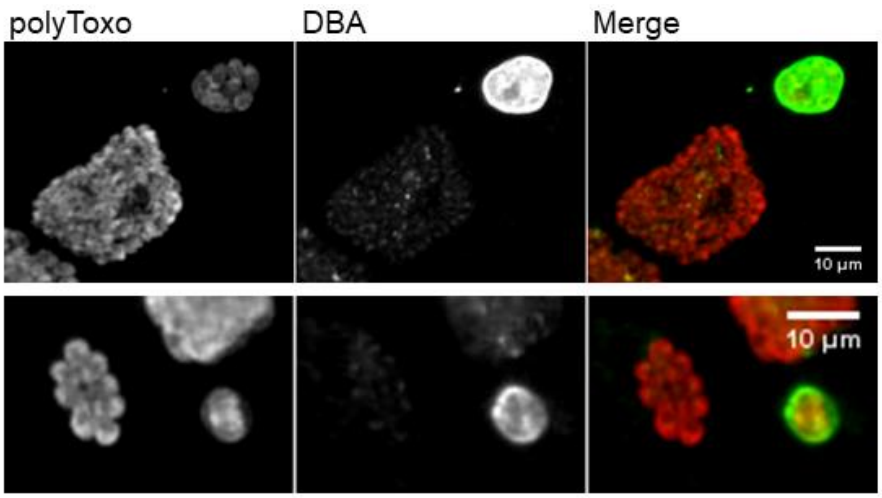

Figure 8. Tachyzoite parasitophorous vacuoles and tissue cysts.

Each panel shows tachyzoite parasitophorous vacuoles, stained only with polyclonal antisera against *T. gondii* surface proteins (polyToxo), and tissue cysts, stained with polyToxo and with *Dolichos biflorus* agglutinin (DBA) lectin, that binds to the tissue cyst wall. The tissue cysts were formed spontaneously *in vitro* culture of the *T. gondii* EGS strain invading confluent HFF. The scale bars represent 10 µm.

The transition from tachyzoite to bradyzoite is an early event, being possible to identify immature tissue cysts containing only one to two zoites (Dubey et al. 1998; Weiss and Kim 2000; Ferguson and Dubremetz 2014). Evidence indicates that the tachyzoite-bradyzoite transition occurs upon host cell invasion or immediately afterwards (Weiss and Kim 2000; Ferguson and Dubremetz 2014). Bradyzoite specific markers are detected within 24 hours of bradyzoite differentiation (Lane et al. 1996). The triggers for tachyzoite-bradyzoite interconversion are not fully understood. *In vitro* studies show that tachyzoites and bradyzoites both spontaneously convert to the other stage (Jacobs et al. 1960; Soete et al. 1993; Soete et al. 1994; Weiss et al. 1995; Weiss and Kim 2000). Tachyzoite replication rate and exposure to stress influence the rate of tachyzoite to bradyzoite conversion. The exposure of tachyzoites to exogenous stress factors may induce or enhance tachyzoite-bradyzoite conversion *in vitro*: treatment with acidic or alkaline pH, heat shock, sodium arsenic or immunity modulators (IFNγ, IL-6, nitric oxide, lipopolysaccharide) have been shown to influence tachyzoite to bradyzoite conversion (Bohne et al. 1993; Bohne et al. 1994; Soete et al. 1994; Weiss et al. 1995). Nutrient depletion can induce tissue cyst formation, namely arginine and cholesterol (Fox et al. 2004; Ihara and Nishikawa 2014). Treatment with several drugs enhanced tissue cyst formation (e.g. pyrimethamine, aphidicolin, atovaquone, myxothiazol, rotenone) (Bohne et al. 1994; Tomavo and Boothroyd 1995). Stress response signaling pathways participate in the regulation of the

cell cycle and bradyzoite differentiation. Inhibition of cAMP and cGMP dependent protein kinases, modules of conserved cyclic nucleotide signaling pathways shown to participate in stress response and differentiation in other organisms, resulted in reduced replication and induction of bradyzoite differentiation in *T. gondii* (Kirkman et al. 2001; Eaton et al. 2006). Phosphorylation of the stress response protein eukaryotic initiation factor-2 (eIF2) is increased in tachyzoites following treatment with alkaline medium or heat shock (Sullivan et al. 2004). Gene regulation through histone mediated chromatin remodeling and epigenetic signaling are also involved in tachyzoite-bradyzoite conversion (Sullivan and Hakimi 2006; Bougdour et al. 2009). Accordingly, the *T. gondii* transcriptome shows clear stage-specific mRNAs, which are altered between virulent and avirulent strains, coherently with its tissue cysts forming abilities (Radke et al. 2005). Metacaspases are a group of cysteine proteases, conserved in plants, fungi, and protozoans, involved in stress response, programmed cell death, and cell proliferation. The *T. gondii* metacaspase 2 is necessary for tissue cyst formation *in vitro* (Song et al. 2020). Transcription factors have also been implicated as key components in tachyzoite-bradyzoite conversion, namely Bradyzoite-formation deficient 1 (BFD1) and various Apicomplexa Apetala-2 (ApiAP2) transcription factors (Huang et al. 2017; Radke et al. 2018; Farhat et al. 2020; Waldman et al. 2020). Bradyzoite to tachyzoite conversion is less understood, but balance of stage-specific ApiAP2 transcription factor seems to control this process (Hong et al. 2017). Stage conversion appears to be intimately connected to cell cycle regulation, with bradyzoites presenting higher enrichment in S/M phase associated genes compared to tachyzoites that present higher enrichment in G1 phase associated genes and are more likely to be in S/M phase when bradyzoite differentiation is triggered (Radke et al. 2003; M.M. Croken et al. 2014). Furthermore, the *T. gondii* transcriptome presents a significantly cyclical profile, with several bradyzoite-specific transcripts peaking at late M phase, and blocking the cell cycle prevents tachyzoite-bradyzoite conversion (Radke et al. 2001; Behnke et al. 2010).

1.1.8. Replication and differentiation: the secret for success?

T. gondii transitions between several cellular stages during its life cycle. The ability to develop resistance structures in the form of tissue cysts in the tissues of intermediate hosts is one of the key features of the *T. gondii* life cycle. When invading a host, *T. gondii* divides inside a parasitophorous vacuole produced by the parasite. Bradyzoites divide at a slower rate inside tissue cysts, a more permanent structure that requires more control regarding parasite number.

The regulation of replication and tachyzoite-bradyzoite differentiation appear to be connected, as slower replication is associated with increased development of tissue cysts. This interconversion ability is dependent on cell cycle regulation and involves, among other events, regulation of cell proliferation and differentiation. Monopolar spindle one binder (MOB) proteins are highly conserved among eukaryotes. MOB1 proteins are kinase adaptors that regulate cytokinesis and division axis orientation in unicellular eukaryotes. In multicellular eukaryotes, MOB1 also regulates cell proliferation versus apoptosis, centrosome duplication and cell differentiation. This led us to select MOB1 as a strong candidate to be involved in the regulation of *T. gondii* replication and stage conversion.

1.2. MOB: pivotal conserved proteins in cytokinesis, cell architecture and tissue homeostasis

In the scope of this study, a review article was published*:* Delgado ILS, Carmona B, Nolasco S, Santos D, Leitão A, Soares H. MOB: Pivotal Conserved Proteins in Cytokinesis, Cell Architecture and Tissue Homeostasis. *Biology*. 2020; 9(12):413. https://doi.org/10.3390/biology9120413. Part of this manuscript was included in this section with minor revisions.

A MOB protein was first identified in 1998 by Luca and Winey (1998), following a two-hybrid screen in budding yeast *Saccharomyces cerevisiae* that detected a monopolar spindle one (Mps1) binder protein. It was not until 2005 that Lai and colleagues (Lai et al. 2005) identified the first metazoan *Mob* gene *mats* (*Mob* as tumor suppressor), in *Drosophila melanogaster*. Since then, research efforts have identified *Mob* genes in further species expanding this family in the eukaryotic lineage. *Mob* genes are found in variable numbers with fungi and fly, typically possessing three to four genes, while humans have up to seven (Maerz et al. 2009; Schmidpeter et al. 2017; Duhart and Raftery 2020).

The MOB family proteins constitute highly conserved eukaryote kinase adaptors that are often essential both for cell and organism survival. MOB proteins were first characterized as regulators of ploidy maintenance, helping to ensure proper chromosome segregation before mitotic exit and allowing the transition from mitosis to cytokinesis (Luca and Winey 1998). This family is also necessary for maintaining cell polarity and morphology during cell division (Tavares et al. 2012; Chalker and Frankel 2014). In multicellular organisms, MOBs have been mostly characterized as tumor suppressors and agents of morphogenesis, frequently by regulating germinal center kinase (GCK) II sterile 20 (STE20) and nuclear dbf2-related (NDR) kinases in the Hippo signaling pathway. Notably, the Hippo pathway interplays with various signaling pathways, like Wnt (wingless integrated), mTOR (mammalian target of rapamycin), Notch, Hedgehog, and the Striatin-interacting phosphatase and kinase (STRIPAK) complex (Shimobayashi and Hall 2014; Hwang and Pallas 2014; Bae et al. 2018). These pathways control a myriad of cellular processes and their activity is largely dependent on intercellular communication. In metazoans, the canonical Hippo signaling pathway comprises a core kinase cascade that includes SAV1/Salvador and MOB1/Mats as signal adaptors. When the Hippo pathway is activated, mammalian sterile 20 1/2 (MST1/2)/Hippo kinase together with SAV1/Salvador phosphorylate, thus activating, MOB1/Mats in a complex with the large tumor suppressor 1/2 (LATS1/2)/Warts kinase that in turn phosphorylates transcriptional co-activators,

preventing its translocation into the nucleus and avoiding the transcriptional activation of target genes (Figure 9). Since yes associated protein (YAP)/TAZ/Yorkie induce the transcription of anti-apoptotic and proliferation-associated genes, such as BIRC5, BIRC2, and MCL1, Hippo signaling activation results in tumor suppression (Dong et al. 2007; Zhang et al. 2008). Alternative interactions between adaptor proteins, GCKII STE20, and NDR kinases result in non-canonical Hippo pathway signaling. MOB adaptor proteins, GCKII STE20 kinases, and NDR kinases are highly conserved protein families from yeast to metazoans. In multicellular eukaryotes, MOB proteins have been mostly characterized in the context of canonical Hippo signaling. However, these proteins also regulate cell biology processes in these species, namely mitotic exit, centrosome duplication and chromosome segregation (Bothos et al. 2005; Shimizu et al. 2008; Hergovich et al. 2009). Significantly, several core Hippo pathway components present homologous proteins in unicellular eukaryotes, most notably the components of the core kinase module MST1/2/Hippo, LATS1/2/Warts, MOB1/Mats. In these organisms, MOB co-activators, GCKII STE20 kinases, and NDR kinases have been mainly characterized in the context of the mitotic exit and septation-initiation networks (MEN/SIN), both ensuring the correct genetic material distribution and cytokinesis (Figure 9). Interestingly, both MEN and SIN networks have a CDC14 phosphatase as an effector protein, a highly conserved protein also present in multicellular eukaryotes (Hergovich and Hemmings 2012).

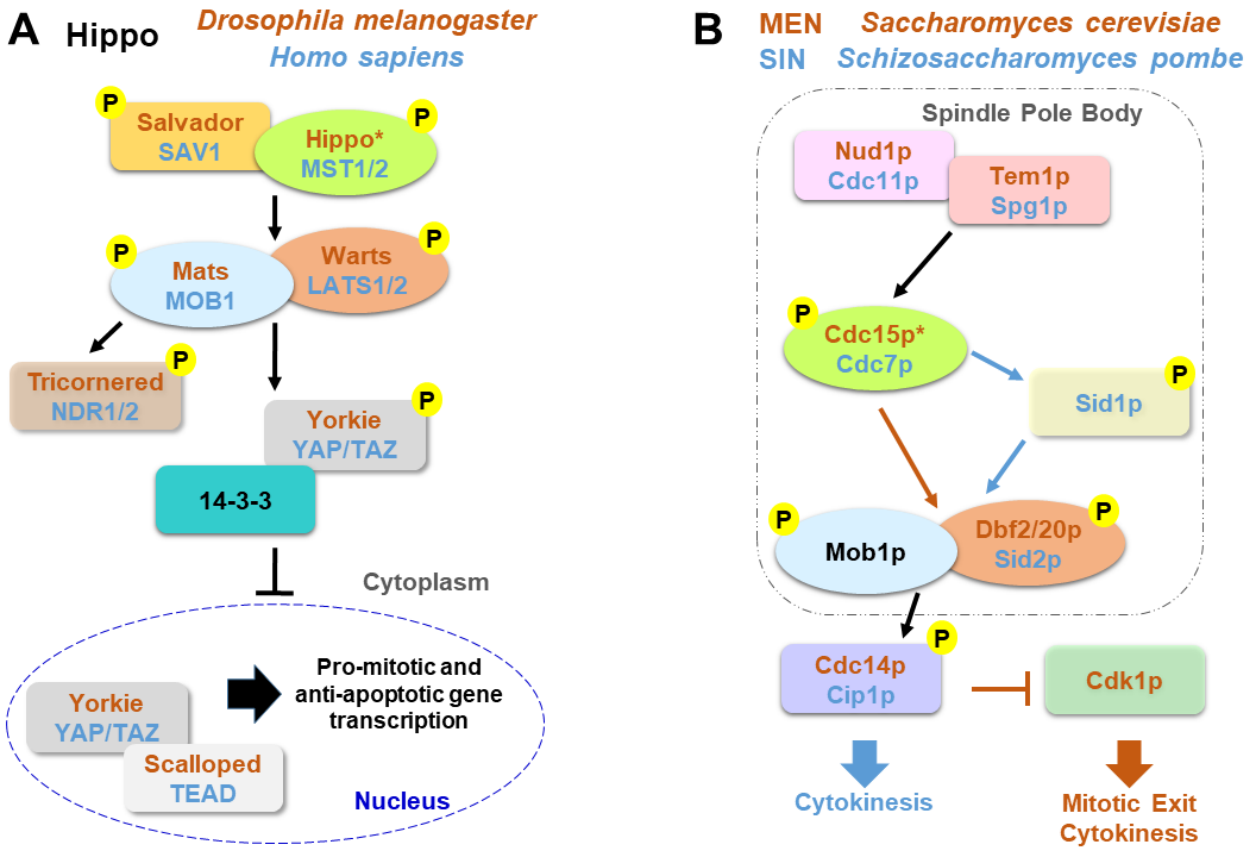

Figure 9. Comparison between MEN/SIN and Hippo pathway.

(A) Schematic representation of the Hippo pathway in *Drosophila melanogaster* (orange) and in *Homo sapiens* (blue). **(B)** Schematic representation of the Mitotic Exit Network (MEN) in *Saccharomyces cerevisiae* (orange) and Septation Initiation Network (SIN) in Schizosaccharomyces pombe (blue). In these pathways, ortholog proteins are represented with oval nodes of the same color (yellow, Salvador/SAV1/Tem1/Spg1; green, Hippo/MST1/2/Cdc15/Cdc7; blue, Mats/MOB1/Mob1; orange, Warts/LATS1/2/Dbf2). * There are some controversies in the literature regarding whether to consider Cdc15 and Hippo as orthologs. This scheme is in accordance with Hergovich (Hergovich 2017).

1.2.1. MOB proteins in multicellular eukaryotes

The MOB family proteins are currently classified into four isotypes that tend to be functionally different within each species: MOB1, MOB2, MOB3, and MOB4/Phocein. Some species, particularly more complex organisms, also present sub-isotypes that tend to be functionally similar or redundant within each species, e.g., MOB1A and MOB1B. In several publications MOB proteins have been referred as MOB3/Phocein (Bernhards and Pöggeler 2011; Dettmann et al. 2013; Hwang and Pallas 2014; Li et al. 2018; Elramli et al. 2019), however this nomenclature has been reviewed based on *Homo sapiens* designations (described by Gundogdu and Hergovich (2019)) and we will refer to these proteins using the updated designation of MOB4/Phocein.

1.2.1.1. Functions of MOB proteins

1.2.1.1.1. Tissue homeostasis: MOB as regulators of cell proliferation and apoptosis

MOB proteins are tumor suppressors playing a critical role in regulating tissue homeostasis maintenance. In *D. melanogaster*, it was shown that DmMOB1 (Mats) controls cell proliferation and apoptosis through interaction with DmLATS (Warts), and its lethal depletion phenotype is rescued by HsMOB1 showing function conservation from invertebrates to vertebrates (Lai et al. 2005; Vrabioiu and Struhl 2015). Indeed, *H. sapiens*, HsMOB1 also presents tumor suppressor activity, by phosphorylating HsLATS1, which can be triggered by HsMST1/2 phosphorylation but this is not essential (Figure 10 and Table 2) (Praskova et al. 2008; Kulaberoglu et al. 2017). HsMOB1 tumor suppressor activity involves apoptotic signaling through Hippo pathway activation (Vichalkovski et al. 2008). DmMOB1 tumor suppressor activity independent of DmMST (Hippo) phosphorylation also occurs in *D. melanogaster* (Vrabioiu and Struhl 2015). Both HsMOB1 and HsMOB2 have been implicated in tissue growth suppression in cancer development (Zhou et al. 2009; Schumacher et al. 2018; Zhang and Zhu 2018; Jiang et al. 2019). Conversely, Chen et al. (2018) showed that the cancer promoter complex HsMST4-HsMOB4/Phocein negatively regulates the tumor-suppressing complex HsMST1-HsMOB1 in pancreatic cancer. HsMOB4/Phocein and HsMST4 integrate the Striatin-interacting phosphatase and kinase (STRIPAK) complex (Gordon et al. 2011). The STRIPAK complex also includes the protein phosphatase PP2A and regulates vesicular trafficking, microtubule cytoskeleton and morphogenesis (Hwang and Pallas 2014). HsMOB3 also shows tumorigenic

properties in glioblastoma cells by suppressing HsMST1 activity (Tang et al. 2014). In *Mus musculus*, MmMOB1 functions as a tumor suppressor and tissue homeostasis factor as a member of Hippo signaling, namely by controlling apoptotic signaling in keratinocytes (Nishio et al. 2012; Nishio et al. 2016; Bae et al. 2018; Kato et al. 2019). MmMOB1 also participates in renal homeostasis, MmMOB1 mediated Hippo activation, through MmLATS1 and MmYAP phosphorylation, is associated with diminished renal fibrosis (Song et al. 2019). The Wnt (wingless integrated) pathway is also activated but seems to have an opposite association. In *Canis familiaris*, CfMOB1-CfLATS1 Hippo signaling appears to regulate photoreceptor homeostasis (Gardiner et al. 2016). In *Gallus gallus*, GgMOB2 interacts with GgSAV1 which acts as a growth suppressor through Hippo signaling (Lyu et al. 2016). *Arabidopsis thaliana* AtMOB1 regulates plant growth and development, and tissue homeostasis through interaction with AtMST, known as SIK1 (Galla et al. 2011; Cui et al. 2016; Xiong et al. 2016). In other angiosperms, *Medicago sativa*, MsMOB1 also regulates cell proliferation (Citterio et al. 2005). However, MsMob1 does not complement budding yeast MOB1 temperature sensitive growth phenotype. In the fungi *Neurospora crassa* and *Colletotrichum higginsianum*, *NcMob1* and *ChMob1* gene deletion results in overall reduced vegetative growth (Maerz et al. 2009; Schmidpeter et al. 2017). *NcMob2* gene deletion exhibited phenotypes similar to deletion of *NcMob1* but with less intensity. NcMob4 gene deletion resulted in a very mild decrease in tissue growth (Maerz et al. 2009). *ChMOB4/Phocein* gene deletion resulted in a very mild colony size reduction lacking a clear phenotype (Schmidpeter et al. 2017). Deletion of the gene coding for *Aspergillus nidulans* AnMOB4/Phocein, which integrates the STRIPAK complex, also showed tumor suppressor properties (Elramli et al. 2019). Overall, several MOB isotypes are involved in the regulation of cell proliferation and apoptosis and its activation induces inhibition or promotion of tissue growth.

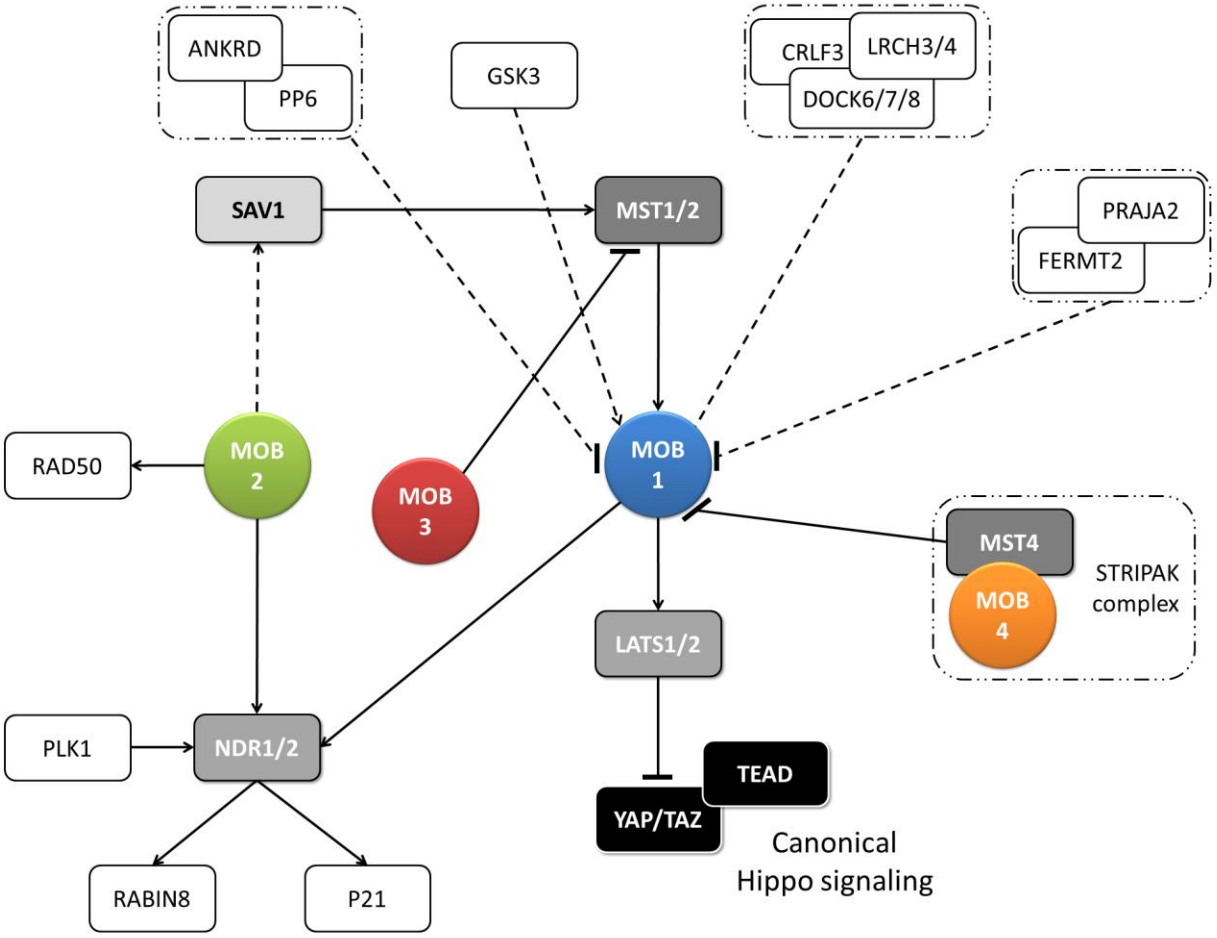

Figure 10. Metazoan MOB proteins present extensive regulation between isotypes.

The canonical Hippo pathway is activated by upstream signals resulting in MST1/2 phosphorylation (which may be mediated by SAV1) and MOB1-LATS1/2 activation, causing YAP/TAZ phosphorylation and cytoplasm retention. The lack of YAP/TAZ transcriptional signaling results in a tumor suppressing effect. However, MOB proteins present several activities beyond canonical Hippo signaling. These include non-canonical Hippo signaling through different interactions with GCKII STE20 or NDR kinases, direct MOB stimulation by upstream signals and direct stimulation by MOBs of non-Hippo proteins. This intricate network results in direct and indirect MOB to MOB regulation. PLK1 regulates mitotic spindle orientation through NDR1 phosphorylation which results in NDR1 binding shifting from MOB1 to MOB2, favoring canonical Hippo activation (Yan et al. 2015). NDR1/2 also regulate P21 and RABIN8 (Cornils et al. 2011; Chiba et al. 2013). MOB3 is a MOB1 antagonist by inhibiting MST1 (Tang et al. 2014). MOB4/Phocein-MST4, part of the STRIPAK complex, also antagonizes MOB1, by disrupting MOB1-MST1/1 binding (M. Chen et al. 2018). MOB1 interacts in a HsMOB1-PPP6R1/2/3-ANKRD28 complex which appears to inhibit MOB1 mediated Hippo activation and in a DOCK6/7/8-CRLF3-LRCH3/4 complex, in a phosphorylation dependent manner (Couzens et al. 2013; Xiong et al. 2017). Both PP6 phosphatase and DOCK6-8 promote actin cytoskeleton polarization signaling via RAC1. The FERMT2-PRAJA2 complex inhibits Hippo signaling by promoting MOB1 ubiquitin-proteasome degradation (Song et al. 2019). MOB1 is stimulated by GSK3β, a signaling hub involved in Wnt,

mTOR, and Notch signaling (Song et al. 2018). MOB2 interacts with RAD50 stimulating the DNA damage response (Gomez et al. 2015). MOB2-SAV1 interaction was detected in *G. gallus* (Lyu et al. 2016). Notably, PP6, DOCK6, FERMT2 and GSK3 are proteins involved in cell-cell junctions. Colored boxes represent Hippo pathway members while other proteins are represented by non-colored boxes. Protein complexes are identified by an interrupted box with dashes and dots lines. Arrows represent activation while dashes represent inhibition. Lack of arrow or dash indicates an uncertain effect. Full lines represent well-established interactions. Interrupted lines represent less documented interactions.

Table 2. MOB functions in multicellular organisms.

	Protein	Described functions	Functional category				Reference
			TH	M	D	CC	
Mammals and birds	HsMOB1	Tissue growth (suppressor); apoptotic signaling; mitotic exit; protein complex positioning to spindle midzone, mitotic spindle orientation; centrosome duplication and disjunction; cytokinesis	X			X	Bothos et al. 2005; Praskova et al. 2008; Vichalkovski et al. 2008; Zhou et al. 2009; Hergovich et al. 2009; Kulaberoglu et al. 2017
	HsMOB2	Tissue growth (suppressor); cortical development; mitotic spindle orientation; centrosome duplication; DNA damage response	X	X		X	Trammell et al. 2008; Maerz et al. 2009; Hergovich et al. 2009; Schulte et al. 2010; Campbell and Ganetzky 2013; Gomez et al. 2015; Yan et al. 2015; Zhang and Zhu 2018
	HsMOB3	Tissue growth (enhancer through MST1 inhibition); apoptotic signaling	X			X	Hergovich et al. 2009; Tang et al. 2014
	HsMOB4	Tissue growth (enhancer through MST1-MOB1 complex inhibition)	X				(Gordon et al. 2011; M. Chen et al. 2018)
	MmMOB1	Tissue growth (suppressor); lung and neuronal morphogenesis; stem cell differentiation and maintenance; centrosome duplication; actin cytoskeleton polarization	X	X	X	X	Nishio et al. 2012; Nishio et al. 2016; Bae et al. 2018; Kato et al. 2019; Song et al. 2019
	MmMOB2	Neuronal and cortical development; actin cytoskeleton organization.		X			Wilmeth et al. 2010; Campbell and Ganetzky 2013
	MmMOB4	Dendritic arborization in neuronal development		X			(Li et al. 2018)
	CfMOB1	Photoreceptor growth; mitosis	X			X	(Gardiner et al. 2016)
	GgMOB2	Tissue growth (suppressor); follicle development	X	X			(Lyu et al. 2016)

Insects	DmMOB1	Tissue growth (suppressor); stem cell differentiation; chromosome segregation	X		X	X	(Lai et al. 2005; Shimizu et al. 2008; Mardin et al. 2010; Vrabioiu and Struhl 2015; Neisch et al. 2017)
	DmMOB2	Wing hair, photoreceptor and neuromuscular junction morphogenesis		X			(Kohler et al. 2010; O'Neill et al. 2018; Jiang et al. 2020)
	DmMOB4	Synapse morphogenesis and microtubule organization; spindle pole assembly; axonal transport of autophagosomes		X		X	(Hergovich et al. 2005; Lin et al. 2011; Mou et al. 2012)
Plants	AtMOB1	Plant growth (enhancer); development of stem and root; sporogenesis and gametogenesis; stem cell differentiation and maintenance; apoptotic signaling; cytokinesis	X	X	X	X	(Galla et al. 2011; Cui et al. 2016; Xiong et al. 2016; Guo et al. 2020)
	MsMOB1	Tissue growth (suppressor); stem cell association	X		X		(Citterio et al. 2005; Citterio et al. 2006)
Fungi	NcMOB1	Tissue growth (enhancer); septum, aerial mycelium and fruiting body development; conidiation; ascosporogenesis; meiosis	X	X	X	X	(Maerz et al. 2009)
	NcMOB2	Tissue growth (enhancer); hypha development; conidiation	X	X	X		(Maerz et al. 2009)
	NcMOB4	Tissue growth (enhancer); fruiting body development; vegetative cell fusion	X	X			(Maerz et al. 2009; Dettmann et al. 2013)
	AnMOB4	Tissue growth (suppressor); ascosporogenesis; meiosis.	X		X	X	(Elramli et al. 2019)
	SmMOB4	Vegetative cell fusion; conidiation and ascosporogenesis; meiosis		X	X	X	(Bernhards and Pöggeler 2011)
	ChMOB1	Conidiation and septum formation	X	X	X		(Schmidpeter et al. 2017)
	ChMOB2	Conidiation and ascosporogenesis; meiosis			X	X	(Schmidpeter et al. 2017)

TH—tissue homeostasis, M—morphogenesis, D—differentiation, CC—cell cycle progression, Dm—*Drosophila melanogaster*, Hs—*Homo sapiens*, Mm—*Mus musculus*, Cf—*Canis familiaris*, Gg—*Gallus gallus*, At—*Arabidopsis thaliana*, Ms—*Medicago sativa*, Nc—*Neurospora crassa*, An—*Aspergillus nidulans*, Sm—*Sordaria macrospora*, Ch—*Colletotrichum higginsianum*.

1.2.1.1.2. Morphogenesis: a MOB function in various species and cell types

MOB proteins are also important cell polarity and tissue morphogenesis regulators (Table 2). *D. melanogaster* DmMOB2 interacts with DmNDR (Trc) and is necessary for wing hair, photoreceptor and neuromuscular junction morphogenesis (Kohler et al. 2010; O'Neill et al. 2018; Jiang et al. 2020). DmMOB4/Phocein is also necessary for synapse morphogenesis and microtubule organization (Hergovich et al. 2005). In *H. sapiens*, HsMOB2 loss of function mutations are associated with defective cortical development (Campbell and Ganetzky 2013). Interestingly, a similar phenotype is produced by mutations in cell adhesion protocadherins HsFAT4-DCHS1 which is compensated by HsYap knockdown (Cappello et al. 2013). *M. musculus* MmMOB1 controls lung morphogenesis through MmYAP/TAZ regulation and neuritogenesis independent of MmYAP (Neisch et al. 2017; Song et al. 2018). MmMOB1 mediated neuritogenesis is stimulated by MmGSK3β (glycogen synthase kinase3β) (Song et al. 2018). Notably, MmGSK3 functions as a signaling hub, integrated into Wnt, mTOR, and Notch pathways (Nagini et al. 2019). MmMOB2 is necessary for neuritogenesis and cortical development, including ciliogenesis (Wilmeth et al. 2010; Campbell and Ganetzky 2013). MmMOB2 RNAi and overexpression studies showed this protein's role in neuritogenesis is synergistic with MmNDR2 and affects the actin cytoskeleton (Wilmeth et al. 2010). Contrary to *H. sapiens*, *M. musculus* MmDCHS1 mutation phenotype could not be compensated by MmYAP knockdown (Campbell and Ganetzky 2013). MmMOB4/Phocein regulates dendritic arborization in neuronal development through STRIPAK complex signaling (Li et al. 2018). In *G. gallus*, GgSAV1-MOB2 interaction also regulates follicle development (Lyu et al. 2016). *A. thaliana*, AtMOB1 is necessary for plant structural development of stem and root (Galla et al. 2011; Cui et al. 2016; Guo et al. 2020). Also, in fungi, MOB proteins participate in morphogenesis. In *N. crassa* NcMOB1 is necessary for septum and aerial mycelium formation and conidiation with NcMob1 gene deletion resulting in increased hyphae branching despite decreased mycelium growth. NcMOB2 controls hyphae polar tip extension through regulation of the NDR kinase NcCOT1 (Maerz et al. 2009). NcMOB4/Phocein is essential for vegetative cell fusion and consequent fruiting body formation in a way unrelated to NDR signaling. NcMOB1 and NcMOB4/Phocein both participate in fruiting body morphogenesis but NcMOB1 activity occurs by interaction with NcLATS (DBF2) while NcMOB4/Phocein integrates the STRIPAK complex (Maerz et al. 2009; Dettmann et al. 2013). Moreover, NcMOB4/Phocein and SmMOB4/Phocein of the Ascomycete *Sordaria macrospora* also control vegetative cell fusion (Maerz et al. 2009; Bernhards and Pöggeler 2011). These data show that the involvement of

MOB proteins in morphogenesis is not exclusive of a specific MOB isotype, but that different MOB isotypes participate in this process (Table 2).

1.2.1.1.3. Cell cycle progression: MOBs as regulators of mitosis, cytokinesis, and centrosome biology

Several core components of the Hippo pathway have been implicated in the regulation of eukaryotic cell cycle progression, including MOB proteins (Figures 10 and 11) (Hergovich 2017). DmMOB1 null mutants present aberrant chromosome segregation during embryogenesis (Shimizu et al. 2008) while DmMOB4/Phocein depleted cells fail to properly assemble the spindle pole (Mou et al. 2012). DmMOB4/Phocein also integrates the STRIPAK complex and is necessary for DmPP2A regulated axonal transport of autophagosomes (Lin et al. 2011). DmMOB1 localizes to the cytoplasm and nucleus, but also to the centrosome (Shimizu et al. 2008). HsMOB1 is required for mitotic exit and its depletion results in prolonged telophase (Bothos et al. 2005). The same is true for its binding partner HsLATS1/2. HsMOB1 is necessary for correct positioning of the mitotic regulator chromosomal passenger complex to the spindle midzone during anaphase (Otsubo et al. 2017). Correct mitotic spindle orientation is regulated through HsNDR1 phosphorylation by HsPLK1 which results in HsNDR1 binding shifting from HsMOB1 to HsMOB2 (Yan et al. 2015). HsMOB1/HsMOB2 competitive binding to HsNDR1 was also observed in centrosome duplication (Hergovich et al. 2009). HsMOB2 binding to HsNDR seems to inhibit its activation which occurs through phosphorylation (Schulte et al. 2010). HsMOB1 has also been implicated in centrosome disjunction by interfering with HsNEK2 centrosome localization (He et al. 2005). HsMOB1 also regulates correct cell abscission and cytokinesis (Bae et al. 2019). HsMOB1 knockdown cells show increased motility immediately after telophase/cytokinesis and persist connected by long intercellular bridges (Bae et al. 2019). Also, HsMOB1 depletion results in centriole separation which supports the idea that HsMOB1 is required for centriole rejoining at the end of mitosis. Interestingly, components of the Hippo pathway, HsSAV1 and MST2 cooperate with the HsNEK2 kinase to regulate centrosome disjunction (He et al. 2005). Additionally, HsMOB1 interacts with serine/threonine phosphatases HsPP6 and an ankyrin repeat–containing protein HsANKRD, forming a HsMOB1-PPP6R1/2/3-ANKRD28 complex. Also, interactions with leucine-rich repeats and calponin homology domain–containing proteins HsLRCH, cytokine receptor–like factor 3 and dedicator of cytokinesis proteins HsDOCK forming an HsDOCK6/7/8-CRLF3-LRCH3/4 complex were described (Couzens et al. 2013; Xiong et al. 2017). Time point analysis suggests the HsPP6 complex may inhibit HsMOB1 mediated Hippo activation. HsMOB1 is mostly localized in the cytoplasm and to

a lesser extent in the cytoplasmic membrane, but it also localizes to various cell cycle associated structures, namely centrosome, kinetochores in early mitosis and spindle midzone in late mitosis (Bothos et al. 2005; Trammell et al. 2008; Hergovich et al. 2009; Otsubo et al. 2017). HsMOB2 induces G1/S cell cycle arrest in response to DNA damage, independently of hsNDR kinases (Gomez et al. 2015). Coincidently, HsMOB2 localizes to the nucleus (Trammell et al. 2008; Hergovich et al. 2009). HsMOB3, a cytoplasmic protein, prevents high cell density growth inhibition by downregulating HsMST1 mediated apoptotic signaling in glioblastoma cells (Hergovich et al. 2009; Tang et al. 2014). Similarly to human, in mouse MmMOB1 regulates centrosome duplication in keratinocytes, through the regulation of MmLATS and MmYAP (Nishio et al. 2012). MmMOB1 also interacts with MmDOCK8 in thymocytes, stimulating MmRAC1 actin cytoskeleton polarization signaling (Florindo et al. 2012). MmMOB1-MmMST1/2 mediate MmRhoA GTP charging and MmRAC1 signaling stimulation. *C. familiaris* CfMOB1 is also necessary for correct mitosis in photoreceptor cells (Gardiner et al. 2016). In plants *A. thaliana* and *M. sativa*, AtMOB1 and MsMOB1 participate in apoptotic signaling during meiotic microsporogenesis and macrosporogenesis and also regulate cytokinesis (Citterio et al. 2005; Galla et al. 2011; Guo et al. 2020). Supporting its role in cytokinesis MsMOB1 is cytoplasmic, but localizes to the cell plate during septum formation and at spindle microtubule structures related to cytokinesis (Citterio et al. 2005). AtMOB1 is present at the cytoplasm, cytoplasmic membrane, and nucleus (Galla et al. 2011; Cui et al. 2016). *A. thaliana* MST1/2/Hippo ortholog SIK1 complements *S. cerevisiae* Ste20 deletion in mitotic exit and SIK1 was shown to bind to AtMOB1 (Xiong et al. 2016). In conclusion, MOB proteins play critical roles in accurate cell division and cytokinesis and, besides other cellular localizations, tend to localize at the centrosome when this structure is present, a localization that is shared by other Hippo components (Table 2).

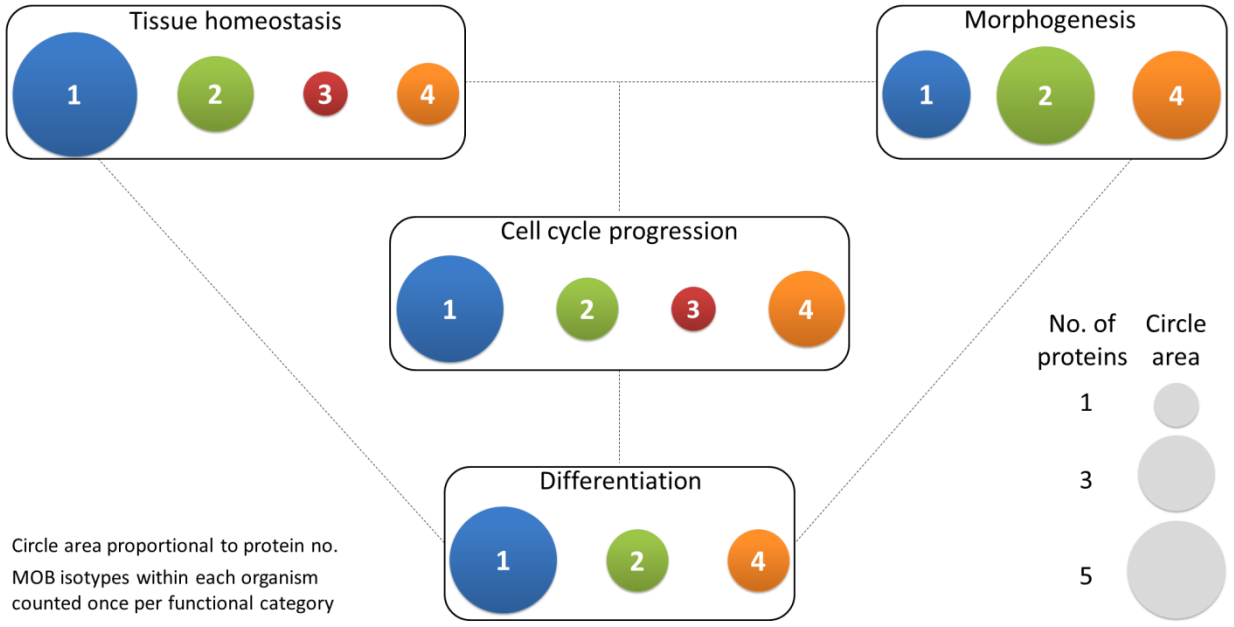

Figure 11. Different MOB isotypes present similar functions.

MOB functions were divided into 4 categories: tissue homeostasis, morphogenesis, differentiation and cell cycle progression (includes mitosis, meiosis, cytokinesis, and centrosome biology). Circle areas are proportional to the number of proteins counted in the literature related to these functions, as is illustrated in the protein count examples at the bottom right. MOB protein isotypes for each organism were counted only once per function category (variants within protein isotypes were not considered). It is obvious that there is no one MOB isotype responsible for a particular function. Various MOB isotypes present similar functions, be it in distinct species or in distinct tissues in the same species. In fungi, NcMOB1, ChMOB2, and SmMOB4/Phocein, all participate in conidiation, ascosporogenesis, and meiosis (Maerz et al. 2009; Bernhards and Pöggeler 2011; Schmidpeter et al. 2017). In *M. musculus*, MmMOB1, MmMOB2, and MmMOB4/Phocein are necessary for neuronal development while MmMOB1 also promotes lung morphogenesis (Wilmeth et al. 2010; Florindo et al. 2012; Neisch et al. 2017; Li et al. 2018; Song et al. 2018). The data also evidence a higher abundance of studies on MOB1 proteins, which are the more represented in each category, except morphogenesis. Colors representing MOB isotypes: 1—blue, 2—green, 3—red, 4—orange.

1.2.1.1.4. Differentiation and stem cell maintenance: MOB in a crossroad between morphogenesis, tissue homeostasis, and cell cycle regulation

In *Drosophila* DmMOB1 is essential for embryonic development (Shimizu et al. 2008). This becomes evident after both zygotic and maternal DmMOB1 depletion that results in non-viable embryos indicating a probable role for DmMOB1 in stem cell differentiation. In mouse, MmMOB1 is necessary for embryonic stem cell differentiation into the three germ layers, an activity that is dependent on YAP regulation (Mardin et al. 2010). MmMOB1 is also involved in

bronchioalveolar cell differentiation and alveolar stem cell maintenance through MmYAP/TAZ regulation (Neisch et al. 2017). Surprisingly, this last study did not find evidence that MmMST or MmLATS kinases were also involved in MmYAP/TAZ regulation. The plant AtMOB1 is necessary for sexual development, namely during sporogenesis and gametogenesis (Galla et al. 2011; Cui et al. 2016). AtMOB1 depleted cells present reduced meristem length and cell number, suggesting a role not only in cell differentiation but also in stem cell maintenance, as documented in mouse (Galla et al. 2011; Cui et al. 2016; Guo et al. 2020). AtMOB1 depleted cells also present a substantially reduced seed output (Galla et al. 2011). The protein localizes to meiocytes, supporting its participation in meiosis. Interestingly, in *M. sativa* MsMOB1 localizes to the meristem in a cell cycle dependent manner (Citterio et al. 2005). Fungi MOB proteins are also involved in the differentiation of cells for sexual development and the meiotic process. NcMOB1, ChMOB2 and SmMOB4/Phocein are involved in conidiation, ascosporogenesis, and meiosis (Maerz et al. 2009; Bernhards and Pöggeler 2011; Schmidpeter et al. 2017). ChMOB1 is also necessary for conidiation and septation following conidiation (Schmidpeter et al. 2017). NcMOB2 exhibited similar properties as NcMOB1 in conidiation, but not in ascosporogenesis and meiosis (Maerz et al. 2009). ChMOB2 interacts with ChNDR, known as Cbk1 (Schmidpeter et al. 2017). *A. nidulans* AnMOB4/Phocein is also necessary for ascospore production through meiosis (Elramli et al. 2019).

1.2.1.2. Regulation of MOB proteins

1.2.1.2.1. Post-Translation Modifications of MOBs

MOB1 can be regulated by different phosphorylation events coordinated by diverse kinases. In 2008, it was described for the first time that the HsMST1/2 kinases catalyzed the phosphorylation of HsMOB1 Thr12 and Thr35 amino acid residues and that these post-translation modifications (PTMs) slowed down the cell cycle progression (Vrabioiu and Struhl 2015). Later, a knowledgebase dedicated to mammalian PTMs reported the existence of additional phosphorylation modifications in HsMOB1 amino acid residues, namely in Tyr26, Ser23, and Ser38 (Hornbeck et al. 2015). Recently, it was described that HsFAK (focal adhesion kinase) regulates HsYAP by phosphorylating the HsMOB1 Tyr26 residue. This modification results in the dissociation of the functional HsMOB1/LATS complex, thus preventing Hippo-dependent inhibition of HsYAP (Feng et al. 2019). It is still unclear whether this regulation could also affect the HsMOB1/NDR complex (Gundogdu and Hergovich 2019). On the other hand, the HsMOB1 Ser23 and Ser38 phosphorylation function remains

unresolved. However, the HsMOB1 Ser23 represents a possible target site for ataxia–telangiectasia-mutated (ATM) serine/threonine kinase (Wong et al. 2007), suggesting a possible link between HsMOB1 and the DNA damage response (DDR). In fact, HsMOB1 and HsMOB2 were detected in RNAi screens to identify modulators of genome integrity (Paulsen et al. 2009; O'Donnell et al. 2010). HsMOB2 was also identified as a suppressor of homologous recombination in a genome-wide RNAi-based screen and was shown to interact with HsRAD50, resulting in recruitment of a HsRAD50 DNA damage sensor complex to damaged chromatin (Adamson et al. 2012; Gomez et al. 2015). Until now, there is no information concerning HsMOB2 phosphorylation. However, HsMOB2 contains several putative ATM phosphorylation sites, which may be related to the DDR function (Wong et al. 2007). Additionally, MmMOB1 Ser146 phosphorylation by the MmGSK3 kinase was described in the context of neurite outgrowth downstream of the PTEN-GSK3β axis, controlling neurite outgrowth after spinal cord injury (Song et al. 2018). Similar to HsMOB1, HsMOB3A, HsMOB3B, and HsMOB3C are modified by several phosphorylation events in distinct amino acid residues: Thr15, Thr26, and Ser38 from HsMOB3A; Thr25 and Thr77 from HsMOB3B; Thr14, Thr25, and Ser37 from HsMOB3C (Hornbeck et al. 2015). Although the role of these modifications is unclear, the sequence motifs surrounding Thr15 and Ser38 of HsMOB3A are quite similar to Thr12 and Thr35 of HsMOB1 (Gundogdu and Hergovich 2019), raising the hypothesis that HsMOB3A is phosphorylated on these residues by HsMST1/2 similarly to what has been described for HsMOB1 (Praskova et al. 2008). The Ser37 residue of HsMOB3C may represent an ATM targeting site (Wong et al. 2007). The phosphorylation of HsMOB4/Phocein, without any associated regulatory role, has also been observed at Ser147 and Tyr141 residues (Hornbeck et al. 2015). Comparable to the phosphorylation of Ser23 of HsMOB1, of Ser37 of HsMOB3C and putative phosphorylation sites of HsMOB2, the Ser147 phosphorylation of HsMOB4/Phocein is probably performed by the DDR-linked ATM kinase (Wong et al. 2007), and will be required for the DNA damage signaling. No other post-translation modifications were identified in MOB proteins, except that HsMOB2 is ubiquitylated, with ubiquitin linked through at Lys23, Lys32, and Lys131 residues (Wagner et al. 2012; Akimov et al. 2018). The function of these unique PTMs in HsMOB2 are unknown since the fate of a ubiquitylated protein is largely determined by the type of ubiquitin modification with which it is decorated (Deol et al. 2019). In human cells, the focal adhesion molecule HsFERMT2 drives Hippo signaling inhibition by interacting with HsMOB1 and the E3 ligase HsPraja2 and promoting HsMOB1 ubiquitin-proteasome degradation (Song et al. 2018).

1.2.1.2.2. Transcriptional and post-transcriptional regulation of MOBs

Data on transcriptional regulation of *Mob* genes is scarce, but alteration of DNA methylation patterns has been proposed as a possible mechanism to affect regulation of the levels of MOB proteins and is often associated to cancer. Studies of DNA methylation patterns revealed that lysine demethylase 2B (KDM2B) directly bound to the promoter region of *HsMob1* gene, inhibited and promoted pancreatic ductal adenocarcinoma progression (Quan et al. 2020). Furthermore, in a study concerning methylation in human breast cancer in response to resveratrol, HsMOB1 promotor presented methylation changes in triple-negative breast cancer cells (Medina-Aguilar et al. 2016). HsMOB3B transcripts were not downregulated in public data sets, it was also observed that the HsMOB3B promoter region is hypermethylated in a significant number of prostate cancer samples (Haldrup et al. 2013). In the last years, non-coding RNAs (ncRNAs) have emerged as critical molecules for the post-transcriptional regulation of gene expression. For example, miRNAs have been considered key regulators of target mRNAs by driving its degradation or translational repression. In the case of the Hippo pathway, multiple miRNAs have been described to target members of this via in cancer (Astamal et al. 2020; Liu et al. 2020). In this context, only three miRNAs were described to target *HsMob1* genes: (i) miR-664a-3p, promotes cell proliferation and invasion in gastric cancer (L. Wang et al. 2019); (ii) miR-135b, promotes migration and invasiveness in lung cancer (Lin et al. 2013); and (iii) miR-181c, promotes tumor progression pancreatic cancer (Chen et al. 2015). Beyond cancer, exosomal miRNAs are important for intercellular communications and functional regulation in recipient cells, being important for several other diseases. Exosomes from human umbilical cord mesenchymal stem cells (HUCMSCs) are effective in inhibiting bone marrow mesenchymal stem cell (BMSC) apoptosis and preventing rat disuse osteoporosis (DOP) by the miR1263/RnMOB1/Hippo signaling pathway (Yang et al. 2020). These few examples on the transcriptional and post-transcriptional regulation of MOB1/Hippo signaling strengthen the need to further understand the molecular mechanisms that regulate/deregulate this pathway. Certainly, it will bring new insights into how this pathway is regulated allowing to define new diagnostic strategies and open new avenues for therapies in, e.g., cancer and developmental diseases.

1.2.2. The MOB proteins in unicellular organisms: the roots of multicellularity?

MOB proteins have been studied in metazoans for more than one decade now, which consolidated their role as signal adaptors that can interact with different kinase families playing critical roles in the Hippo signaling pathway and Hippo-like signaling pathway (Duhart and Raftery 2020). Most studies were carried out in multicellular organisms, strongly suggesting that the Hippo pathway, in crosstalk with other signaling pathways, presents a conserved role throughout the bilaterian animals, thus being a probable hallmark of multicellularity. To trace the evolutionary roots of the Hippo signaling pathway, researchers focused their attention on the presence of genomic sequences coding for the main effector of the pathway, the YAP/Yorkie (Yki). Genome wide analysis and comparative genome approaches associated with heterologous gene expression studies clearly showed that orthologs of several components of the Hippo pathway, including YAP/Yki, were present in cnidarians (e.g., sea-anemone *Nematostella vectensis*), placozoans (e.g., *Trichoplax adhaerens*), and sponges, that are non-bilaterian animals (Hilman and Gat 2011; Zhu et al. 2013). Similar studies identified YAP/Yki homologs in two holozoan protists that are assumed to be the closest unicellular relatives of metazoans, namely the filastereans *Capsaspora owczarzaki* and the choanoflagellate *Monosiga brevicollis* (Sebé-Pedrós et al. 2012). Noteworthy, the functional analysis of *C. owczarzaki* Hippo components showed that they were able to regulate tissue growth in *Drosophila* by activating DmYki. Based on these data, the authors proposed that the Hippo pathway originated in unicellular organisms within the holozoa, before the divergence of filastereans, choanoflagellates, and metazoans (Sebé-Pedrós et al. 2012). Later, Ikmi et al. (2014), also using heterologous gene expression assays, showed that YAP/Yki proteins from *M. brevicollis*, *A. queenslandica*, *T. adhaerens*, *N. vectensis*, and their non-phosphorylatable forms (YAP activity is regulated through phosphorylation by LATS1/2/Warts kinases) were able to regulate growth in *Drosophila*, and to be regulated by phosphorylation, similarly to what is observed for HsYAP/DmYki.

Currently, most of the core components of the Hippo pathway (e.g., MOB1/Mats, MST1/2/Hippo, and LATS1/2/Warts) have been identified in the genome of animal lineages that diverged before the bilaterians and seem to have similar functions. This suggest that MOB1/Mats, MST1/2/Hippo, and LATS1/2/Warts are evolutionarily more conserved than their upstream regulators (i.e., FAT/Fat, DCHS/Dachsous, CBR/Crumbs) and downstream partners in the via (YAP/TAZ/Yki and transcriptional enhanced associate domain (TEAD)/Scalopped (Sd)) (Zhu et al. 2013). However, there are still some discrepancies between different studies, for example YAP/Yki was identified in *C. owczarzaki*, but bona fide YAP/Yki orthologue is

apparently absent from ctenophore genomes (Coste et al. 2016). Nevertheless, atypical sequences may be present in the genome of these organisms. Only TAZ proteins, that are YAP paralogs, were not found in non-vertebrates and seem to have appeared late in evolution. Recently, it was suggested that YAP and TAZ seem to share the same evolutionary origin since TAZ was originated from YAP/Yki during the whole genome duplication in fish, which may explain their redundant roles in the mammalian Hippo pathway (Chen et al. 2020). Although YAP/Yki exhibit a high degree of coevolution with MOB1/Mats (Hilman and Gat 2011), this last protein is conserved throughout the eukaryotic lineage, whereas SAV1/Salvador, another adaptor of the core pathway, is only present in choanoflagellates and metazoa (Sebé-Pedrós et al. 2012). By analyzing the evolutionary history of the Hippo pathway in a variety of unicellular organisms like the ciliate *Tetrahymena thermophila*, the centric diatom *Thalassiosira pseudonana*, the algae *Chlamydomonas reinhardtii*, the flagellated protozoan parasite *Trichomonas vaginalis*, and the excavate *Naegleria gruberi*, Chen et al. (2020) concluded that MOB1/Mats was the earliest member of the Hippo pathway to be identified in these unicellular species. According to this study, the MST1/2/Hippo kinase was the next member of this via to emerge and was identified in the Amoebozoa (e.g., *Acanthamoeba castellanii*), Dictyostelia (e.g., *Dictyostelium discoideum*), and Apusozoa (e.g., *Thecamonas trahens*). The LATS1/2/Warts kinase was first identified in the cellular slime mold *Fonticula alba* and in *S. cerevisiae*. The Hippo/Warts/Mats or MST1/2/LATS1/2/MOB1 core kinase complex was revealed in the chytrid fungus *Spizellomyces punctatus*, whereas the Yki/Sd or YAP/TEAD transcriptional complex was found in the unicellular choanozoan *Corallochytrium limacisporum*, an organism belonging to the supergroup Opisthokonta and assumed to be important to understand the evolutionary origin of animals and fungi. Finally, a complete Hippo pathway was attained in *C. owczarzaki* (Chen et al. 2020) which agrees with the data of Sebé-Pedrós et al. (2012). The ancestor components of the Hippo pathway, (i.e., MOB1/Mats, MST1/2/Hippo, and LATS1/2/Warts) from *T. thermophila*, *A. castellanii*, and *F. alba* not only share key domains and regulatory amino acid residues with *C. owczarzaki*, *Drosophila*, and human orthologs but also present conserved functions in human cells as revealed by heterologous gene expression assays (Chen et al. 2020).

The presence of a complete Hippo pathway in a unicellular organism is now undoubtedly accepted but its function is still uncertain. In metazoans, Hippo signaling plays critical roles during development and is in crosstalk with other signaling cascades, for example Notch, Hedgehog, and Wnt signaling, all absent in unicellular organisms. Sebé-Pedrós et al. (2012) proposed that the Hippo pathway in unicellular organisms may be involved in the coordination of

cell proliferation in response to cell density or cell polarity. This assumption was based on the fact that the metazoan apical proteins NF2/Merlin (neurofibromin 2, recognized as a critical mediator of contact inhibition of proliferation and regulator of Hippo pathway), KIBRA/Kibra (kidney and brain protein, functions as a scaffold protein in various cell processes, such as cell polarity, cell migration, and membrane trafficking (Elbediwy and Thompson 2018), aPKC (atypical protein kinase C, plays a critical role in the regulation of apical-basal polarity in epithelial cells and asymmetrically dividing cells (Hong 2018)) and Lgl (Lethal-2-giant larvae, makes part of the Scribble cell polarity module involved in cell polarity, control of tissue growth, differentiation and directed cell migration (Stephens et al. 2018)) are encoded in the *C. owczarzaki* genome (Sebé-Pedrós et al. 2012). Moreover, recent studies in ciliates showed that some Hippo proteins link accurate cell division and cytokinesis to morphology (Chalker and Frankel 2014). In unicellular organisms, the maintenance of morphology likely relies more on self-organization than in extrinsic/intrinsic cues as it occurs in metazoa, with the Hippo proteins having a crucial role in the perpetuation of cell pattern and organization. Thus, Hippo signaling research in unicellular organisms may reveal the ancestral regulatory routes of cell division and cell number control in metazoans

Probably, the establishment of a tight regulation control may have contributed to the establishment of multicellularity. Studies in unicellular organisms will allow for the definition of core and pivotal conserved modules of these signaling pathways. Consequently, in the next sections, we will focus our attention on the role of MOB proteins in two groups of unicellular organisms where the functional role of this protein has been largely studied, namely the yeast and members of the alveolate clade.

1.2.2.1. MOB proteins in yeast: from cell division to signaling pathways

The budding yeast *S. cerevisiae* divides asymmetrically originating two daughter cells that differ in cell size and specific inheritance of molecules (Juanes and Piatti 2016). This asymmetrical division requires cell polarization, and many polarity factors are recruited to the site where cell division will take place, i.e., the bud neck. Interestingly, the fission yeast *Schizosaccharomyces pombe* that present a rod-shape cell grows by polarized tip extension and divides symmetrically by medial fission (Piel and Tran 2009). Both yeasts do not contain centrioles or basal bodies, but they possess a structure designated spindle pole body. This structure is a MTOC that can organize the nuclear microtubules required for nuclear positioning, and the cytoplasmic microtubules that are involved in chromosome segregation during cell division (Seybold and Schiebel 2013). Spindle pole bodies are proteinaceous, multi-layered

structures that duplicate only once per cell cycle. In budding yeast *S. cerevisiae*, this structure is permanently embedded in the nuclear envelope whereas in fission yeast it is inserted into the nuclear envelope before mitosis (Seybold and Schiebel 2013).

In *S. cerevisiae*, the essential MOB protein (ScMob1p) is an interactor of the ScMps1p kinase required for the spindle pole body duplication and control of the mitotic checkpoint (Luca and Winey 1998). Conditional alleles of ScMob1p showed that the protein was necessary for successful mitosis end and maintenance of ploidy. Also, genetic and biochemical studies showed interactions between ScMob1p and three genes involved in mitosis completion, namely the GTP exchange factor ScLte1p that encodes a daughter specific protein, and the kinases ScCdc5p, ScCdc15p, ScDbf2p and ScDbf20 (counterparts of mammalian NDR/LATS kinases) (Luca and Winey 1998; Komarnitsky et al. 1998). In yeast, these proteins are involved in the regulation of cell cycle transition from mitosis to G1 that implies the degradation of the mitotic cyclins and the inactivation of cyclin-dependent kinase. The major signaling via that regulates these events is the MEN which plays important role in the coordination of the spindle orientation with mitotic exit. The final outcome of MEN is the onset of cytokinesis through the inactivation of the mitotic cyclin ScCdk1p (McCollum and Gould 2001; Hotz and Barral 2014). Indeed, the MEN is a critical component of the checkpoint that controls the correct spindle position in anaphase (Meitinger et al. 2012). The establishment of ScMob1p as an interactor of the MEN kinases and the phenotype of conditional ScMob1p mutants of late mitotic arrest, positioned this protein as a component of the MEN (Luca et al. 2001). In fact, at late mitosis, ScMob1p localizes to spindle pole bodies and the bud neck where ScDbf2p kinase is also detected which is consistent with their role in cytokinesis (Frenz et al. 2000). Mah et al. (2001) showed that ScCdc15p kinase promotes the exit from mitosis by directly activating the ScDbf2p kinase in a ScMob1p dependent manner. In turn, the activation of the ScCdc15p kinase is dependent on the initial activation of the GTPase ScTem1p that occurs at the spindle poles starting the MEN signaling (Luca and Winey 1998; Lee et al. 2001; Hergovich 2011). Interestingly, the MEN proteins that are required for ScDbf2 kinase activity are also necessary for actin ring formation at the bud neck (Lee et al. 2001). Finally, the phosphorylation of the ScCdc14p phosphatase by the complex ScDbf2p-Mob1p complex promotes its transport from the nucleolus to the cytoplasm thereby causing a dephosphorylation wave through which the ScCyclin B-Cdk1p complex is inactivated triggering the mitosis exit (Mohl et al. 2009).

In the fission yeast *S. pombe* the SIN signaling cascade is equivalent to MEN and is essential to regulate the time and place of cytokinesis in connection with cell cycle progression, but is not part of the checkpoint that monitors spindle position (Meitinger et al. 2012; Simanis

2015). SIN via triggers the actomyosin ring constriction and septum formation after chromosome segregation (McCollum and Gould 2001; Bardin and Amon 2001). Like in *S. cerevisiae*, the *S. pombe Spmob1* gene is essential and the protein is located on both spindle pole bodies throughout mitosis. Later in mitosis SpMob1p localizes at the medial ring and when the ring starts to constrict it borders the septum (Salimova et al. 2000). This localization and the phenotypes of the spores lacking SpMob1p, which are not viable elongated multinucleated cells, are typical of a role in septation (Salimova et al. 2000). Also, the SpSid2p kinase (the counterpart of *S. cerevisiae* ScDbf2p and ScDbf20p kinases) localizes at the spindle pole body at all stages of the cell cycle and transiently at the cell division site where medial ring constricts and septation occurs (Sparks et al. 1999). SpSid2p kinase activation and localization are dependent on SpMob1p, with the SpSid2p-Mob1p kinase complex being a key element of this via and determining the time and local of cell division (septation) (Hou et al. 2000; Hou et al. 2004).

The SIN signaling cascade (Figure 9) is similar to the MEN in *S. cerevisiae* and the Hippo signaling pathway in mammalian cells (Hergovich 2017). Indeed, all these signaling pathways possess a conserved core of NDR-family kinases composed of ScDbf2p in *S. cerevisiae*, LATS1/2 in mammals, and SpSid2p in *S. pombe* (Simanis 2015). However, the SIN pathway contains an additional kinase module composed of a p21-activated kinase (PAK)/GCK family protein kinase, SpSid1p and its activator SpCdc14p, that act downstream of the STE20 family kinase SpCdc7p (the fission yeast counterpart of ScCdc15p) which interacts with SpSpg1p (ScTem1p in *S. cerevisiae*) and upstream of SpSid2p-Mob1p kinase complex regulating the onset of cytokinesis (Guertin et al. 2000). This module may be involved in the integration of signals from other pathways with those of SpCdc7p and SpSpg1 GTPase to activate the SpSid2p-Mob1p kinase complex (Simanis 2015).

Notably, most MEN and SIN components localize at the spindle pole body (Jaspersen and Winey 2004). In during mitosis, some of the components of SIN signaling associate asymmetrically with the duplicated spindle pole bodies being SIN hyperactivated on the “new” spindle pole body (Schmidt et al. 1997; Sohrmann et al. 1998; Grallert et al. 2004). This polarized localization seems to be important for SIN regulation and to shut off the signal cascade after cytokinesis completion (García-Cortés and McCollum 2009; Johnson et al. 2012). Contrary to SIN, MEN is active on the ‘‘old’’ spindle pole body (Pereira et al. 2001), still, its activity is also asymmetric in both spindle bodies. The MEN signaling asymmetry seems to be established through microtubule-bud cortex interactions (Monje-Casas and Amon 2009).

Interestingly, the SIN signaling pathway is not exclusive of the unicellular *S. pombe* but most of its components, e.g., SpMob1p and the SpSid1p and SpSid2p kinases, are encoded by genes present in the genomes of syncytial ascomycete fungi *N. crassa* and *A. nidulans* (Galagan et al. 2003; Galagan et al. 2005). However, in these fungi that possess multinuclear hyphal, SIN components localization and how this via is regulated significantly differs from that of yeast (Heilig et al. 2013). This clearly shows that these conserved signaling networks have evolved to cope with cell morphology diversity.

A second member of the MOB family is present in both yeast genomes, the nonessential *mob2* gene. In *S. cerevisiae* ScMob1p presents a 43% sequence similarity at the amino acid level and 33% identity with ScMob2p (Luca and Winey 1998). ScMob2p regulates polarized cell growth through its interaction with the other members of the NDR/LATS kinase family, namely ScCbk1p in budding yeast (Colman-Lerner et al. 2001) and SpOrb6p kinase in fission yeast (Hou et al. 2004). In fact, in *S. cerevisiae* both ScCbk1p and ScMob2p localize, at late mitosis, to the bud neck, exactly when the transcription factor ScAce2p starts to accumulate in the daughter nucleus. In the nucleus, this factor activates daughter-specific genes and genes involved in mother/daughter separation after cytokinesis (Colman-Lerner et al. 2001). After mitotic exit ScMob2p–Cbk1p are required to avoid the daughter nuclear export of ScAce2p. Consequently, they participate in the coordination of ScAce2p-dependent transcription with MEN activation, establishing a connection between cell morphology and cell cycle transitions with cell fate determination and development (Weiss et al. 2002). ScMob2p in complex with ScCbk1p are indeed core components of the regulation of Ace2 and morphogenesis (RAM) network that besides controlling polarized growth also regulates cell separation, mating, maintenance of cell wall integrity, and stress signaling (Bidlingmaier et al. 2001; Weiss et al. 2002; Kuravi et al. 2011; Saputo et al. 2012). This signaling pathway is conserved among eukaryotes from yeasts to humans, including the pathogenic fungal species (e.g., *Candida albicans*, *Candida glabrata*, *Cryptococcus neoformans*, *Aspergillus fumigatus*, and *Pneumocystis* spp.), where it also plays an important role in the pathogenesis of these organisms (Saputo et al. 2012).

1.2.2.2. MOB proteins in Protozoa: a conserved family

Mob genes were identified in protozoan parasites such as the kinetoplastid *Trypanosoma brucei*, a member of the Euglenozoa phylum, which expresses two closely related MOB1 proteins, TbMOB1A and TbMOB1B (92.4% identity). Hammarton et al. (2005) showed that TbMOB1 exhibits a punctate cytoplasmic localization in the bloodstream form and is

required for cytokinesis but not for mitosis in the bloodstream and procyclic forms. This research also demonstrated that TbMOB1A interacts with the *T. brucei* NDR kinase TbPK50, a protein with high homology to the *T. gondii* NDR kinases. More recently, MOB proteins were also detected and are conserved in other kinetoplastids, i.e., *Trypanosoma rangeli*, *Trypanosoma cruzi*, and *Leishmania major* (de Oliveira et al. 2006; Prestes et al. 2019) and in the Fornicata *Giardia* (Ankarklev et al. 2010; Markova et al. 2016; Emery-Corbin et al. 2020). Conserved *Mob1* genes have also been identified in *Trichomonas vaginalis* and *Entamoeba histolytica*, protozoans belonging to the phyla Parabasalia and Amoebozoa, respectively (Grewal and Lohia 2015; Wang et al. 2018). An analysis of the genome of the protozoan and obligate intracellular plant parasite *Plasmodiophora brassicae* also identified a conserved *PbMob1* gene (Bulman et al. 2006). These data clearly indicate that MOB encoding genes and other members of the Hippo signaling pathway are generally present in protozoa parasites.

1.2.2.3. MOB proteins in the Alveolata: from cytokinesis to morphology

Alveolata is a morphologically and ecologically varied clade of organisms that include the Ciliates, Dinoflagellates, and Apicomplexa. These organisms are characterized by the presence of cortical alveoli (membrane-bound sacs underlying the cell membrane) that gives the name to the clade (Cavalier-Smith 1991). The Alveolata have extraordinarily large and complex cells that can reach millimeters in length. Dinoflagelates diverged from apicomplexans and both reside within a membranous sac (the PV for apicomplexans) but while dinoflagelates harbor a photosynthetic plastid, apicomplexans present an apicoplast which is non-photosynthetic (McFadden and Yeh 2017).

1.2.2.3.1. MOB in Ciliata

Ciliates, that are characterized by the presence of cilia and the separation of the somatic lineage (vegetative macronucleus) from the germ lineage (micronucleus only active during sexual reproduction), demonstrate a tremendous morphological diversity (Wloga and Frankel 2012). For example, the ciliate *Tetrahymena* is a complex permanently polarized unicellular organism. This ciliate displays an elaborated cortex characterized by the specific pattern organization of thousands of basal bodies, most harboring motile cilia, and high diversity of microtubule structures (Wloga and Frankel 2012).The basal bodies are organized in longitudinal rows that extend from the anterior to the posterior region of the cell. This organization is broken in specific regions by the occurrence of complex structures like the oral apparatus and

cytoprocts that create specific cell territories. Therefore, *Tetrahymena* cells present a permanent anteroposterior axis and left-right asymmetry and this organism is an excellent biological model to study development and morphogenetic mechanisms. The complex ciliate cortical organization of *Tetrahymena* cells is perpetuated during the symmetrical division of the ciliate cell. During this event, the continuity of longitudinal rows of basal bodies is interrupted, and a fission furrow develops at the equatorial region of the cell. The cell grows throughout the antero-posterior axis by the addition of new basal bodies to the preexisting longitudinal rows (Iftode et al. 1989; Frankel 1999; Wloga and Frankel 2012).

Interestingly, in the ciliate *Tetrahymena* vegetative cells, TtMob1 accumulates in the basal bodies of the posterior pole creating a gradient through the antero-posterior axis of the cell. When cells divide TtMob1 is recruited to the basal bodies that are localized at the cell midzone, just above the region where the cleavage furrow will be established. Thus, TtMob1 localizes at the new posterior pole of the anterior daughter cell. The localization of TtMob1 at basal bodies is mediated by TtSas4 that promotes scaffolds for TtMob1 localization to the cell cortex (Ruehle et al. 2020). The *Tetrahymena* TtSas4 is required, not only for basal body assembly and maintenance but integrates these events with the surrounding environment linking the perpetuation of cortical organization to cell division (Ruehle et al. 2020). The depletion of TtMob1 in *Tetrahymena* causes the abnormal establishment of the cell division plane and cytokinesis arrest. In these cells, as far as the division continues, TtMob1 progressively accumulates with TtCdaI protein at the region where the furrow will be established and the future posterior pole of the anterior daughter cell develops (Florindo et al. 2012; Jiang et al. 2017). Notably, the TtCdaI protein is absent in non-dividing cells and starts to localize at the ciliary rows of the anterior half of the cell when division initiates. Also, TtCdaI mutants phenocopy the depletion of TtMob1 (Frankel 2008; Jiang et al. 2017). Moreover, the posterior boundary of the TtCdaI stained region is affected by the TtElo1 protein suggesting that the size of this region is regulated by these two proteins (Jiang et al. 2017; Jiang et al. 2019). In fact, loss-of-function of *TtElo1* gene moves the division plane to the posterior pole, whereas the depletion of TtCdaI displaces it to the anterior pole of the cell (Jiang et al. 2019). Resembling the TtMob1 localization, the TtElo1 protein localizes at the posterior basal bodies in non-dividing cells and is recruited to the midline when division starts (Florindo et al. 2012; Jiang et al. 2019). The TtCdaI and TtElo1 proteins are orthologues of the human MST1/2 and NDR/LATS kinases, respectively, showing that *Tetrahymena* possesses the core kinase module of the human Hippo signaling, which is coincident with the recent data obtained by Chen et al. (2020). The fact that the *Tetrahymena* genome seems to contain a gene for a MOB4/Phocein ortholog and the

existence of the interplay between TtCdaI and TtElo1, led Jiang et al. (2019) to propose the existence in *Tetrahymena* of different Hippo signaling routes using different kinases belonging to MST1/2 and NDR/LATS kinase families, or even different MOB molecules. The studies in *Tetrahymena* clearly showed that TtMob1 is a critical factor in cell polarity establishment apart from its role in cytokinesis. On the other hand, experiments carried out in *Stentor coeruleus*, a ciliate that can regenerate an entire cell-organism from a fragment of one cell, clearly showed that ScMob1 is a critical factor for morphogenesis. In *S. coeruleus* ScMob1 was surgically removed from the anterior and posterior pole of the ciliate's cells in a ScMob1 knockdown background. These cells, contrary to controls, were unable to regenerate a normal morphology showing that ScMob1 plays a role in the establishment of both anterior and posterior polarity in *S. coeruleus* (Slabodnick et al. 2014). Altogether, the studies in ciliates showed that Mob1 is essential for the perpetuation of the complex patterning and axiation of the ciliate's cells and morphogenesis that are linked to accurate cell division ultimately required to maintain cell ploidy and genomic stability (Florindo et al. 2012; Slabodnick et al. 2014).

1.2.2.3.2. MOB in Apicomplexa

Mob genes are present and conserved in the genome of Apicomplexan parasites like the cyst-forming Coccidia *T. gondii*, *Hammondia hammondi*, *Neospora caninum*, and *Besnoitia besnoiti*, in the monoxenic Coccidia *Eimeria tenella* and *Eimeria maxima*, and the most basal Apicomplexa *Cryptosporidium*, e.g., *Cryptosporidium muris* and *Cryptosporidium parvum*. Current analyses were not able to identify *Mob* genes in the genomes of Hematozoans (data available at VEuPathDB.org) namely, *Plasmodium* spp., *Babesia* spp., or *Theileria* spp.

To the best of our knowledge, the only study on Apicomplexan MOBs was performed by Alexandra Tavares in the scope of her doctoral thesis, within our research group (Tavares 2015). This work identified a single *Mob1* gene in the *T. gondii* genome, coding for a protein with high homology to MOB1 proteins of other Apicomplexan parasites. *In house* produced *T. gondii* specific polyclonal anti-MOB1 sera were used to identify the MOB1 subcellular localization mainly concentrated at the basal pole of tachyzoites, compatible with the basal complex. MOB1 was also localized in a central dot and as a cytoplasmic pool. *Mob1* expression dramatically decreased upon tachyzoite invasion of host cells, maintaining low expression levels during parasite replication. Furthermore, MOB1 overexpression strains showed a marked delay in tachyzoite replication, with no effect on invasion. The results of this work indicate that MOB1 is a critical player in the regulation of cell division and proliferation in *T. gondii*, suggesting a role similar to the described for MOB1 proteins of unicellular organisms as regulators of cell

division (Luca and Winey 1998; Tavares et al. 2012) and in multicellular organisms as tumor suppressor agents (Lai et al. 2005; Praskova et al. 2008; Maerz et al. 2009; Galla et al. 2011; Nishio et al. 2012; Gardiner et al. 2016; Lyu et al. 2016).

Chapter 2. Research questions and objectives

T. gondii affects a variety of definitive and intermediate hosts, including various farm animal species and humans, causing high economic losses as well as health and food safety concerns. The ability for stage conversion is paramount in this parasite's life cycle. Specifically, tachyzoite-bradyzoite interconversion and production of tissue cysts is key for the dissemination and persistence of *T. gondii*. Research showing that depletion of MOB1 impaired cell division in unicellular eukaryotes led us to hypothesize that MOB1 regulates replication in *T. gondii* affecting tachyzoite proliferation and eventually tachyzoite-bradyzoite interconversion and cyst formation. MOB1 is a kinase adaptor present in signaling pathways controlling cytokinesis in unicellular eukaryotes (MEN/SIN) and cell proliferation vs. apoptosis in multicellular eukaryotes (Hippo pathway) (McCollum and Gould 2001; Ma et al. 2019). Hippo is a signaling pathway that culminates in the activation/deactivation of transcription factors controlling the expression of genes involved in many developmental processes, including cell proliferation, apoptosis and cell differentiation. The study of a multicellular pathway becomes even more relevant in *T. gondii*, a cyst forming Coccidia, where zoites are interdependent within the tissue cyst and the schizont, multicellular units that can be comparable to an organ, with controlled cell number and size. Initially considered to be inert, the bradyzoite is a life stage now recognized to have a slow replication rate (Watts et al. 2015). The Hippo signaling pathway is a central regulator of organ size in metazoan but key proteins of this pathway have been found in unicellular organisms as well (Sebé-Pedrós et al. 2012). This pathway is regulated by extracellular signals, namely mechanical and chemical stimuli perceived through the plasma membrane, and a significantly higher frequency of gene ontology terms related to "response to stimulation" and "organism process" was detected in a transcriptome analysis of *T. gondii* bradyzoites compared to tachyzoites (L.F. Chen et al. 2018; Rausch and Hansen 2020).

We hypothesize that a MEN/SIN/Hippo like signaling pathway is crucial in the *T. gondii* replication process and parasite number regulation. Proteins involved in this pathway would be promising potential targets for therapeutic strategies to control parasite proliferation. In addition to the currently published data on MOB1 in unicellular and multicellular organisms (Luca and Winey 1998; Weiss et al. 2002; Hammarton et al. 2005; Hergovich 2011; Florindo et al. 2012), data obtained by our research group (Tavares 2015) on *T. gondii* MOB1 led us to consider this protein as a probable key player in the regulation of parasite replication, prompting us to select it as a starting point for this project. This work intends to contribute to the current understanding of the molecular mechanisms underlying parasite replication and parasite number regulation (proliferation/replication versus latency) in order to better understand and control the parasitic

disease. To achieve this, we will use cell culture and molecular biology techniques to reach the following objectives:

- assess the MOB1 function in replication using reverse genetics to obtain the *Mob1* knockout and characterize the MOB1 depletion phenotype, namely its impact on replication and parasite number regulation;

- characterize the MOB1 subcellular localization, specifically with regard to its relation with structures and organelles implicated in mitosis and cytokinesis;

- identify the MOB1 interactome in light of the proposed MOB1 function of replication and parasite number regulation acting through a hypothetical *T. gondii* MEN/SIN/Hippo like signaling pathway;

- characterize the expression of *Mob1* during the *T. gondii* lytic cycle in order to understand the relationship between *Mob1* regulation and MOB1 function.

At the end of this project we expect have expanded our understanding of the MOB1 function in the *T. gondii* life cycle, namely in regard to its involvement in tachyzoite replication and number regulation. We also expect to have obtained a comprehensive database allowing us to begin unraveling the pathways that are involved in the MOB1 function and regulation in *T. gondii*.

Chapter 3. Material and Methods

3.1. *Toxoplasma gondii* strains

In this work, we used *T. gondii* strains classified as type I (RH) and recombinant type I/III (EGS). RH strains were kindly provided by Markus Meissner (Department of Veterinary Sciences, Ludwig-Maximilians-Universität, Munich, at the time located at Wellcome Centre for Molecular Parasitology, University of Glasgow). These include the RHΔ*Hx* referred here as RH (Donald et al. 1996), RH:splitCas9 referred here as splitCas9, and ku80::diCre referred here as diCre (also a RHΔ*Hx* strain*)*. The diCre strain was provided with permission from Vern B. Carruthers, Department of Microbiology & Immunology, University of Michigan Medical School (Andenmatten et al. 2013). The EGS strain was kindly provided by Érica Martins Duarte, Laboratório de Ulstraestrutura Celular Hertha Meyer, Carlos Instituto de Biofísica Chagas Filho Universidade Federal do Rio de Janeiro (Paredes-Santos et al. 2013).

3.2. Strategies

3.2.1. *Mob1* inducible knockout in the RH strain

MOB1 has been shown to be an essential protein both in unicellular (Luca and Winey 1998; Weiss et al. 2002; Hammarton et al. 2005; Florindo et al. 2012; Slabodnick et al. 2014) and in multicellular eukaryotes (Galla et al. 2011; Florindo et al. 2012; Bae et al. 2018). As the MOB protein family is highly conserved in metazoans (Hergovich 2011), it is probable that this characteristic of MOB proteins is also conserved in *T. gondii*. Studying the loss of function phenotype of an essential gene can be a challenge, as the incompatibility with sustained life often translates to a very reduced timeframe in which it is possible to gather data and an inability to isolate individual clones with the desired phenotype. In the case of *Mob1*, and to circumvent partially these issues, we adopted an inducible knockout system.

3.2.1.1. CRISPR/Cas9 technology and splitCas9

The CRISPR/Cas9 system takes advantage of a naturally occurring prokaryotic defense mechanism against mobile genetic elements based on clustered regularly interspaced short palindromic repeats or CRISPR (Ishino et al. 2018). A CRISPR associated endonuclease (Cas) produces DNA double stranded breaks (DSBs). The Cas forms a complex with two RNA molecules: a protospacer or guide RNA (gRNA) that anneals to the target DNA sequence and a transactivating RNA (trRNA). These RNA molecules may be substituted by a single chimeric RNA that aggregates the two, designated single guide RNA (sgRNA). The gRNA or protospacer

must be followed by a specific trinucleotide sequence known as protospacer-adjacent motif (PAM) which allows the system to distinguish between the target and the RNA-coding DNA sequence. The DSBs produced by the Cas are repaired by the cellular machinery either through non-homologous end joining or, less frequently, through homologous recombination. Reparations through the error-prone non-homologous end joining pathway frequently produce small insertions or deletions (indels) which can result in frame shift mutations. The coding sequence of the gene of interest (GOI) is modified from the point of DSB, translating to an altered protein sequence and/or to a premature Stop codon which may lead to a functional knockout of the GOI.

In order to obtain an inducible knockout for *Mob1*, we used the *T. gondii* splitCas9, developed by the Markus Meissner Laboratory. *T. gondii* RH parasites were modified to express Cas9 divided into 2 sub-units (Figure 12). Both Cas9 sub-units are overexpressed by the *Tub8* promoter and each sub-unit is fused to a rapamycin binding protein: C-terminal Cas9 is associated to FK506 binding protein (FKBP) and N-terminal Cas9 is associated to FKBP rapamycin binding (FRB). To obtain a GOI functional knockout strain, two steps are required. First, a plasmid harboring the sequence for a sgRNA targeting the GOI is stably transfected into splitCas9 tachyzoites using the dihydrofolate reductase (DHFR) selection marker. This generates the GOI inducible Cas9 strain that overexpress the sgRNA in addition to both Cas9 sub-units. Second, addition of rapamycin to the culture medium triggers dimerization of both rapamycin-binding proteins and, consequently, of the 2 Cas9 fragments which activates the endonuclease (Putyrski and Schultz 2012). This enables the sgRNA to direct the endonuclease activity to the GOI and leads to a functional knockout of this gene.

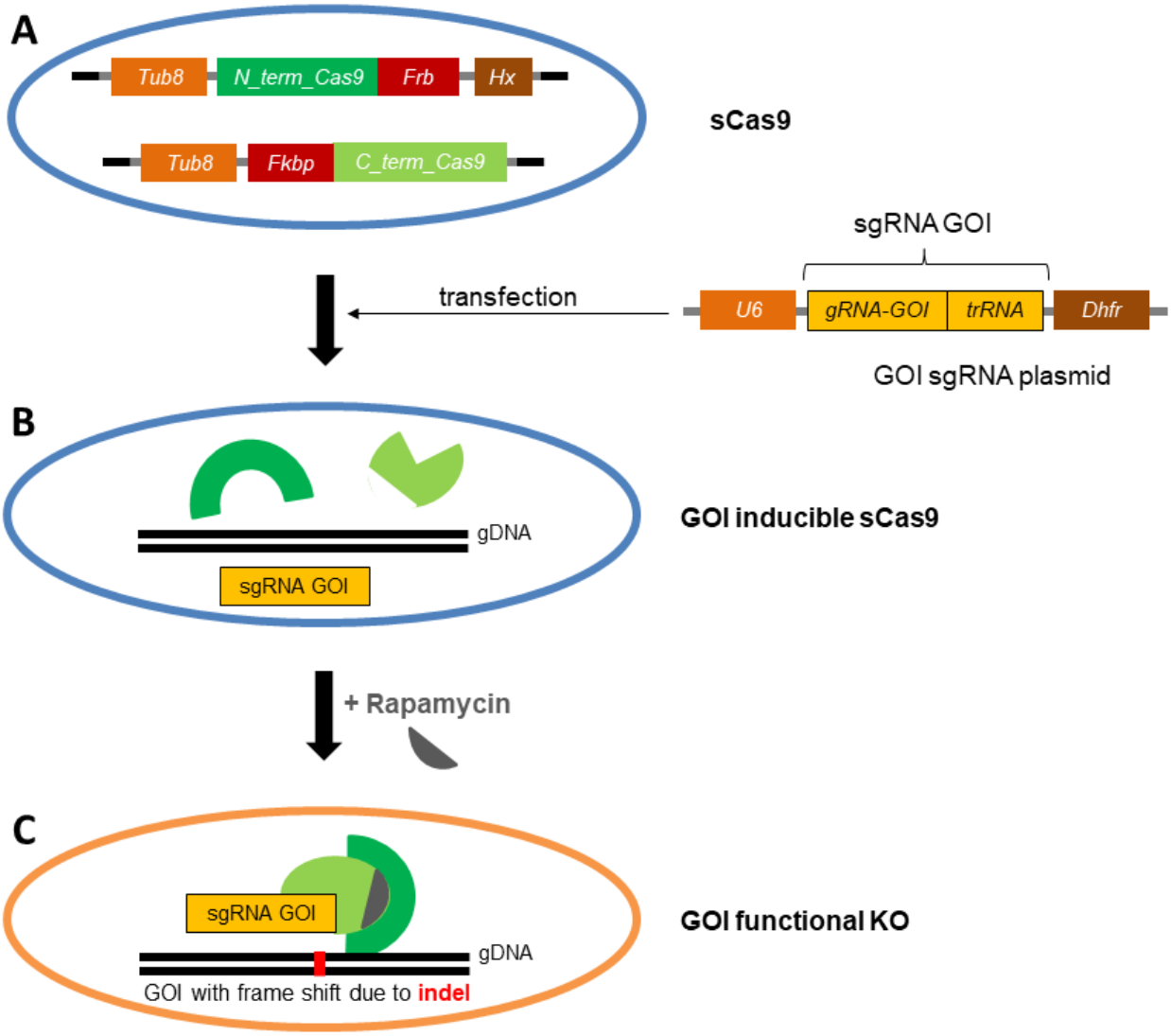

Figure 12. Strategie of the splitCas9 system.

A) *T. gondii* splitCas9 overexpress Cas9 divided into two sub-units. Each Cas9 sub-unit is fused to a rapamycin binding protein: C-terminal Cas9 is associated to FK506 binding protein (FKBP) and N-terminal Cas9 is associated to FKBP rapamycin binding (FRB). **B)** A gene of interest (GOI) inducible knockout strain is generated by a stable transfection of the GOI single guide RNA (sgRNA) plasmid which produces an overexpression of the guide RNA fused to the transactivating RNA, forming the sgRNA. **C)** Rapamycin triggers dimerization of both rapamycin-binding proteins and, consequently, of the two Cas9 fragments which enables endonuclease activity. Addition of rapamycin to the culture medium in the presence of the sgRNA directs the endonuclease activity to the GOI and causes its functional knockout. *Tub8* – *Tub8* promoter; *U6* – *U6* promoter; *N_term_Cas9* - N-terminal Cas9; *C_term_Cas9* - C-terminal Cas9; *Hx* - hypoxanthine-xanthine-guanine phosphoribosyl transferase (selection marker); *Dhfr* - dihydrofolate reductase (selection marker); gDNA – genomic DNA; indel – insertion or deletion.

3.2.1.2. Generation of inducible *Mob*1 splitCas9 *Toxoplasma gondii*

To obtain inducible *Mob1* splitCas9 (iC) tachyzoites, we employed three gRNAs targeting each of the first three exons of *Mob1* (Table 3, Figure 13). The gRNAs were designed with the Eukaryotic Pathogen CRISPR sgRNA Design Tool (EuPaGDT) using the *T. gondii* GT1 ToxoDB-26 release, the most fully annotated genome available at the time closest to the RH genome (Peng and Tarleton 2015). The design of the sgRNAs took into account the specificities of the Cas9, namely, sequences with 20 nucleotides figuring immediately before a 5'-NGG-3' PAM. We targeted the beginning of the coding sequence to increase the chances of achieving a functional knockout using the CRISPR/Cas9 system as it enables the disruption at the beginning of the protein sequence, ensuring a maximum chance of not having a partially functional protein. Each gRNA (Table 3) was cloned independently into the vector *pU6-sgRNA-Dhfr* in order to form a sgRNA by fusion with the trRNA the plasmid harbors. The resulting plasmid constructs (*pU6-sgRNA1-Dhfr*, *pU6-sgRNA2-Dhfr*, and *pU6-sgRNA3-Dhfr*) were independently transfected into splitCas9 tachyzoites and caused to stably and randomly integrate the genome by selection for the DHFR resistance using pyrimethamine (1 µM, Fluka). After selection, clones were isolated through limit dilutions. Isolated clones were cryopreserved and processed for *Mob1* functional knockout induction.

Table 3. Sequences of gRNAs used to obtain *Mob1* functional knockouts.

gRNA ID	Target sequence (5' - 3')	Annealing location
gRNA1	GGACGTCTTGGCGACTACCA	exon 1
gRNA2*	GCCTCACTCATCCACCCAGAT	exon 2
gRNA3	GACGGCTGCCCGGGCATCTC	exon 3

*The first "G" was manually added to the 5' of the gRNA target sequence.

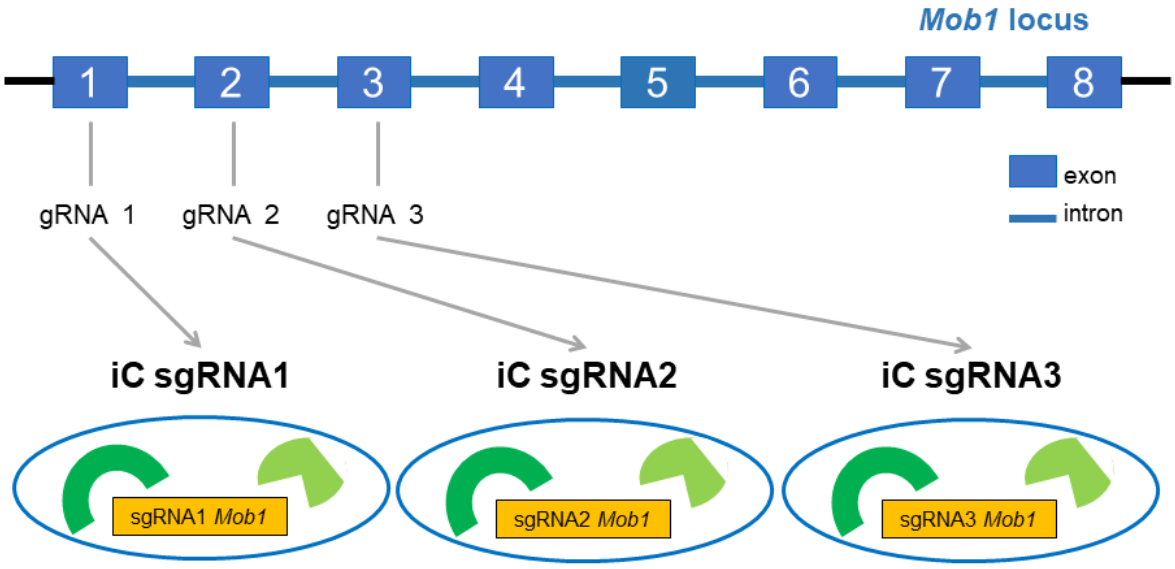

Figure 13. Strategy to obtain inducible Mob1 splitCas9 (iC) Toxoplasma gondii.

Three gRNAs were designed targeting each of the first three exons of *Mob1*. Each gRNA was cloned independently into the vector pU6-sgRNA-DHFR harboring the trRNA to form a fused sgRNA (*pU6-sgRNA1-Dhfr*, *pU6-sgRNA2-Dhfr*, and *pU6-sgRNA3-Dhfr*). The resulting plasmid constructs were independently transfected into splitCas9 tachyzoites. Clonal lines were isolated overnight by limit dilution in 96-well plates.

3.2.1.3 Generation of *Mob1* functional knockout *Toxoplasma gondii*

3.2.1.3.1. Activation of the splitCas9 and initial assessment

Following the isolation of iC clonal lines harboring the three *Mob1* sgRNAs, the splitCas9 of iC clonal lines was activated by addition of a final concentration of 50 nM of rapamycin (Sigma-Aldrich) to the culture medium in order to obtain *Mob1* splitCas9 functional knockout (Cko) tachyzoites. As it was likely that MOB1 depletion could be lethal, we tested various induction protocols including intracellular and extracellular tachyzoites, variations in tachyzoite number, and various rapamycin exposure times ranging from four to 72 hours. To verify that splitCas9 induced DSBs and reparation had occurred at the expected locus according to the sgRNA expressed, we isolated gDNA from induced iC tachyzoites. Two distinct subpopulations were observed after splitCas9 activation, normal and abnormal replicating tachyzoites. The parasites that presented normal cellular division were collected from the supernatant. To isolate the abnormal replication parasites, we allowed the normal division parasites to fully lyse the host cell monolayer, removed the supernatant with the normal division parasites, washed the still adherent cells with PBS to eliminate contamination by normal division parasites and finally scraped the adherent cells. For each subpopulation, gDNA was extracted and used to amplify

the *Mob1* region were the Cas9 activity was expected, namely the region of expected annealing with the gRNA expressed by each clonal line. The primers used are described in Table 4. Two primer pairs were designed for each sgRNA using a nested strategy: a more external pair for gDNA amplification and a more internal pair for sequencing, which was also used for amplification when necessary. Additionally, the successful genome integration of *Mob1* sgRNAs was also confirmed. Primers were designed to anneal with the *pU6-sgRNA-Dhfr* sequence spanning the sgRNA and using the same nested primer strategy described above (Table 4).

Table 4. Primers used to develop *Mob1* knockouts using splitCas9.

Primer ID	Sequence (5' - 3')	Purpose
gRNA1_Mob1_pFext	GGTCTGCTTGTGATGCTGAA	Clonal line testing
gRNA1_Mob1_pRext	CATGACGCTACGAGGATCAA	Clonal line testing
gRNA1_Mob1_pFint	ATTGCTTTCCCGTGATAGTCC	Sequencing, clonal line testing
gRNA1_Mob1_pRint	TTCGACTCCAAGGAACAGAG	Sequencing, clonal line testing
gRNA2_Mob1_pFext	AGGCAATCCGAATCCTCTTT	Clonal line testing
gRNA2_Mob1_pRext	TTCACAGCAAGTGGCAGAAC	Clonal line testing
gRNA2_Mob1_pFint	TGGCGAATCTGTGCCTATAA	Sequencing, clonal line testing
gRNA2_Mob1_pRint	TGGTTCCAGTCAAAGCGATA	Sequencing, clonal line testing
gRNA3_Mob1_pFext	CATTTGTCGTTGCTTGCTGT	Clonal line testing
gRNA3_Mob1_pRext	ACGTCAAATGCTGAGGGAAG	Clonal line testing
gRNA3_Mob1_pFint	ACCTCCCAACTTCCCAGAGT	Sequencing, clonal line testing
gRNA3_Mob1_pRint	TTAAAGTGTCATCGTGCAGTCA	Sequencing, clonal line testing
CRISPR_ext_F	GCCACATGTTGGAGACACTG	Clonal line testing
CRISPR_ext_R	ACAGTCTCACCTCGCCTTGT	Clonal line testing
CRISPR_int_F	AGTCTTTCACGCTGCGAAGT	Sequencing, clonal line testing
CRISPR_int_R	TGTATGCCGCTAGAGTGCTG	Sequencing, clonal line testing

3.2.1.3.2 Genotypic and phenotypic characterization of Cko tachyzoites

DSBs caused by Cas9 are primarily repaired through the non-homologous end joining pathway. Therefore, the same sgRNA guided break will be repaired in different ways in different tachyzoites which will thus harbor different genotypes. Cko tachyzoites from the normal replication subpopulation were inoculated into 96-well plates using limit-dilutions in order to

isolate clonal lines with a single *Mob1* genotype. This was performed for Cko tachyzoites expressing the three *Mob1* sgRNAs. Clonal lines were characterized after gDNA extraction and amplification of the *Mob1* locus, spanning the site of gRNA annealing, and cloning into the pJET1.2 vector followed by Sanger sequencing, using the primers described in Table 4. We confirmed that the recombination events we detected at the gDNA level were also present at the RNA level by total RNA extraction and cDNA synthesis followed by cDNA amplification, cloning and into the pJET1.2 vector and sequencing with the same primers. Clonal lines presenting a genomic modification compatible with MOB1 depletion were selected for phenotypic characterization through cell culture *in vivo* assays, immunofluorescence and western blot.

3.2.1.3. Gene-swap recombination strategy

Parallel to the CRISPR/Cas9 strategy, we also employed an alternative method to obtain gene knockouts, the gene-swap recombination strategy published by Andenmatten et al. (2013) (Figure 14). This strategy employs the *T. gondii* DiCre system that is expressed in the *T. gondii* strain ku80::diCre (diCre). Two inactive Cre recombinase (Cre) fragments are each fused to a rapamycin-binding protein, N-terminal Cre fused to FKBP and C-terminal Cre to FRB, and randomly integrated into the diCre genome. The GOI's complimentary DNA (cDNA), flanked by two 34 bp *loxP* (locus of X-over P1) sequences arranged in the same direction, is inserted into the diCre genome in a site-specific manner, by homologous recombination using homology arms, and is exchanged with the endogenous GOI. These tachyzoites are deleted for the endogenous GOI but overexpress the GOI cDNA due the presence of the strong promoter *Tub8*. The knockout can be induced, as previously described for splitCas9, by addition of rapamycin to the cell medium which triggers the dimerization of FKBP and FRB and consequently joins the Cre fragments. The active Cre recognizes the *loxP* sequences and causes a rearrangement with excision of the *loxP* flanked DNA, namely the GOI cDNA, which is eliminated. This produces a knockout of the GOI and the expression of the YFP open reading frame as its position causes *Tub8* promoter led transcription.

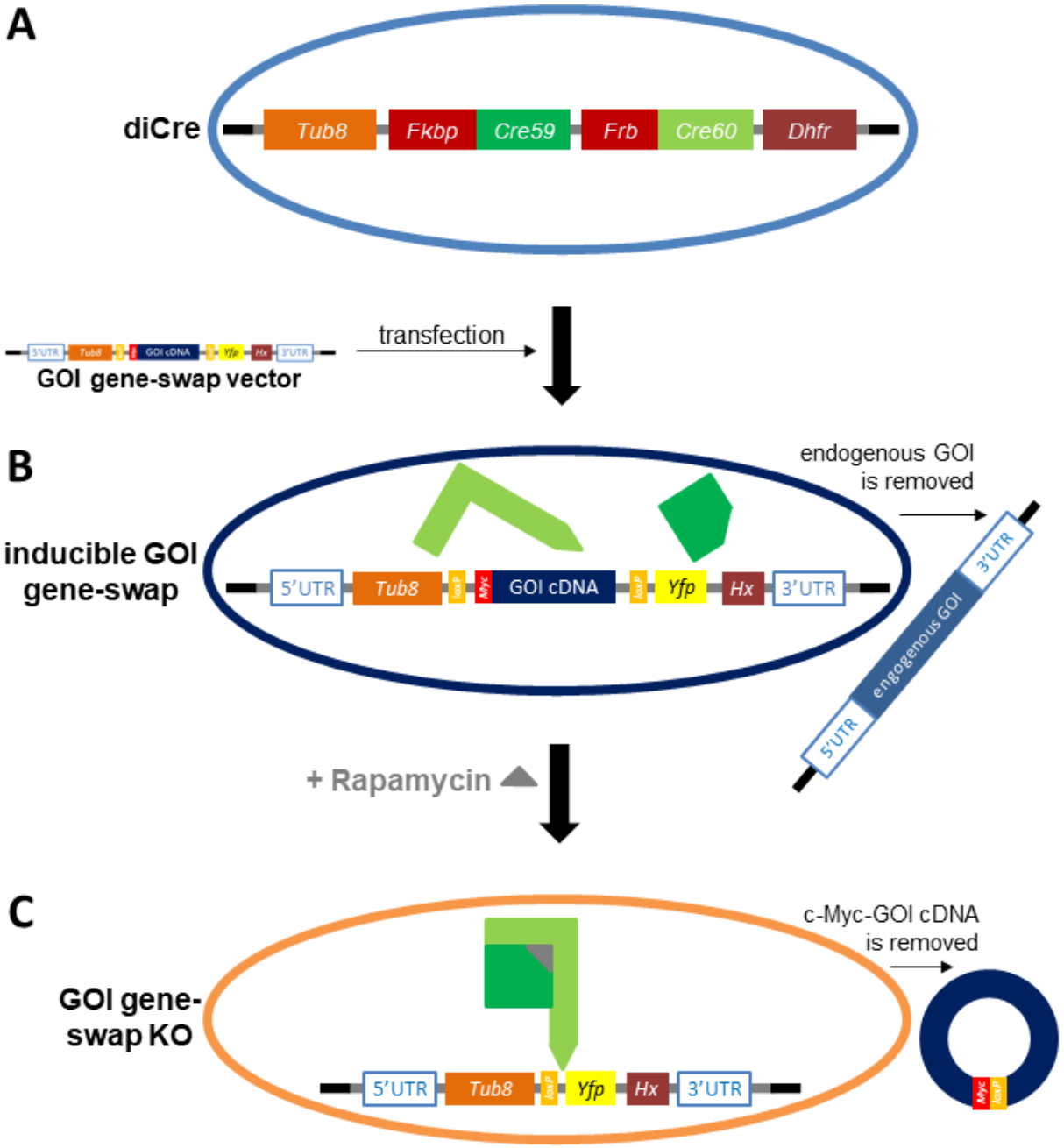

Figure 14. Strategie of the gene-swap inducible knockout system.

A) *T. gondii* diCre tachyzoites overexpress Cre divided into two sub-units. Each Cre sub-unit is fused to a rapamycin binding protein: N-terminal Cre59 is fused to FK506 binding protein (FKBP) and C-terminal Cre60 is fused to FKBP rapamycin binding (FRB). **B)** The inducible GOI gene-swap strain is obtained by homologous recombination, after the transfection of the GOI gene-swap vector into diCre tachyzoites. The vector replaces the endogenous GOI which is removed from the genome. **C)** Upon addition of rapamycin to the culture medium, the Cre59 and Cre60 fragments form an active dimer and produce double stranded DNA breaks at the *loxP* sites included in the GOI gene-swap vector, originating the GOI gene-swap knockout. The *Myc*-GOI cDNA portion of the DNA construct is removed from the genome and a GOI knockout is obtained. GOI gene-swap knockout tachyzoites express YFP due to the excision

of the *Myc*-GOI cDNA. The *loxP* sequences are represented by the small orange rectangle. The *Myc* tag is represented by the small red rectangles. *Tub8* – *Tub8* promoter; *Fkbp* and *Frb* – rapamycin binding domains; *Cre59* – Cre fragment 1-59 aa; *Cre60* – Cre fragment 60-343 aa; *Dhfr* - dihydrofolate reductase (selection marker); UTR - untranslated region; *loxP* - 34 bp Cre recognition sequence; *Myc* - DNA sequence coding for the Myc protein tag; cDNA - complimentary DNA; *Yfp* - yellow fluorescent protein; *Hx* - hypoxanthine-xanthine-guanine phosphoribosyltransferase (selection marker).

3.2.1.3.1. Assembly of the MOB1 gene-swap vector

The *Mob1* gene-swap vector 5'UTR-*pTub8-loxP-Myc-Mob1-loxP-Yfp-Hx*-3'UTR was obtained by modification of the gene-swap vector *pTub8-loxP-KillerRed-loxP-Yfp-Hx* (Andenmatten et al. 2013). For the assembly of the *Mob1* gene-swap vector, we amplified and cloned the *Mob1* complimentary DNA (cDNA) fused to the *Myc* tag and two homology arms, which were amplified from the *Mob1* 5' and 3' untranslated regions (UTRs). For each homology arm, a 2 kb genomic region was selected, upstream of the ATG codon for the 5'UTR and downstream of the Stop codon for the 3'UTR. The three amplicons were cloned into the pJET1.2 plasmid, sequenced and subcloned into the original gene-swap vector plasmid using the primers described in Table 5. The amplification of the 3'UTR was difficult to achieve, requiring additional gDNA extraction to ensure a good quality source of amplification, restriction of total gDNA with *Bam*HI to facilitate primer and polymerase access to the target region (no *Bam*HI restriction site is present in this region), design of additional primers, cross PCR of all primer pairs, and optimization of primer annealing temperatures using temperature gradients ranging from 50 ºC to 63 ºC. The restriction sites available in this plasmid and present in the amplicons determined that these must be inserted in the plasmid in a specific order: first the 3'UTR, second the 5'UTR and third the *Mob1* cDNA. The resulting *Mob1* gene-swap vector was sequenced to confirm the correct insertion of the three amplicons.

Table 5. Primers used to assemble the *Mob1* gene-swap vector.

Primer ID	Sequence (5' - 3')	Purpose
F – 5' Mob[1]	GGACTAGTGCGACGCCCTTCGAAACC	Cloning
R – 5' Mob[2]	CGGGATCCAAGGCGACGGCAAACGAAG	Cloning
5 UTR Mob F	GGGTTTGCTTTTCTCTGCGG	Colony testing, sequencing
5 UTR Mob R	AATCATGAAGCGAATGCGGC	Colony testing, sequencing
5 - 5UTR Mob Seq	TGCGTACGACCTATATTGCC	Sequencing
3 - 5UTR Mob Seq	AGTGCGCACTGCCATCGC	Sequencing
F Mob KO[3]	CCCCTTAAGAACTACTGGACGTCTTGGC	Cloning
R Mob KO[4]	CCCTTAATTAATCAAAAACTGGCCTGAGAGC	Cloning
Mob Tg F int	GAAGAAAGCGTCCCATGCAC	Colony testing, sequencing
Mob Tg R int	CACGAGATTTGCCACAGCAG	Colony testing, sequencing
MobTg F_int2	CGAAGTCCAGTTGGTGTGGA	Colony testing, sequencing
MobTg R_int2	GCAGTTCGAGTGGTACGGAG	Colony testing, sequencing
MobTg 3 seq	CTAAGTGTTCATTGTCTCCG	Sequencing
MobTg 5 seq	GTGGATGAGTGAGGAAGGC	Sequencing
F – 3' Mob	ATCCCCTTAAATCAGAGTTTC	Amplification test
R – 3' Mob	TATGAAAATGACCCGAACGC	Amplification test
F1 - 3' Mob	GACAACGGACACAGACAGA	Amplification test
F2 – 3'3' Mob	TGTCTCCGGTGTGCTTGAG	Amplification test
R1 - 3' Mob	CAGGAAGCAATGGACTTTGA	Amplification test
R2 - 3' Mob	GACAGCAAGCCTGCGGTT	Amplification test
F1 - 3' Mob_not[5]	ATAAGAATGCGGCCGCGACAACGGACACAGACAGA	Cloning
R2 - 3' Mob_mfe[6]	CCCCAATTGGACAGCAAGCCTGCGGTT	Cloning
F_3_int_Mob	GATCTGCATTGCTAGCGACA	Colony testing, sequencing
R_3_int_Mob	GACAGGAAAGGCACAGAGGA	Colony testing, sequencing
New 3' – 5' seq	TATGTATATGCGCATACACG	Sequencing
New 3' - 3' seq	CGTCGTTGCCACCCTCG	Sequencing

The sequence targeted by the restriction endonuclease (RE) is highlighted in grey. The nucleotides upstream of these were added to increase the efficiency of the restriction activity on the amplicons. [1]RE is *Spe*I. [2]RE is *Bam*HI. [3]RE is *Afl*II. [4]RE is *Pac*I. [5]RE is *Not*I. [6]RE is *Mfe*I.

3.2.1.3.2. Generation of inducible gene-swap *Mob1* tachyzoites

The *T. gondii* diCre strain was transfected with the *Mob1* gene-swap vector by electroporation to obtain inducible *Mob1* gene-swap overexpressing MOB1 (iGSoe) tachyzoites (Figure 15). The diCre parental strain is deleted for *ku80*, a DNA repair gene involved in the non-homologous end joining pathway. This deletion inhibits random integration and highly favors integration of DNA through homologous recombination. The transfected tachyzoites were put under positive selection pressure for the *Hx* resistance with mycophenolic acid and xanthine. The selected parasites were isolated into clonal lines which were tested for correct vector integration.

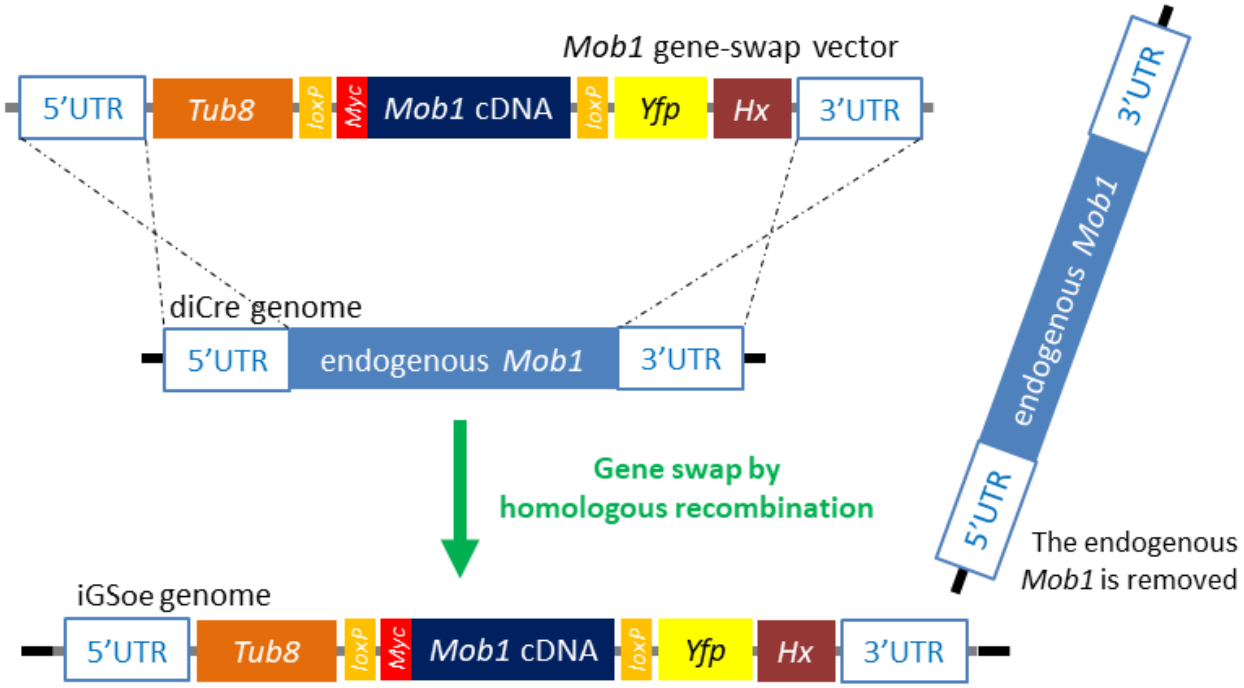

Figure 15. iGSoe tachyzoites were obtained by transfection of the diCre strain with the *Mob1* gene-swap vector.

The *Mob1* gene-swap vector was transfected into diCre tachyzoites. Gene-swap by homologous recombination occurs when the endogenous *Mob1* is removed from the *T. gondii* diCre genome and replaced by the *Mob1* gene-swap vector. This produces the iGSoe tachyzoites which overexpress Myc-MOB1cDNA, under the influence of the strong promoter *Tub8*. Tachyzoites where vector integration occurred are selected for the presence of the *Hx* marker by addition of mycophenolic acid and xanthine to the culture medium. UTR – untranslated region; *loxP* - 34 bp Cre recognition sequence; *Myc* – DNA sequence coding for the *Myc* protein tag; *Yfp* – yellow fluorescent protein; cDNA – complimentary DNA; *Hx* – hypoxanthine-xanthine-guanine phosphoribosyl transferase (selection marker).

Two types of PCR tests were designed: intron spanning PCR, where both forward and reverse primers anneal with exons (these primers anneal with both the endogenous *Mob1* and the integrated *Mob1* cDNA), and exon spanning PCR, where both forward and reverse primers

anneal with introns, only detecting the endogenous *Mob1* (Table 6). Several primer pairs were designed for both intron spanning and exon spanning PCR tests. Clonal lines that show the amplicon corresponding to the *Mob1* cDNA but not the amplicon corresponding to the endogenous *Mob1* represent the iGSoe tachyzoites. These parasites suffered integration of the *Mob1* gene-swap vector through homologous recombination at the *Mob1* locus by exchange with the endogenous *Mob1* and not at random in the genome.

Table 6. Primers used to obtain GSko tachyzoites

Primer ID	Sequence (5' - 3')	Purpose
Mob Tg F int	GAAGAAAGCGTCCCATGCAC	Intron spanning PCR
testKO-WTmob R1	GCAGGCATTTTCACAGCAAGT	Intron spanning PCR
MobTg F_int2	CGAAGTCCAGTTGGTGTGGA	Intron spanning PCR
testKO-WTmob R2	TCCTGCAAGATGCTCCTCAAT	Intron spanning PCR
testKO-WTmobF3	ATGCCTGCAACTTGTGTGGA	Intron spanning PCR
testKO-WTmobR3	TCGACACTGGCACTGGTCTT	Intron spanning PCR
testKO-WTmobR4	TGCATGAGTTGAGCCAAGATG	Intron spanning PCR
testKO-WTmobF4	TCCCAGCGTTGATGGTGATA	Intron spanning PCR
testWTmob F1	GTTGTCTTCACGTGCGCTGT	Exon spanning PCR
testWTmob R1	CGTTGTAGGCGTTCGGAGAT	Exon spanning PCR
testWTmobF2	GTCGCCTTATGGCTGTTCGT	Exon spanning PCR
testWTmobR2	CAGGACAGGGCAGCTGAAAT	Exon spanning PCR
testWTmobF3	CAGTGGTGTTGGGAACGACA	Exon spanning PCR
testWTmobR3	TTCAGGAACTGGACGCCTTC	Exon spanning PCR
F 2 _ FRB-Cre60/FKBP-Cre59	ATGGCCCCTAAGAAGAAGAG	Testing induction iGSoe
R 2 _ FKBP-Cre59	TCAGTTCAGCTTGCACCAG	Testing induction iGSoe
F_int_Icre	GTCCCTGGTGATGAGGAGAA	Testing induction iGSoe
R_int_Icre	TGATTTCAGGGATGGACACA	Testing induction iGSoe
F_ICre_EcoRI_V1[1]	GGAATTCATGGTGCCCAAGAAGAAGAG	Cloning
R_ICre_Pac_V1[2]	CCCTTAATTAATCAGTTCAGCTTGCACCAG	Cloning
testKOindF1	TTCGCCCTTTCCTTCTCTTT	*Mob1* cDNA excision test
testKOindR1	TGGTGCAGATGAACTTCAGG	*Mob1* cDNA excision test

The sequence targeted by the restriction endonuclease (RE) is highlighted in grey. The nucleotides upstream of these were added to increase the efficiency of the restriction activity on the amplicons. [1]RE is *Eco*RI. [2]RE is *Pac*I.

3.2.1.3.3. Generation and characterization of GSko tachyzoites

Tachyzoites of the iGSoe strain possess the diCre strain background which expresses Cre divided into two inactive fragments, each fused to a rapamycin-binding protein. The N-terminal Cre fragment, Cre59, consists of nuclear localization signal (NLS), FKBPP, linker and Cre 1–59 nucleotides while the C-terminal Cre fragment, Cre60, consists of NLS, FRB, linker and Cre 60–343 nucleotides (Andenmatten et al. 2013). Addition of rapamycin to the culture medium enables the union of both rapamycin-binding proteins and consequently the two fragments of Cre form an active dimer (Putyrski and Schultz 2012). The active Cre produces double stranded DNA breaks at the *loxP* sites (Jullien 2003).

The *Mob1* gene-swap vector present in iGSoe tachyzoites includes two *loxP* sites surrounding the *Myc-Mob1* cDNA (Figure 15). To obtain *Mob1* gene-swap knockout tachyzoites (GSko), we added rapamycin to the culture medium of iGSoe tachyzoites which causes Cre activation and excision of the floxed *Myc-Mob1* resulting in a *Mob1* knockout. The excision of the *Myc-Mob1* cDNA causes the YFP to be under the influence of the *Tub8* promoter and leads to YFP expression (Figure 14.C).

Addition of rapamycin to the culture medium of iGSoe tachyzoites failed to induce Cre activity. In order to assess why, we tested the genome of diCre and iGSoe tachyzoites for the presence of both Cre subunits using the primers described in Table 6, and Cre59 was not detected. At this point we had concluded that the *Mob1* is not an essential gene, enabling us to transfect the missing Cre59 subunit for transient expression and directly trigger the *Mob1* knockout. Therefore, this subunit was cloned into the *pTub8-Myc-Gfp-MyoATy-Hx* vector forming the p*Tub8-Cre59-Hx* vector which was transfected into iGSoe tachyzoites. Immediately after the transfection, rapamycin was added to the medium. Cre59 transfected tachyzoites were inoculated into 96-well plates using limit-dilutions in order to isolate clonal lines. Clonal lines were characterized after gDNA extraction and amplification of the *Mob1* cDNA using the primers described in Table 6, to test for the successful activation of Cre activity (Figure 16). PCR results were confirmed at the protein level by western blot using anti-Myc and anti-GFP monoclonal antibodies. Clonal lines presenting PCR and western blot results compatible with *Mob1* knockout were selected for phenotypic characterization through cell culture *in vivo* assays, immunofluorescence and western blot.

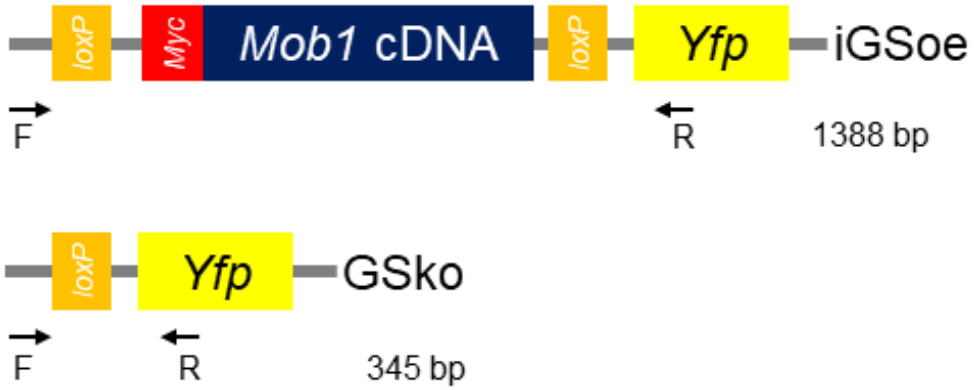

Figure 16. PCR analysis of iGSoe tachyzoites transfected with the *pTub8-Cre59-Hx* vector.

A PCR test was designed to confirm the excision of *Mob1* cDNA after Cre activation, to be performed on gDNA. The PCR produces amplicons with different sizes for iGSoe and GSko tachyzoites. Forward (F) and reverse (R) primers annealing locations are indicated. F – primer testKOindF1; R – primer testKOindF1; bp – base pairs.

3.2.2. Direct *Mob1* knockout in the EGS strain

The RH *Mob1* knockout strains (Cko and GSko) present a moderate but significant increase of the tachyzoite replication rate when compared to the respective parental strains (iC and iGSoe). This suggests an involvement of *Mob1* in the regulation of the tachyzoite replication rate, which is thought to be a key factor for tachyzoite-bradyzoite transition. However, RH strains, or type I strains in general, are not a good model to study this transition (Jeffers et al. 2018): (i) *in vitro*, these parasites usually are very resistant or have lost the ability to make the tachyzoite to bradyzoite transition, probably due to long term adaptation to *in vitro* conditions; (ii) *in vivo*, in the mouse model, RH tachyzoites are a virulent strain, usually causing mortality in a short time, limiting the possibility of producing bradyzoite cysts, which is a key feature of the chronic stage of the infection. This led us to delete *Mob1* in strains more prone to produce bradyzoite cysts *in vitro*, which tend to be less virulent, by employing the CRISPR/Cas9 system. Our previous results show that *Mob1* knockout does not impair the tachyzoite cell cycle or survival.

3.2.2.1. Generation and isolation of *Mob1* knockout using CRISPR/Cas9

In order to obtain a *Mob1* knockout in the EGS strain, we employed the CRISPR/Cas9 system. We obtained a vector for the transient expression of Cas9, *pTub8-Cas9-Yfp-Ha_U6-gRNAintron*. This vector was originally developed to improve the efficiency homologous recombination at the locus targeted by the gRNA of a vector harboring homology arms. Thus it also codes for a sgRNA, gRNAintron, which was designed for the target sequence 5'-

GAGTAGAGGGTCGTCAGAAA -3' located in the first *Mob1* intron. Knowing that *Mob1* knockout tachyzoites are viable, we decided to co-transfect the *pTub8-Cas9-Yfp-Ha_U6-gRNAintron* with the *pU6-sgRNA1-Dhfr* to produce functional *Mob1* knockouts in EGS tachyzoites (Figure 17). Following transfection, we used pyrimethamine to select parasites for the selection marker DHFR present in the vector expressing the sgRNA1. This way, if we obtained a low efficiency of transient Cas9 activity and did not obtain *Mob1* functional knockout clonal lines with this strategy, we would still be able to isolate clonal lines expressing the sgRNA1. Clones were isolated by limit-dilutions in 96-well plates.

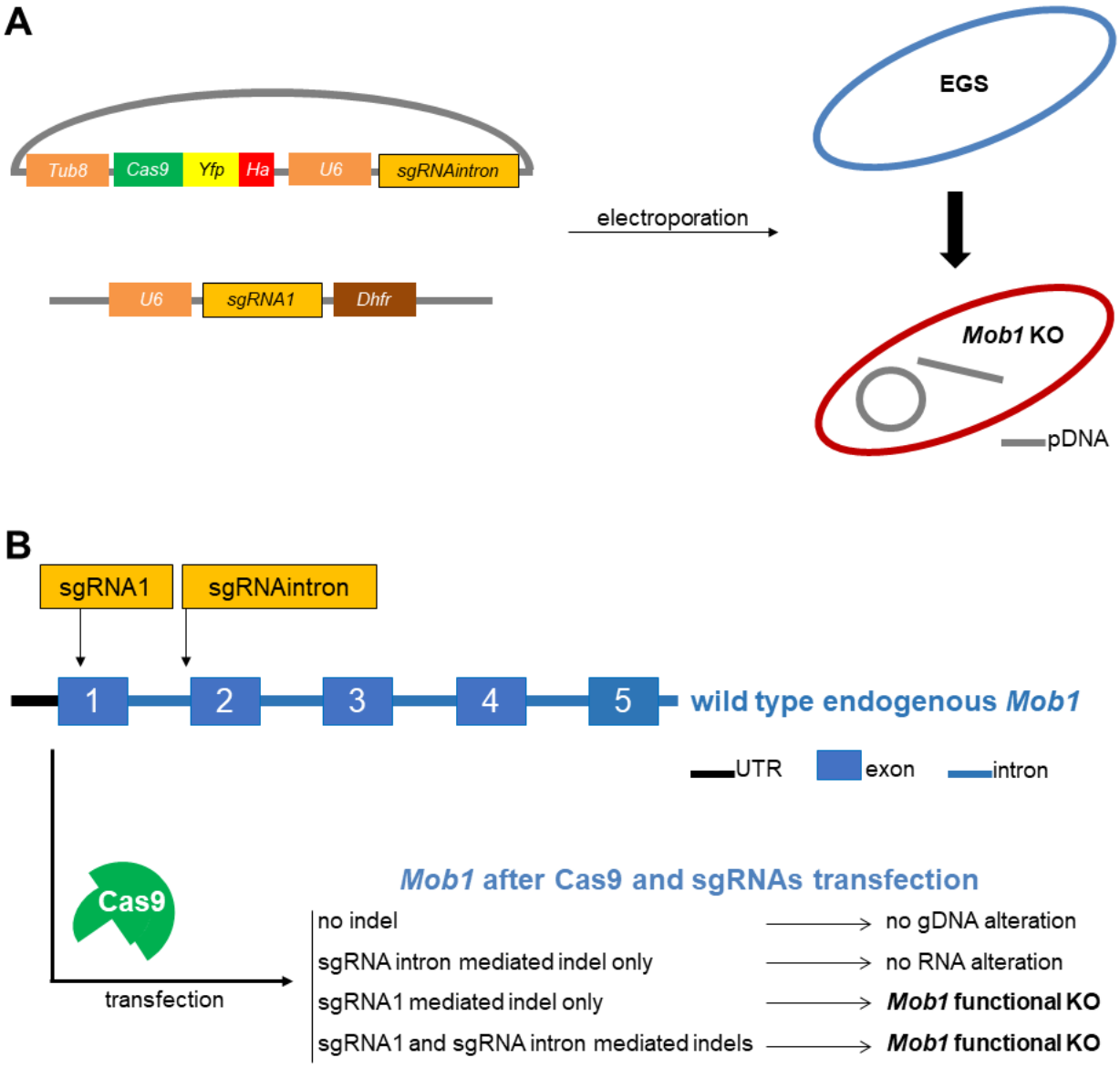

Figure 17. Generation of *Mob1* knockout in the EGS strain.

A) The *T. gondii* EGS strain was co-transfected with two plasmid vectors, *pTub8-Cas9-Yfp-Ha_U6-gRNAintron* (not linearized) and *pU6-gRNA1-Dhfr* (linearized). **B)** Various outcomes are possible following transfection, which may or may not result in a *Mob1* functional knockout. Therefore, it is necessary to isolate and characterize the clonal lines.

3.2.2.2. Genotypic and phenotypic characterization of EGS *Mob1* functional knockout tachyzoites

We initiated the genotypic characterization of the EGS *Mob1* functional knockout (Eko) clonal lines as described previously for the Cko clonal lines. However, primer pairs that had performed at that stage did not produce the expected amplicons with the Eko clonal lines, despite presenting the expected result with the EGS parental strain. This led us to suspect that the *Mob1* locus had suffered a more marked remodeling than we expected. Thanks to a fortuitous unspecific amplicon, we realized that part of the *pU6-gRNA1-Dhfr* vector had been inserted into the *Mob1* locus. After this initial series of PCR > amplicon purification > Sanger sequencing, we developed a strategy to pinpoint the extent of the insertion. To this end, we performed multiple series of primer design > PCR > amplicon purification > Sanger sequencing. Whenever needed, the amplicon was cloned into the pJET1.2 vector for sequencing. The primers used in this strategy are described in Tables 4 and 7. Clonal lines presenting a genomic modification compatible with MOB1 depletion were selected for phenotypic characterization through cell culture *in vivo* assays, immunofluorescence and western blot.

Table 7. Primers used to characterize the *Mob1* locus of Eko clonal lines

Primer ID	Sequence (5' – 3')	Purpose
dKO_Crispr_Fext	TTTATGCCCGTTTTGAAAGAA	Amplification
dKO_Crispr_Rext	TGTTGCGGTTTCTGACTCAT	Amplification
dKO_Crispr_Fint	GCTGTTCGTCAGTGTTTTGG	Sequencing, amplification
dKO_Crispr_Rint	CTCCCCCTTATGCAAATGAA	Sequencing, amplification
pKOinsert_F1	ACTGGACGTCTTGGCGACTA	Amplification
pKOinsert_R1	CTGCCGTGTGGTAAAATGAA	Amplification
pKOinsert_R2	GCATGCTTTCCCAGGTTTT	Amplification
pKOinsert_R3	ACGCAGGGAAGAAAACGTC	Amplification
pKOinsert_R4	CGAAGAAGGAGCCTGCAA	Amplification
pKOinsert_Rstop	AAGAAAACAAGGCGAGGTGA	Amplification
pKOinsert_F2	TCGACCAGCTGAAGAATGTG	Amplification
pKOinsert_F3	GTACAAGGATTCTGTCGACC	Amplification
pKOinsert_R5	GTGCATGGGACGCTTTCT	Amplification
pKOinsert_F4	TTCATGTGGCATTTCACACAG	Sequencing
seqRNA_MOB1_F	CGGAGTTTCCTTTCCACG	RT-PCR
seqRNA_MOB1_R	TACGCATCTACAGAGAAACT	RT-PCR
Tg*Gapdh1*_F	CGTGGAGGTTTTGGCGATC	RT-PCR
Tg*Gapdh1*_R	GACTTCGCCGGGGTAGTG	RT-PCR

* Primers used to develop *Mob1* KOs using splitCas9 were also used to characterize the *Mob1* locus of Eko clonal lines (Table 4).

3.2.3. MOB1 overexpression

3.2.3.1. BirA expressing strains for BioID analysis

In order to gain a more comprehensive understanding of MOB1´s function we identified its interactome using the proximity-dependent biotin labeling method BioID (Roux et al. 2012). BioID is a genetic tool that identifies interacting and neighbor proteins in their native cellular environment by proximity labeling. This technique employs the rare protein modification biotinylation. To obtain this modification, a bacterial biotin ligase was modified to a promiscuous form named BirA. BirA biotinylates proteins by proximity and, when fused to the protein of interest, it will label its neighbors and interacting partners with biotin (provided to the medium). Biotinylation occurs in the native cellular environment, a key aspect of this methodology, and produces a very resistant bond that withstands stringent and denaturing processing. This allows

the detection of stable but also transient and weak interactions as well as the detection of interactions with proteins harder to isolate as membrane-bound proteins. The naturally high affinity between biotin and streptavidin molecules allows easy detection of biotin labeled proteins by western blot with streptavidin-HRP and pull-down with streptavidin labeled beads (Figure 18). The characteristics of the BioID method are especially useful for the detection of an interaction network, including transient and weak interactions, enabling the identification of stable and the dynamic parts of an interactome. This applies to proteins that typically produce brief interactions, namely proteins that participate in a kinase cascade as the kinase adaptor MOB proteins.

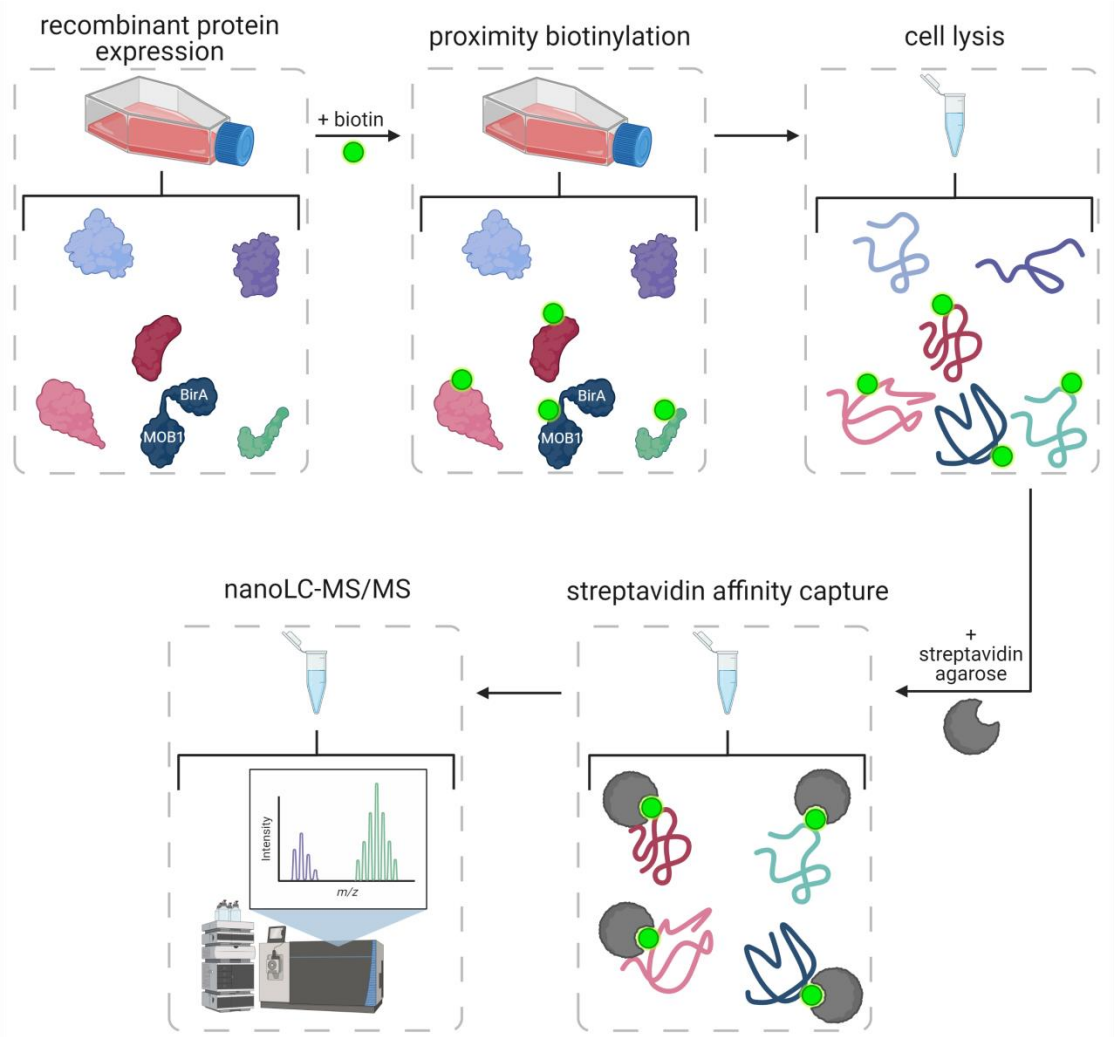

Figure 18. BioID system operation.

We set up a MOB1 BioID system using a FLAG tag as part of the DNA constructs for easy detection of the recombinant proteins. For this system, we obtained two strains: a BirA

control expressing FLAG-BirA (FB), and a BirA-MOB1 test strain expressing FLAG-BirA-MOB1 (FBMOB1). To obtain the FLAG-BirA and FLAG-BirA-MOB1 strains, RH tachyzoites were transfected with the linearized vectors *pTub8-Flag-BirA-Hx* and *pTub8-Flag-BirA-Mob1-Hx* for random integration in the genome. Tachyzoites that had successfully integrated the constructs were selected by addition of xanthine and mycophenolic acid to the culture medium and isolated into clonal lines by limit dilutions in 96-well plates. Clonal lines were tested for the expression of recombinant proteins. Strains expressing FLAG-BirA, and FLAG-BirA-MOB1 with similar recombinant protein expression levels were selected for further characterization.

3.2.3.2. Recombinant MOB1 strain driven by a low expression promoter

Commonly used overexpression promoters, such as the *T. gondii Tub8* tubulin promoter present in the iGSoe and FLAG-BirA-MOB1strains, often result in constitutively high protein expression that may overwhelm the cell making it impossible to distinguish its sub-cellular localization. In order to obtain a probable sub-cellular localization of MOB1 in *T. gondii*, the MOB1 cDNA was cloned into a vector plasmid fused to a FLAG tag and driven by the *T. gondii* MORN1 promoter, morn1. MORN1 is a protein constitutively expressed at low levels, with known sub-cellular localization (Gubbels et al. 2006). Its promoter has been used as a transgene expression promoter for MORN1 and other *T. gondii* proteins as it allows for protein expression with low levels. The *pmorn1-Flag-Mob1-Cat* plasmid vector, a kind gift from Marc-Jan Gubbels (Department of Biology, Boston College, USA) was transfected into RH tachyzoites that were selected for plasmid integration with mycophenolic acid and xanthine supplementation. Tachyzoites that survived drug selection were used to isolate clones through limit dilutions in 96-well plates. Clones were tested for FLAG-MOB1 expression through immunofluorescence and western blot analysis.

3.3. Cell culture

Human foreskin fibroblasts (HFF) were used as host cells to maintain *T. gondii*. The cell line HFF-1 (SCRC-1041, ATCC) was grown in Gibco Dulbecco's Modified Eagle Medium (DMEM) medium with GlutaMAX Supplement supplemented with 10% Gibco heat inactivated fetal bovine serum (FBS). For passaging, HFF were washed twice with phosphate-buffered saline (PBS, Gibco), detached from the Petri dish using 800 µl of Trypsin-EDTA (0.05%) phenol red (Gibco), and resuspended in an appropriate volume of DMEM GlutaMAX 10% FBS. HFF were grown to confluent monolayers to maintain *T. gondii* cultures and were used no further

than passage 30. Cell cultures were kept at 37 ºC, in a humidified atmosphere with 5% CO_2. *T. gondii* were cultured using DMEM GlutaMAX supplemented with 1% FBS. HFF and *T. gondii* strains were cryopreserved in DMEM GlutaMAX supplemented with 20% FBS and 10% dimethyl sulfoxide (DMSO, Sigma-Aldrich) using liquid nitrogen. *T. gondii* strains were cryopreserved while infecting HFF, following 36 hours of infection.

3.3.1. *Toxoplasma gondii* transfection

For reverse genetics experiments, *T. gondii* tachyzoites were transfected by electroporation using program U-033 of the Nucleofector™ 2b and the Amaxa® Basic Parasite Nucleofector Kit 2 (Lonza). Approximately $2x10^7$ tachyzoites and 10-15 µg of plasmid were used for each transfection. For stable transfections, tachyzoites were then selected for successful plasmid integration through drug selection for at least 3 passages with the drug, considering the drug resistance gene present in the plasmid. Following transfection and drug selection, clonal lines were isolated by limit dilution in 96-well plates seeded with confluent HFF. Wells where a single lysis plaque formed in the host cell monolayer likely were selected as a *T. gondii* clonal line. Clonal lines were subsequently cryopreserved and characterized.

3.4. Nucleic acid molecular biology

3.4.1. Nucleic acid isolation

For DNA isolation, cells were collected and washed twice with PBS (Gibco). Genomic DNA was isolated using the DNeasy Blood & Tissue Kit (QIAGEN), following the manufacturer's instructions regarding the tissue protocol. PCR amplified DNA was purified using the QIAquick PCR Purification Kit (QIAGEN) or the QIAquick Gel Extraction Kit (QIAGEN), depending on the visualization results. Alternatively, we also used the Zymoclean Gel DNA Recovery kit (ZymoResearch) for low starting DNA amounts. Plasmid DNA (pDNA) was purified using the QIAprep Spin Miniprep Kit (QIAGEN), following the manufacturer's instructions. DNA was quantified using the NanoDrop 2000c spectrophotometer (Thermo Scientific).

For RNA isolation, cells were collected and washed twice with PBS (Gibco). Total RNA was isolated using the E.Z.N.A. Total RNA Kit I (Omega Bio-Tek), following the manufacturer's instructions. The optional step of addition of β-mercaptoethanol (Sigma-Aldrich) was performed.

3.4.2. DNA amplification

DNA amplification was performed using Phusion High-Fidelity DNA Polymerase (Thermo Scientific) when proofreading activity or blunt ended amplicons were necessary. Solutions were prepared using Phusion HF Buffer with addition of 0.02 U/µl of enzyme, deoxynucleotides (including dATP, dTTP, dGTP, and dCTP; Thermo Scientific) at a final concentration of 200 µM, and forward and reverse primers at a final concentration of 0.5 µM each. PCRs with a final volume of 25-50 µl were processed as follows: initial denaturation at 98 ºC for 2 minutes; 30 to 40 cycles of denaturation at 98 ºC for 10 seconds, annealing at the primer pair specific temperature for 20 seconds, extension at 72 ºC during 30 seconds per 1000 bp of the expected amplicon; and a final extension at 72 ºC for five minutes.

DNA amplification was performed using DreamTaq DNA Polymerase (Thermo Scientific) for everyday purposes or when sticky ended amplicons were necessary. Solutions were prepared using DreamTaq Buffer with addition of 0.025 U/µl of enzyme, deoxynucleotides (including dATP, dTTP, dGTP, and dCTP; Thermo Scientific) at a final concentration of 200 µM, and forward and reverse primers at a final concentration of 0.5 µM each. PCRs with 20-50 µl were processed as follows: initial denaturation at 95 ºC for 5 minutes; 30 to 40 cycles of denaturation at 95 ºC for 60 seconds, annealing at the primer pair specific temperature for 60 seconds, extension at 72 ºC during 60 seconds per 1000 bp of the expected amplicon; and a final extension at 72 ºC for ten minutes.

Electrophoresis was performed using agarose gels with 1-1.5% of agarose (w/v, NZYTech) in TAE buffer [40 mM Tris-Acetate (Calbiochem-Fluka), 1mM EDTA (Bio-Rad)] with GreenSafe Premium nucleic acid stain (NZYTech). Amplicon sized was evaluated based on the O'GeneRuler 1 kb DNA Ladder (Thermo Scientific). The reactions were visualized using the imager ChemiDoc XRS+ (BioRad).

3.4.3. Molecular cloning

Generally, molecular cloning was performed by restriction endonuclease activity and ligation. Amplicons and target vectors were hydrolyzed overnight at the restriction endonuclease specific temperature using two units of endonuclease per 1 µg of DNA. The vector's 5'ends were dephosphorylated using Antarctic Phosphatase (NEB), following the manufacturer's instructions. The hydrolyzed DNA fragment and vector were purified following agarose gel electrophoresis. Alternatively, amplicons were cloned in the *pJET1.2/blunt* cloning vector

(Thermo Scientific) following the manufacturer's instructions. These were sequenced and/or subcloned in a *T. gondii* destination vector.

Ligations were prepared in 10 µl reactions with 50 ng of vector, the equivalent amount of fragment, and two units of T4 DNA Ligase (Thermo Scientific) in T4 DNA Ligase Buffer. The reactions were incubated at 4 ºC during 16 to 72 hours. Following ligation, 50 µl of competent *Escherichia coli* (strains DH5α or JM109) were incubated with 5 µl of the ligation reaction in ice. Transformation was achieved through heat shock: from ice to 42 ºC for 90 seconds, to ice again for two minutes. Bacteria were subsequently allowed to recover in sterile LB medium (NZYTech) at 37 °C and 180 rpm for 60 minutes. Following recovery, bacteria were plated onto LB agar (NZYTech) supplemented with an antibiotic compatible with the destination vector resistance. Bacterial colonies were allowed to grow at 37 ºC overnight and were tested through colony PCR for fragment insertion using DreamTaq DNA Polymerase (Thermo Scientific). Colonies were sampled using a micropipette tip, streaked on LB Agar (NZYTech) for maintenance, and dipped in 20 µl of Milli-Q water for use as PCR template. Positive colonies were grown in antibiotic supplemented LB medium (NZYTech) at 37 ºC and 180 rpm overnight, for plasmid purification.

3.4.3.1. Alternative molecular cloning methods

The vectors *pU6-sgRNA1-Dhfr, pU6-sgRNA2-Dhfr, pU6-sgRNA3-Dhfr,* and *pTub8-Cas9-Yfp-Ha_U6-gRNAintron* were a kind gift from Markus Meissner (Department of Veterinary Sciences, Ludwig-Maximilians-Universität, Munich, at the time located at Wellcome Centre for Molecular Parasitology, University of Glasgow). Cloning of sgRNAs in the *pU6-sgRNA-Dhfr* vector was achieved through direct mutagenesis using the Q5 Site-Directed Mutagenesis Kit (New England Biolabs, Inc) following the manufacturer's instructions. Cloning of sgRNAs in the *pTub8-Cas9-Yfp-Ha_U6-ccdB* vector was performed by annealing of single-stranded oligonucleotides. The vector *pTub8-Cas9-Yfp-Ha_U6-ccdB* was linearized with the restriction endonuclease *Bsa*I, which removes the *ccdB* fragment. Oligonucleotides were designed with ends complementary to the ends of the *Bsa*I digested plasmid vector. The oligonucleotides were resuspended in annealing buffer [10 mM Tris (Calbiochem), pH 7.5–8.0, 50 mM NaCl (Merck), 1 mM EDTA (Bio-Rad)] at equimolar concentrations (100 µM). Equal volumes of complementary oligonucleotides were mixed and heated at 95 ºC for five minutes. The heat block was removed from the apparatus and allowed to cool overnight. Annealed oligonucleotides were ligated with the linearized vector using two units of T4 DNA Ligase (Thermo Scientific) in T4 DNA Ligase Buffer at 16 ºC overnight. The sgRNAs used are described in Table 3. The primers used to

clone the sgRNAs in the *pU6-sgRNA-Dhfr* and *pTub8-Cas9-Yfp-Ha_U6-ccdB* vectors are described in Table 8. The vectors *pU6-sgRNA1-Dhfr, pU6-sgRNA2-Dhfr, and pU6-sgRNA3-Dhfr* were transfected into splitCas9 tachyzoites to obtain the iC strains. The *pU6-sgRNA1-Dhfr* and *pTub8-Cas9-Yfp-Ha_U6-gRNAintron* vectors were transfected into EGS tachyzoites to obtain the Eko strain.

Table 8. Primers used to clone the *Mob1* sgRNAs.

Primer ID	Sequence (5' - 3')	Purpose
Mob1gRNA_Exon_1_F	GCGACTACCAGTTTTAGAGCTAGAAATAGC	Cloning (direct mutagenesis)
Mob1gRNA_Exon_1_R	CAAGACGTCCAACTTGACATCCCCATTTAC	Cloning (direct mutagenesis)
Mob1gRNA_Exon_2_F	CCACCCAGATGTTTTAGAGCTAGAAATAGC	Cloning (direct mutagenesis)
Mob1gRNA_Exon_2_R	ATGAGTGAGGCAACTTGACATCCCCATTTAC	Cloning (direct mutagenesis)
Mob1gRNA_Exon_3_F	CGGGCATCTCGTTTTAGAGCTAGAAATAGC	Cloning (direct mutagenesis)
Mob1gRNA_Exon_3_R	GGCAGCCGTCAACTTGACATCCCCATTTAC	Cloning (direct mutagenesis)
Mob1gRNA_intron_1_F	AAGTTGAGTAGAGGGTCGTCAGAAAG	Cloning (oligonucleotide annealing)
Mob1gRNA_intron_1_R	AAGTT TTTCTGACGACCCTCTACTCG	Cloning (oligonucleotide annealing)

Cloning in the *pmorn1-Morn1-Myc-Cat* vector, a kind gift from Marc-Jan Gubbels (Biology Department of Biology, Boston College, USA), as performed through ligation independent cloning (LIC) using the In-Fusion HD Cloning Kit (Takara), following the manufacturer's instructions. The *pmorn1-Morn1-Myc-Cat* vector was linearized using the *Bgl*II and *Asc*I restriction endonucleases which simultaneously removed the *Morn1-Myc* fragment. The *Flag-Mob1* fragment was amplified from the *pTub8-dd-Myc-Gfp-Mob1-Hx* vector (Tavares 2015) and first cloned in the *pJET1.2/blunt* cloning vector (Thermo Scientific) in order to fuse the *Flag* and *Mob1* sequences (the *Flag* sequence was inserted in the forward primer). From the *pJET1.2/blunt-Flag-Mob1* vector, the *Flag-Mob1* fragment was amplified with the LIC primers. Finally the *Flag-Mob1* fragment was exchanged with the *Morn1-Myc* fragment obtaining the *pmorn1-Flag-Mob1-Cat* vector using the In-Fusion HD Cloning Kit (Takara) protocol. The primers used to obtain the *pmorn1-Flag-Mob1-Cat* vector are described in Table 9. The *pmorn1-Flag-Mob1-Cat* vector was transfected into RH tachyzoites for random integration to obtain the morn1-FLAG-MOB1 strain.

Table 9. Primers used to obtain the *pmorn1-Flag-Mob1-Cat* vector.

Primer ID	Sequence (5' - 3')	Purpose
FLAGMob1Tg_BamHI_F[1]	GGATCCATGGACTACAAAGACGATGACG ATAAAAACTACTGGACGTCTTGGC	Cloning
FLAGMob1Tg_NdeI_R[2]	GGAATTCCATATGTCAAAAACTGGCCTGA GAGC	Cloning
morn1FLAGMob1_F	ACCGTTGTCCACCAGATCATGGACTACAA AGACGATGAC	Cloning (ligation independent)
morn1Mob1_Asc_Rnew	CGGGCAGCTTCTGGCGCGTCAAAAACTG GCCTGAGAGC	Cloning (ligation independent)
morn1_F	GTATCTCCTGTCTTGAATTA	Colony testing, sequencing
morn1_R	GCAACTCGCTTTCGTTC	Colony testing, sequencing

The sequence targeted by the restriction endonuclease (RE) is highlighted in grey. The nucleotides upstream of these were added to increase the efficiency of the restriction activity on the amplicons. [1]RE is *Bam*HI. [2]RE is *Nde*I.

3.4.4. DNA constructs cloned by restriction endonuclease activity and ligation

The vector *pTub8-loxP-Myc-loxP-Yfp-Hx* was modified to include the multiple cloning site *EcoRI-Myc-AflII-AseI-BstZ17I-PacI* (Francisco 2019). The modified *pTub8-loxP-Myc-loxP-Yfp-Hx* is referred as the gene swap vector.

To obtain the *Mob1* gene swap vector, the *Mob1* cDNA, a 2 kbp *Mob1* 5'UTR fragment (5'UTR) and a 2 kbp *Mob1* 3'UTR fragment (3'UTR) were cloned in the gene swap vector *pTub8-loxP-Myc-loxP-Yfp-Hx*. The *Mob1* cDNA was amplified with the *Afl*II and *Pac*I restriction sites in its 5' and 3' ends, respectively. The 5'UTR was amplified with the *Spe*I and *Bam*HI restriction sites in its 5' and 3' ends, respectively. The 3'UTR was amplified with the *Not*I and *Mfe*I restriction sites in its 5' and 3' ends, respectively. These restriction sites were used to clone the three fragments in the gene swap vector but, due to availability of the restriction sites in the various fragments, these had to be inserted in a specific order: first the 3'UTR, second the 5'UTR and third the *Mob1* cDNA. At the end of this cloning process, we obtained the *Mob1* gene swap vector *p5'UTR-Tub8-loxP-MycMob1-LoxP-Yfp-Hx-3'UTR*. The primers used to obtain the *Mob1* gene swap vector are described in Table 5. The *Mob1* gene swap vector was subsequently transfected into diCre tachyzoites to obtain the iGSoe strain through homologous recombination. The original vector *pTub8-loxP-Myc-loxP-Yfp-Hx* was provided by Markus Meissner.

To obtain the recombinant vectors for the MOB1 BioID system, we modified the gene swap vector to express FLAG tagged BioID constructs. The gene swap vector *pTub8-loxP-Myc-loxP-Yfp-Hx* was linearized with *Afl*II and *Nde*I which simultaneously removed the *loxP-Yfp* fragment. The *Flag-BirA* and *Flag-BirA-Mob1* fragments were amplified fused to *Afl*II and *Nde*I restriction sites and were inserted into the hydrolyzed gene swap vector, resulting in the *pTub8-loxP-Myc-Flag-BirA-Hx* and *pTub8-loxP-Myc-Flag-BirA-Mob1-Hx* vectors. The constructs were transfected into RH tachyzoites for random integration, to obtain the FLAG-BirA and FLAG-BirA-MOB1 strains. The *Flag-BirA* fragment was amplified from the *pcDNA5-Flag-BirA* vector that was provided by Helena Soares (Escola Superior de Tecnologia da Saúde de Lisboa, Instituto Politécnico de Lisboa and Centro de Química Estrutural–Faculdade de Ciências da Universidade de Lisboa). *Mob1* was cloned in the *pcDNA5-Flag-BirA* vector fused to *Flag-BirA* using the *Xho*I and *Not*I restriction sites, and *Flag-BirA-Mob1* was amplified from this construct. The primers used to obtain these constructs are described in Table 10.

Table 10. Primers used to obtain the *Mob1* BioID vectors.

Primer ID	Sequence (5' - 3')	Purpose
FlagBirAMob1vKO_AflII_F[1]	AATCGCCTTAAGATGGACTACAAAGACGATGAC	Cloning
FlagBirAvKO_NdeI_R[2]	GGAATTCCATATGTCAAGATATCTGTACAGGCGCG	Cloning
FlagBirAMob1vKO_NdeI_R[2]	GGAATTCCATATGTCAAAAACTGGCCTGAGAGC	Cloning
vKO_fillin_apa_bamh_R	ACTGGGACTGCGAACAGC	Colony testing, sequencing
F_vectorKO	TAAAGGCGGCGAATATTAGC	Colony testing, sequencing
vKO_fillin_apa_bamh_F	TGTGCTGCAAGGCGATTA	Colony testing, sequencing
BirA F_int	GACAGCACCAACCAGTACCT	Colony testing, sequencing
BirA R_int	AGTTGTCCAGCTTCTCCCAC	Colony testing, sequencing
BirA5' seq	GTTCACCGTGCCCGGCAA	Colony testing, sequencing
BirA 3' seq	GGAGCAGGACGGCATCATC	Colony testing, sequencing

The sequence targeted by the restriction endonuclease (RE) is highlighted in grey. The nucleotides upstream of these were added to increase the efficiency of the restriction activity on the amplicons. [1]RE is *Afl*II. [2]RE is *Nde*I.

3.4.5. DNA precipitation

When necessary, DNA was precipitated overnight at -20 ºC in a 1.5 ml tube using a 10% volume of 3 M sodium acetate pH 5.2 (Sigma-Aldrich) and a 250% volume of ice-cold absolute ethanol (Panreac). To isolate the DNA, the tube was centrifuged at 16000 g and 4 ºC for 60

minutes and the supernatant was discarded. The DNA pellet was washed with 750 µl of 70% (v/v) ethanol (Panreac) and centrifuged again at 16000 g and 4 ºC for 15 minutes. After discarding the supernatant, the pellet was air-dried. For *T. gondii* transfection, 10-15 µg of pDNA was precipitated, air-dried in the laminar flow hood and resuspended in the transfection solution provided with the Amaxa Basic Parasite Nucleofector Kit 2 (Lonza).

3.4.6. RNA characterization and expression analysis

Complimentary DNA (cDNA) was synthesized using SuperScrip III Reverse Transcriptase (Invitrogen) following the manufacturer's instructions. Genomic DNA (gDNA) contamination was eliminated with RNase-free DNase Set I (Omega Bio-Tek). When the purpose was to amplify and/or sequence a specific cDNA, the maximum amount of total RNA and oligodT universal primers (Invitrogen) were used for the cDNA synthesis. This cDNA was processed using conventional PCR. When the purpose was to quantify RNA expression, 1 µg of total RNA and random primers (Invitrogen) were used for the cDNA synthesis. This cDNA was processed for qPCR using PerfeCTa SYBR Green SuperMix with ROX reference dye, on an ABI Prism 7700 Sequence system (Applied Biosystems), for 40 cycles. Relative quantification was performed using the standard curve method based on *Gapdh* and *α-Tubulin* as *T. gondii* endogenous controls. Standard curve samples were run in triplicate and test samples were run in duplicate. Data are presented as mean ± standard error (SE) of three independent experiments. Specific primers used for RNA isolation and/or quantification are described in Table 11.

Table 11. Primers used for RNA characterization and expression analysis.

Primer ID	Sequence (5' - 3')	Purpose
TgGapdh1_qPCR_F	CGTGGAGGTTTTGGCGATC	Quantification, amplification
TgGapdh1_qPCR_R	GACTTCGCCGGGGTAGTG	Quantification, amplification
TgATub_qPCR_F	CGCCTGCTGGGAGCTCTT	Quantification, amplification
TgATub_qPCR_R	GAAGGTGTTGAAGGCGTCG	Quantification, amplification
TgMob1_qPCR_F	CTGCCACATCTACAGACAAC	Quantification, amplification
TgMob1_qPCR_R	GAGTGGTACGGAGACAATG	Quantification, amplification
seqRNA_MOB1_F	CGGAGTTTCCTTTCCACG	Isolation, amplification, sequencing, quantification
seqRNA_MOB1_R	TACGCATCTACAGAGAAACT	Isolation, amplification, sequencing, quantification

3.4.6.1. *Mob1* strand specific RNA analysis

In order to assess *Mob1* strand specific transcript expression, *Mob1* strand specific cDNA was synthesized from total RNA using a specific primer for each strand (Table 11 and Figure 18). Both primers anneal in the UTR regions, close to the ATG and to the Stop codons. A control cDNA was synthesized using the universal oligodT primer. *Mob1* strand specific cDNA was used for conventional PCR followed by molecular cloning and sequencing. *Mob1* strand specific cDNA was also used for qPCR.

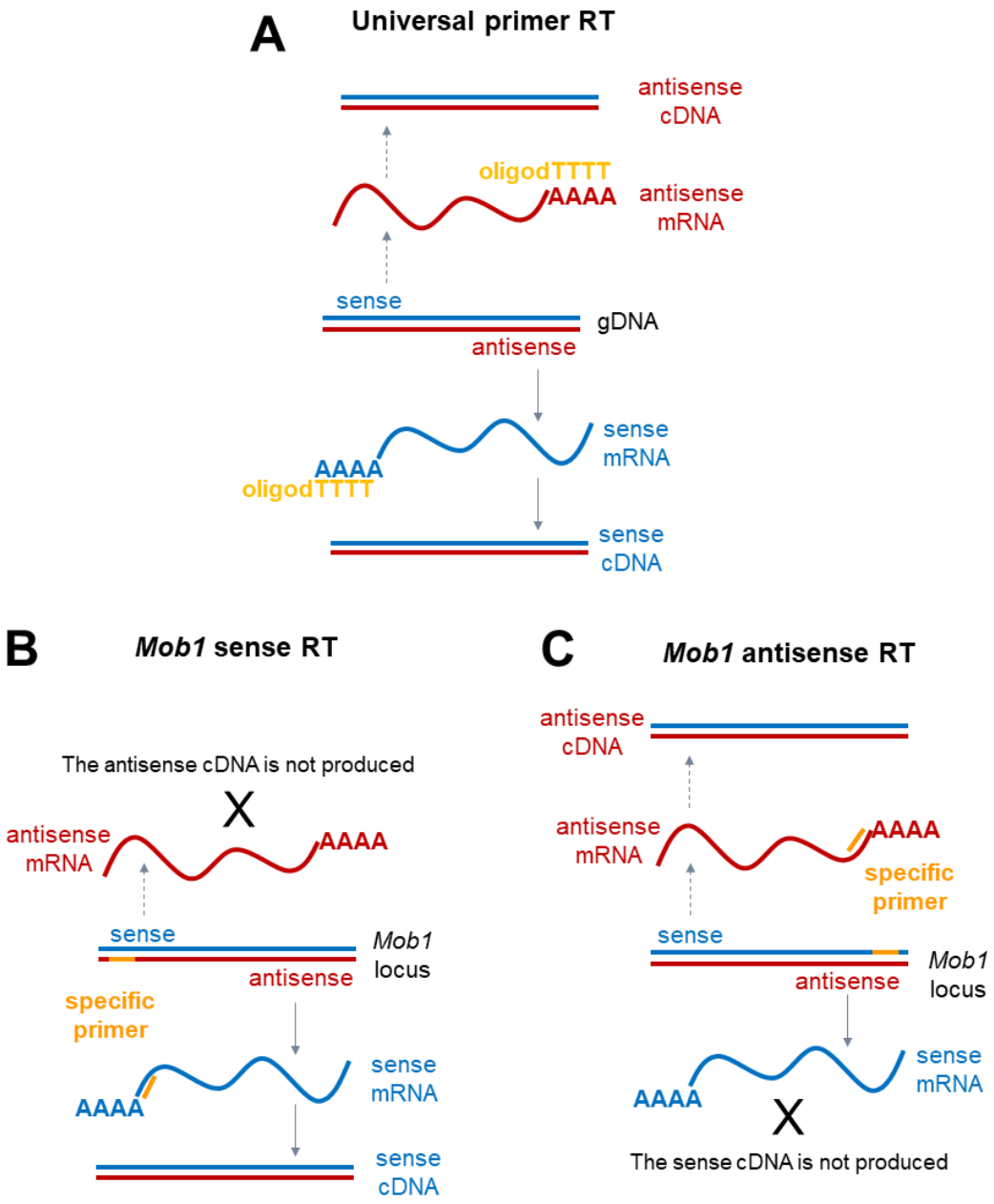

Figure 18. *Mob1* strand specific cDNA strategy.

If Mob1 gene is transcribed in both directions, the cDNA synthesis, using universal primers, can occur from any transcripts, sense or antisense (A). In order to assess *Mob1* strand specific transcription, specific primers were designed to amplify *Mob1* sense (B) and antisense (C) cDNA templates. RT - retro transcription; cDNA – complimentary DNA; mRNA – messenger RNA; oligodTTTT – universal oligodT primer; AAAA – polyA tail.

3.5. Cell culture *in vivo* assays

The *T. gondii* strains used during this study were summarized in Table 12.

Table 12. Summary of the *Toxoplasma gondii* strains used during this study.

PS	Strain	Description	Source of strain
_	RHΔHX	Type I	Markus Meissner
RHΔHX	sCas9	expresses Nterm_Cas9 and Cterm_Cas9	Markus Meissner
sCas9	iC	expresses *Mob1* specific gRNAs	vector random integration
iC	Cko	expresses a *Mob1* functional KO	induction of Cas9 activity
RHΔku80	diCre	expresses Nterm_Cre and Cterm_Cre	Markus Meissner
diCre	iGSoe	expresses Myc-MOB1cDNA	vector homologous integration
iGSoe	GSko	Δ*Mob1* and expresses YFP	induction of Cre activity
RH	FB	expresses FLAG-BirA	vector random integration
RH	FBMOB1	expresses FLAG-BirA-MOB1	vector random integration
RH	mFMOB1	expresses FLAG-MOB1 with the morn1 promoter	vector random integration
RH	dMGMOB1	expresses dd-Myc-GFP-MOB1	Alexandra Tavares
_	EGS	Recombinant type I/III	Érica Martins Duarte
EGS	Eko	expresses a *Mob1* functional KO	Cas9 transient expression

PS - parental strain; KO – knockout; sCas9 – splitCas9.

3.5.1. Tachyzoite growth assays

3.5.1.1. Invasion assay

To evaluate the invasion stage of the *T. gondii* lytic cycle, $1x10^6$ freshly egressed parasites were inoculated onto confluent HFF seeded on 24-well plates over glass coverslips and kept in standard culture conditions during 2 hours. At this point, the wells were washed abundantly with PBS (Gibco) to remove any extracellular tachyzoites, fresh culture medium was added to the wells and the invaded parasites were allowed to grow for 24 hours counting from inoculation. Following the 24 hours period, wells were washed twice with PBS (Gibco), fixed with ice-cold methanol (Fluka) during 20 minutes at -20 ºC, washed twice with PBS (Gibco) again and kept in PBS (Gibco) at 4 ºC until processed for immunofluorescence assay. Cells were stained with polyglutamylated tubulin monoclonal antibody (to stain the apical complex),

polyclonal sera for *T. gondii* surface proteins, and 4′,6-diamidino-2-phenylindole (DAPI). Data are presented as percentage of the mean number of parasitophorous vacuoles ± SE. The normalized means were analyzed with a two-factor ANOVA for a significance level (α) of 0.05. All vacuoles were counted in at least five randomly chosen fields per coverslip using the 40x objective. A total of three independent experiments were performed per assay, including three technical replicates per experiment.

3.5.1.2. Replication assay

To evaluate the replication stage of the *T. gondii* lytic cycle, $1x10^6$ freshly egressed parasites were inoculated onto confluent HFF seeded on 24-well plates over glass coverslips and kept in standard culture conditions during 2 hours. At this point, the wells were washed abundantly with PBS (Gibco) to remove any extracellular tachyzoites, fresh culture medium was added to the wells and the invaded parasites were allowed to grow for 24 hours counting from inoculation. Slower developing strains were also allowed to growth during 44 hours. These instances are indicated in the results. At this point, the wells were washed twice with PBS (Gibco), fixed with ice-cold methanol (Fluka) during 20 minutes at -20 ºC, washed twice with PBS (Gibco) again and kept in PBS (Gibco) at 4 ºC until processed for immunofluorescence. Cells were stained with polyglutamylated tubulin monoclonal antibody (to stain the apical complex), polyclonal sera for *T. gondii* surface proteins, and DAPI. The number of parasites inside the parasitophorous vacuole was counted in at least five randomly chosen fields per coverslip using the 40x objective. Each parasitophorous vacuole was assigned to a class following the expected 2^n progression (i.e. 2, 4, 8, 16, and 32). One tachyzoite vacuoles were not included in the count. Whenever the number of tachyzoites per vacuole did not correspond to the 2^n progression, the number of tachyzoites was rounded to the nearest class. Data are presented as mean percentage of the number of parasitophorous vacuoles ± SE per vacuole type, where the total number of counted vacuoles was normalized to 100% for each strain. Numbers of parasites per parasitophorous vacuole were analyzed with a two-factor ANOVA for $\alpha=0.05$. A total of three independent experiments were performed per assay, including three technical replicates per experiment.

3.5.1.3. Parasitophorous vacuole regularity assay

PV regularity assays were used to evaluate the degree to which tachyzoite replication is in line with the theoretical exponential 2^n replication. When analyzing the number of tachyzoites

in a PV, we considered the norm synchronous replication through endodyogeny, the generally accepted division process of *T. gondii* tachyzoites. This replication process implies a replication rate of 2^n, with n being the number of replication cycles, therefore the number of tachyzoites inside a PV is stratified by the number of cell cycles. PVs harboring a number of tachyzoites not compatible with the expected 2^n replication rate were designated as irregular. Assays were performed together with the replication assays. The number of parasites inside the parasitophorous vacuole was counted in at least five randomly chosen fields per coverslip using the 40x objective. Each PV was assigned to one of two classes: regular number, when the vacuole followed the expected 2^n progression (e.g. 4, 8, 16, 32), or irregular number, when the vacuole presented a tachyzoite number different from the expected. One and two tachyzoite vacuoles were not included in the count. Data are presented as mean percentage of the number of PVs ± SE per vacuole type, where the total number of counted vacuoles was normalized to 100% for each strain. Numbers of parasites per PV were analyzed with a two-factor ANOVA for α=0.05. A total of three independent experiments were performed per assay, including three technical replicates per experiment.

3.5.2. Bradyzoite conversion assay

Cell culture assays were used to assess the spontaneous formation of bradyzoite cysts. Parasites were inoculated according to the strains replication rate. For strains with a faster replication rate (diCre and morn1-FLAG-MOB1), $2x10^4$ freshly egressed parasites were inoculated. For strains with a slower replication rate (iGSoe, GSko, EGS, Eko), $4x10^4$ freshly egressed parasites were inoculated. Parasites were inoculated onto confluent HFF seeded on 24-well plates over glass coverslips and kept in standard culture conditions during 50 hours. At this point, the wells were washed twice with PBS (Gibco), fixed with ice-cold methanol (Fluka) during 20 minutes at -20 ºC, washed twice with PBS (Gibco) again and kept in PBS (Gibco) at 4 ºC until processed for immunofluorescence assays. Cells were stained with *Dolichos biflorus* agglutinin (DBA) lectin (Biotinylated, 1:500 dilution, Vector Laboratories), which presents a high affinity to the bradyzoite cyst wall, polyclonal sera for *T. gondii* surface proteins, and DAPI. The biotinylated DBA was detected with Alexa Fluor 488-conjugated streptavidin (1:500 dilution, Invitrogen). The DBA staining was performed was reported for antibody staining in section 3.6. The number of parasites inside the parasitophorous vacuole was counted in at least five randomly chosen fields per coverslip using the 20x objective. A total of three independent experiments were performed per assay, including three technical replicates per experiment.

3.5.3. Time course assay for qPCR analysis

Freshly egressed $9x10^6$ tachyzoites were inoculated onto confluent HFF cells in T-25 flasks and kept in standard culture conditions during 2 hours. At this point, the wells were washed with PBS (Gibco) to remove extracellular tachyzoites and fresh culture medium was added to the flasks. Flasks were processed for the recovery of total RNA at determined times after infection so as to follow the full course of infection. RH and RH based strains were sampled at 0 (extracellular, freshly egressed), 4, 24, 38 and 44 (extracellular, freshly egressed) hours. For the EGS strain, to obtain equivalent time points and follow the full course of infection, we increased the total time sampling that occurred at 0 (extracellular, freshly egressed), 4, 24, 42 and 54 (extracellular, freshly egressed) hours. To ensure that the final collection consisted of freshly egressed tachyzoites, the flasks were washed and new medium was added at 38 (RH) or 42 (EGS) hours post infection. A total of three independent experiments were performed per assay.

3.5.4. Biotinylation assays

Freshly egressed $2x10^7$ FLAG-BirA or FLAG-BirA-MOB1 tachyzoites were inoculated onto HFF confluent cells in T-75 flasks in DMEM GlutaMAX™ 1% FBS. Following 14 hours of host cell infection, biotin was added to a final concentration of 150 µM and incubated for 56 hours. At this point, tachyzoites had fully lysed the host cell monolayer and the culture medium was harvested to recover the parasites. The medium was centrifuged at 800 g for ten minutes. The resulting pellets were washed twice with PBS (Gibco) and centrifuged at 800 g for 10 minutes to obtain medium free parasite pellets. These were weighted and prepared for protein electrophoresis and precipitation. We prepared 10 T-75 flasks per *T. gondii* strain for one experiment in the first assay and 20 T-75 flasks per *T. gondii* strain per experiment, in a total of three independent experiments, in the second assay.

3.6. Immunofluorescence assays

Freshly egressed tachyzoites were inoculated onto confluent HFF seeded on 24-well plates over glass coverslips and kept in standard culture conditions during the assay appropriate time. At this point, the wells were washed twice with PBS (Gibco), fixed with ice-cold methanol (Fluka) during 20 minutes at -20 ºC, washed twice with PBS (Gibco) again and kept in PBS (Gibco) at 4 ºC until processed. Fluorescence staining was performed at room temperature. Fixed cells were incubated with the blocking solution, PBS (Gibco) 3% (w/v)

bovine serum albumin (BSA, Calbiochem), for 30 minutes. Primary and secondary antibodies were incubated with the preparations for one hour, diluted in blocking solution. Following primary and secondary antibodies incubation, the fixed cells were washed twice with PBS (Gibco). Before secondary antibodies' incubation, the preparations were washed with PBS (Gibco) 0.1% (v/v) Tween 20 (Merck). DNA staining with was achieved by assembling the coverslips on glass slides with DAPI Fluoromount-G Mounting Medium (SouthernBiotech). Slides were imaged through a Leica DMR microscope equipped with a Leica DFC340FX camera (CIISA BioImaging Unit) or an Andor Spinning Disk equipped with an Andor iXon+ 512 EMCCD camera (IGC Imaging and Cytometry Unit). Antibodies used for immunofluorescence assays are described in Table 13.

Table 13. Antibodies used for immunofluorescence.

Antibody	Species	Dilution	Source
polyclonal anti-*T. gondii* MOB1	mouse	1:100	in house
polyclonal anti-*T. gondii* TBCB	rabbit	1:100	in house
polyclonal anti-*T. gondii* surface proteins	cat	1:500	Helga Waap
polyclonal anti-*T. gondii* surface proteins	rabbit	1:2000	Andrew Hemphill
polyclonal anti-*T. gondii* CenH3 (50% glycerol)	rabbit	1:50	Boris Striepen
polyclonal anti-*T. gondii* IMC1	rabbit	1:500	Andrew Hemphill
anti-Ndc80	mouse	1:1500	Marc Jan Gubbels
anti-Myc	mouse	1:200	Sigma
anti-GFP	mouse	1:100	Roche
anti-FLAG	mouse	1:200	Sigma
anti-polyglutamylation modification GT335	mouse	1:200	Adipogen
Alexa Fluor 594-conjudated anti-mouse IgG	goat	1:500	Invitrogen
Alexa Fluor 594-conjudated anti-rabbit IgG	chicken	1:500	Invitrogen
Alexa Fluor 488-conjudated anti-mouse IgG	goat	1:500	Invitrogen
Alexa Fluor 488-conjudated anti-rabbit IgG	donkey	1:500	Invitrogen
FITC-conjugated anti-cat	goat	1:500	Helga Waap

3.7. Protein molecular biology

3.7.1. Protein quantification

Soluble proteins were quantified through the Bio-Rad protein microassay for low protein concentrations using the Bradford reagent and adapted from the Bradford dye-binding method. A quantification solution was prepared at the moment by diluting the Bradford reagent stock solution 1:5 in distilled H_2O. The quantification solution mixed with 1.0 µl of soluble protein for 1.0 ml of solution per sample to quantify. For the control, 1.0 µl of lysis buffer was added to 1.0 ml of solution. Mixed samples were allowed to incubate at room temperature for 15 minutes. Following incubation, the samples' absorbance was measured at 595 nm using a 1.5 ml cuvette adapted to the NanoDrop 2000c spectrometer (Thermo Scientific). The absorbance values were used to calculate protein concentration values according to a protein standard curve set with known BSA concentrations.

3.7.2. Protein extracts and electrophoresis

Protein extracts were prepared from freshly egressed parasites from one T-25 flask. Parasites were centrifuged at 800 g for 10 minutes. The pellet was transferred to 2.0 ml tubes and washed twice with PBS (Gibco). Parasites were lysed in 100 µl of sucrose based lysis buffer [250 mM sucrose (Sigma-Aldrich), 100 mM NaCl (Merck), 50 mM 4-(2-hydroxyethyl)-1-piperazineethanesulfonic acid (HEPES, Sigma-Aldrich) pH 7.6, 2 mM ethylenediaminetetraacetic acid (EDTA, Bio-Rad), 0.1% (v/v) Triton X-100 (Sigma-Aldrich), 1x Halt Protease and Phosphatase Inhibitor Cocktail EDTA-free (Thermo Scientific)] and centrifuged at 16000 g for 20 minutes at 4 ºC. The soluble fraction was transferred to a new tube and quantified by the Bradford Protein assay. Following protein quantification, the soluble fraction was prepared for gel electrophoresis by addition of 25 µl of 5x protein loading buffer [250 mM Tris-HCl pH 6.8 (Calbiochem), 30% (v/v) glycerol (Invitrogen), 16% (v/v) β-mercaptoethanol (Sigma-Aldrich), 4% (w/v) sodium dodecyl sulphate (SDS, Bio-Rad), 0.2% (w/v) bromophenol blue]. The insoluble fraction was resuspended in 62.5 µl of urea 8 M (Sigma-Aldrich) and 62.5 µl of 2x protein loading buffer [125 mM Tris-HCl pH 6.8 (Calbiochem), 20% (v/v) glycerol (Invitrogen), 10% (v/v) β-mercaptoethanol (Sigma-Aldrich), 4% (w/v) SDS (Bio-Rad), 0.2% (w/v) bromophenol blue]. The samples were heated at 100 ºC for 10 minutes. Polyacrylamide mini-gels (7x8x0.15cm^3) were loaded with 50 µg of each sample. The polyacrylamide mini-gels included a 5% stacking gel and a 10%, 12% or 15% resolving gel for

SDS polyacrylamide gel electrophoresis (SDS-PAGE), prepared according to Table 14. The gels were run in electrophoresis buffer [192 mM glycine (Merck), 25 mM Tris-Base (Calbiochem), 0.1% (w/v) SDS (Bio-Rad)] at 20-25 mAmp per gel. Following protein migration, the gels were transferred to a nitrocellulose membrane or stained. Proteins were transferred to a Amersham Protran nitrocellulose membrane (0.45 µm, GE Healthcare) in transfer buffer [192 mM glycine (Merck), 25 mM Tris-Base (Calbiochem), 10% (v/v) methanol (VWR)] at 30 V overnight using a wet Mini Trans-Blot transfer system (Bio-Rad). Membranes were stained with Ponceau S solution (Sigma-Aldrich) to confirm the success of the protein transfer process. Stained membranes were captured in the imager ChemiDoc XRS+ (BioRad). After imaging, the Ponceau S stain was washed in PBS [137 mM NaCl (Merck), 2.68 mM KCl (Merck), 8.10 mM Na2HPO4 * 2H2O (Fluka), 1.75 mM KH2PO4 (Merck)].

For BioID assays, an alternative lysis method was also tested in parallel to the described above. Freshly egressed parasites were counted and the same amount of parasites was centrifuged at 800 g for 10 minutes for each strain to be analyzed. The pellet was transferred to 2.0 ml tubes and washed twice with PBS (Gibco). Parasites were lysed in 100 µl of RIPA buffer [50 mM Tris-HCl pH 8.0 (Calbiochem), 150 mM NaCl (Merck), 2 mM EDTA (Bio-Rad), 1% (v/v) NP-40 Alternative (Calbiochem), (v/v) 0.5% (w/v) sodium deoxycholate (Sigma-Aldrich), 0.1% (w/v) SDS (Bio-Rad), 1x Halt Protease and Phosphatase Inhibitor Cocktail EDTA-free (Thermo Scientific)] and centrifuged at 16000 g for 20 minutes at 4 ºC. Protein extracts were prepared for gel electrophoresis and subsequent procedures as previously described.

Table 14. Preparation of mini-gels for SDS-PAGE.

Components	Stock solutions	Stacking	Resolving
Acrylamide/bis-acrylamide 29:1 (VWR)	40% (w/v)	5%	10%, 12% or 15%
Tris-HCl (Calbiochem)	1 M pH 6.8	62.5 mM	_
Tris-HCl (Calbiochem)	1.5 M pH 8.8	_	375 mM
SDS (Bio-Rad)	20% (w/v)	0.1%	0.1%
TEMED (Sigma-Aldrich)	_	0.1%	0.05%
APS (Bio-Rad)	10% (w/v)	0.1%	0.05%

3.7.3. Protein gel staining

3.7.3.1. BlueSafe stain

Following protein migration through SDS-PAGE, mini-gels were stained using the single step BlueSafe stain following the manufacturer's instructions. Proteins were stained by immersion of a mini-gel in 25 ml of BlueSafe stain for approximately one hour. At this point, the stain was removed and the mini-gel was washed briefly in distilled water to remove excess stain. Stained mini-gels were captured in the imager ChemiDoc XRS+ (BioRad).

3.7.3.2. Copper stain

Following protein migration through SDS-PAGE, polyacrylamide gels were immersed in a CuCl2 (300 mM, Merck) solution using a plastic container. The gels were incubated at room temperature using an orbital shaker (GyroTwister) at 45 rpm during five minutes. After incubation, the gels were washed in distilled water for two minutes. This method produces negative stain of colorless proteins against a colored background which can be visualized with a white light (Lee et al. 1987).

3.7.4. Western blot

Membranes were incubated with blocking solution [PBS 5% (w/v) Molico skimmed milk (Nestlé)] overnight at 4 ºC. After blocking, membranes were probed with a primary antibody, diluted in blocking solution, during one hour with orbital shaking at room temperature, followed by three wash steps with PBS 0.1% (v/v) Tween 20 (Merck) for 10 minutes and one rinse step in blocking buffer to remove residual Tween 20. Membranes were then probed with a horseradish peroxidase (HRP) labelled secondary antibody, diluted in blocking solution, during one hour with orbital shaking at room temperature, followed by three wash steps with PBS for 10 minutes. HRP was detected with Amersham ECL Prime Western Blotting Detection Reagent (GE Healthcare) according to the manufacturer's instructions, in the imager ChemiDoc XRS+ (BioRad). Alternatively, the signal acquisition was performed mannualy using Amersham Hyperfilm ECL (GE Healthcare) sheets and D-19 Developer and Fixer Carestream Processing Chemicals (Kodak). Antibodies used for western blot are described in Table 15.

Table 15. Antibodies used for western blot.

Antibody	Species	Dilution	Source
polyclonal anti-*T. gondii* MOB1	mouse	1:1000	in house
polyclonal anti-*T. gondii* TBCB	rabbit	1:1000	in house
polyclonal anti-*B. besnoiti* PDI	rabbit	1:5000	in house
anti-Myc	mouse	1:2000	Sigma
anti-GFP	mouse	1:1000	Roche
anti-FLAG	mouse	1:2000	Sigma
HRP-conjugated anti-rabbit IgG	goat	1:1000	Invitrogen
HRP-conjugated anti-mouse IgG	goat	1:5000	Jackson ImmunoResearch

3.7.4.1. Biotinylation detection

Membranes were incubated with blocking solution [PBS 2.5% (w/v) BSA (NZYTech), 0.4% (v/v) Triton X-100 (Sigma-Aldrich)] overnight at 4 ºC. After blocking, membranes were probed with Streptavidin-HRP, diluted in blocking solution (1:50.000), during one hour with orbital shaking at room temperature, followed by three wash steps with PBS 10 minutes. HRP was detected with Amersham ECL Prime Western Blotting Detection Reagent (GE Healthcare) according to the manufacturer's instructions, in the imager ChemiDoc XRS+ (BioRad).

3.8. Anti-MOB1 sera production

GST-MOB1 was produced by expression of *pGEX4T.2-Mob1* in *E. coli* Rosetta(DE3)pLysS following the protocol previously used to obtain the anti-MOB1 mouse sera (Tavares 2015). Protein expression was induced with isopropyl β-D-1-thiogalactopyranoside (IPTG, NZYTech) during 3 hours. Bacteria were collected through centrifugation and lysed. GST-MOB1 was isolated through acrylamide gel electrophoresis. Following electrophoresis, the protein was visualized using the negative stain copper chloride (300 mM, Merck) for gel band excision. GST-MOB1 was purified through electroelution in a dialysis membrane (cut-off 10 kDa) and using dialysis buffer [Tris 20mM (Calbiochem), glycine 150 mM, 0.01% (w/v) SDS (Bio-Rad)]. The resulting purified protein was quantified using the Bradford reagent and inoculated in five Balc/c mice: 50 µg of GST-TgMOB1 + saponin adjuvant in two injection sites subcutaneously, repeated twice with two weeks interval between each inoculation, sacrifice of the mice and retrieval of total serum one week after the third inoculation. Mice inoculation and

sera recovery steps were performed at Andrew Hemphill's laboratory (Institute of Parasitology, Vetsuisse Faculty, University of Bern).

3.9. BioID precipitation and mass spectrometry analysis

3.9.1. First assay

FLAG-BirA and FLAG-BirA-MOB1 tachyzoites grown in 10 T-75 flasks produced pellets weighing around 50 mg which were lysed in 2 ml of sucrose based protein lysis buffer. About 8 mg of soluble protein extracts (2 ml) were incubated with 100 µl of pre-washed agarose-streptavidin beads (equivalent to 200 µl of resin) in 1.5 ml protein low-bind tubes (5 tubes per strain) overnight at 16 ºC using an orbital shaker (GyroTwister) at 45 rpm. Following binding, beads were washed 5 times with lysis buffer and 3 times with 8M urea. For each washing step, beads were centrifuged at 2500 g for 10 minutes. Urea buffer was removed with a syringe and beads were boiled in 2x SDS loading buffer for 20 minutes. 2x SDS loading buffer was added so it completely covered the bead pellet. The eluates were collected by syringe, which resulted in a final volume of ~370 µl of eluted proteins per strain. 1 µl of each sample was loaded onto a 10% gel for SDS-PAGE and transferred to a nitrocellulose membrane to confirm the success of the precipitation. Eluates were run in 5% SDS gels in duplicate (165 µl per well) for 15 minutes at 20 mAmp/gel so that the full samples entered the gel. Gel bands were cut and stored at 4 ºC in Milli-Q water in protein low-bind tubes until the mass-spectrometry analysis which was performed by the proteomics service UniMS (ITQB-UNL, Oeiras, Portugal).

Samples were subjected to trypsin in-gel digestion coupled with mass spectrometric analysis (GeLC-MS/MS). Each strain was analyzed in technical duplicates. Briefly, protein sample was reduced with 10 mM DTT (Sigma) for 40 min at 56 ºC followed by alkylation with iodoacetamide (Sigma) 55 mM for 30 min in the dark. Excessive iodoacetamide was quenched by further incubation with DTT (10 mM for 10 min in the dark). The resulting sample was digested overnight with trypsin (Proteomics grade from Promega) at 37 ºC (1:50 protein/trypsin ratio), dried and resuspended in 8 µL LCMS water 0.1% formic acid (Fisher Chemicals). Nano-liquid chromatography-tandem mass spectrometry (nanoLC-MS/MS) analysis was performed on an ekspert NanoLC 425 cHiPLC system coupled with a TripleTOF 6600 with a NanoSpray III source (Sciex). Peptides were separated through reversed-phase chromatography (RP-LC) in a trap-and-elute mode. Trapping was performed at 2 µl/min on a Nano cHiPLC Trap column (Sciex 200 µm x 0.5 mm, ChromXP C18-CL, 3 µm, 120 Å) with 100% A for 10 min. Separation was performed at 300 nl/min, on a Nano cHiPLC column (Sciex 75 µm x 15 cm, ChromXP C18-

CL, 3 µm, 120 Å). The gradient was as follows: 0-1 min, 5% B (0.1% formic acid in acetonitrile, Fisher Chemicals, Geel, Belgium); 1-91 min, 5-30% B; 91-93 min, 30-80% B; 93-108 min, 80% B; 108-110 min, 80-5% B; 110-127 min, 5% B. Peptides were sprayed into the MS through an uncoated fused-silica PicoTip emitter (360 µm O.D., 20 µm I.D., 10 ± 1.0 µm tip I.D., New Objective, Oullins, France). The source parameters were set as follows: 15 GS1, 0 GS2, 30 CUR, 2.5 keV ISVF and 100 ºC IHT. An information dependent acquisition (IDA) method was set with a TOF-MS survey scan of 400-2000 m/z. The 50 most intense precursors were selected for subsequent fragmentation and the MS/MS were acquired in high sensitivity mode for 40 msec. The obtained spectra were processed and analyzed using ProteinPilot software, with the Paragon search engine (version 5.0, Sciex). A TrEMBL database (127701 entries, accessed in 08-01-2019) containing the sequences of the proteins from the *T. gondii* (Taxon ID: 5811) was used. The following search parameters were set: Iodoacetamide, as Cys alkylation; Trypsin, as digestion; TripleTOF 6600, as the Instrument; ID focus as biological modifications and Amino acid substitutions; search effort as thorough; and a FDR analysis. Only the proteins with Unused Protein Score above 0.45 and 66% confidence were considered. The analysis is the result of two replicate analyses of one experiment.

3.9.2. Second assay

FLAG-BirA and FLAG-BirA-MOB1 tachyzoites grown in 20 T-75 flasks produced pellets weighing around 200 mg which were lysed in 3 ml of protein lysis buffer, to a ratio of approximately 1:15 (w/v). About 24 mg of soluble protein (3 ml) were incubated with 275 µl of pre-washed beads agarose-streptavidin beads (equivalent to 550 µl of resin) overnight at room temperature (approximately 16 ºC) in 50 ml centrifuge tubes using an orbital shaker (GyroTwister) at 45 rpm. Following binding, beads were washed twice with 4 ml of lysis buffer followed by centrifugation at 2000 g for 5 minutes. Next, the beads were washed three times with 15 ml of PBS (Gibco) and centrifuged at 3220 g for 5 minutes. 10% of the bead volume was separated for assay analysis. After the final centrifugation step, the PBS was removed using a needle and syringe before storage at -35 ºC. The frozen agarose beads were sent for mass-spectrometry analysis to be performed by the i3S Proteomics Scientific Platform (Porto, Portugal).

Each sample was reduced and alkylated and processed for proteomics analysis following the solid-phase-enhanced sample-preparation (SP3) protocol as described in PMID30464214. Enzymatic digestion was performed with Trypsin/LysC (2 µg) overnight at 37 ºC at 1000 rpm. Protein identification and quantitation was performed by nanoLC-MS/MS.

This equipment is composed by an Ultimate 3000 liquid chromatography system coupled to a Q-Exactive Hybrid Quadrupole-Orbitrap mass spectrometer (Thermo Scientific). Samples were loaded onto a trapping cartridge (Acclaim PepMap C18 100Å, 5 mm x 300 µm i.d., 160454, Thermo Scientific) in a mobile phase of 2% ACN, 0.1% FA at 10 µl/min. After 3 min loading, the trap column was switched in-line to a 50 cm by 75 µm inner diameter EASY-Spray column (ES803, PepMap RSLC, C18, 2 µm, Thermo Scientific) at 250 nl/min. Separation was generated by mixing A: 0.1% FA, and B: 80% ACN, with the following gradient: 5 min (2.5% B to 10% B), 120 min (10% B to 30% B), 20 min (30% B to 50% B), 5 min (50% B to 99% B) and 10 min (hold 99% B). Subsequently, the column was equilibrated with 2.5 % B for 17 min. Data acquisition was controlled by Xcalibur 4.0 and Tune 2.9 software (Thermo Scientific). The mass spectrometer was operated in data-dependent (dd) positive acquisition mode alternating between a full scan (m/z 380-1580) and subsequent HCD MS/MS of the 10 most intense peaks from full scan (normalized collision energy of 27%). ESI spray voltage was 1.9 kV. Global settings: use lock masses best (m/z 445.12003), lock mass injection Full MS, chrom. peak width (FWHM) 15s. Full scan settings: 70k resolution (m/z 200), AGC target 3e6, maximum injection time 120 ms. dd settings: minimum AGC target 8e3, intensity threshold 7.3e4, charge exclusion: unassigned, 1, 8, >8, peptide match preferred, exclude isotopes on, dynamic exclusion 45s. MS2 settings: microscans 1, resolution 35k (m/z 200), AGC target 2e5, maximum injection time 110 ms, isolation window 2.0 m/z, isolation offset 0.0 m/z, spectrum data type profile.

The raw data was processed using Proteome Discoverer 2.4.0.305 software (Thermo Scientific) and searched against the ToxoDB-46_TgondiiME49 database. The Sequest HT search engine was used to identify tryptic peptides. The ion mass tolerance was 10 ppm for precursor ions and 0.02 Da for fragment ions. Maximum allowed missing cleavage sites was set 2. Cysteine carbamidomethylation was defined as constant modification. Methionine oxidation and protein N-terminus acetylation were defined as variable modifications. Peptide confidence was set to high. The processing node Percolator was enabled with the following settings: maximum delta Cn 0.05, decoy database search target FDR 1%, validation based on q-value. Protein label free quantitation was performed with the Minora feature detector node at the processing step. Precursor ions quantification was performing at the consensus step with the following parameters: Peptides to use unique plus razor, precursor abundance was based on intensity, normalization mode was based on total peptide amount, pairwise protein ratio calculation, hypothesis test was based on t-test (background based). The analysis is the result of three independent experiments.

3.10. Media supplements

T. gondii selection drugs were prepared for regular use. Xanthine and mycophenolic acid were both prepared as 500x stock solutions. Xanthine (Sigma-Aldrich) was diluted in 1 M potassium hydroxide (Merck) to a concentration of 20 mg/ml. The stock solution was kept in 100 µl aliquots at -20 ºC. Mycophenolic acid (Sigma-Aldrich) was diluted in methanol (Fluka) to a concentration of 12.5 mg/ml. The stock solution was kept at -20 ºC. Pyrimethamine and chloramphenicol were prepared as 1000x stock solutions. Pyrimethamine was diluted in ethanol to a concentration of 1 µM. The stock solution was kept at -20 ºC. Chloramphenicol was diluted in ethanol to a concentration of 20 µM. The stock solution was kept at -20 ºC.

The ligand Shield1 (0.5 mM, Clontech) was kept as a stock solution at -20 ºC.

Rapamycin (Sigma-Aldrich) was prepared as a 1000x stock solution by dilution in DMSO (Sigma-Aldrich) to a concentration of 50 µM. The stock solution was kept at -20 ºC.

Biotin was prepared as a 10x stock solution by dilution in DMEM GlutaMAX™ to a concentration of 1.5 mM. The stock solution was kept at 4 ºC and used in a maximum of one month after preparation.

Ampicillin (NZYTech) was prepared as a 1000x stock solution by dilution in Milli-Q water to a concentration of 100 mg/ml. Isopropyl β-D-1-thiogalactopyranoside (IPTG) was prepared as a 1000x stock solution by dilution in Milli-Q water to a concentration of 1 M.

All stock solutions were filter sterilized with a 0.22 µm pore membrane after dilution.

3.11. Bioinformatics and statistical analysis

Sequence analysis was performed using the Multalin interface (Corpet 1988) and the BioEdit sequence alignment editor (Hall 1999). Homology inference and functional categorization was based on the aggregated information from various sources: NCBI blastp, gene ontology terms (available on ToxoDB, Uniprot, and/or InterPro), the InterProScan resource (www.ebi.ac.uk/Tools/pfa/iprscan/), the ScanProsite tool (prosite.expasy.org/scanprosite/), and literature review. The functional analysis categories were based on the FunCat a functional annotation scheme (Ruepp et al. 2004). The expected subcellular localization was determined using the Hyper LOPIT Global mapping of protein subcellular location data set available on ToxoDB.org (Barylyuk et al. 2020), gene ontology terms, and literature review. Network analysis was performed using the STRING database (Szklarczyk et al. 2019).

Statistical analysis was performed using R (R_Core_Team 2017). The data was processed for statistical analysis and data visualization using the Microsoft Excel spreadsheet application.

Chapter 4. Results

4.1. *Mob1* knockout studies indicate a function in the regulation of tachyzoite replication and tachyzoite to bradyzoite transition

Taking into account the described functions of MOB1 proteins in several organisms and the data previously obtained by our group regarding the *T. gondii* MOB1, we hypothesized that MOB1, the most conserved member of the MEN/SIN/Hippo signaling pathways, is essential for the *T. gondii* life cycle regulating the parasite's replication process and number control. We developed *Mob1* knockout strains in order to assess this hypothesis.

4.1.1. Part of the tachyzoites presented abnormal replication following Cas9 activity

Following isolation of the iC (inducible *Mob1* splitCas9) strains expressing sgRNA1, sgRNA2, or sgRNA3, we activated the splitCas9 to obtain functional knockouts for *Mob1*, the Cko strains. After induction of splitCas9 activity, we documented a failure in replication simultaneous with a normally replicating pattern in the same clonal line (Figure 20). Part of the parasite population was not dividing properly while the rest of the population maintained an apparently normal division process. These parasites presented enlarged, aberrant nuclei and abnormal cellular morphology, suggesting a continued nuclear multiplication without nuclear division or cytokinesis. After the first lytic cycle, the abnormal replication phenotype was no longer present in the parasite population as its failure to divide is incompatible with egress and re-invasion. This phenotype was present after activation of splitCas9 activity in Cko tachyzoites expressing the three *Mob1* sgRNAs. The rate of abnormal tachyzoites was variable between induced iC clonal lines but did not appear to be related to the gRNA being expressed.

In order to verify that the splitCas9 system was functioning properly and to assess if both the populations identified were a *Mob1* functional knockout, we proceeded to amplify and sequence the sites of gRNA annealing with the *Mob1* locus. Non-induced iC tachyzoites were compared to the two subpopulations of induced iC tachyzoites: free parasites present in the medium (normally replicating) and parasites that failed host cell egress scraped from the bottom of the flasks (abnormally replicating), after full lysis of the cell monolayer by the normal parasites (Figure 21). We verified that the *Mob1* locus had been modified at the expected nucleotides for each of the three expressed gRNAs in both parasite subpopulations. Thus, our initial assessment was that both subpopulations (normally and abnormally replicating tachyzoites) were *Mob1* functional knockouts. We considered the abnormal replication phenotype to be a consequence of MOB1 depletion as it is consistent with MOB1 depletion phenotypes in other

protozoans (Hammarton et al. 2005; Tavares et al. 2012) and in multicellular eukaryotes (Galla et al. 2011; Florindo et al. 2012; Bae et al. 2018). However, at the time we were obtaining our transgenic lines, Markus Meissner's Laboratory was also using the splitCas9 system to knockout various genes in *T. gondii*. The Meissner group detected a cytotoxicity phenotype in the study of several genes when employing Cas9, characterized by nuclear and cellular morphology compromise, with varying rates of affected tachyzoites that could be as high as 65%. This repeated phenotype for various genes, similar to what we detected, prompted the Meissner group to assess if it was solely a consequence of the genes' knockout or if it was also related to the splitCas9 system as the cytotoxic effect was present only following splitCas9 activation during the parasites' first lytic cycle. Comparing different knockout systems for the same gene, the Meissner group concluded that the cytotoxicity phenotype was related to the Cas9 activity, most likely due to a failure to repair the DSBs caused by the Cas9, justifying its occurrence limited to the first lytic cycle.

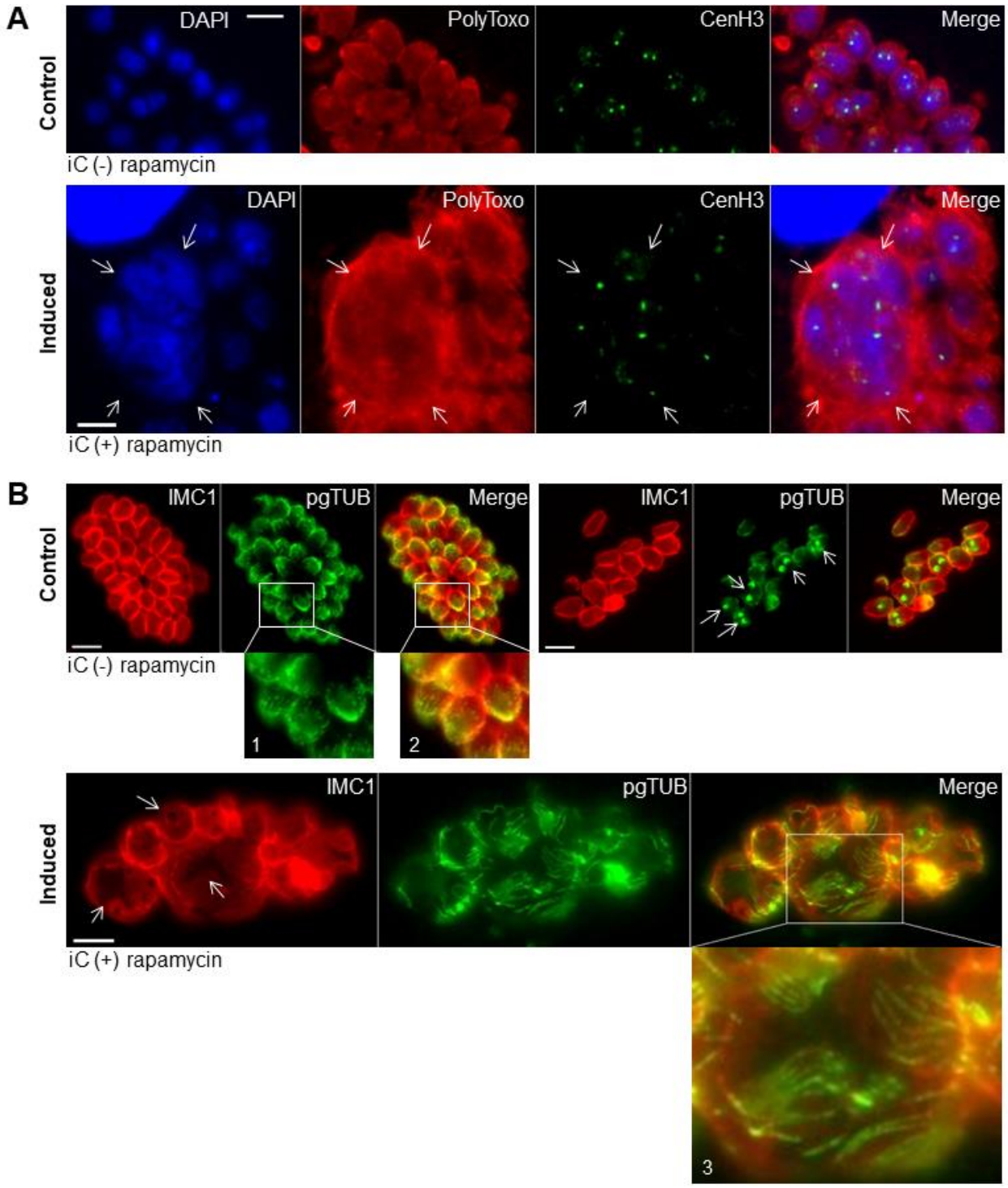

Figure 20. An abnormal replication phenotype is observed after splitCas9 activation.

Following activation of splitCas9 of iC tachyzoites, we observed two separate populations: one presented an apparently normal division process (similar to control tachyzoites) while the other presented an abnormal replication phenotype. The abnormal replication phenotype tachyzoites were analyzed by immunofluorescence assay at 24 to 96 hours following splitCas9 activation. Images presented here correspond to 48 hours after host cell infection and splitCas9 activation. **A)** Immunofluorescence assay staining *T. gondii* surface proteins with polyclonal sera

(PolyToxo), centromeric H3 variant proteins (CenH3) and DNA (DAPI). The induced tachyzoites present enlarged, aberrant nuclei and abnormal cellular morphology (arrows). The presence of 3 or more centromeres (stained with CenH3) per nucleic mass suggests a continued nuclear multiplication without nuclear division or cytokinesis. **B)** Immunofluorescence assay staining the inner membrane complex 1 (IMC1) and polyglutamylated tubulin (pgTUB). The left control panel shows the position of the glutamylated microtubules preferentially the apical pole of the parasite, with pgTUB staining the apical complex and subpellicular microtubules and functioning as a *T. gondii* polarity marker (see details 1 and 2). The control right panel shows pgTUB accumulating at the apical poles of the forming daughter cells in tachyzoites going through endodyogeny (arrows). The induced tachyzoites present enlarged and abnormal cellular morphology. IMC1 present large areas of discontinuity (arrows). The tubulin cytoskeleton is also altered with glutamylated microtubules presenting in decreased number with a disorganized pattern and increased thickness (see detail 3). Scale bars represent 5 µm.

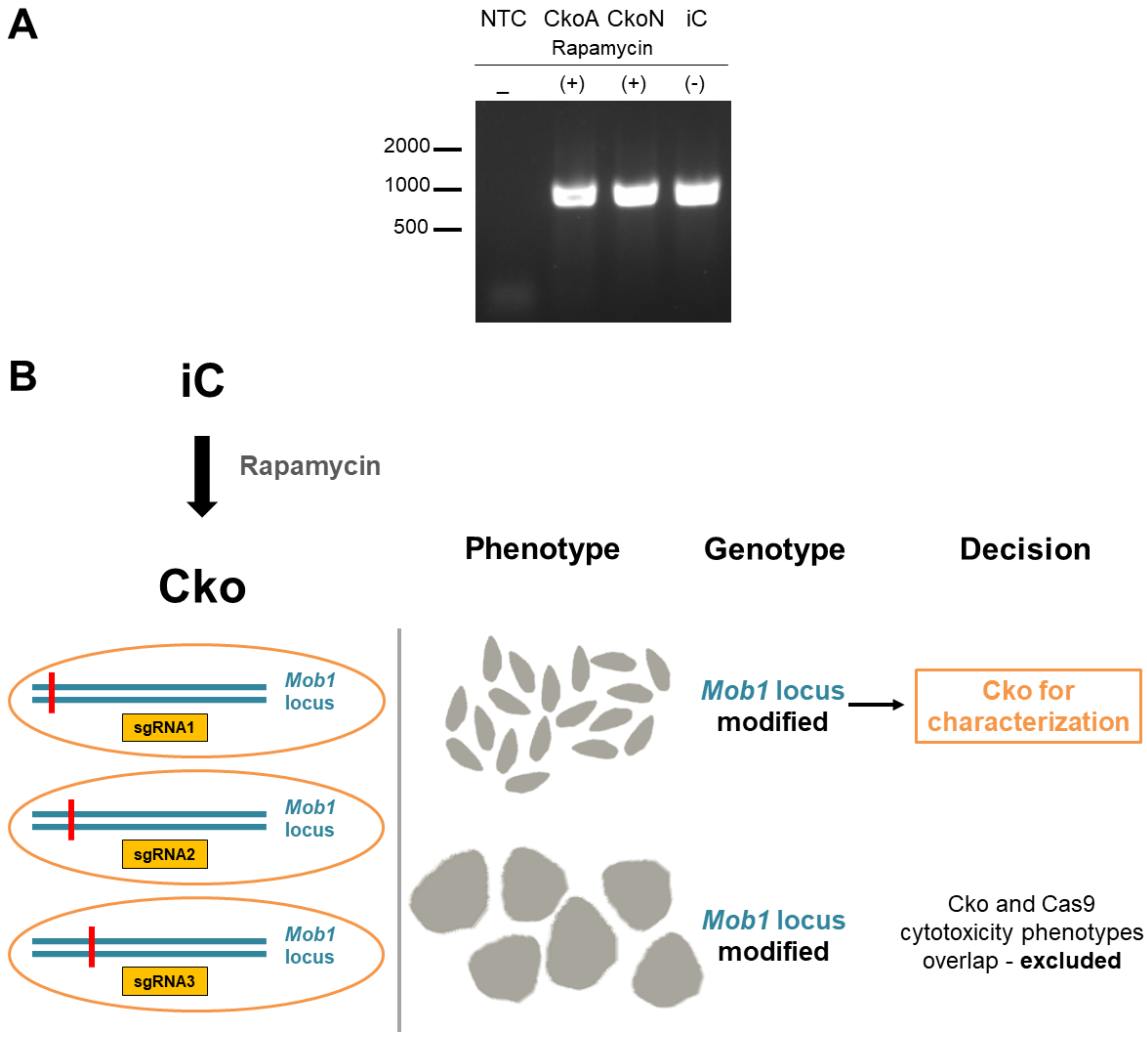

Figure 21. Cko tachyzoites presented two subpopulations following splitCas9 activity.

After activation of splitCas9, we documented an abnormal replication in part of the parasite population, while the rest of the population maintained an apparently normal division process. **A)** Genomic DNA was used to amplify the *Mob1* target region, where the Cas9 activity was expected. Numbers on the left represent molecular weight in bp. NTC –

non-template control; CkoA – *Mob1* functional knockout tachyzoites presenting abnormal replication; CkoN – *Mob1* functional knockout presenting normal replication; iC – inducible *Mob1* splitCas9 (non-induced control) **B)** Sanger sequencing showed that the *Mob1* locus was modified in both subpopulations of Cko tachyzoites. Taking into account the data collected by our group and the Meissner group, we concluded that the Cko tachyzoites with normal replication are the most appropriate parasites to study the effect of *Mob1* knockout. The red lines represent the location of Cas9 activity for each sgRNA. iC – inducible *Mob1* splitCas9; Cko – *Mob1* functional knockout; sgRNA – single guide RNA

In our study, the abnormal replication or cytotoxicity phenotype was also detected only during the first lytic cycle following splitCas9 activation, from around 12 hours after exposure to rapamycin. The phenotype occurred even when the iC tachyzoites were exposed to rapamycin for only four hours. Tachyzoites exposed to rapamycin for at least five passages did not continue to present this phenotype after the first lytic cycle. Also, tachyzoites re-exposed to rapamycin after two drug-free passages did not show any replication problems. This was assessed for clonal lines expressing the three *Mob1* sgRNAs. Our group also employed the splitCas9 system to knockout the *T. gondii Tbcb* gene. *Tbcb* functional knockout tachyzoites presented impaired invasion and replication, with a reduced proliferation rate and altered division axis (Francisco 2019). The cellular masses of *Mob1* and *Tbcb* functional knockout tachyzoites appear to be morphologically distinct. Furthermore, TBCB proved to be an essential protein with *Tbcb* functional knockout tachyzoites losing viability after 2 passages. Therefore and taking into account the data from our group and the Meissner group, we concluded that the abnormal replication phenotype that we initially attributed to MOB1 depletion is the result of Cas9 cytotoxicity during the first lytic cycle, likely due to DSBs repair failure, the hypothesis put forward by the Meissner group. Although the sequencing results indicated that both normally and abnormally replicating tachyzoite subpopulations had an altered genome, the amplification detected in the abnormal replication fraction could be due to contamination by normal replicating tachyzoites, despite our efforts to separate both subpopulations before gDNA extraction. It is noteworthy to state that we did not detected evidence of wild type genomes in any of the Cko subpopulations. Hence, the available evidence indicates that the abnormally replicating tachyzoites are *Mob1* functional knockouts and accumulate the Cas9 cytotoxicity phenotype while the normally replicating tachyzoites are *Mob1* functional knockouts with no confounding phenotype (Figure 20). This made us select the normally replicating tachyzoites as the most appropriate subpopulation to study the effects of *Mob1* knockout.

4.1.2. *Mob1* functional knockout tachyzoites are viable and present a slight increase in the replication rate

Contrary to expectations, Cko (*Mob1* splitCas9 functional knockout) tachyzoites are viable. This allowed us to isolate clonal lines from Cko tachyzoites expressing the three sgRNAs, characterize its *Mob1* genotype and select the clonal lines most compatible with MOB1 depletion. We used Sanger sequencing to identify the recombination event present in each clonal line and confirm that the clonal line was appropriately isolated and did not present more than one recombination type. We identified indels that occurred at the site directed by the gRNA, namely three nucleotides before the PAM: *Mob1* nucleotide 27 with gRNA1, nucleotide 175 with gRNA2, and nucleotide 208 with gRNA3 (Figures 21 and 22). Deletions ranged from 1 to 4 nucleotides. Insertions ranged from 1 to 8 nucleotides, with varying nucleotides or nucleotide combinations being inserted. Only one substitution event was detected, of a single nucleotide. The most frequent events were single or two nucleotide indels. We did not detect endogenous *Mob1* in any of the characterized clonal lines. The recombination events detected at the gDNA level were also present at the RNA level. Most recombination events detected resulted in predicted protein sequence compatible with a presumably inactive protein caused by disruption of the open reading frame and presence of a premature Stop codon (Figures 21 and 22). To study the effect of *Mob1* knockout, we selected Cko clonal lines harboring a maximum protein disruption for each gRNA. From the sgRNA1 clonal lines, we selected a clonal line that suffered a ‘TA’ deletion (Figure 22, dTA). From the sgRNA2 and sgRNA3 clonal lines, we selected a clonal line that suffered an ‘A’ and ‘T’ insertion, respectively (Figure 23). While endogenous MOB1 presents a predicted molecular weight of 35 kDa, the selected Cko strains expressing the *Mob1* sgRNA1, sgRNA2, and sgRNA3 are predicted to express truncated proteins with 4.1 kDa, 10.5 kDa, and 10.6 kDa respectively. The characterized *T. gondii* clonal lines expressing *Mob1* sgRNA1, which were more extensively characterized, are presented in Figure 22. The characterized clonal lines expressing *Mob1* sgRNA2 and sgRNA3 presented similar recombination events to those presented for sgRNA1.

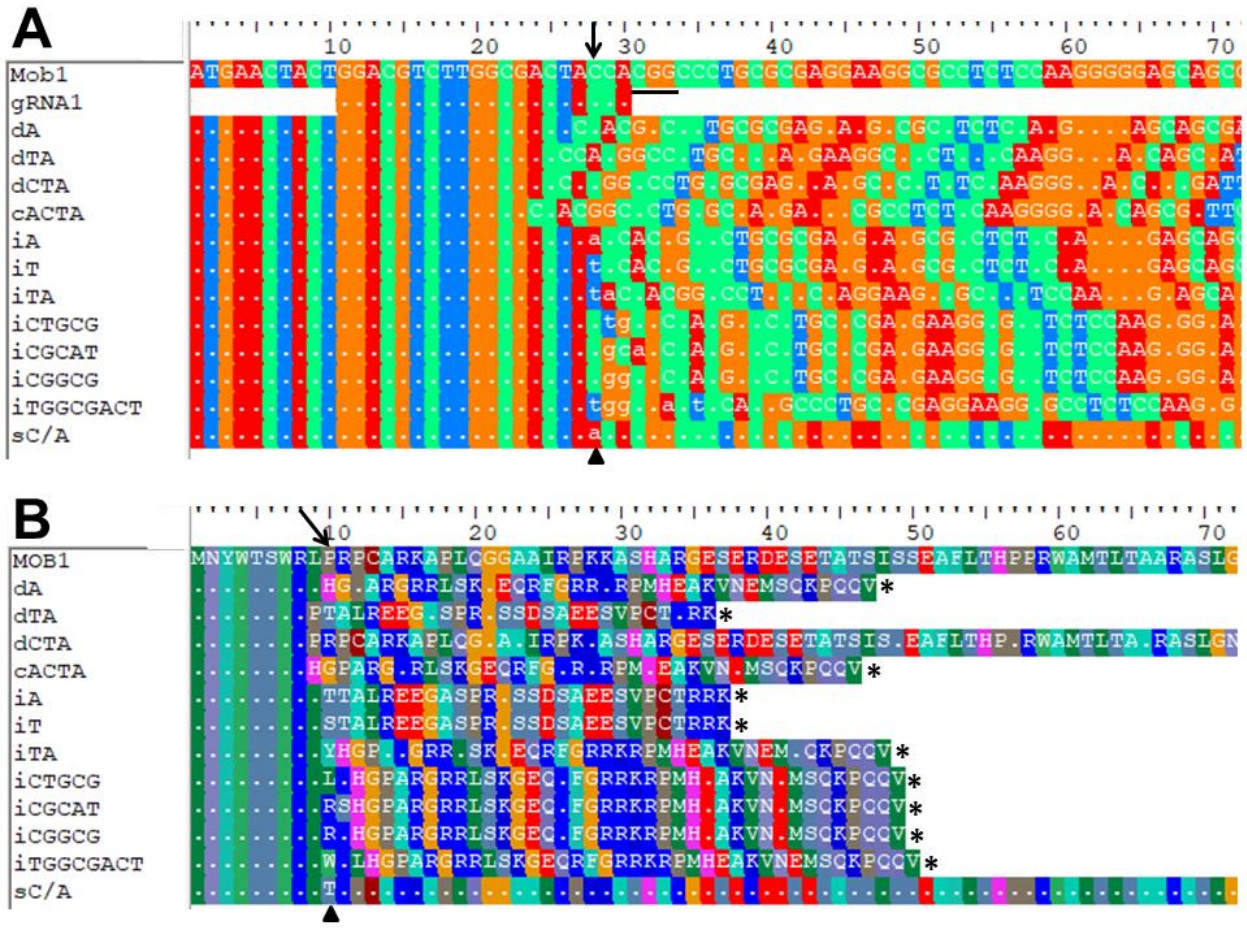

Figure 22. Genotypic characterization of Cko sgRNA1 clonal lines.

The characterized *T. gondii* clonal lines expressing *Mob1* sgRNA1 are presented. *Mob1*/MOB1 endogenous sequences are presented in comparison to the sequences resulting from the diversity of recombination events that were detected. Each event type is designated by “d”, “i” or “s”, indicating if a deletion, an insertion, or a substitution occurred, respectively, followed by the nucleotides that were inserted, deleted or substituted. **A)** Nucleotide sequences of endogenous *Mob1* (Mob1), *Mob1* gRNA1 target sequence (gRNA1) and *Mob1* of clonal lines expressing the *Mob1* sgRNA1 (12 bottom sequences). The arrow indicates the residue of expected Cas9 DSB. The PAM triplet ‘CGG’ associated to the *Mob1* gRNA1 is underlined in black. In sC/A the arrowhead highlights the substituted nucleotide, the only difference to the endogenous *Mob1* nucleotide sequence. **B)** Amino acid sequences of endogenous MOB1 (MOB1) and MOB1 of clonal lines expressing *Mob1* sgRNA1 (12 bottom sequences). The arrow indicates the residue of expected Cas9 DSB. In sC/A the arrowhead highlights the substituted nucleotide, the only difference to the endogenous MOB1 amino acid sequence. The asterisks indicate MOB1 recombinant amino acid sequences that present a premature Stop codon in comparison with the endogenous sequence. The clonal lines dCTA and sC/A are not considered Cko as the MOB1 sequence remains mostly unchanged. The numbers at the top represent the number of residues. The dots indicate the residue is similar to the one on the same position of the top sequence.

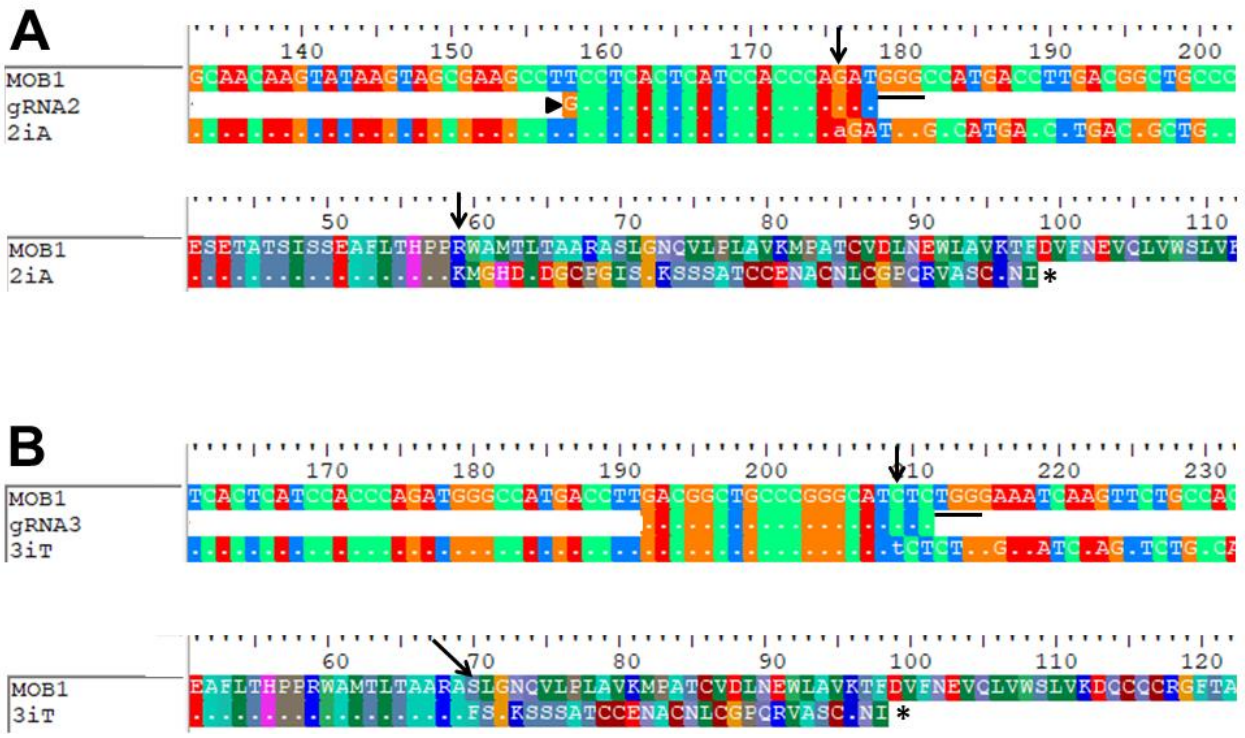

Figure 23. Genotypic characterization of selected Cko sgRNA2 and sgRNA3 clonal lines.

The selected *T. gondii* clonal lines expressing *Mob1* sgRNA2 and sgRNA3 are presented, which ensure a maximum disruption of the MOB1 protein. The top panel shows nucleotide sequences of endogenous *Mob1* (Mob1), the gRNA expressed by the clonal line and the recombinant *Mob1* (bottom sequence). The bottom panel shows the amino acid sequences of endogenous MOB1 (MOB1) and recombinant MOB1 (bottom sequence). Each event is designated by 2 or 3, according to the gRNA expressed by the clonal line, followed by "i", indicating an insertion occurred, and finally by the nucleotide that was inserted. The arrow indicates the residue of expected Cas9 DSB. The PAM triplet 'NGG' associated to the gRNA is underlined in black. The asterisk indicates the premature Stop codon present in the MOB1 recombinant amino acid sequence. **A)** Nucleotide and amino acid sequence of endogenous *Mob1*/MOB1 and selected Cko clonal line expressing the sgRNA2. The sequence targeted is designated by gRNA2. The arrowhead highlights a 'G' that was manually added to the gRNA2 target sequence and therefore does not align with the endogenous *Mob1* nucleotide sequence. **B)** Nucleotide and amino acid sequence of endogenous *Mob1*/MOB1 and selected Cko clonal line expressing the sgRNA3. The sequence targeted is designated by gRNA3. The numbers at the top represent the number of residues. The dots indicate the residue is similar to the one on the same position of the top sequence.

We detected no significant difference between iC and Cko strains in invasion efficiency, with F=1.682 and p=0.3241 (Figure 24.A). A significant difference was detected between the iC and Cko strains regarding replication efficiency, with F=19.77 and p<0.0001 (Figure 24.B). Cko tachyzoites present an increased replication rate compared to iC tachyzoites. *Post hoc* tests using the Tukey multiple comparisons of means identified significant differences between

strains within groups. While the iC strains presented significantly more vacuoles with 4 parasites (difference in means=-11.90 and adjusted p=0.0087), the Cko strains presented significantly more vacuoles with 8 parasites (difference in means=11.06 and adjusted p=0.0158) and with 16 or more parasites (difference in means=9.781 and adjusted p=0.0390). The difference between vacuoles with 2 parasites was not significant (difference in means=-8.94 and adjusted p=0.0695). We also evaluated the PV regularity by estimating the percentage of irregular vacuoles (number of tachyzoites per vacuole different from 2^n). We detected significantly higher irregular vacuoles in Cko tachyzoites (20.47%) when compared to iC tachyzoites (10.54%) with F=33.97 and p=0.0004 (Figure 24.C). *Post hoc* tests using the Tukey multiple comparisons of means identified significant differences between strains within the regular (2^n) and irregular classes (difference in means=9.925 and adjusted p=0.0142). The invasion, replication, and PV regularity assay data presented refer to iC and Cko tachyzoites expressing the sgRNA1. Analysis of clonal lines expressing the sgRNA2 and sgRNA3 presented the same replication and PV number regularity phenotypes as detected for sgRNA1 expressing tachyzoites (Annex I, Figures 1 and 2). This indicates that the phenotypes detected are specific to *Mob1* and not the result of an off-target effect of a single sgRNA.

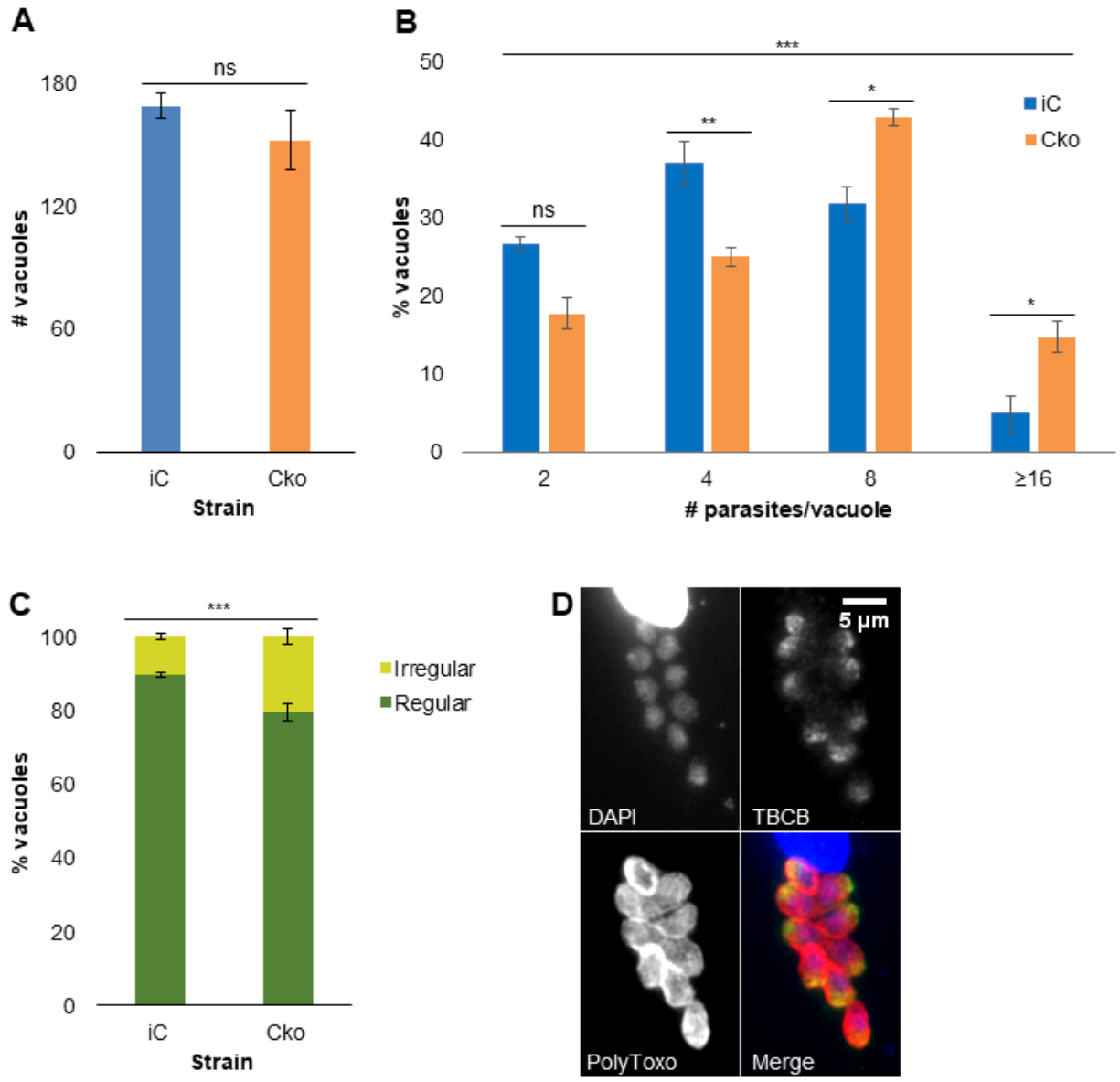

Figure 24. Analysis of *in vitro* phenotypes of Cko tachyzoites.

Cko tachyzoites were analyzed for its invasion efficiency, replication efficiency, and PV regularity in comparison to the control iC tachyzoites. **A)** Invasion assays did not detect significant differences between iC and Cko tachyzoites (p=0.3241). **B)** Replication assays detected significant differences between iC and Cko tachyzoites (p<0.0001). Cko tachyzoites present a higher replication rate compared to iC tachyzoites. **C)** PV regularity assays detected significantly higher irregular vacuoles in Cko tachyzoites compared to iC tachyzoites (p=0.004). Data are presented as mean ± SE of three independent experiments. **D)** Immunofluorescence assay of Cko tachyzoites invading HFF, presenting an irregular vacuole with 9 tachyzoites. The cells were stained using *T. gondii* surface proteins with polyclonal sera (PolyToxo), *T. gondii* tubulin cofactor B polyclonal sera (TBCB) and DNA (DAPI). iC – inducible *Mob1* splitCas9; Cko – *Mob1* splitCas9 functional knockout; Irregular – vacuoles with a number of tachyzoites different from 4, 8, 16 or 32; Regular – vacuoles with a number of tachyzoites equal to 4, 8, 16 or 32.

4.1.3. Our in house anti-MOB1 sera failed to confirm MOB1 depletion

Previous work by the group developed in house produced mouse anti-MOB1 sera (Tavares 2015). However, when testing the anti-MOB1 sera on the Cko tachyzoites, we saw no change in signal when compared to the control iC tachyzoites through western blot and immunofluorescence (Figure 25). This occurred even though, in Cko tachyzoites, the *Mob1* genomic locus and transcripts are both altered and the MOB1 protein predicted to be produced is mutated and truncated. The selected Cko clonal lines are predicted to express truncated proteins ranging from 4.1 kDa to 10.6 kDa. It is therefore not possible to detect MOB1 with a molecular weight close to 35 kDa. Therefore, we concluded that our anti-MOB1 sera successfully detect an endogenous protein in tachyzoites however this is not the endogenous MOB1. Consequently, we cannot use the anti-MOB1 sera to confirm MOB1 depletion in *Mob1* knockout tachyzoites. Efforts were also put into the production of additional in house produced anti-MOB1 sera. These were produced using GST-MOB1, the same recombinant protein used to produce the first batch of anti-MOB1 sera. The new sera variably detect the same endogenous 35 kDa protein and recognize MOB1 recombinant proteins in overexpression but do not detect any endogenous protein compatible with the endogenous MOB1 in wild type strains (data presented in 4.2).

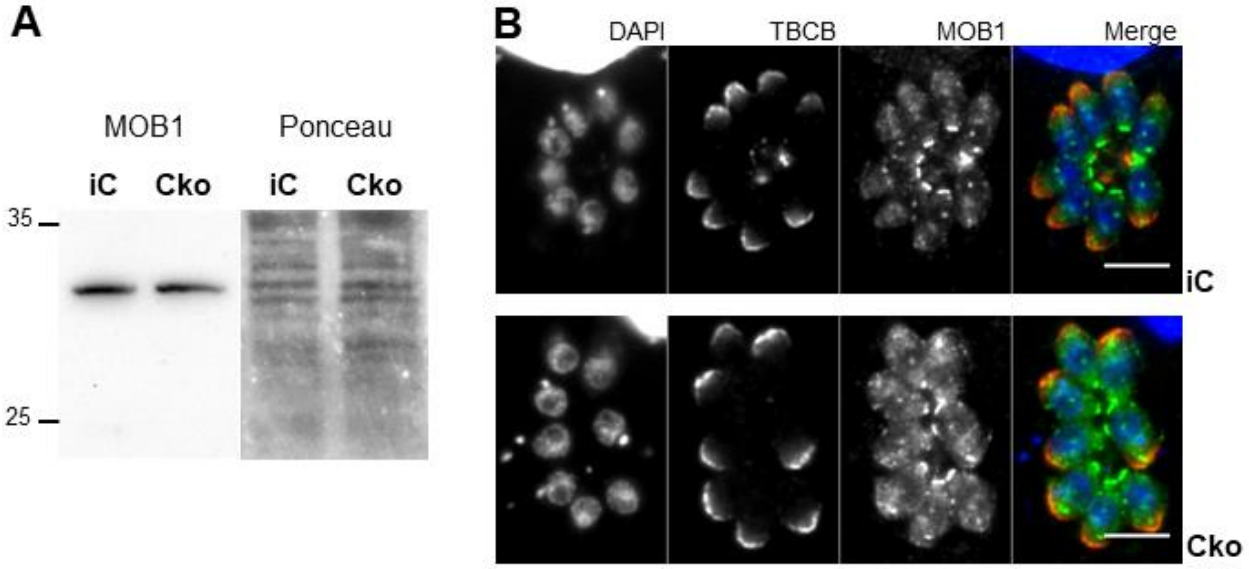

Figure 25. The polyclonal anti-MOB1 sera do not detect endogenous MOB1.

The polyclonal anti-MOB1 sera were used to detect MOB1 depletion in Cko tachyzoites (*Mob1* knockout). **A)** Western blot analysis showed no change to the stained band we previously considered to correspond to the endogenous *T. gondii* MOB1 protein. Ponceau S reversible staining was used as a loading control. Numbers on the left represent the molecular weight in kDa. **B) I**mmunofluorescence assay staining the assumed *T. gondii* endogenous MOB1 protein, *T. gondii* tubulin cofactor B (TBCB), and DNA (DAPI). The assay also detected no difference in the signal of

in house polyclonal anti-MOB1 sera between strains. The scale bar corresponds to 5 µm. iC - inducible *Mob1* splitCas9 strain; Cko - *Mob1* splitCas9 functional knockout strain.

The specificity of the original anti-MOB1 sera had been confirmed through western blot and immunofluorescence assays (Figure 26). For this, we used three *T. gondii* strains: RH (harboring only endogenous *Mob1*), dd-Myc-GFP-MOB1 (Tavares 2015), and morn1-FLAG-MORN1. The strain dd-Myc-GFP-MOB1 includes the destabilizing domain ddFKBP (dd) that is used to control the levels of recombinant protein in a Shield1 concentration dependent manner, allowing us to control the levels of dd-Myc-GFP-MOB1 in the cell (Herm-Götz et al. 2007). MORN1 is a *T. gondii* protein that presents a very specific location at the centrocone (a structure involved in the regulation of the mitotic spindle) and at the ring-like structures formed by the inner membrane complex in the apical and basal poles of the parasite (Gubbels et al. 2006). This subcellular localization was compatible with the localization documented for MOB1 by Tavares (2015). Western blot analysis of dd-Myc-GFP-MOB1 tachyzoites labeled with anti-MOB1 sera detected the recombinant protein in a Shield1 concentration dependent manner presenting a molecular weight compatible with the predicted of 81 kDa (Figure 26.A). The analysis detected additionally an endogenous protein, present in all samples, not dependent on Shield1 concentration, with a molecular weight close to the predicted for the endogenous MOB1 (35 kDa). The ~35 kDa protein was consistently detected in RH tachyzoites and at the time it was considered the endogenous MOB1 protein. We also used RH and morn1-FLAG-MORN1 tachyzoites for immunofluorescence analysis with the anti-MOB1 sera (Figure 26.B). The assumed endogenous MOB1 presented a consistent staining between different experiments, accumulating mostly at the basal pole, as well as at a centrally located dot and in a cytoplasmic pool, as previously documented by Tavares (2015). The basal pole and central dot staining co-localized with the FLAG-MORN1 recombinant protein at the basal polar ring and the centrocone, respectively. The central dot also presented a side-by-side location with the kinetochore complex component protein NDC80.

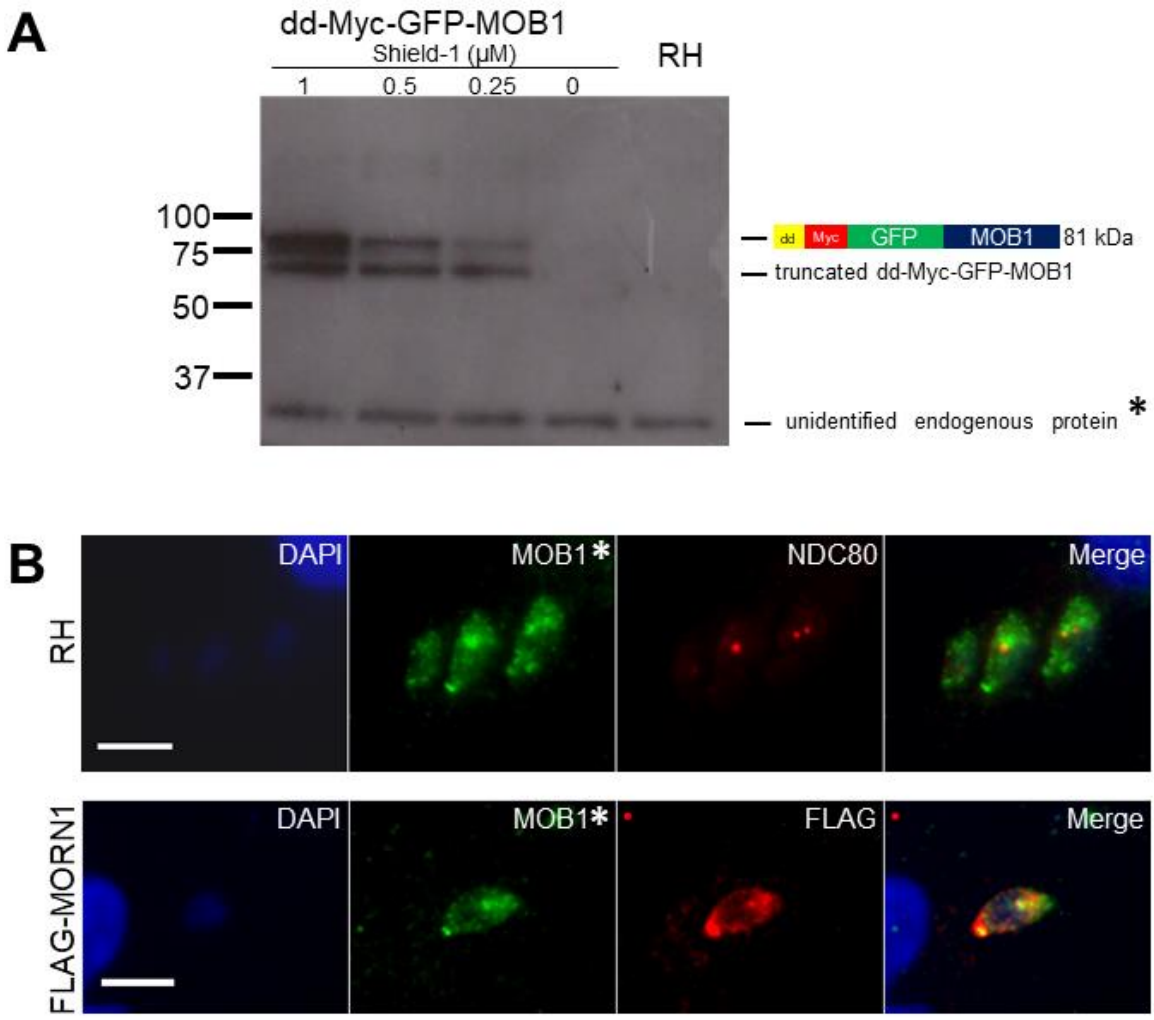

Figure 26. Characterization of an endogenous protein proven not to be MOB1 with in house produced polyclonal anti-MOB1 sera.

A) Western blot analysis of anti-MOB1 sera on dd-Myc-GFP-MOB1 tachyzoites using decreasing concentrations of Shield1. The recombinant protein dd-Myc-GFP-MOB1 was detected in a Shield1 dependent manner presenting a molecular weight compatible with the predicted. A truncated version of dd-Myc-GFP-MOB1, that appears to be less responsive to Shield1 concentration, is also detected with a slightly lower molecular weight. An unidentified endogenous protein was also detected with a molecular weight slightly below the 35 kDa predicted for MOB1 (previously thought to be the endogenous MOB1 but disproven using *Mob1* deleted *T. gondii* strains). *T. gondii* strains are indicated on the top of the panel. Numbers on the left represent the molecular weight in kDa. Numbers on the right correspond to predicted molecular weights in kDa. The small yellow rectangle represents the destabilizing domain ddFKBP (dd). The small red rectangle represents the Myc tag. **B)** Immunofluorescence analysis of anti-MOB1 sera showed a consistent staining over different assays with the signal accumulating mostly at the basal pole but also present in a centrally located dot and in the cytoplasm with a punctate pattern (MOB1*). The signal co-localized with the FLAG-MORN1 recombinant protein at the basal pole and the central dot (FLAG). The central dot also presented a side-by-side location with the *T. gondii* kinetochore complex component protein NDC80. DNA is identified using DAPI. The scale bar represents 5 µm. * Although we used anti-MOB1 sera, the endogenous protein detected is not the endogenous MOB1.

Overall, the ~35 kDa endogenous protein detected by the original anti-MOB1 sera presented gel mobility consistent with the expected for the endogenous MOB1. It also presented a subcellular localization compatible with a function related to replication, namely in the centrocone and the basal complex, structures intimately connected to the replication process. This was congruent with our data at the time on *T. gondii* MOB1 which showed a decrease in expression during the replicative phase of the lytic cycle and a decrease in replication efficiency with MOB1 overexpression, indicating a role in *T. gondii* replication. This resulted in our wrongful identification of the ~35 kDa endogenous protein as MOB1, which was disproven by testing the sera with *Mob1* knockout parasites.

4.1.4. The results obtained with CRISPR/Cas9 were replicated using a homologous recombination system

Beyond the CRISPR/Cas9 strategy, we also employed a homologous recombination strategy to study the effects of *Mob1* knockout. This consists of an inducible knockout system using the site-specific gene-swap recombination strategy (Andenmatten et al. 2013). The parallel use of two strategies to knockout *Mob1* provided us with a confirmation for the phenotypes we detected in each.

4.1.4.1. *Mob1* homologous recombination knockout tachyzoites were obtained following overexpression of Myc-MOB1

The execution of the gene-swap recombination strategy proved technically challenging throughout multiple steps of the process. The correct assembly of the *Mob1* gene-swap vector implied that the 3'UTR homology arm be the first amplicon inserted into the original gene-swap vector, however this amplification proved to be problematic and was the last to be achieved. Only one of nine primer combinations tested produced the desired amplicon with various tested conditions, F1 - 3' *Mob* and R2 - 3' *Mob* (Table 5). Additionally, in our first attempt to insert the *Mob1* cDNA into the gene-swap vector, after inserting the 3'UTR and 5'UTR amplicons, the resulting plasmids integrated the *Mob1* cDNA but lost the 3'UTR. This made us go back to different 3'UTR-5'UTR-gene-swap vector clones to test the insertion of the cDNA fragment. Although the deletion of the 3'UTR was detected again in part of the resulting clones, we were able to isolate the complete *Mob1* gene-swap vector.

We used the correctly assembled *Mob1* gene-swap vector to transfect diCre tachyzoites in order to obtain iGSoe (inducible *Mob1* gene-swap overexpressing MOB1) tachyzoites.

Positive iGSoe tachyzoites would have integrated the *Mob1* gene-swap vector through homologous recombination using the 5'UTR and 3'UTR homology arms. However, even using a ∆ku80 strain (that favors homologous recombination), positive results were relatively rare. From 34 tested clonal lines only one was positive for correct replacement of the endogenous *Mob1*. Representative results of PCR tests using the two types of primers designed, exon spanning and intron spanning, are presented in Figure 27. Several primer pairs of the two types of PCR were used and confirmed the results (Table 6). The most common results were clonal lines positive for the presence of both the endogenous *Mob1* and the *Mob1* cDNA, due to random integration. Clonal lines positive for the presence of the endogenous *Mob1* and negative for the presence of the *Mob1* cDNA were observed rarely, though not expected. Most likely these clonal lines are the result of a random partial integration of the vector DNA, including the HX selectable marker, which allowed for survival during the mycophenolic acid + xanthine selection.

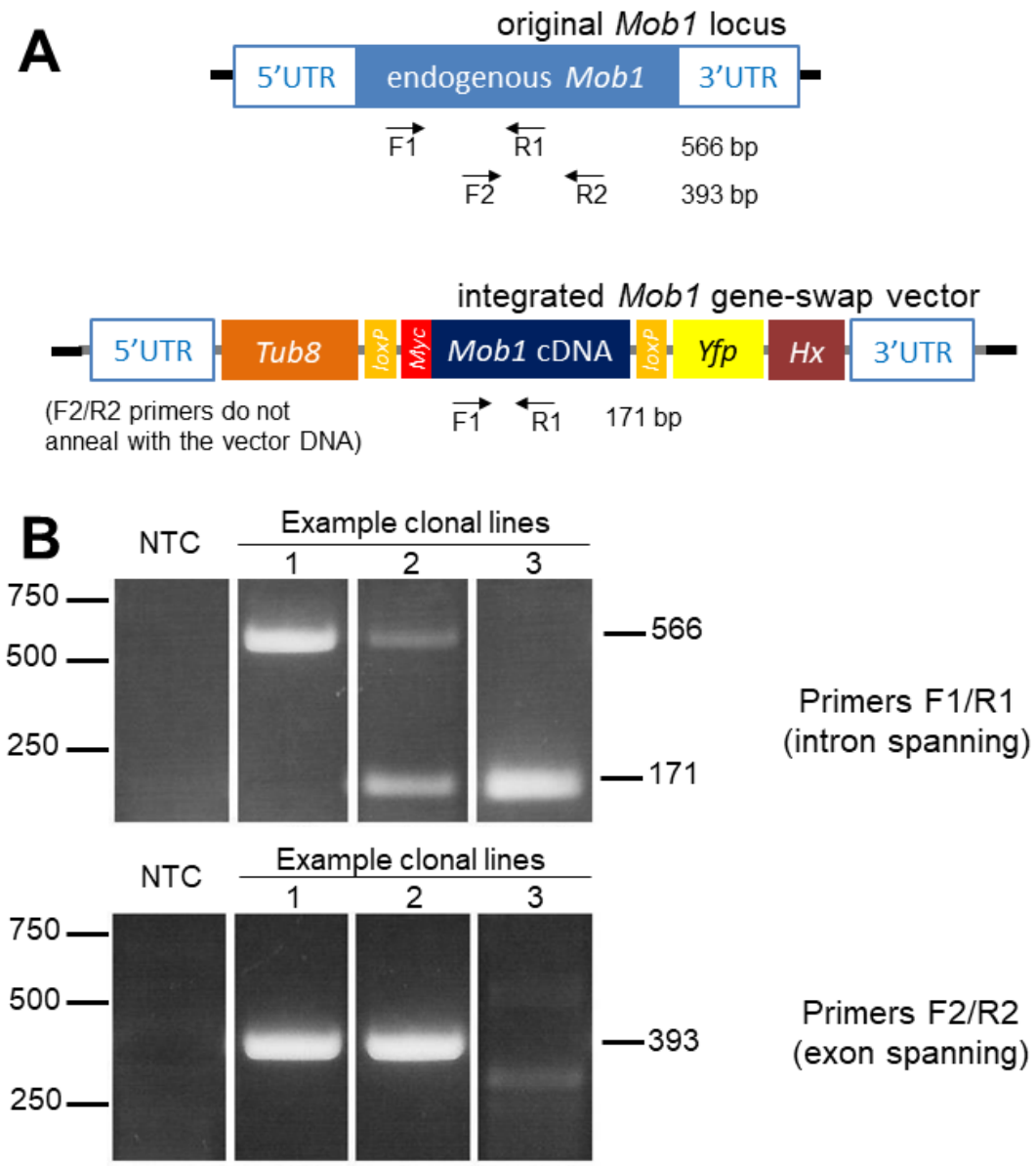

Figure 27. Analysis of the correct integration of the *Mob1* gene-swap vector.

A) PCR analysis strategy to test the integration of the *Mob1* gene-swap vector. The F1/R1 primer pair is an example of an intron spanning PCR (annealing with two exons in a row). The F2/R2 primer pair is an example of an exon spanning PCR (annealing with two introns in a row). The primers F1 and R1 hybridize with exons 2 and 3, respectively, producing 2 different PCR amplicons: 566 bp for the original Mob1 locus and 171 bp for the Mob1 cDNA. Successful gene-swap by homologous recombination will produce the 171 bp amplicon only. The primers F2 and R2 hybridize with the introns 2 and 3, respectively, amplifying a 393 bp amplicon. Successful homologous recombination will produce no PCR product. F1 – primer Mob Tg F int; R1 - primer testKO-WTmob R1; F2 - primer testWTmobF3; R2 - primer testWTmobR3; UTR – untranslated region; *loxP* - 34 bp Cre recognition sequence; *Myc* – Myc protein tag; *Yfp* – yellow fluorescent protein; *Hx* – hypoxanthine-xanthine-guanine phosphoribosyl transferase (selection marker). **B)** Clonal lines were tested by PCR using gDNA. The primer pair F1/R1 is an example of an intron spanning PCR test, therefore both the endogenous *Mob1* and the *Mob1* cDNA may be detected by this test. The

primer pair F2/R2 is an example of an exon spanning PCR test, therefore only the endogenous *Mob1* may be detected by this test. The example clonal line 1 is positive for the endogenous *Mob1* and negative for the *Mob1* cDNA, a result we obtained rarely and that is likely a partial integration of the *Mob1* gene-swap vector. The example clonal line 2 is positive for both the endogenous *Mob1* and the *Mob1* cDNA, therefore integrated the vector at a random locus of the genome, the most frequent result we obtained. The example clonal line 3 is positive only for the *Mob1* cDNA, indicating the homologous integration of the *Mob1* gene-swap vector and respective replacement of the endogenous *Mob1* by the *Mob1* cDNA. In this case, primers F2/R2 that only anneal with the endogenous *Mob1* sequence did not produce an amplicon of the expected size (393 bp). However, two weak intensity amplicons are visible, with sizes of approximately 300 and 500 bp, which are likely the result of unspecific amplification in a reaction where no specific annealing site was available for the primers. Numbers on the left represent the molecular weight in bp. Numbers on the right represent the expected amplicon's molecular weight in bp. NTC – non-template control.

4.1.4.2. Isolation of the MOB1 gene-swap knockout

The iGSoe parasites possess the diCre strain background which expresses Cre recombinase divided into two inactive fragments, each fused to a rapamycin-binding protein (Andenmatten et al. 2013). Addition of rapamycin to the culture medium enables the union of both rapamycin-binding proteins and consequently the two fragments of Cre form an active dimer (Putyrski and Schultz 2012). The active Cre produces double stranded DNA breaks at loxP sites (Jullien 2003). The MOB1 gene-swap vector inserted into the iGSoe tachyzoites includes two LoxP sites surrounding Myc-MOB1 (Figure 15). To obtain knockout tachyzoites, we added rapamycin to the culture medium of iGSoe tachyzoites which should cause Cre activation and excision of the floxed Myc-MOB1 resulting in the knockout of MOB1 and expression of YFP (Figure 14). However, our initial attempts to induce the MOB1 knockout were not successful as the tachyzoites continued to express Myc-MOB1 and were negative for the expression of YFP. To confirm if the Cre system was working properly, we tried to amplify both Cre fragments from the gDNA of iGSoe parasites but were only able to amplify the Cre60 fragment, indicating the Cre59 fragment had been lost from the iGSoe genome (Figure 28).

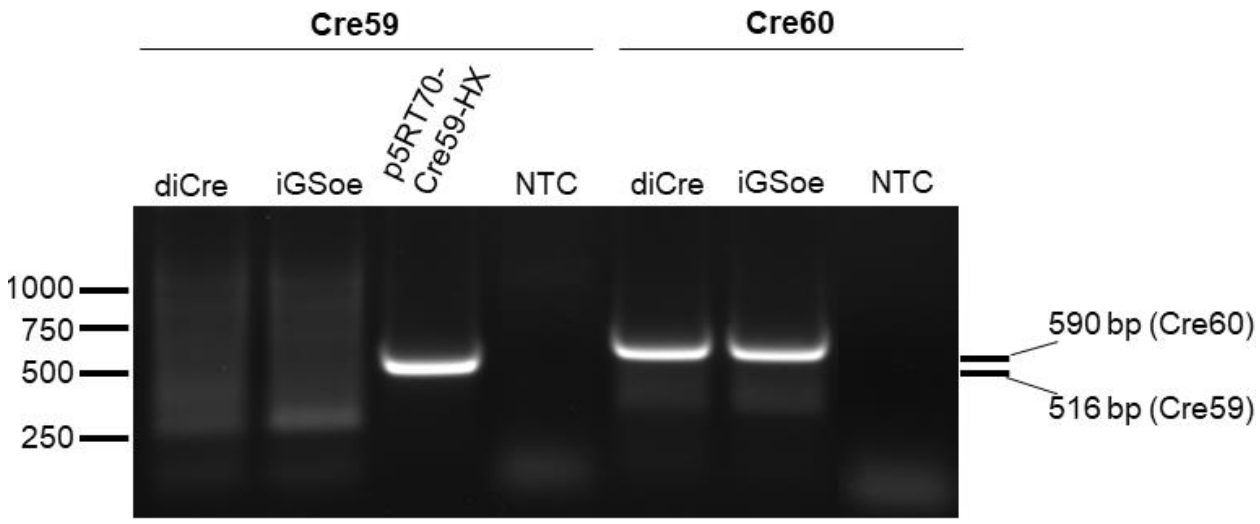

Figure 28. Evaluation of the diCre system upon failure to induce Cre activity.

As addition of rapamycin to the culture medium of iGSoe tachyzoites did not result in the removal of *Myc-Mob1* and concomitant activation of YFP expression, we designed a PCR assay to confirm if the Cre system was working properly. Amplification of Cre59 failed while amplification of Cre60 was successful, indicating the Cre59 fragment had been lost from the iGSoe tachyzoites' genome and from the diCre genome of tachyzoites used to originate the iGSoe tachyzoites. Numbers on the left represent the molecular weight in bp. The numbers on the right represent the expected molecular weight of the Cre59 and Cre60 amplicons. *pTub8-Cre59-Hx* - positive control of the PCR with the Cre59 primers (plasmid vector harboring the Cre59 sequence). Cre59 – Cre fragment 1-59 aa; Cre60 – Cre fragment 60-343 aa; diCre - ku80::diCre tachyzoites; iGSoe – *Mob1* inducible gene-swap tachyzoites; NTC – non-template control.

Considering our results with the Cko *T. gondii* lines, that showed *Mob1* as non-essential for parasite survival, we decided to perform a transient transfection of the Cre59 fragment to obtain LoxP excision. We obtained a plasmid vector that constitutively expresses Cre59 and transfected it into iGSoe tachyzoites by electroporation. Following electroporation, we added rapamycin to the culture medium to induce Cre activity and, after the tachyzoites lysed the host cell layer, we performed clonal line selection through limit dilutions. The isolated clonal lines were tested by PCR and western blot which confirmed successful recombination by Cre activity with removal of the Myc-MOB1 sequence and consequent activation of YFP expression (Figure 29). From 12 isolated clonal lines, three were positive for YFP expression. These clonal lines were designated as *Mob1* gene-swap knockout (GSko).

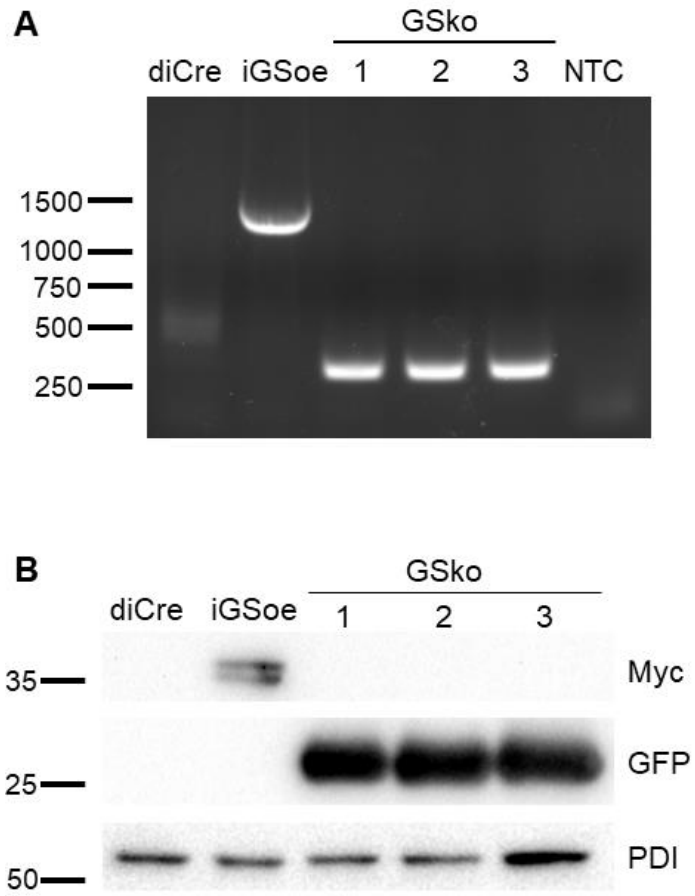

Figure 29. Evaluation of the induction of Cre activity upon transfection of the Cre59.

A plasmid harboring the Cre59 sequence was transfected into iGSoe tachyzoites and Cre activity was induced. Clonal lines were tested for successful recombination. **A)** The isolated clonal lines (1-3) tested positive for loss of the *Mob1* cDNA in the genome. Numbers on the left represent the molecular weight in bp. NTC – non template control. **C)** Western blot analysis for the detection of Myc protein tag, and yellow fluorescent protein (YFP) which has been stained using an antibody against the related green fluorescent protein (GFP). The *T. gondii* protein disulfide isomerase (PDI) was used as loading control. The analysis confirmed that the isolated clonal lines do not express Myc but express YFP, thus are knocked out for the *Mob1* gene. The numbers on the left represent molecular weight in kDa. iGSoe – inducible *Mob1* gene-swap overexpressing MOB1 tachyzoites; GSko – *Mob1* gene-swap knockout tachyzoites.

4.1.4.3. The phenotypes of GSko tachyzoites indicate *Mob1* is involved in replication and tachyzoite to bradyzoite differentiation

We saw a marked difference in proliferation between diCre tachyzoites and iGSoe and GSko tachyzoites during routine culturing, with iGSoe and GSko tachyzoites presenting an obviously decreased proliferation rate compared to diCre tachyzoites. Although these strains present a type I RH background, the proliferation rate of iGSoe and GSko tachyzoites is closer

to that of tachyzoites belonging to the slower replicating recombinant type I/III strain EGS or type II strains. The proliferation delay observed in iGSoe tachyzoites, readily detected in routine cell culture maintenance, presents a greater magnitude then that observed in other MOB1 overexpression strains obtained by our group, as the FLAG-BirA-MOB1 strain which harbors the same *Tub8* strong promoter as the iGSoe strain. Significantly, iGSoe tachyzoites needed to be passaged with a slower rate, at the same pace as the slower proliferating EGS strain, while other MOB1 overexpression strains with RH backgrounds needed to be passaged at the same pace as the faster proliferating RH strains. This difference may be explained by the location of the genome remodeling of each strain. While other strains suffered random integration, the iGSoe tachyzoites integrated the plasmid at the *Mob1* locus by gene-swap with the endogenous *Mob1*.

Tachyzoites of the iGSoe and GSko strains did not present significant differences in efficiency of host cell invasion when compared each to diCre tachyzoites or when compared between each other, with F=2.36 and p=0.1750 (Figure 30.A). Comparing the three strains in terms of replication efficiency at 24 hours, we detected a statistically significant overall difference between strains with F= 1060.8 and p<0.0001 (Figure 30.B). *Post hoc* tests using the Tukey multiple comparisons of means identified significant differences, with the diCre strain presenting a significantly faster replication rate when compared to both iGSoe and GSko strains in all vacuole type factor levels, except for vacuoles with two tachyzoites where only the GSko strain is significantly different from diCre (vacuoles with two tachyzoites - diCre/iGSoe difference in means=0.0625 and adjusted p=0.0812, diCre/GSko difference in means=0.1448 and adjusted p<0.0001; vacuoles with four tachyzoites - diCre/iGSoe difference in means=0.6575 and adjusted p<0.0001, diCre/GSko difference in means=0.5446 and adjusted p<0.0001; vacuoles with eight tachyzoites - diCre/iGSoe difference in means=-0.6456 and adjusted p<0.0001, diCre/GSko difference in means=-0.6204 and adjusted p<0.0001; vacuoles with sixteen tachyzoites - diCre/iGSoe difference in means=-0.0690 and adjusted p=0.0399, diCre/GSko difference in means=-0.0746 and adjusted p= 0.0209). In this analysis, iGSoe and GSko strains present statistically significant differences only in vacuoles with two and four tachyzoites, however the overall results are incoherent, not allowing to conclude if any of the strains presents higher replication efficiency (vacuoles with two tachyzoites - difference in means=-0.082 and adjusted p=0.0026; vacuoles with four tachyzoites - difference in means=0.1129 and adjusted p<0.0001; vacuoles with eight tachyzoites - difference in means=-0.0249 and adjusted p=0.9146; vacuoles with sixteen tachyzoites - difference in means=-0.0057 and adjusted p=1). Furthermore, when comparing only the iGSoe and GSko strains, no

significant differences are observed with F=8.23 and p=0.1030, thus the 24 hour assay was inconclusive for this comparison. This led us to perform a replication assay using a larger incubation time of 44 hours as the iGSoe and GSko strains present a slower replication rate. In the 44 hour assay, we detected statistically significant overall differences between these strains, with F=58.47 and p<0.0001 (Figure 30.C). *Post hoc* tests using the Tukey multiple comparisons of means identified significant differences between strains within vacuole types. While the iGSoe strains presented significantly more vacuoles with 8 parasites (difference in means=0.1167 and adjusted p<0.0001), the GSko strains presented significantly more vacuoles with 16 parasites (difference in means= 0.1373 and adjusted p<0.0001). The differences between strains in vacuoles with 2 parasites (difference in means=0.0253 and adjusted p=0.5637), with 4 parasites (difference in means=0.0273 and adjusted p=0.4657), and with 32 or more parasites (difference in means=0.0327 and adjusted p=0.2486) were not significant. But the overall tendency of the differences was coherent. We evaluated the PV regularity of tachyzoite replication by estimating the percentage of irregular vacuoles, namely vacuoles that presented a number of parasites different from 4, 8, 16 or 32 (vacuoles with 1 or 2 parasites were excluded from this analysis). We detected significant differences in PV regularity between the iGSoe and GSko strains with higher percentages of irregular vacuoles in GSko compared to iGSoe tachyzoites (64.04% and 55.72% respectively) with F=40.54 and p=0.0238 (Figure 30.D). The high percentages detected in this assay are likely related to the fact the PV regularity was evaluated at 44 hours post inoculation, with a higher percentage of vacuoles presenting high numbers of tachyzoites which contributes to a higher percentage of less organized PVs.

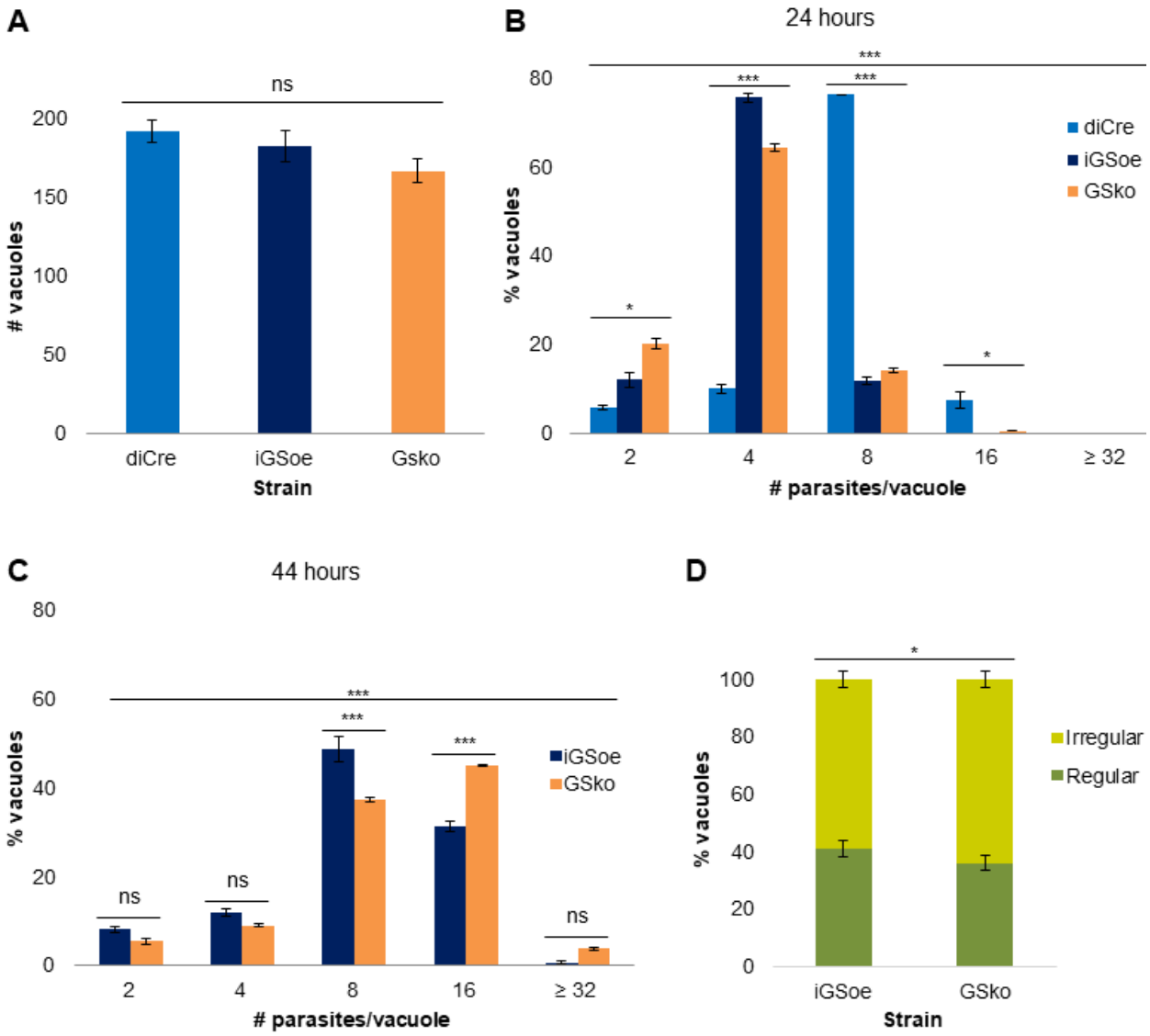

Figure 30. GSko tachyzoites also present an increased replication rate.

GSko tachyzoites were compared to iGSoe and diCre tachyzoites with *in vivo* assays to analyze the *Mob1* knockout phenotype. **A)** The invasion assay did not detect significant differences in between diCre, iGSoe, and GSko tachyzoites (p=0.1750). **B)** The diCre strain presented a significantly faster replication rate when compared to both iGSoe and GSko strains after a 24 hour incubation period (p<0.0001). **C)** The GSko strain a faster replication rate compared to the iGSoe strain after a 44 hour incubation period (p<0.0001). **D)** The PV regularity assay detected a significantly higher percentage of irregular vacuoles in GSko tachyzoites compared to iGSoe tachyzoites (p= 0.0238). PV regularity was measured at 44 hours. Data are presented as mean ± SE of three independent experiments. iGSoe – inducible *Mob1* gene-swap overexpressing MOB1 tachyzoites; GSko – *Mob1* gene-swap knockout tachyzoites; ns – p-value not significant; * - p ≤ 0.05; ** - p ≤ 0.01; *** - p ≤ 0.001.

Finally, we assessed if the iGSoe and GSko strains present altered patterns of spontaneous tachyzoite-bradyzoite conversion during *in vitro* culturing (Figure 31). Type I RH

tachyzoites typically do not spontaneously convert from tachyzoite to bradyzoite in cell culture and, as expected, we saw no spontaneous formation of bradyzoite cysts in the control strain diCre (0%). Surprisingly, because the diCre, iGSoe and GSko strains have a RH background (type I), although with a low frequency, we detected spontaneous formation of bradyzoite cysts in the iGSoe strain (2.8%), which overexpresses Myc-MOB1. However, this spontaneous formation of bradyzoite cysts was almost completely reversed in the GSko strain (0.1%). The spontaneous formation of bradyzoite cysts is significantly different between strains ($F=32.74$ and $p<0.001$). *Post hoc* tests using the Tukey multiple comparisons of means identified significant differences between strains. The iGSoe strain presents a significant increase in bradyzoite cysts compared to the diCre strain (difference in means=2.767 and adjusted p=0.0102). The GSko strain presents a significant decrease in bradyzoite cysts compared to the iGSoe strain (difference in means=-2.616 and adjusted p=0.0012). The difference in spontaneous formation of bradyzoite cysts between the diCre and GSko strains is not significant (difference in means=0.1507 and adjusted p=0.92).

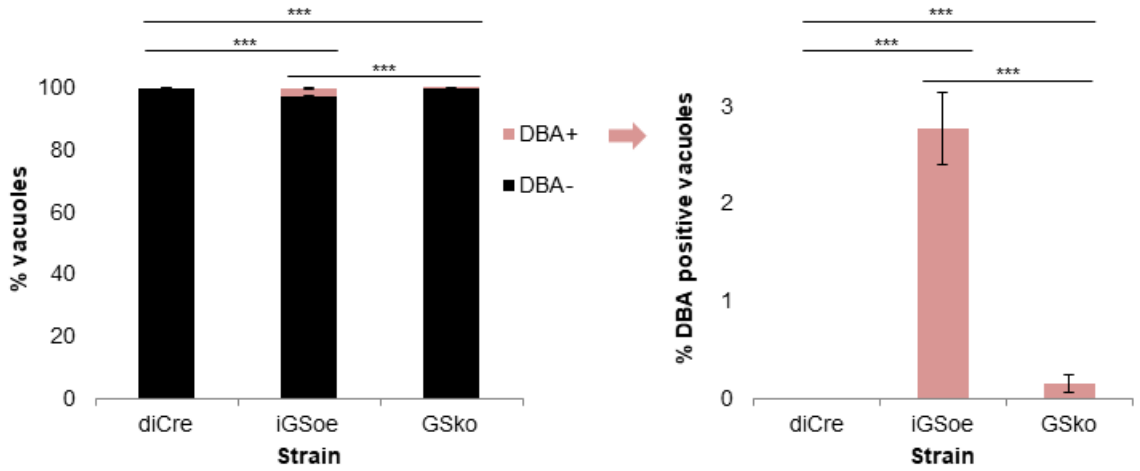

Figure 31. MOB1 overexpression iGSoe tachyzoites show increased tachyzoite to bradyzoite differentiation which decreases in GSko tachyzoites.

The strains diCre, iGSoe and GSko present significant differences in spontaneous formation of bradyzoite cysts ($p<0.001$). The iGSoe strain presents spontaneous formation of bradyzoite cysts significantly increased compared to diCre (2.8% vs. 0%). The GSko strain presents a significant decrease in bradyzoite cysts compared to the iGSoe strain (2.8% vs. 0.1%). The difference in spontaneous formation of bradyzoite cysts between the diCre and GSko strains is not significant. Bradyzoite cyst formation was detected using *Dolichos biflorus* agglutinin (DBA) lectin. Data are presented as mean ± SE of three independent experiments. iGSoe – inducible *Mob1* gene-swap overexpressing MOB1 tachyzoites; GSko – *Mob1* gene-swap knockout tachyzoites; ns – p-value not significant; * - $p \leq 0.05$; ** - $p \leq 0.01$; *** - $p \leq 0.001$.

4.1.5. Eko tachyzoites present a reduction in tachyzoite to bradyzoite differentiation

We employed the vectors *pTub8-Cas9-Yfp-Ha_U6-gRNAintron* and *pU6-gRNA1-Dhfr* to obtain direct *Mob1* functional knockouts in the EGS strain, using the CRISPR/Cas9 system (see material and methods 3.2.2). Following co-transfection of the vectors, eight clonal lines were isolated. We tested the clonal lines by PCR using primer pairs that anneal before and after the annealing site of the *Mob1* gRNA1 (Figure 32).

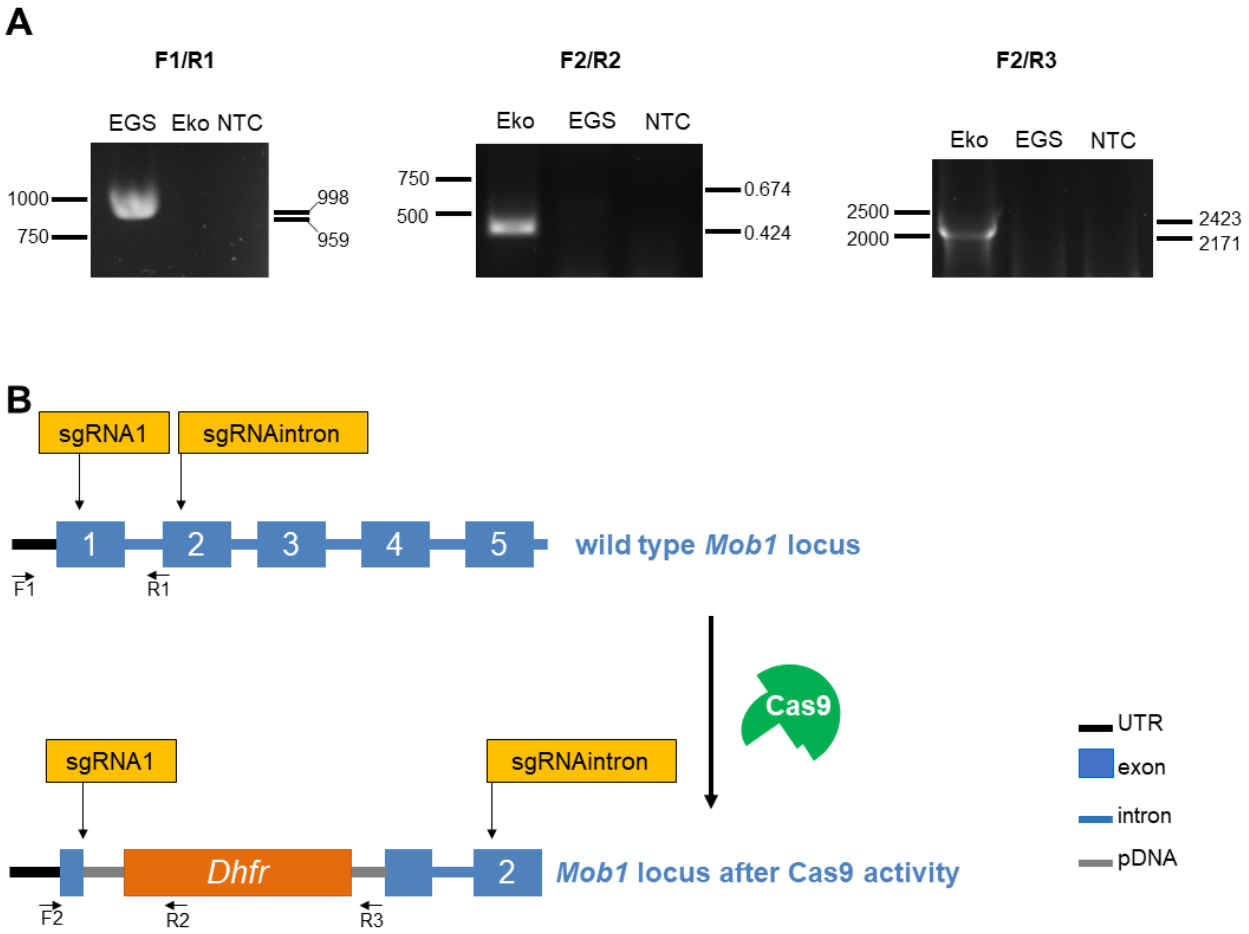

Figure 32. Eko clonal lines inserted part of the *pU6-gRNA1-Dhfr* vector.

T. gondii EGS tachyzoites were co-transfected with the vectors *pTub8-Cas9-Yfp-Ha_U6-gRNAintron* and *pU6-gRNA1-Dhfr*. The resulting Eko clonal lines were tested by PCR to characterize the *Mob1* locus at the expected sites of recombination. **A)** The isolated Eko clonal lines suffered a large insertion of part of the *pU6-gRNA1-Dhfr* vector. This is evident by example PCR results that are presented: primers F1/R1 that span exon 1 only produce an amplicon from endogenous *Mob1*; primers F2/R2 and F2/R3 that anneal with the *pU6-gRNA1-Dhfr* vector and the Mob1 genome produce amplicons from Eko *Mob1*. F1 - gRNA1_*Mob1*_pFext; R1 - gRNA1_*Mob1*_pRext; F2 - pKOinsert_F1; R2 - pKOinsert_R2; R3 - pKOinsert_Rstop. Numbers on the left represent the molecular weight in bp.

Numbers on the right represent the molecular weight of the detected amplicons in bp. NTC – non template control. Eko – EGS *Mob1* functional KO. **B)** Diagram depicting the recombination event detected in the Eko clonal lines. *Dhfr* - dihydrofolate reductase (selection marker); UTR – untranslated region; pDNA – plasmid DNA; sgRNA – single guide RNA.

Although this strategy had been efficient to test the Cko clonal lines, the same primer pairs did not produce amplicons from the gDNA of Eko clonal lines. We hypothesized that the gDNA region between the gRNA1 and gRNA intron Cas9 activity residues had been removed however primer pairs spanning this hypothetical deletion also did not produce amplicons in the isolated clonal lines. Sanger sequencing of a fortuitous unspecific amplicon allowed us to recognize that a portion of the *pU6-gRNA1-Dhfr* vector had been integrated into the genome at the *Mob1* locus. We were able to confirm this by PCR with primer pairs that anneal with the genome and with the vector DNA. This showed that the Eko clonal lines suffered a similar recombination event, a partial insertion of the *pU6-gRNA1-Dhfr* linearized vector at the *Mob1* locus. We selected one knockout clonal line to assess the extent of the insertion and performed various series of primer design > PCR > amplicon purification > Sanger sequencing. The inserted vector DNA included the full *Dhfr* coding sequence and upstream and downstream plasmid. Though the *pU6-gRNA1-Dhfr* vector had been linearized before transfection, neither the N-terminal or C-terminal ends of the insertions correspond to the ends produced by the linearization. The Eko clonal line presented an insertion of 3890 bp and the inserted residues started 140 bp before the *Dhfr* ATG and 1665 bp after the *Dhfr* stop. The partial vector insertion causes disruption of the *Mob1* genomic locus. But, to assess the effect of these insertions at the RNA level, we performed RT-PCR to compare the transcript levels of control and knockout clonal lines. A PCR test detected no *Mob1* cDNA in knockout clonal lines (Figure 33). Thus, the insertion impairs *Mob1* transcription which consequently produces a *Mob1* functional knockout. We selected the Eko clonal line that was more thoroughly characterized in the *Mob1* locus for phenotypic analysis.

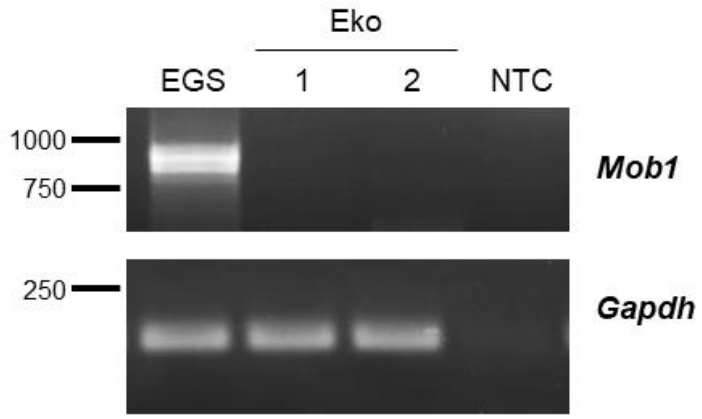

Figure 33. Eko clonal lines do not present detectable levels of *Mob1* transcripts.

Eko clonal lines were tested by RT-PCR and no detectable levels of *Mob1* transcripts were detected. *Gapdh* was used as control. Numbers on the left represent the molecular weight in bp. NTC – non template control. Eko – EGS *Mob1* functional knockout.

We evaluated spontaneous cyst formation in the Eko clonal line. The rate of spontaneous bradyzoite cyst formation was relatively high in wild type EGS (10.9%). The strains Eko and EGS presented significant differences in spontaneous formation of bradyzoite cysts, with F=57.65 and p=0.0169 (Figure 34.A). The Eko strain presented a marked decrease in the formation of bradyzoite cysts compared to EGS (0.3% vs. 10.9%). We further analyzed the phenotype of Eko tachyzoites regarding PV number regularity, invasion and replication. We detected a significantly higher percentage of irregular vacuoles in Eko tachyzoites compared to EGS tachyzoites, with F=18.83 and p=0.0492 (Figure 34.B). Finally, we evaluated the efficiency of the Eko strain regarding invasion and replication. Comparing Eko tachyzoites to the control strain, EGS, we saw no difference in invasion, with F=2.594 and p=0.2486, or in replication, with F=0.786 and p=0.5346 (Figure 34.C).

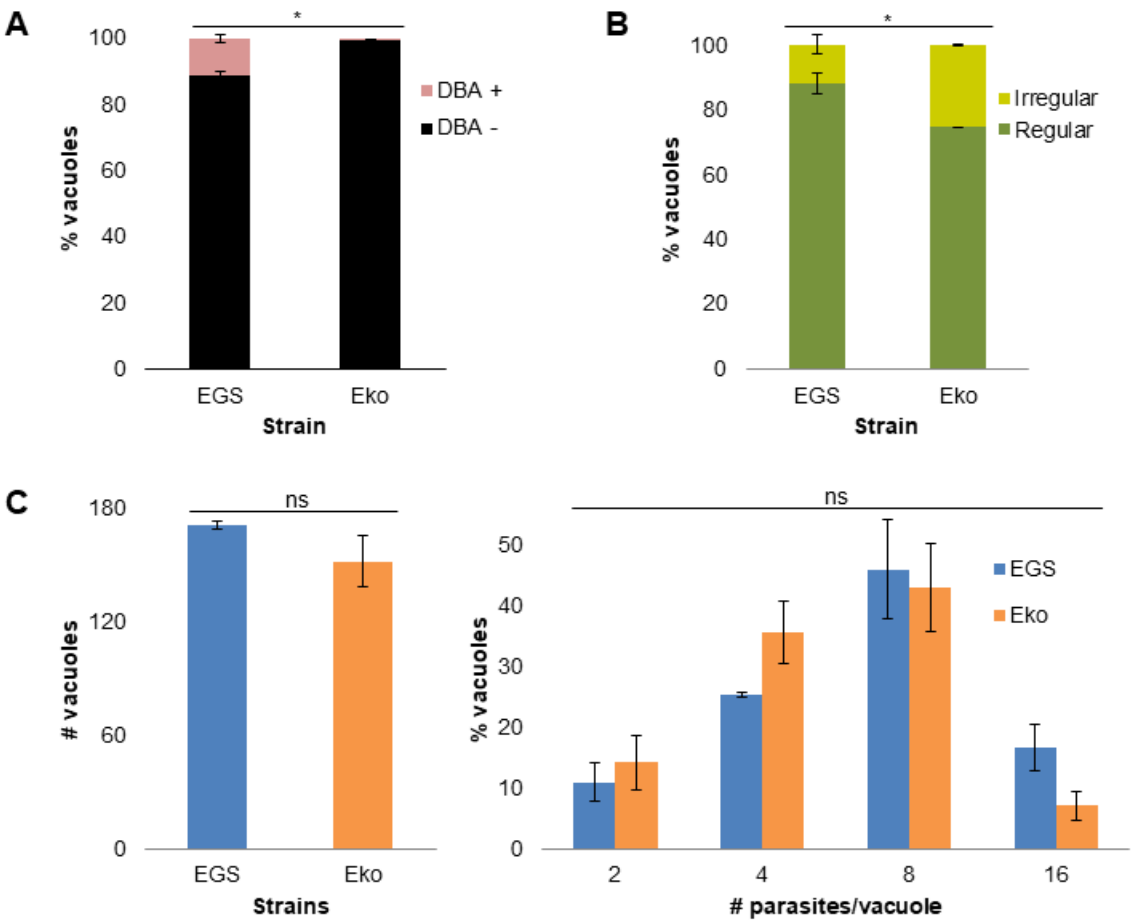

Figure 34. Eko tachyzoites show a marked decrease in the tachyzoite-bradyzoite transition.

Eko tachyzoites were compared to EGS tachyzoites with cell culture assays to analyze the *Mob1* functional knockout phenotype. **A)** The strains Eko and EGS present significant differences in spontaneous formation of bradyzoite cysts (p=0.0169) with the Eko strain presenting a marked decrease in the formation of bradyzoite cysts compared to EGS (0.3% vs. 10.9%). *In vitro* cyst formation was detected using *Dolichos biflorus* agglutinin (DBA) lectin. **B)** PV regularity assays detected significantly higher percentages of irregular vacuoles in Eko tachyzoites compared to EGS tachyzoites (p=0.0492). **C)** Invasion assays did not detect significant differences between EGS and Eko tachyzoites (p=0.2486). **D)** Replication assays did not detect significant differences between EGS and Eko tachyzoites (p=0.5346). Data are presented as mean ± SE of three independent experiments. Eko – EGS *Mob1* functional knockout; ns – p-value not significant; * - $p \leq 0.05$.

4.2. MOB1 presents a cytoplasmic subcellular localization and accumulates between the two forming nuclei at the end of mitosis

When starting this project we were using in house produced anti-MOB1 polyclonal sera (Tavares 2015). According to the data available at the time, the sera specifically identified endogenous MOB1 and MOB1 recombinant proteins and identified the subcellular localization of MOB1 in *T. gondii.* However, when tested in our *Mob1* knockout clonal lines Cko, we realized it only detected MOB1 recombinant proteins and that the endogenous protein detected could not be the endogenous MOB1 (see section 4.1.1.3). This drawback led us to start new efforts to identify the MOB1 subcellular localization in order to characterize the function of *Mob1* in *T. gondii*.

4.2.1. Recombinant MOB1 presents a largely cytoplasmic localization

We obtained RH tachyzoites expressing a FLAG-MOB1 recombinant protein driven by the low expression promoter morn1 (Figure 35). FLAG-MOB1 expression shows a dotted pattern and a cytoplasmic location excluded from the nucleus. FLAG-MOB1 is also excluded from the apical pole, which is identified by the *T. gondii* tubulin cofactor B (TBCB) protein, a polarity marker that accumulates mostly at the *T. gondii* apical pole (Francisco 2019). The expression of the recombinant FLAG-MOB1 is not constant through tachyzoites from the same clonal line at the same time point. All tested clonal lines were positive for FLAG-MOB1 expression and showed similar staining patterns. Western blot showed the recombinant protein at a molecular weight slightly above 35 kDa, compatible with the FLAG-MOB1 predicted molecular weight of 36 kDa (Figure 35).

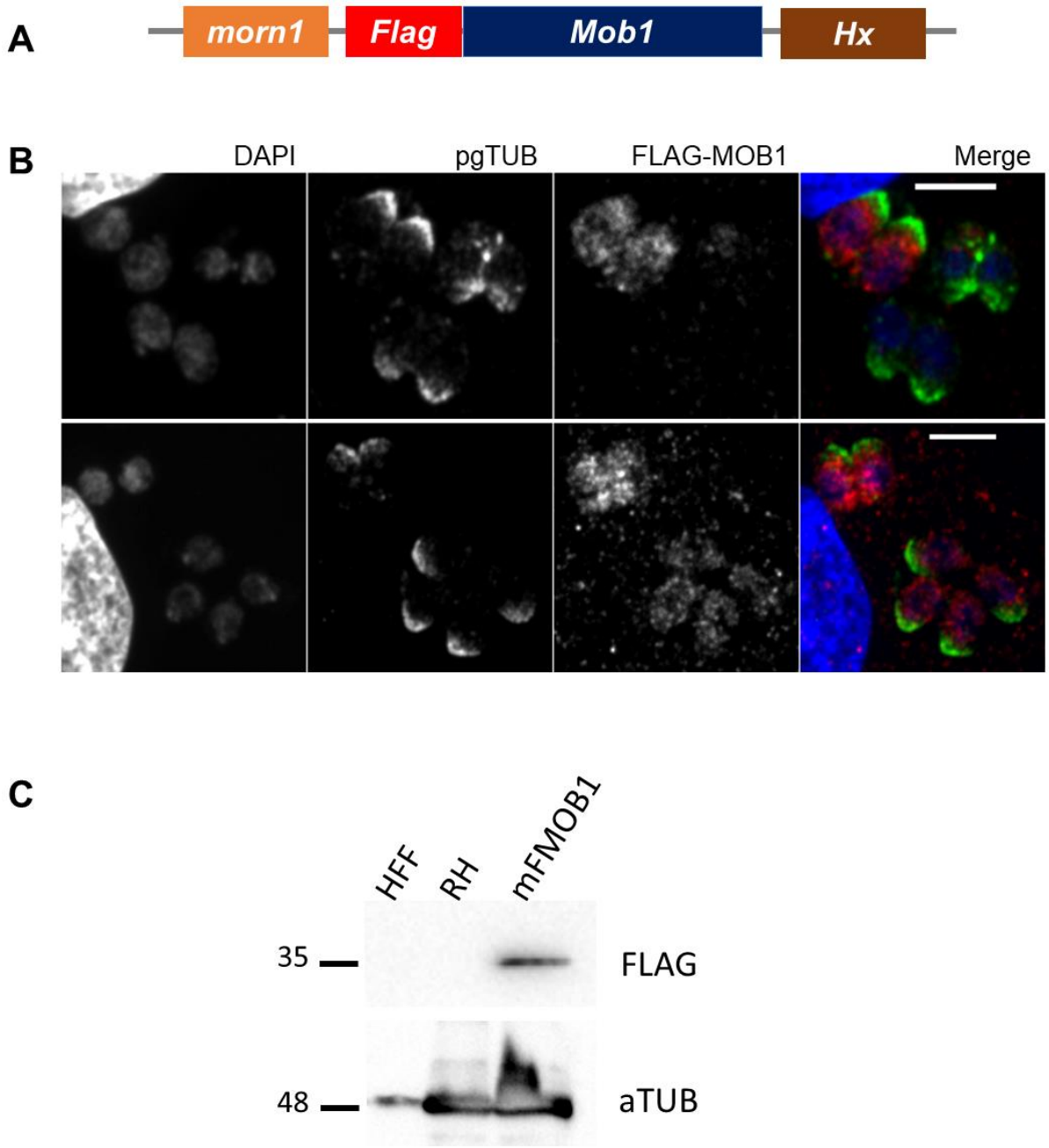

Figure 35. The recombinant FLAG-MOB1 protein presents a cytoplasmic punctate localization.

A) Plasmid vector used to transfect RH tachyzoites, harboring the MORN1 promoter, morn1, and the *Mob1* cDNA fused to *Flag*. **B)** Tachyzoites expressing FLAG-MOB1 driven by the morn1 promoter (mFMOB1) present a dotted pattern with a cytoplasmic localization, excluded from the apical pole, indicated by the glutamylated tubulin staining (pgTUB), and from the nucleus, indicated by DNA staining (DAPI). Tachyzoites from the same clonal line present varying expression levels. Scale bars represent 5 µm. *C)* Western blot analysis shows FLAG-MOB1 at a molecular weight near 35 kDa, compatible with the predicted molecular weight of 36 kDa. Acetylated tubulin (aTUB) was used as a loading control. FLAG-MOB1 recombinant protein was detected using anti-FLAG. Numbers on the left represent

molecular weight in kDa. morn1 – morn1 promoter; *Hx* - hypoxanthine-xanthine-guanine phosphoribosyltransferase (selection marker); HFF – human foreskin fibroblasts; DAPI - 4,6-diamidino-2-phenylindole.

4.2.2. Additional anti-MOB1 sera showed similar properties to our original anti-MOB1 sera

We produced additional anti-MOB1 sera using the GST-MOB1 recombinant protein expressed in *E. coli* and used wild type and recombinant MOB1 expressing *T. gondii* strains to test the sera. Sera produced with GST-MOB1 showed similar properties to our original sera, which had been produced with the same recombinant protein when analyzed through western blot (Figure 36). The sera detected MOB1 recombinant proteins with varying degrees of specificity and sensitivity. Recombinant MOB1 driven by high expression promoters were consistently detected, although with varying levels of sensitivity. All GST-MOB1 sera detected the recombinant MOB1 expressed by the FLAG-BirA-MOB1 strain and all but sera 2.2 detected the recombinant MOB1 expressed by the iGSoe strain. Sera 2.2 presented higher specificity but lower sensitivity then the other GST-MOB1 sera. When we incubated the GST-MOB1 sera with protein extracts from FLAG-BirA-MOB1 and iGSoe strains (express high levels of recombinant MOB1) simultaneously with protein extracts from wild type RH and morn1-FLAG-MOB1 strains (morn1-FLAG-MOB1 expresses low levels of recombinant MOB1), no MOB1 compatible signal was detected in the RH or morn1-FLAG-MOB1 strains. When we incubated the GST-MOB1 sera with protein extracts from wild type RH and morn1-FLAG-MOB1 strains separately from the FLAG-BirA-MOB1 and iGSoe strains, we detected a weak signal compatible with FLAG-MOB1 in the morn1-FLAG-MOB1 strain. However other unspecific signals were also detected, sometimes with much higher intensity than the FLAG-MOB1 signal. Both the Myc-MOB1 (iGSoe strain) and the FLAG-MOB1 (morn1-FLAG-MOB1 strain) proteins presented a double band pattern with sera 1, and 2.4 but a single band pattern with sera 2.1. The Myc-MOB1 protein (iGSoe strain) also presented a double band pattern with sera 2.3 and 2.5. The Myc-MOB1 protein (iGSoe strain) also presented a double band pattern when detected by the anti-Myc antibody (Figure 29.B). No MOB1 compatible signal was detected in RH protein extracts. The protein that was previously thought to be the endogenous MOB1 was only detected with high sensitivity by the sera 1, our original sera, but sera 2.1, 2.2, 2.4 and 2.5 also detect a protein of the same molecular weight although with a much less intense signal. Overall, the various GST-MOB1 sera are specific for highly expressed MOB1 recombinant proteins, in particular sera 1, 2.1, 2.2, 2.3, and 2.5. Sera 1, 2.1, and 2.4 also detect the low expressed FLAG-MOB1

recombinant protein but present low specificity for this level of expression. No sera detected endogenous MOB1.

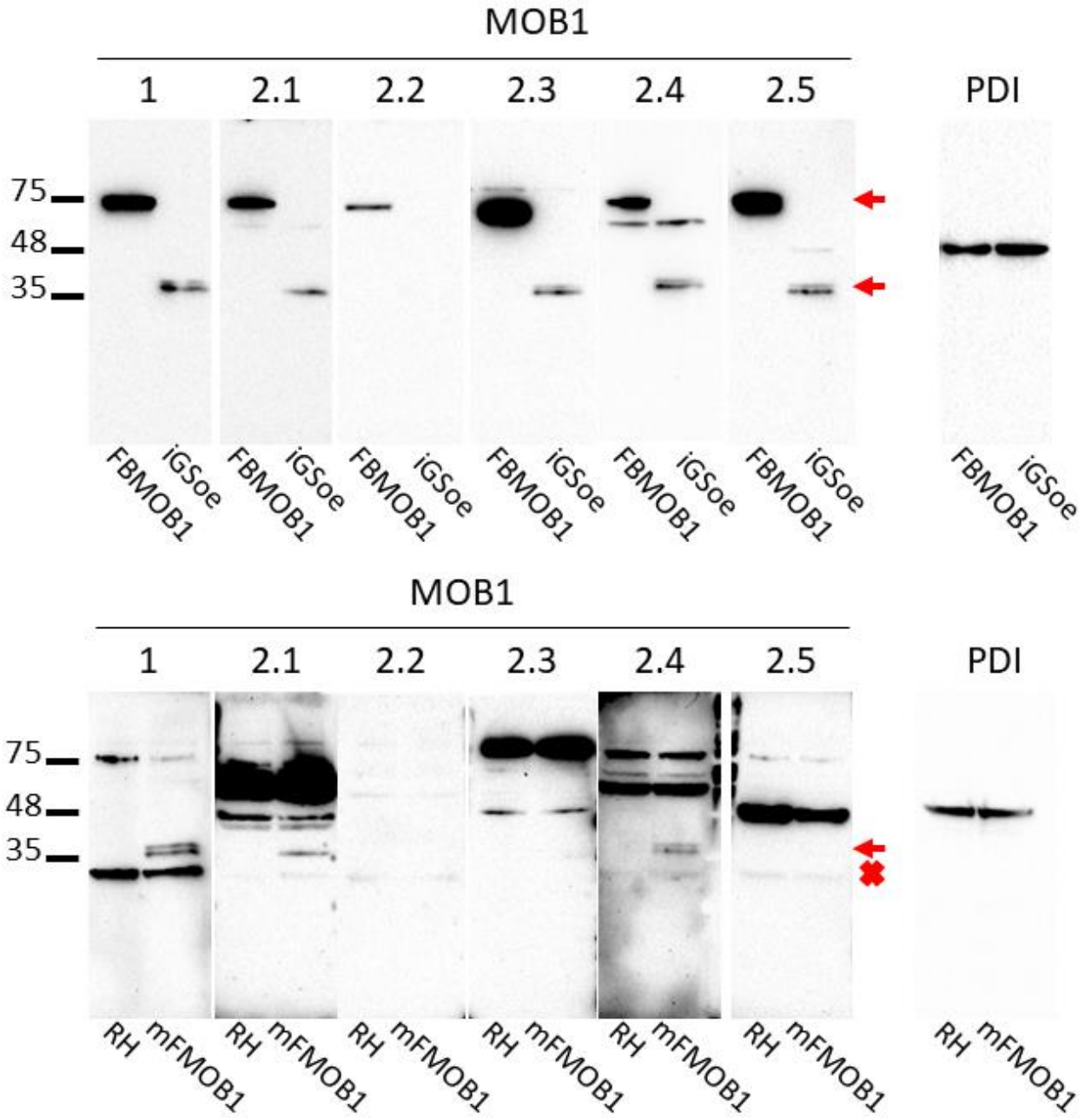

Figure 36. Anti-MOB1 sera produced with GST-MOB1 show specificity for recombinant MOB1 but not for endogenous MOB1.

To assess the specificity and sensitivity of in house produced anti-MOB1 sera we used western blot analysis and compared a control strain, RH, to MOB1 overexpression strains FLAG-BirA-MOB1 (FBMOB1), iGSoe (expresses Myc-MOB1) and morn1-FLAG-MOB1 (mFMOB1). FLAG-BirA-MOB1 and iGSoe tachyzoites express high levels of the recombinant proteins while mFMOB1 tachyzoites express low levels of the recombinant protein. All sera produced with GST-MOB1 detect highly expressed recombinant MOB1 while only sera 1, 2.1 and 2.4 detect the low

expression recombinant MOB1. No sera detect the endogenous MOB1. Recombinant MOB1 are sometimes detected in a double band pattern. Protein disulfide isomerase (PDI) was used as loading control. Recombinant MOB1 proteins are highlighted by a red arrow (FLAGBirAMOB1 – 74.1 kDa; Myc-MOB1 – 36.8 kDa; FLAGMOB1 - 36 kDa). The protein that was previously thought to be the endogenous MOB1 is highlighted by a red cross. The numbers on the left represent molecular weights in kDa. 1 – first production of anti-MOB1 sera, using GST-MOB1 (Tavares 2015); 2.1 to 2.5 – second production of anti-MOB1 sera, using GST-MOB1; iGSoe – *Mob1* inducible gene-swap.

4.2.3. Recombinant MOB1 accumulates at the end of mitosis between the two nuclei

We used anti-MOB1 sera, produced with GST-MOB1, and strains that express recombinant MOB1 to further study the MOB1 subcellular localization. Immunofluorescence assays performed at various points of the *T. gondii* cell cycle allowed us to identify a time point of recombinant MOB1 accumulation in a pattern different than the cytoplasmic localization routinely observed. At the end of mitosis, when the two new forming nuclei are visibly separated but still very close, recombinant MOB1 accumulates between the two newly divided nuclei (Figure 37). The accumulation appears to be very time sensitive, being detected just as the nuclei finish segregating and while they are still very close to each other. It is no longer detected when the nuclei move apart. This localization was observed using several anti-MOB1 sera (GST-MOB1 batches 1 and 2) and in two *T. gondii* strains expressing recombinant MOB1, namely the high expression FLAG-BirA-MOB1 strain and the low expression morn1-FLAG-MOB1 strain. The same accumulation was also observed when staining the morn1-FLAG-MOB1 and FLAG-BirA-MOB1 strains with anti-FLAG monoclonal antibody (Figure 38). Recombinant MOB1 was also observed to accumulate in the residual body. The basal complex and centrocone localization that was originally considered as the MOB1 subcellular localization, detected only with the anti-MOB1 sera 1, was ignored from this analysis whenever the sera 1 were used as we concluded this is not a MOB1 specific signal.

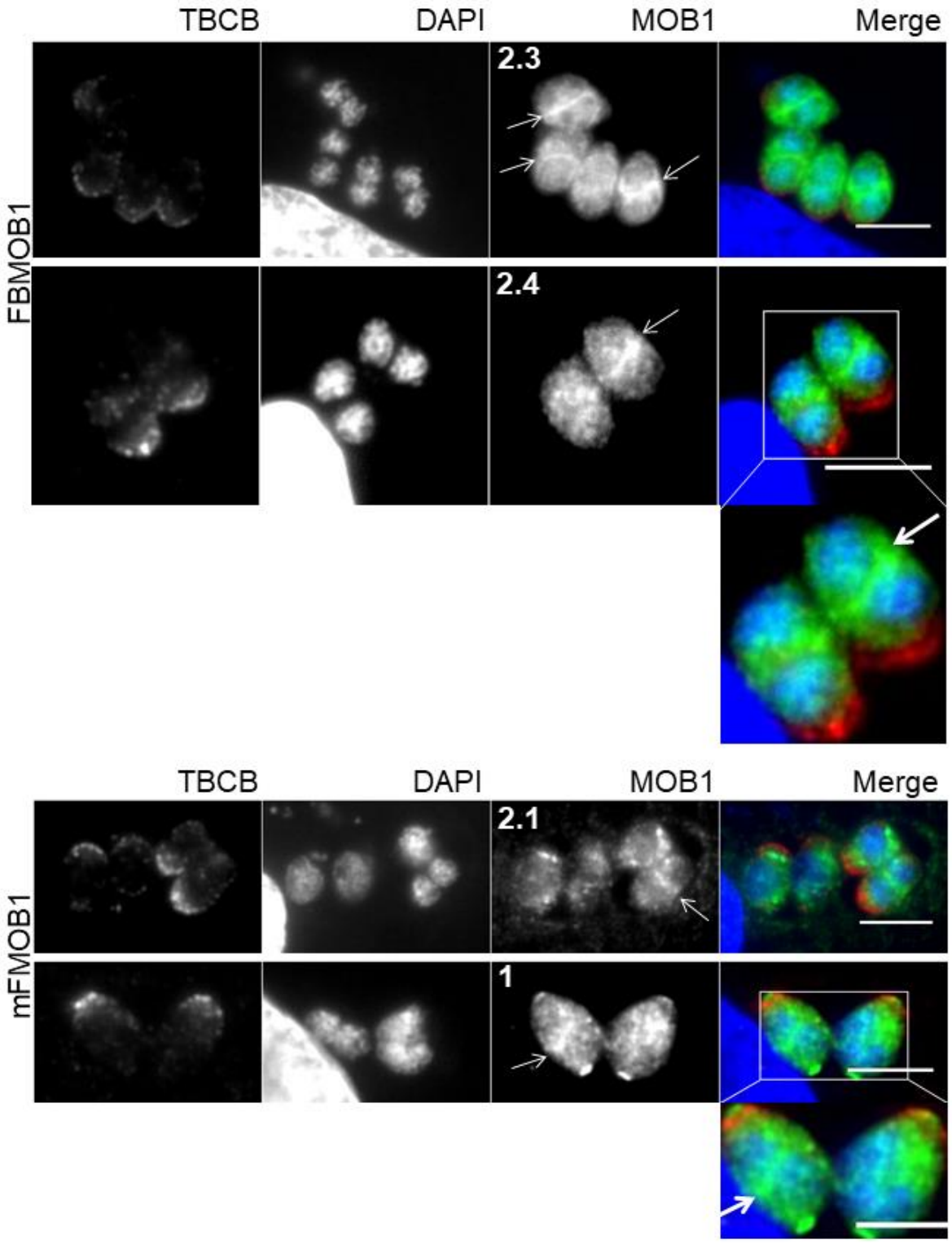

Figure 37. Anti-MOB1 sera detect recombinant MOB1 accumulating at the end of mitosis.

Recombinant MOB1 accumulates between the two newly divided nuclei at the end of mitosis when the new nuclei finish segregation but are still very close (arrows). This accumulation fades rapidly as the nuclei move further apart (panel with sera 2.4). This localization was observed in *T. gondii* strains expressing recombinant MOB1 with a high

expression promoter (FBMOB1), a low expression promoter (mFMOB1) and using various anti-MOB1 sera. The tachyzoites' apical pole is identified by the *T. gondii* tubulin cofactor B polyclonal sera (TBCB). DNA is identified using DAPI. Scale bars represent 5 µm. 1 – first production of anti-MOB1 sera, using GST-MOB1 (Tavares 2015); 2.1 to 2.5 – second production of anti-MOB1 sera, using GST-MOB1; FBMOB1 - FLAG-BirA-MOB1; mFMOB1 – morn1-FLAG-MOB1. DAPI - 4,6-diamidino-2-phenylindole.

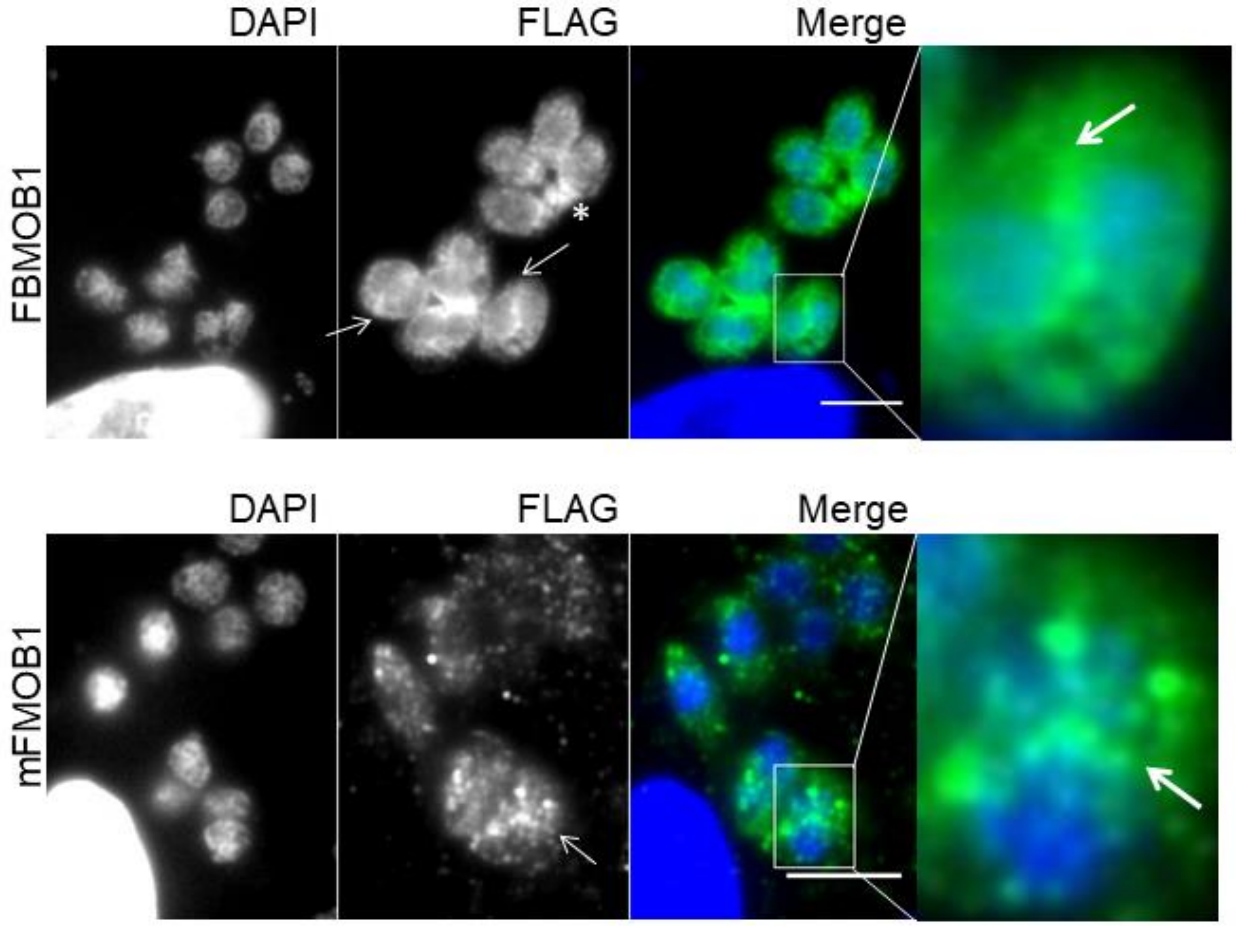

Figure 38. Anti-FLAG antibody detects the same accumulation as the anti-MOB1 sera.

The same accumulation of recombinant MOB1 between the new newly divided nuclei was observed when staining the morn1-FLAG-MOB1 and FLAG-BirA-MOB1 strains with anti-FLAG monoclonal antibody. In the top panel we see through the DAPI staining that the nuclei are just finishing its segregation. MOB1 recombinant protein was also observed in the residual body (*). DNA is identified using DAPI. Scale bars represent 5 µm. FBMOB1 - FLAG-BirA-MOB1; mFMOB1 – morn1-FLAG-MOB1.

4.3. The Interaction Network of *Toxoplasma gondii* MOB1

Our data indicates that MOB1 is involved in the regulation of replication and tachyzoite to bradyzoite transition in *T. gondii*. In order to understand the molecular pathways through which MOB1 acts in this organism, we worked to identify its interacting partners using predictive and experimental approaches.

4.3.1. *Toxoplasma gondii* expresses key elements of MEN and Hippo signaling beyond MOB1

The MOB1 function has been described mostly in the context of MEN/SIN/Hippo signaling. MOB1 appears as the most conserved component of these signaling pathways, having been identified in unicellular organisms that appear earliest in the evolutionary tree. However, other core components of the MEN/SIN/Hippo signaling pathways also emerge in unicellular organisms, indicating that MEN/SIN/Hippo signaling may also be present in these species. Protein kinases ScCdc15p/ SpCdc7p/ HsMST1/2/ DmHippo, and ScDbf2/20p/ SpSid2p/ HsLATS1/2/ DmWarts, essential proteins for MEN/SIN and Hippo signaling make up its core kinase modules together with the kinase adaptors Sc/SpMob1p/ HsMOB1/ DmMats. Analyses of predicted apicomplexan kinomes detected a high number of divergent kinases but also highly conserved eukaryotic kinase families (Peixoto et al. 2010; Talevich et al. 2011). The analyses identified several AGC kinases, including two NDR kinases, and one STE kinase in *T. gondii*. Sequence comparison indicates that the *T. gondii* NDR kinases S8ESP0 (TGME49_215670) and S8F1R4 (TGME49_272200) are possible orthologs of ScDbf2/20p/ SpSid2p/ HsLATS1/2/ DmWarts and HsNDR1/2/ DmTricornered, respectively (Figure 39). Significantly, *Mob1* presents an expression pattern similar to that of the TGME49_215670 and TGME49_272200 genes throughout the *T. gondii* life cycle, indicating a possible concerted action by these genes (this is further explored in section 4.4). While the single predicted *T. gondii* STE family kinase S8F0U9 (TGME49_225960) was not successfully classified into STE subfamilies, it presents high homology with the *N. caninum* F0VLX7 (NCLIV_046870) kinase which is classified as a STE20 kinase, the subfamily that includes the ScCdc15p/ SpCdc7p/ HsMST1/2/ DmHippo kinases. *T. gondii* S8F0U9 (TGME49_225960) and *N. caninum* F0VLX7 (NCLIV_046870) do not possess the HsMST1/2/ DmHippo SARAH (Salvador/Rassf/Hippo) domain. Notably, the SARAH domain is also absent in ScCdc15p/ SpCdc7p, the *S. cerevisiae* and *S. pombe* HsMST1/2/ DmHippo orthologs. Additionally, the *T. gondii* kinome appears to lack kinases containing a citron homology CNH domain (CNH)

which is present in the STE20 kinases HsMAP4K4/6/7/ DmMisshapen and HsMAP4K1/2/3/5/ DmHappyhour. Still, the *T. gondii* uncharacterized protein A0A125YQ80 (TGME49_306220) presents two WW domains, similarly to YAP, the most conserved Hippo effector protein. The *T. gondii* genome also codes for four 14-3-3 proteins, highly conserved phospho-binding regulator proteins which regulate HsYAP/HsTAZ/DmYorkie activity. CDK1 and CDC14, highly conserved proteins that regulate the cell cycle, are also present in the *T. gondii* genome. The cyclin-dependent related kinase 2 (CRK2) (A0A125YRL7; TGME49_218220) and the phosphatase CDC14 (A0A125YZF0; TGME49_314430) are likely orthologous to ScCdk1p and ScCdc14p/ SpCip1, respectively. No clear counterparts to ScNud1p, ScTem1p, SpSid1, HsSAV1/ DmSalvador, HsKIBRA/ DmKibra, HsTEAD/ DmScalloped, HsNF2/ DmMerlin, or HsYAP/TAZ/ DmYorkie were identified in *T. gondii* (Figure 39).

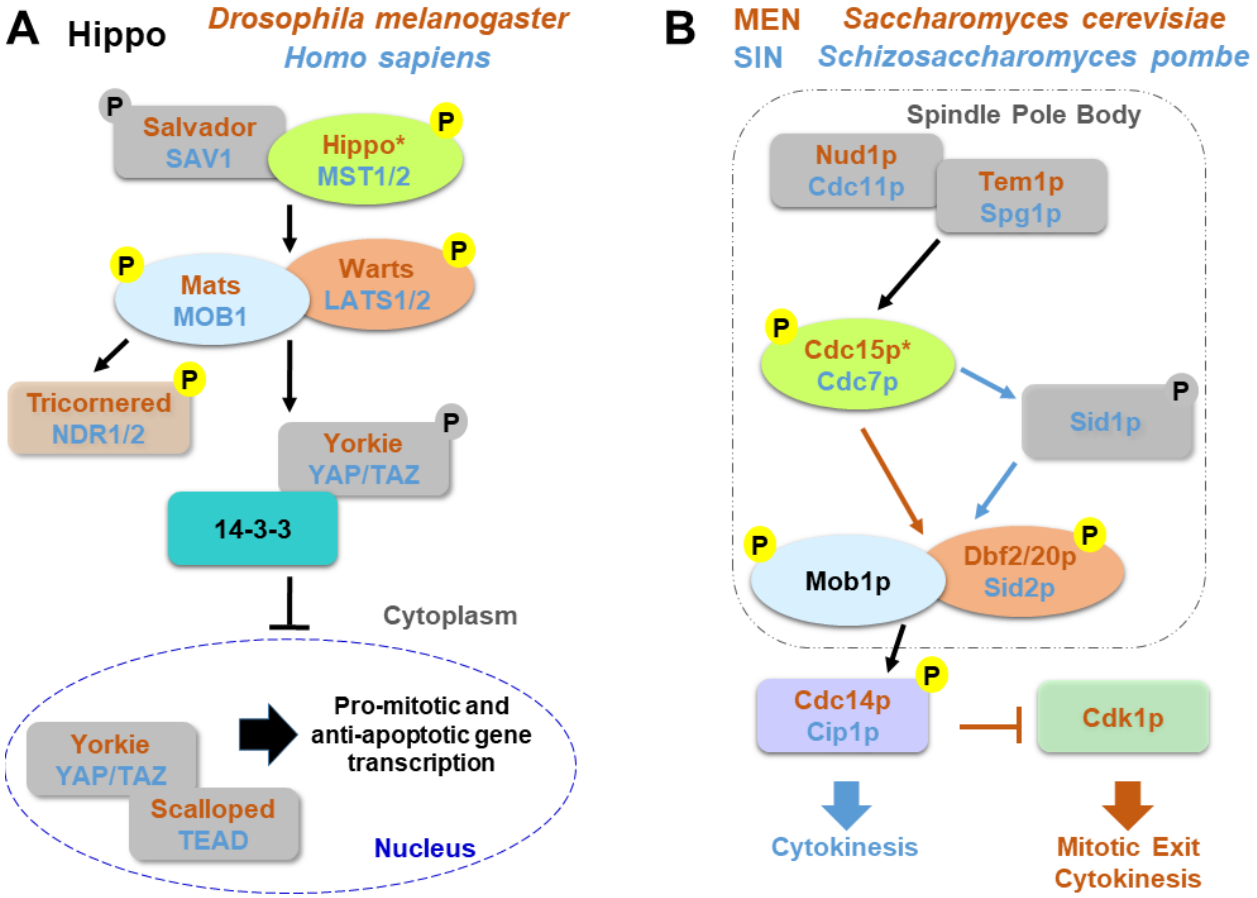

Figure 39. Hippo/MEN/SIN components with possible *Toxoplasma gondii* counterparts.

Figure 9 was updated to highlight the predicted components of a hypothetical *T. gondii* MEN/SIN/Hippo pathway. **A)** *D. melanogaster* and *H. sapiens* Hippo pathway core components. **B)** *S. cerevisiae* MEN and *S. pombe* SIN core components.

The STRING database, accessed December 2020, lists nine proteins as probable interactors of MOB1 that form a network with a protein-protein interaction enrichment value of $1.29*10^{-07}$. The network includes 11 nodes and 32 connections (Figure 40, Table 16). The *T. gondii* gene TGME49_256880 codes one protein but is misidentified by STRING as two separate proteins coded by the genes TGME40_056880 and TGME49_056890. Meaning that this network actually includes ten nodes and 28 connections. Therefore, the real protein-protein interaction enrichment value is lower than $1.29*10^{-07}$. Of the nine identified nodes, seven proteins are kinases, one is a Tre-2/Bub2/Cdc16 (TBC) domain-containing protein and one is a tyrosine phosphatase. More specific classifications of the seven kinases include one rhoptry kinase, one serine/threonine kinase, two CMGC kinase including one CRK, and three AGC kinases with one being an NDR kinase. The high frequency of this protein type evidences the probable kinase related signaling activity of the *T. gondii* MOB1. These predictions are based on text mining, experiments and co-expression data. Notably, the CDC14 (TGME49_314430) and the NDR kinase S8F1R4 (TGME49_272200) are proteins identified as probable counterparts to MEN/SIN/Hippo components. TGME49_314430 codes for the predicted *T. gondii* CDC14 while TGME49_272200 codes for the predicted *T. gondii* NDR. Two other AGC kinases and one CRK were also identified in the MOB1 interaction network. The identification of a rhoptry protein indicated a MOB1 action related to apicomplexan specific biology. Furthermore, the ScBub2 participates in MEN activation and one of the predicted *T. gondii* MOB1 interactor belongs to the TBC family. Altogether, these data support the possibility that a MEN/SIN/Hippo-like pathway may be conserved in *T. gondii*.

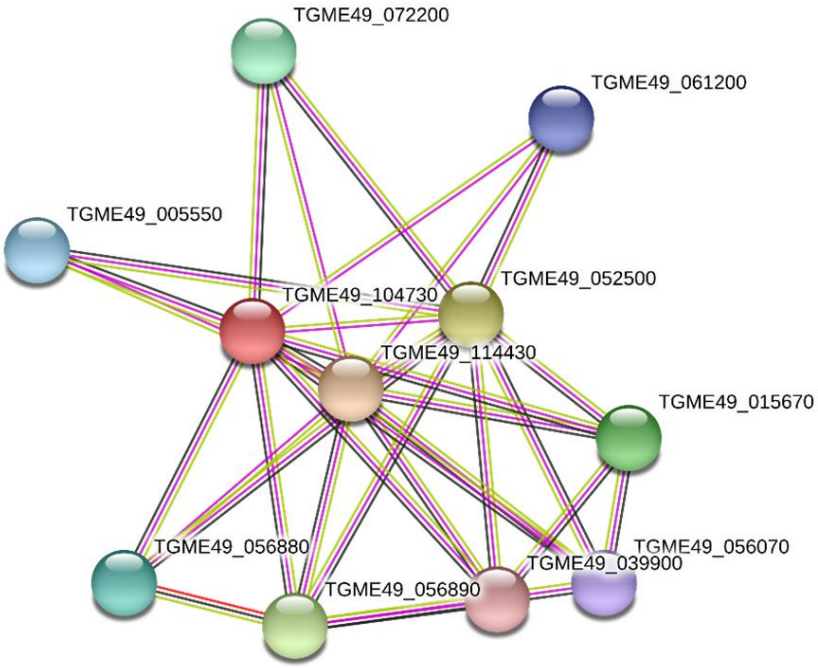

Figure 40. MOB1 interaction network predicted by STRING.

STRING generated diagram depicting the predicted MOB1 interaction network. The STRING database identifies nine proteins as probable interactors of the *T. gondii* MOB1. Two proteins identified in the diagram (TGME49_056880 and TGME49_056890) consist of a single protein identified coded by TGME49_256880.

Table 16. *Toxoplasma gondii* proteins predicted as MOB1 interactors by STRING.

STRING[1]	ToxoDB[2]	Uniprot	Description	Score
114430	314430	A0A125YZF0	CDC14	0.803
052500	252500	S8F7N5	ROP kinase	0.693
056880 056890	256880	S8GBL3	Ser/Thr kinase	0.576
015670	215670	S8ESP0	AGC kinase	0.576
072200	272200	S8F1R4	NDR kinase	0.517
05550	205550	S8GN25	AGC kinase	0.517
061200	261200	S8GLW6	Rab-GAP TBC protein	0.487
056070	256070	A0A125YUD7	CMGC kinase	0.468
039900	239910	S8FAP4	CRK-like	0.468

The genes that code for each protein are identified with STRING, ToxoDB and Uniprot identifiers. A functional description and the STRING interaction score are provided for each protein. 1 – STRING gene ID number; 2- TGME49_ gene ID number.

4.3.2. The FLAG tagged MOB1 BioID system shows a high biotinylation capacity

We assembled a FLAG tagged MOB1 BioID system in order to experimentally asses the MOB1 interactome in *T. gondii*. Clonal lines were tested for the expression of the recombinant proteins FLAG-BirA and FLAG-BirA-MOB1 (Figure 41). As a first approach the clonal lines were tested through immunofluorescence using a monoclonal antibody to detect the FLAG tag. Positive clones by immunofluorescence were also tested by western blot to confirm the expected recombinant protein size: FLAG-BirA is predicted to have 41 kDa while FLAG-BirA-MOB1 is predicted to have 76 kDa. We selected FLAG-BirA and FLAG-BirA-MOB1 strains with similar expression levels of the FLAG-BirA and FLAG-BirA-MOB1 recombinant proteins for interactome identification assays (Figure 41). Notably, the FLAG-BirA-MOB1 recombinant protein presents a cytoplasmic localization and we can observe a variation in signal strength in tachyzoites of different parasitophorous vacuoles, which is not observed in FLAG-BirA tachyzoites, although these are clonal lines. These results confirmed those observed for the FLAG-MOB1 recombinant protein in morn1-FLAG-MOB1 tachyzoites (Figure 35).

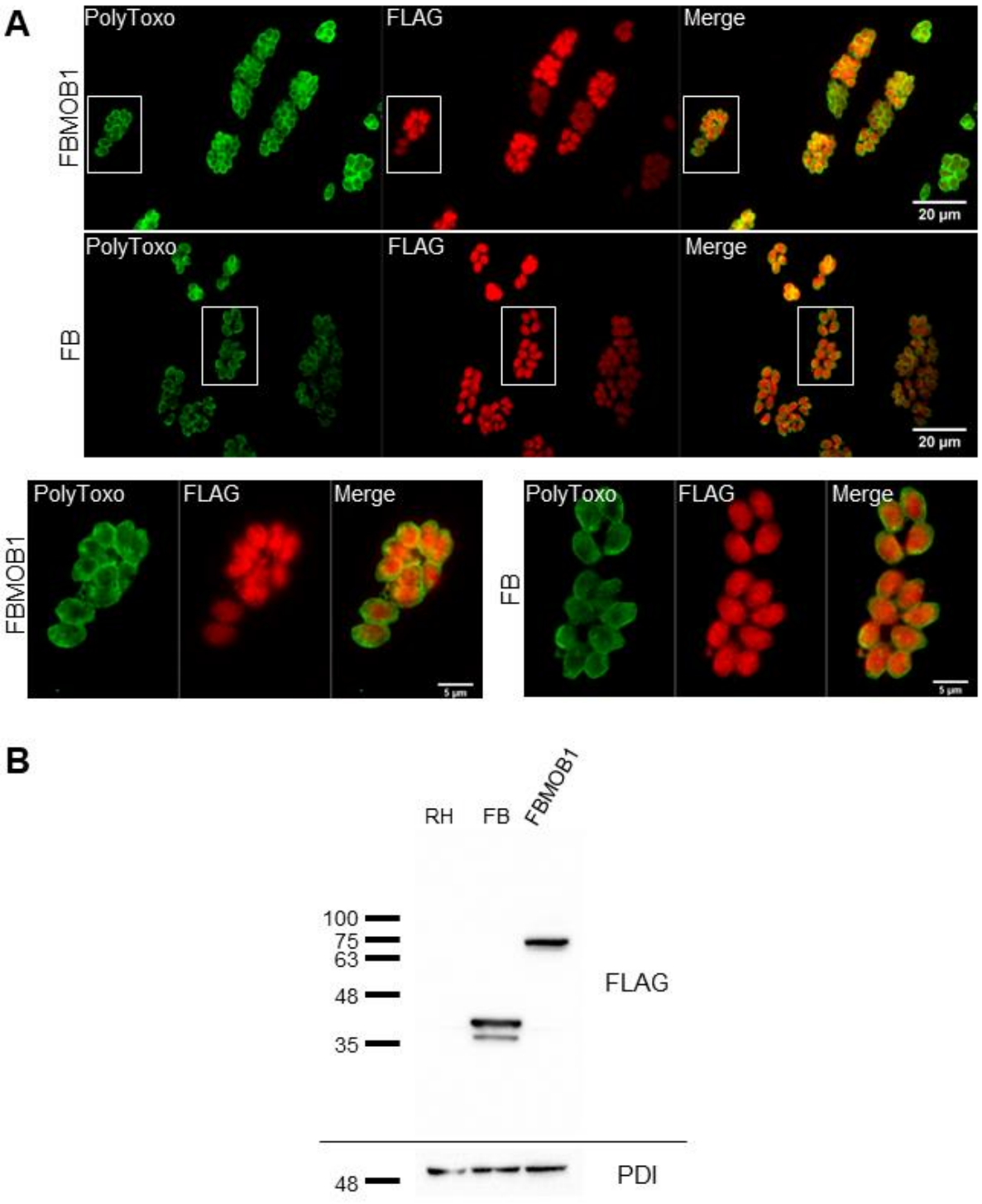

Figure 41. The FLAG-BirA and FLAG-BirA-MOB1 strains adequately express the respective recombinant proteins.

FLAG-BirA and FLAG-BirA-MOB1 clonal lines were tested for the expression of the recombinant proteins using anti-FLAG monoclonal antibody. **A)** We detected the expression of the predicted recombinant proteins in FLAG-BirA and FLAG-BirA-MOB1 clonal lines through immunofluorescence. Tachyzoites constitutively expressing FLAG-BirA-MOB1

and FLAG-BirA, driven by the strong promoter *Tub8*, present a cytoplasmic location. FLAG-BirA-MOB1 tachyzoites from the same clonal line present varying expression levels, which is not observed in the control FLAG-BirA tachyzoites. *T. gondii* surface proteins are identified with polyclonal sera (PolyToxo). The two bottom panels are details amplified from the two top panels, indicated by the white line rectangles. The scale bars of the two top panels represent 20 μm while those of the two bottom panels represent 5 μm. **B)** We confirmed the expression of the FLAG-BirA and FLAG-BirA-MOB1 recombinant proteins by western blot analysis. The molecular weight of the recombinant proteins expressed in the FLAG-BirA and FLAG-BirA-MOB1 clonal lines is compatible to the predicted 41 kDa for FLAG-BirA and 76 kDa for FLAF-BirA-MOB1. The *T. gondii* protein disulfide isomerase (PDI) was used as loading control. Numbers on the left represent molecular weights in kDa.

Following this, we confirmed our BioID system was functional as the BirA recombinant proteins were able to biotinylate other proteins *in vivo* (Figure 42). We used western blot coupled to streptavidin-HRP to assess functionality and to evaluate the experimental conditions regarding biotin concentration, time of biotin incubation, and lysis buffer used. We tested different concentrations of biotin (50 and 150 μM), biotin incubation times (24, 48, and 64 hours) and cell lysis using two protein lysis buffers, a sacharose based and a RIPA buffer. We confirmed that both recombinant proteins are functional as both FLAG-BirA and FLAG-BirA-MOB1 protein extracts present substantially higher amounts of biotinylated proteins when biotin is added to the culture medium compared to the control strain and to when no biotin is supplied (Figure 42). The best experimental conditions were achieved by incubating the parasites with 150 μM of biotin during 48 hours. The sacharose and RIPA buffers performed similarly, but we observed slightly more obvious differences between the biotinylated proteins pattern of FLAG-BirA and FLAG-BirA-MOB1 tachyzoites using the sacharose buffer and used this buffer in future analyses.

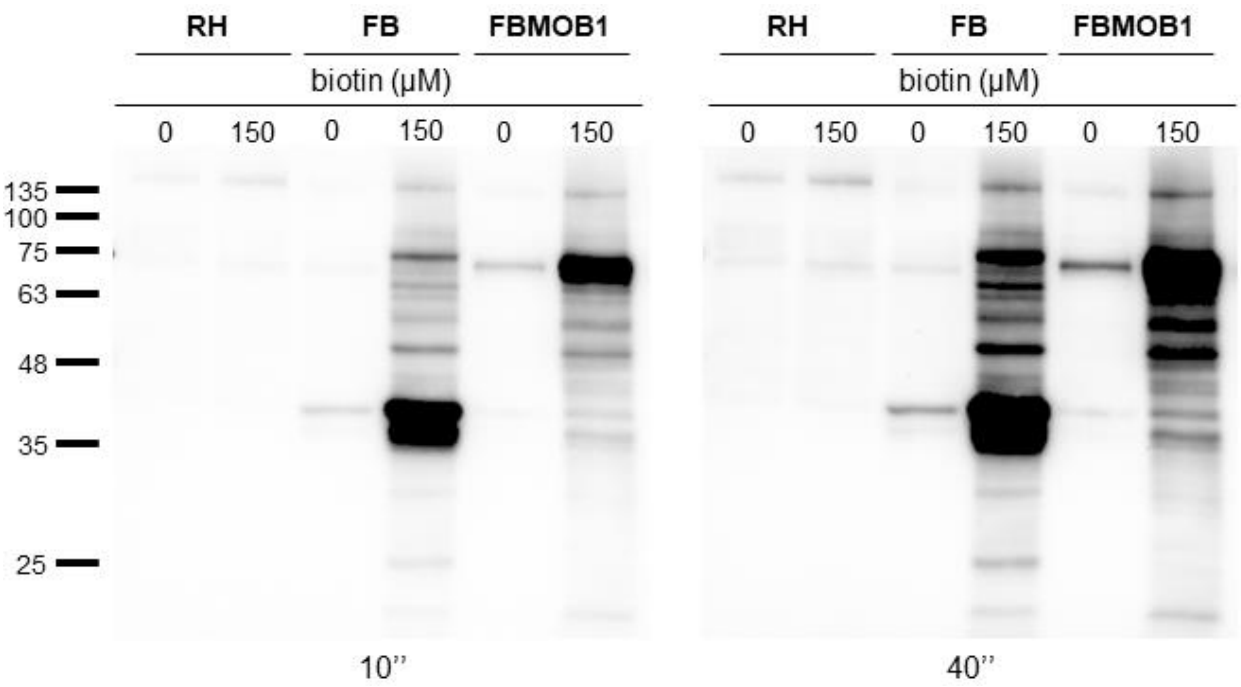

Figure 42. FLAG-BirA and FLAG-BirA-MOB1 strains successfully biotinylate proteins *in vivo*.

We confirmed that the BirA recombinant proteins can biotinylate other proteins *in vivo* through western blot using streptavidin-HRP. FLAG-BirA and FLAG-BirA-MOB1 protein extracts present substantially higher amounts of biotinylated proteins when biotin is added to the culture medium compared to the control strain and to when no biotin is supplied. Numbers on the left represent molecular weights in kDa. Numbers on the bottom indicate the exposure time in seconds. FB - FLAG-BirA; FBMOB1 - FLAG-BirA-MOB1.

4.3.3. The BioID assay identified a *Toxoplasma gondii* MOB1 interactome

For the first BioID assay, FLAG-BirA and FLAG-BirA-MOB1 tachyzoite pellets weighing approximately 50 mg were lysed in 2 ml of lysis buffer and approximately 8 mg of soluble protein of each extract were incubated with agarose-streptavidin beads. Following binding, beads were washed with lysis buffer and with 8M urea. The full beads volume was boiled in 2x loading buffer to elute the biotinylated proteins. Western blot analysis of the eluates confirmed that the precipitation was successful in purifying biotinylated proteins (Figure 43). The eluates were run in an acrylamide gel and were subjected to trypsin in-gel digestion coupled with mass spectrometric analysis by nanoLC-TripleTOF (UniMS iBET/ITQB-UNL Mass Spec Services, Oeiras, Portugal) with technical duplicates for a single experiment. The analysis resulted in a very low intensity signal which translated in a low total number of identified proteins: 25 for FLAG-BirA and 17 for FLAG-BirA-MOB1 considering only identified proteins with Unused Protein Score above 1.3 and peptides with confidence above 95%. Including proteins identified with Unused Protein Score above 0.47 and peptides with confidence above 66%, we obtained a

protein total of 35 for FLAG-BirA and 24 for FLAG-BirA-MOB1 (Figure 43). The technology used in this assay only allows identification of proteins, therefore, the criteria to define differentially biotinylated proteins was presence in FLAG-BirA-MOB1 and absence in FLAG-BirA. Of the 35 identified proteins, 11 were unique to FLAG-BirA-MOB1 thus considered differentially biotinylated, including the FLAG-BirA-MOB1 recombinant protein. As we used an overexpression system with high expression levels, we expected a higher total number of detected proteins. The protein used for this analysis resulted in a very weak intensity signal and a relatively low number of identified proteins based on a single peptide with confidence higher than 95% or between 66-95%, compatible to a very low amount of detected protein as shown by the total ion chromatograms (TIC) in Figure 43. In order to improve this assay and our confidence in the results, we decided to optimize our precipitation protocol in an effort to increase total biotinylated protein yield, namely by increasing the amount of starting material, obtaining more concentrated extracts of biotinylated proteins, increasing the ratio of protein to streptavidin-agarose beads, performing less stringent washes by substituting 8M urea by PBS, and performing the trypsinization step directly on the agarose beads, bypassing the elution step and electrophoresis steps.

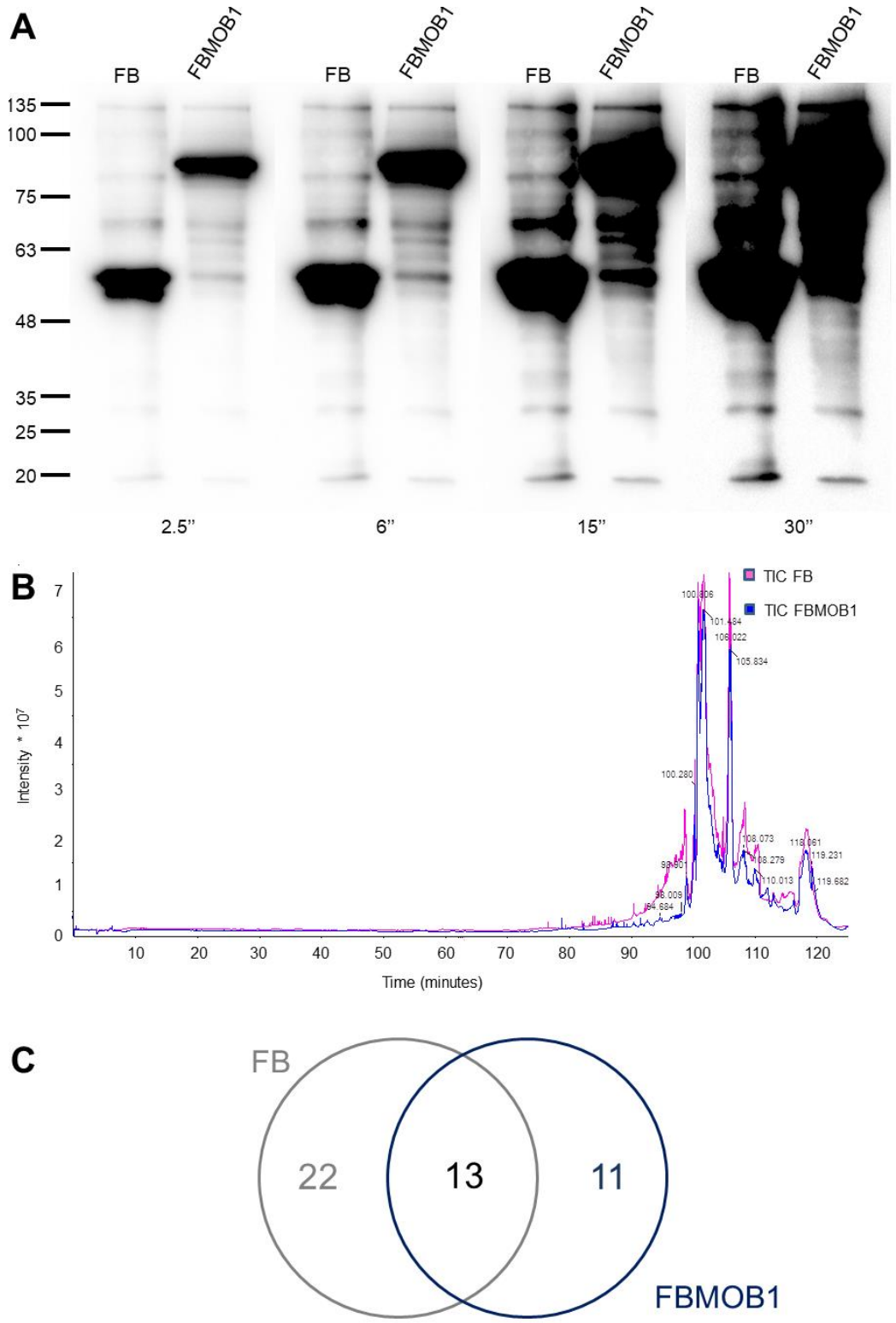

Figure 42. The first BioID precipitation assay yielded poor results.

A) Precipitation with streptavidin-agarose beads successfully isolated biotinylated proteins from FLAG-BirA and FLAG-BirA-MOB1 protein extracts. Numbers on the left represent molecular weights in kDa. The numbers on the bottom represent exposure time in seconds. **B)** Total ion chromatogram (TIC) resulting from the nanoLC-TripleTOF

analysis of the FLAG-BirA and FLAG-BirA-MOB1 precipitated proteins. An appropriate signal for detection would consist in a series of peaks with intensities ranging from $1x10^7$ to $12x10^7$, forming a curve between 20 and 100 minutes, where the FLAG-BirA and FLAG-BirA-MOB1 TICs present baseline values. **C)** Venn diagram illustrating the results from the mass spectrometry analysis. FB - FLAG-BirA; FBMOB1 - FLAG-BirA-MOB1.

For the second BioID assay, FLAG-BirA and FLAG-BirA-MOB1 tachyzoite pellets weighing approximately 200 mg (4 times more) were lysed in 3 ml of lysis buffer. Approximately 24 mg of soluble protein of each extract were incubated with agarose-streptavidin beads. Following binding, beads were washed with lysis buffer and with PBS. The supernatant was removed and the streptavidin-agarose beads were frozen at -70 ºC until the mass spectrometry analysis. To evaluate the assay, 10% of the bead volume was transferred to a separate tube and boiled in 2x loading buffer for analysis through western blot. Proportional volumes of protein extracts pre-precipitation and post-protein extracts precipitation, and three times concentrated volume of the final wash buffer (PBS) were also analyzed. The western blot analysis confirmed that the precipitations were successful in purifying biotinylated proteins (Figure 44). The post-precipitation protein extracts still maintained some biotinylated protein and we also detect a small amount of biotinylated proteins in the last wash buffer, mostly the recombinant proteins FLAG-BirA and FLAG-BirA-MOB1. Therefore, there is room to further improve the precipitation conditions.

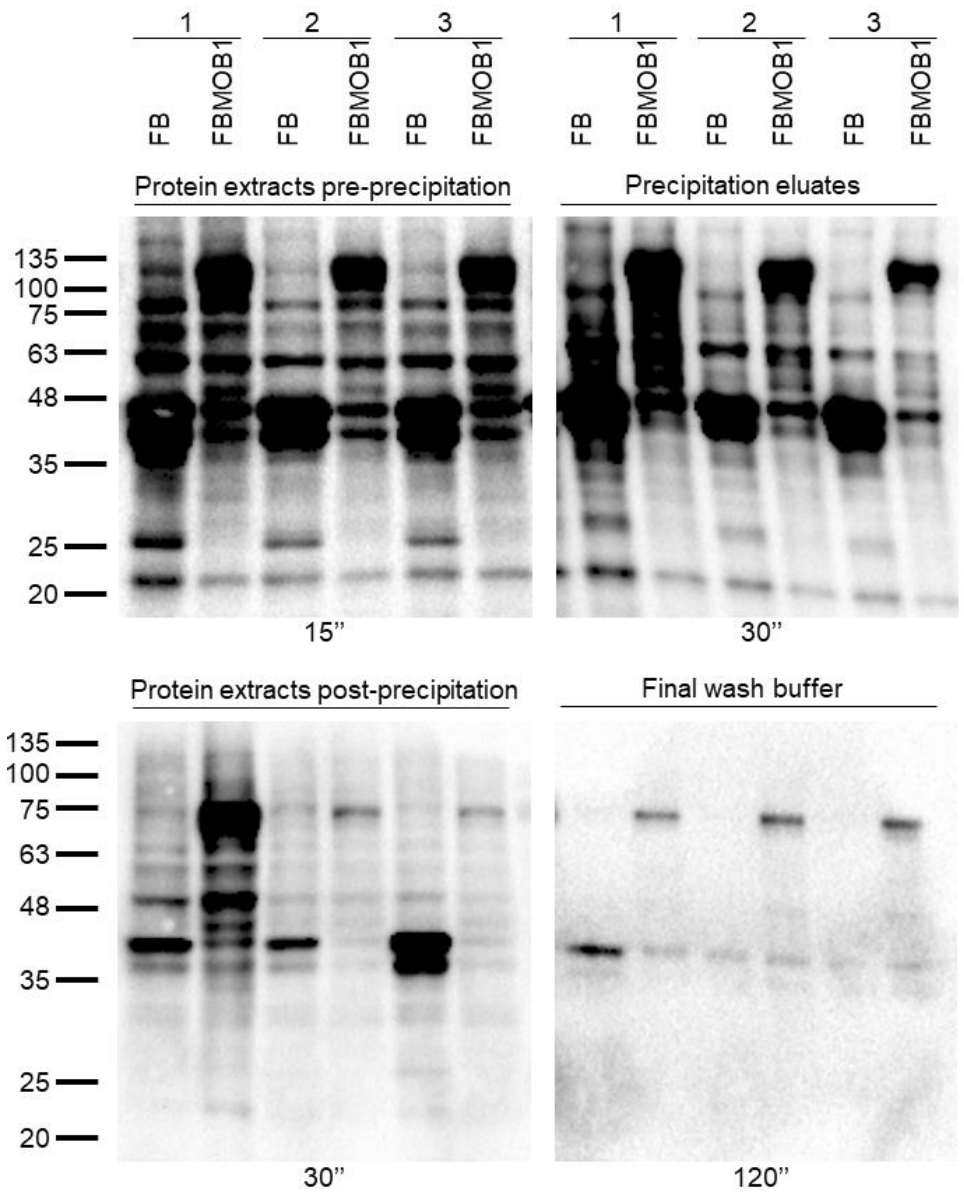

Figure 44. Evaluation of the precipitation of the second BioID assay.

Precipitation successfully isolated biotinylated proteins from FLAG-BirA and FLAG-BirA-MOB1 protein extracts of three independent experiments. Numbers on top indicate the BioID assay. Numbers on the left represent molecular weights in kDa. Numbers on the bottom represent exposure time in seconds.

The mass spectrometry analysis of the three independent experiments was performed at the I3S Proteomics Platform (Porto, Portugal). The samples were processed for proteomics analysis following a solid-phase-enhanced sample-preparation protocol, starting with an on-bead trypsinization, for protein identification and quantitation through nanoLC-MS/MS. The technology used in this assay allows for protein identification and quantification, therefore, the

criteria to define differentially biotinylated proteins was either presence in the FLAG-BirA-MOB1 strain and absence in the FLAG-BirA strain or a significantly higher level of presence in the FLAG-BirA-MOB1 *versus* the FLAG-BirA samples. We considered proteins identified with FDR experimental q-value≤0.05 and abundance ratio adjusted p-value≤0.05. Proteins that were detected in only one of the three independent samples of FLAG-BirA or FLAG-BirA-MOB1 strains were also excluded from the analysis. A total of proteins 3123 biotinylated proteins were significantly detected, 128 uniquely or significantly more biotinylated in the FLAG-BirA-MOB1 strain (Figure 45). Principal component analysis shows that the samples FLAG-BirA and FLAG-BirA-MOB1 cluster together according to strain and independently from the other group, with the principal component 1 accounting for 98.5% of the variance between samples (Figure 45).

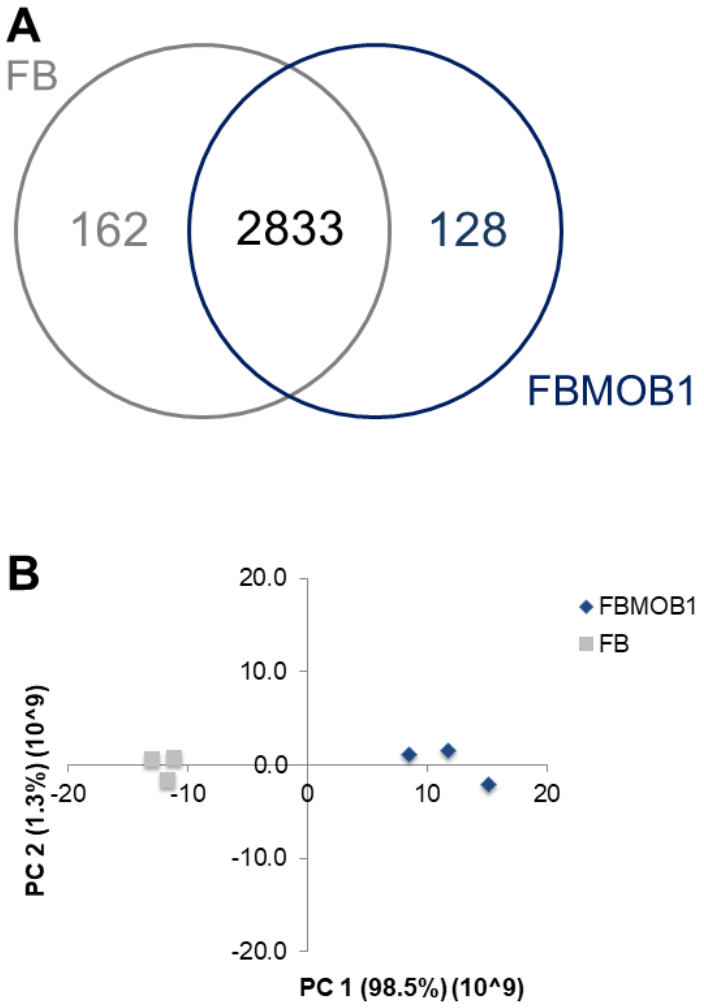

Figure 45. The second BioID assay resulted in the detection of a high number of proteins with samples clearly clustering according to strain.

A) Venn diagram illustrating the distribution of the 3123 proteins significantly detected in the mass spectrometric analysis. **B)** Principal component analysis shows clear clustering of FLAG-BirA and FLAG-BirA-MOB1 samples

according to strain. The first factor (PC 1) accounts for 98.5% of the variance between samples. FB - FLAG-BirA; FBMOB1 - FLAG-BirA-MOB1.

Total peptide quantification prior to sample loading onto the mass spectrometer detected an average of 360 ŋg/µl in a total of 100 µl of sample. A maximum of 500 ŋg of peptides was used per analysis, so the total amount of protein isolated was more than enough for a successful analysis. This calls into question our previous assessment concerning the first BioID assay. Based on protein quantification of protein extracts pre-precipitation, the protein produced for the first assay was roughly 1/10 of the produced for the second assay (per analysis), however that would still be more than sufficient for a successful analysis. Therefore, we hypothesize that there must have been loss of protein during the process, perhaps during the urea washing steps or the step of gel loading, or downstream during the mass spectrometry analysis process, namely during in-gel digestion by trypsinization.

4.3.4. The BioID assays point to a MOB1 interactome with high involvement of nucleic acid and ubiquitin-proteasome system related proteins

4.3.4.1. The MOB1 differentially biotinylated proteins identified in the first BioID assay belong to diverse functional categories

In the first BioID assay, 11 proteins were identified as FLAG-BirA-MOB1 differentially biotinylated, including FLAG-BirA-MOB1 which was the top identified protein presenting the highest unused protein score (Table 17). The differentially biotinylated proteins include, with 95% confidence, a transmembrane protein, a protein that harbors a structural maintenance of chromosomes domain (SMC), 3 ribosomal proteins, a dense granule protein (GRA5) and, with 66-95% confidence, a histone, a protein with a Ku70 domain, a ribosomal protein and an uncharacterized protein with no known domains. These results point to an involvement of MOB1 with several *T. gondii* processes, namely, cellular signaling, translation and DNA replication. However, these proteins were identified based on a single peptide with confidence higher than 95% or between 66-95% originating from a single experiment and the identifications resulted from a very low signal. Therefore, these results may give us a biased vision of the MOB1 interactome.

Table 17. Differentially biotinylated proteins identified in the first BioID precipitation assay.

ToxoDB #	Description
N/A	FLAG-BirA-MOB1
TGME49_201390	Transmembrane protein
TGME49_212780	SMC domain uncharacterized protein
TGME49_300200*	Histone H2A
TGME49_248160*	Ku70 domain uncharacterized protein
TGME49_225080	Ribosomal protein S18
TGME49_229670	Ribosomal protein S23
TGME49_263050	Ribosomal protein L13
TGME49_310490*	Ribosomal protein L22
TGME49_286450	Dense granule 5
TGME49_266380*	Uncharacterized protein (no known domains)

* proteins identified with 66-95% confidence; SMC – structural maintenance of chromosomes.

4.3.4.2. The MOB1 differentially biotinylated proteins identified in the second BioID assay confirmed and expanded on the functional categories identified in the first assay

In the second BioID assay, 128 proteins were identified as FLAG-BirA-MOB1 differentially biotinylated, including FLAG-BirA-MOB1 and endogenous MOB1 (Annex II, Table 1). We were able to identify one peptide with high confidence that, due to the trypsin cleavage sites available on the recombinant FLAG-BirA-MOB1 and on the endogenous MOB1, is coherent with belonging to the endogenous MOB1 (Figure 46). The peptide corresponds to the most N-terminal endogenous MOB1 peptide cleaved at the first arginine residue and was detected harboring the post-translational modification methionine loss. This evidence indicates that MOB1 is expressed in *T. gondii* although likely at very low levels, consistent with our findings of phenotypes following knockout of *Mob1*.

Figure 46. Identification of the endogenous MOB1 through nanoLC-MS/MS.

A single peptide compatible only with the endogenous MOB1 was identified through nanoLC-MS/MS. Trypsin digestion cleaves the peptide bond between arginine (R) or lysine (K) and the adjacent amino acid.

We performed functional categorization of the FLAG-BirA-MOB1 significantly biotinylated proteins and were able to atribute 94 proteins into 9 functional categories: metabolism, cell cycle and DNA processing, transcription, protein synthesis and fate, ubiquitin-proteasome system (UPS), signal transduction, cell transport, secretory system and cell structure (Figure 47). For lack of information, 32 proteins (25.2%) were not atributed to any functional category (ND). Analysis using blastp showed that 24 of the not assigned proteins are apicomplexan specific proteins with 14 being specific to cyst-forming coccidia.

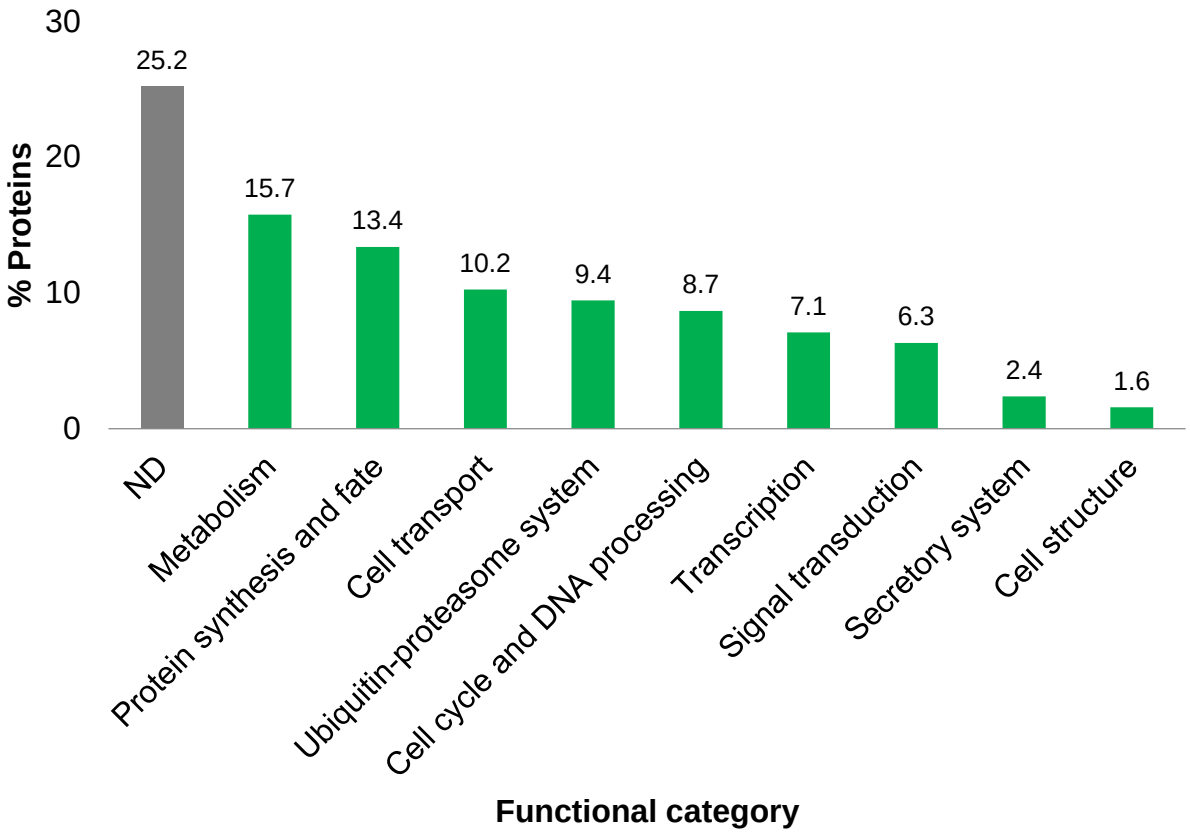

Figure 47. Distribuition of FLAG-BirA-MOB1 differentially biotinylated proteins by functional category.

ND – not determined.

The most frequently identified category was metabolism with 20 proteins, namely eight hydrolases (including a DNA glycosylase, a phospholipase C-like phosphodiesterase, a phospholipase DDHD1, a peptidase amidohydrolase and an aspartyl aminopeptidase), seven proteins involved in amino acid metabolism (including two methyltransferases, glutamate-5-kinase and adenylosuccinase), two redox related thioredoxins, one mannose-6-phosphate isomerase, one thiamin pyrophosphokinase, and one Pleckstrin-like protein. The metabolism category is followed in protein number by the protein synthesis and fate category which includes 17 proteins. We detected four proteins involved in rRNA biogenesis and processing, five proteins involved in translation (three ribosomal proteins, a mitochondrial glycoprotein and a translation initiation factor 2A), two proteins involved in folding, and five proteins involved in protein modification, including constitutive photomorphogenesis 9 signalosome complex subunit 5 (CSN5), an oligosaccharyl transferase, and a Mir domain-containing protein related to glycosylation. Regarding cell transport, 13 proteins were assigned to this category, including an ATG6 (autophagy-related protein 6)/Beclin1-like protein, a soluble N-ethylmaleimide sensitive

factor attachment protein receptor (SNARE) protein, a RAS-associated protein 5 (Rab5)-interacting protein, a protein translocation complex SEC61 gamma subunit, and a thrombospondin type 1. Proteins related to ubiquitin-dependent protein degradation were also frequent in the MOB1 interactome with 12 identified proteins, including an ubiquitin receptor protein DA1-like (da is Chinese for “large”), an ubiquitin family protein, an ubiquitin-activating enzyme E1, an ubiquitin-conjugating enzyme E2, two proteins containing ubiquitin-ligase E3 domains (a RING (really interesting new gene)-type E3 domain and a Gid (glucose induced degradation deficient complex)-type RING domain), two proteasome subunit beta proteins (PSMB1 and PSMB5), a S-phase kinase-associated protein 1 (SKP1), and a regulatory particle non-ATPase 13 (RPN13). Proteins involved in cell cycle regulation and DNA processing were also among the most detected. From 11 proteins related to cell cycle regulation and DNA processing, five proteins are involved in DNA replication (including a an helicase and a SMC domain-containing protein), three proteins participate in DNA repair (RAD25, RAD26, and RAD51), and four proteins are involved in cell cyle regulation (including the anaphase-promoting complex subunit 1 (APC1), dual specificity tyrosine phosphorylation regulated kinase (DYRK), and the cytokinesis related coiled-coil domain containing protein 124 (CCDC124)). We also detected nine proteins involved in transcription, including the ApiAP2 AP2VIIA4 transcription factor, the mediator of RNA polymerase II transcription subunits (MED) MED8 and MED10 transcription regulators, two DEAD/DEAH (Asp-Glu-Ala-Asp/Asp-Glu-Ala-His) box helicases and a polyadenylation factor subunit. In the signal transduction category, we identified eight proteins including five kinases (cAMP-dependent protein kinase catalytic subunit 1 (PKAc1), cAMP-dependent protein kinase regulatory subunit (PKAR), calcium/calmodulin dependent protein kinase 1 (CAMK1), phosphofructokinase (PFK), a tyrosine kinase-like kinase (TKLK), and two phophatases). Secretory system proteins were also detected, namely two ROPs (ROP1 and an uncharacterized ROP) and one uncharacterized ROM. Finaly, we detected two cytoskeleton related proteins, Myosin B/C and an engulfment and cell motility (ELMO) protein.

The expected subcellular localization of the FLAG-BirA-MOB1 differentially biotinylated proteins was determined using available experimental and predictive data (Figure 48). There is a clear tendency for a nuclear subcellular localization, with 30 (23.6%) proteins predicted to be present in this organelle. Together with the nucleus, the plasma membrane (PM) with 16 (12.6%) proteins, the cytoplasm with 15 (11.8%) proteins, the endoplasmic reticulum (ER) with 12 (9.4%) proteins, the Golgi with 10 (7.9%), and the mitochondrion with 9 (7.1%) represent 72.4% of the predicted subcellular localizations of the FLAG-BirA-MOB1 differentially biotinylated proteins. Apicoplast, proteasome, and ribosome localizations were predicted for

seven or six proteins each. Less than five proteins were predicted to be localized to the organelles/subcelular spaces apical, IMC, dense granules, rhoptries, cytoskeleton, endomembrane vesicles, micronemes, or extracellular. For lack of information, no subcellular localization was determined for 22 (17.3%) proteins (ND).

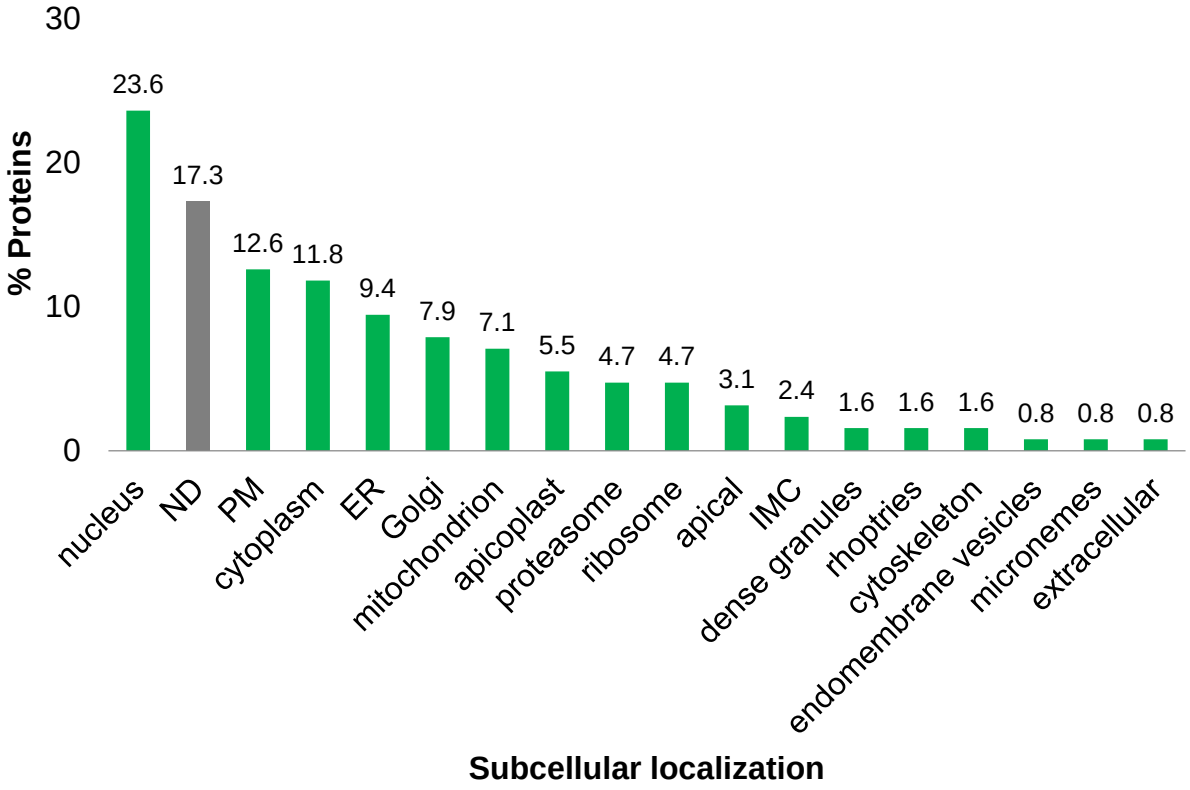

Figure 48. Distribuition of FLAG-BirA-MOB1 differentially biotinylated proteins by subcellular localization.

ND – not determined.

We performed a literature review to identify possible FLAG-BirA-MOB1 differentially biotinylated protein counterparts that have been characterized as related to MOB, MEN, and/or the Hippo pathway. We detected reports of two possible counterparts related to MOB, two possible counterparts related to MEN and of 17 possible counterparts related to the Hippo pathway, which are listed in Table 18. We included in the analysis seven proteins that, although not specifically reported with functions relating to MOB/MEN/Hippo in other organisms, belong to the same protein families or have roles intimately connected with other proteins detected as counterparts of FLAG-BirA-MOB1 differentially biotinylated protein, namely proteins related to the UPS and PKAR. Using this inferrence criteria, we considered the two E3 ligase domain-

containing as possible counterparts to the *H. sapiens* RING-type E3 ligase HsPraja2, the PSMB1, E1, E2, and ubiquitin family protein for its roles in the UPS, and the PKAR for its association to the PKAc1. Considering the functional category, we identified counterpart/related proteins classified mostly to the UPS (nine or 52.9%), cell cycle and DNA processing (three or 17.6%), and signal transduction (three or 17.6%) (Figure 49). Considering the subcellular localization, MOB1/MEN/Hippo counterpart/related proteins are predicted to localize mostly to the nucleus (six or 35.3%), proteasome (four or 25.3%), and cytoplasm (three or 17.6%) (Figure 50).

Table 18. Differentially biotinylated proteins with counterpart/related proteins characterized as associated to MOB/MEN/Hippo.

ToxoDB[a]	UniProt	Protein	Association	Reference
219120	S8EN13	E3	MOB/H	[b] Lignitto 2013, Song 2019
265390	S8GGY5	E3	MOB/H	
218920	A0A125YL46	PSMB5	Hippo	Kapoor 2014
290005	S8F038	PSMB1	Hippo	
290290	S8G8F6	E1	Hippo	[b] Lignitto 2013, Kapoor 2014, Song 2018, Song 2019
202820	A0A125YRV8	E2	Hippo	
254600	A0A125YWZ9	Ubi	Hippo	
224110	S8G5J3	RPN13	MEN	Zhou 2020
207680	A0A125YIV5	SKP1	MEN/H	Liu 2010, Zhao 2010, Kim 2006
272900	A0A125YQJ7	RAD51	Hippo	Pefani 2014
204280	S8F8Y6	DYRK	Hippo	Tschop 2011, Degoutin 2013
275410	S8ESM4	APC1	Hippo	Kob 2009, Kim 2019
308590	S8G413	CSN5	Hippo	Kob 2009, Zou 2018
226030	A0A125YVN4	PKAc1	Hippo	Kim 2013, Yu 2013, Zhang 2019
242070	A0A125YLM6	PKAR	Hippo	[b] Kim 2013, Yu 2013, Zhang 2019
209950	A0A125YN61	TRX	Hippo	Cae 2012, Wu 2013, López-Grueso 2019
281400	S8F3K1	PFK	Hippo	Enzo 2015

a - TGME49 gene ID; b - inferred from; H - Hippo; E3 – ubiquitin ligase enzymePSMB5 - proteasome subunit beta type 5; PSMB1 - proteasome subunit beta type 1; E1 - ubiquitin-activating enzyme; E2 - ubiquitin-conjugating enzyme; Ubi – ubiquitin family protein; DYRK - dual specificity tyrosine phosphorylation regulated kinase; APC1 - anaphase-promoting complex subunit 1; CSN5 - constitutive photomorphogenesis 9 signalosome subunit 5; PKA - cAMP-dependent protein kinase; PKAR - cAMP-dependent protein kinase regulatory subunit; TRX – thioredoxin; PFK – phosphofrutokinase.

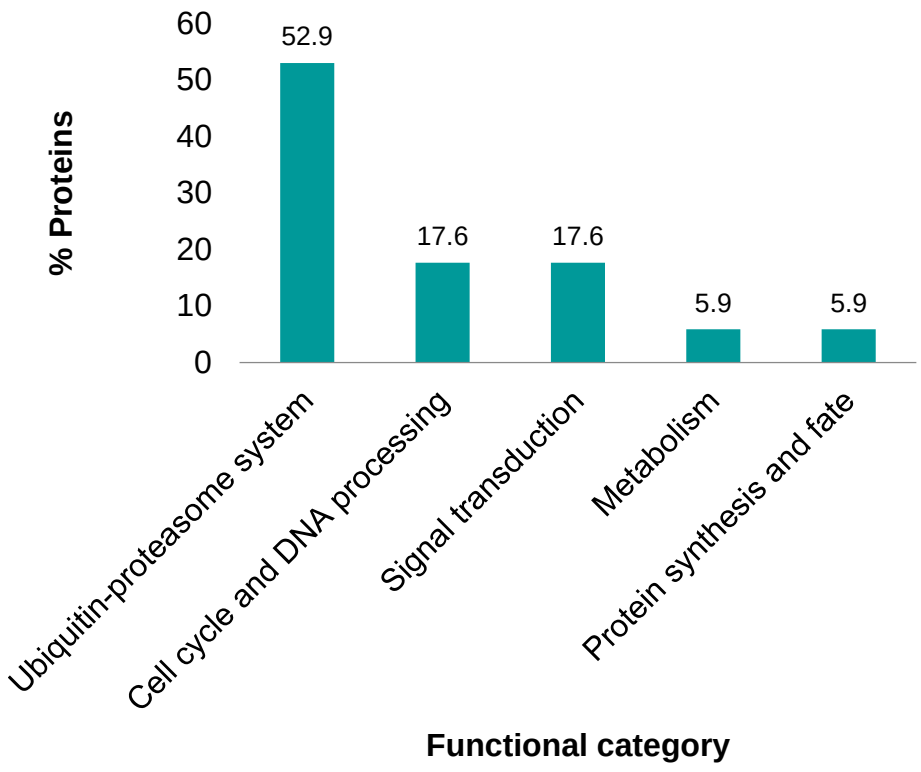

Figure 49. Functional category distribuition of FLAG-BirA-MOB1 differentially biotinylated proteins with counterpart/related proteins characterized as associated to MEN/Hippo.

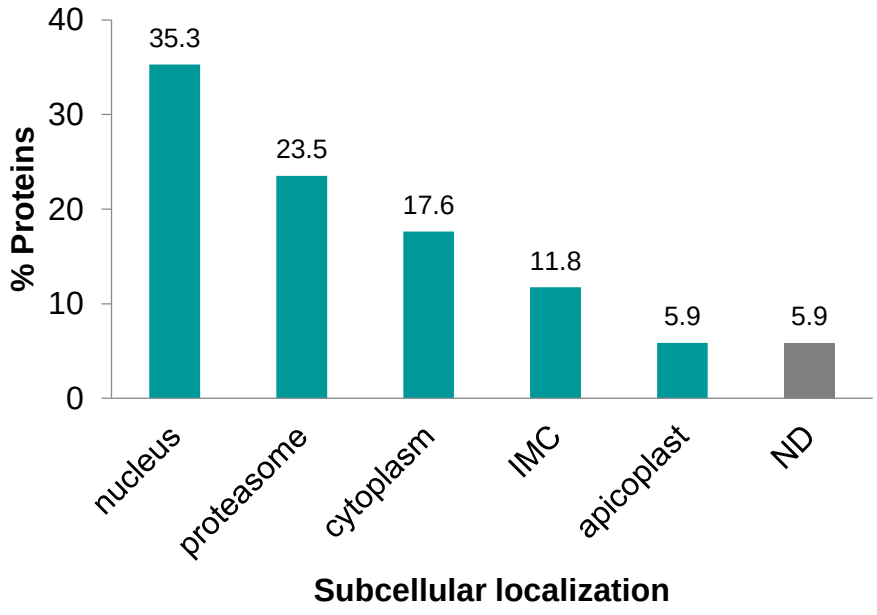

Figure 50. Subcellular localization distribuition of FLAG-BirA-MOB1 differentially biotinylated proteins with counterpart/related proteins characterized as associated to MEN/Hippo.

ND – not determined.

The STRING databse was used to analyze predicted interactions among the FLAG-BirA-MOB1 differentially biotinylated proteins (Figure 51). Of the 127 proteins identified in the MOB1 interactome (including MOB1), STRING predicted connections between 39 proteins while five proteins were not included in the analysis because the gene code was not identified by STRING. The network predicted from the accepted 122 nodes presents 67 edges and a protein-protein interaction enrichment value of p=0.0006 denoting the presence of more interactions than those expected by chance. This analysis predicted interactions between 39 proteins forming ten clusters, with the clusters 1 and 2 being most represented. Cluster 1 includes nine proteins which were mostly classified into the UPS functional category. Cluster 2 includes nine proteins mostly classified into the metabolism category and five of these proteins relate to amino acid metabolism. Clusters 6, 7, 9, and 10 predominantly include proteins classified in cell cycle and DNA processing, transcription, and signal transduction functional categories. Cluster 8 includes three helicases and one ribosomal protein relating to the protein synthesis and fate category. The small clusters 3, 4, and 5 include a mix of proteins categorized in metabolism, protein synthesis and fate, cell transport, and UPS. The only statistically significant cluster is the ubiquitine-proteasome system rich cluster 1 with the FDR presenting an adjusted p-value=0.0260. STRING detected two keywords statistically enriched in the network: ATP-binding and nucleotide-binding (adjusted p-value=0.0184 for both). The 13 proteins associated to these keywords are included in clusters 1, 6, 7, 8, and 9 and in four instances are not included in any cluster. Proteins that were included in the clusters are indicated in Annex II, Supplementary table 1.

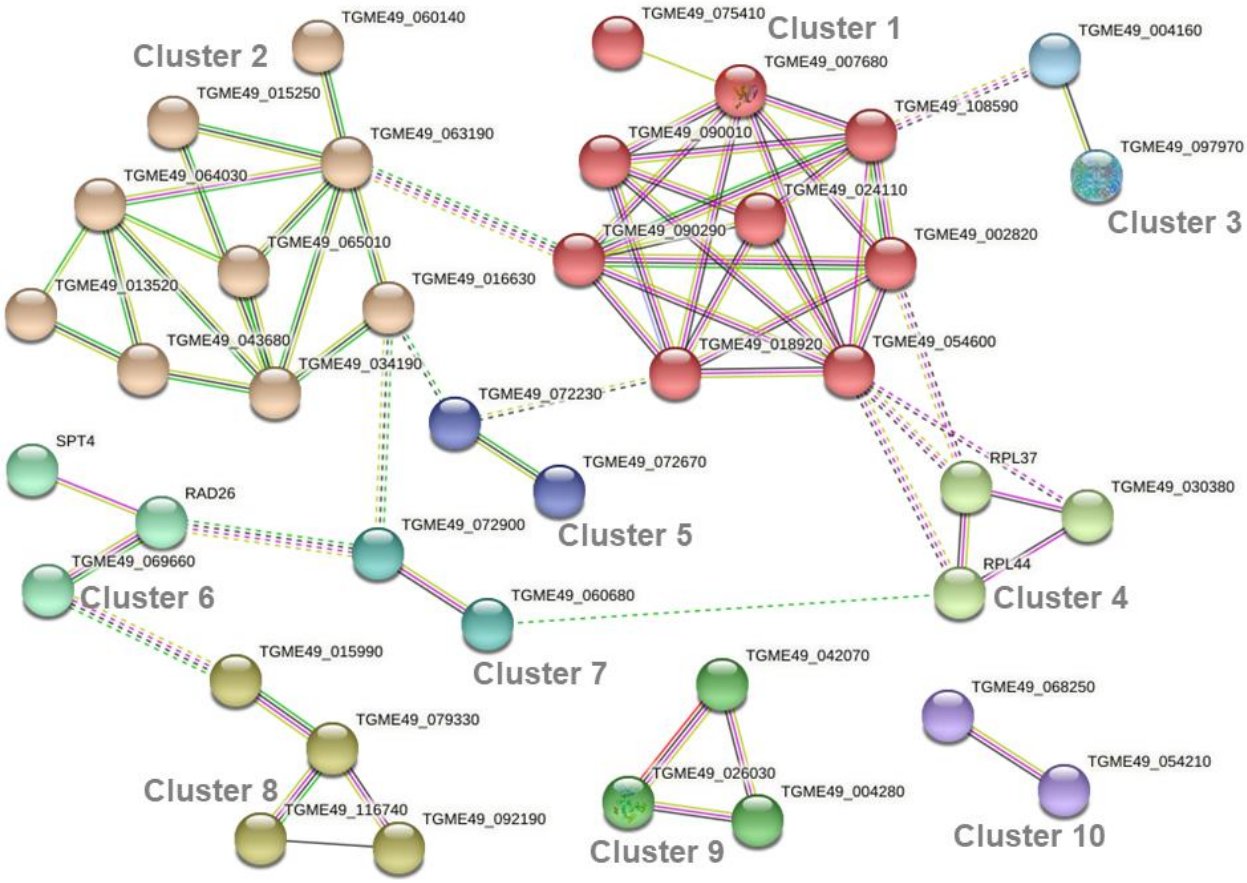

Figure 51. Network analysis of the FLAG-BirA-MOB1 differentially biotinylated proteins using STRING.

STRING clustered proteins are highlighted in the same color. Five proteins were not included in this analysis as STRING was not able to identify the gene code (TGME49_202750, TGME49_209060, TGME49_210778, TGME49_213415, and TGME49_215420).

4.4. *Mob1* expression is highly regulated in *Toxoplasma gondii*

During the characterization of the Cko clonal lines, total RNA was converted to cDNA and MOB1 transcripts were amplified, cloned and sequenced in order to validate that the genomic alterations identified in the *Mob1* locus were also present in *Mob1* transcripts. This confirmed that the *Mob1* transcripts detected originate from the endogenous *Mob1* locus identified in the *T. gondii* genome and that the clonal lines isolated express *Mob1* transcripts with the modifications detected in the gDNA. During this verification, several alternatively spliced transcripts were identified which led us to investigate further the expression of *Mob1*.

4.4.1. RH and EGS strains present a similar *Mob1* transcription pattern

T. gondii Mob1 was originally identified and studied by our group in the scope of Alexandra Tavares' PhD thesis (tese Xana). In this work, *Mob1* transcript expression was characterized as highest in free tachyzoites, dropping with tachyzoite invasion and replication in the host cell and plummeting to the lowest levels at 24 hours post invasion. Considering our current data on *Mob1* transcriptional and post-transcriptional regulation, we decided to further characterize *Mob1* expression during tachyzoite infection of host cells. Through qPCR analysis, we were able to confirm the variation in transcript levels described by Tavares 2015 and expand the *Mob1* transcript characterization in RH tachyzoites (Figure 183). Free, invasion-ready tachyzoites present higher amounts of *Mob1* transcripts (0 hours). There is subsequent downregulation of the transcript levels following host cell invasion, during the active phase of tachyzoite replication inside the host cell (4, 24, and 38 hours). Finally there is an upregulation of *Mob1* transcript levels in freshly egressed tachyzoites (44 hours). We also quantified *Mob1* transcript levels of EGS tachyzoites in comparison to RH tachyzoites (Figure 52). RH and EGS strains, type I and II *T. gondii* strains respectively, present distinct replication rates and consequently distinct lytic cycle durations. Therefore, we adapted the time points sampled for the EGS tachyzoites in order to capture the full course of infection of both strains at comparable time points (invasion to egress). EGS tachyzoites consistently presented lower Mob1 transcript levels compared to RH tachyzoites. Notably, EGS and RH Mob1 transcript levels present the same pattern of variation over time. This is more obvious analyzing a simple coefficient of EGS/RH *Mob1* transcript levels. The coefficients of the various time points are similar, with a mean ± SE of 43.2 ± 8.2%. Overall, we observed the same expression pattern in EGS tachyzoites compared to RH tachyzoites however with lower transcript levels throughout all time points, indicating a possible strain specific regulation of *Mob1* transcript levels.

A

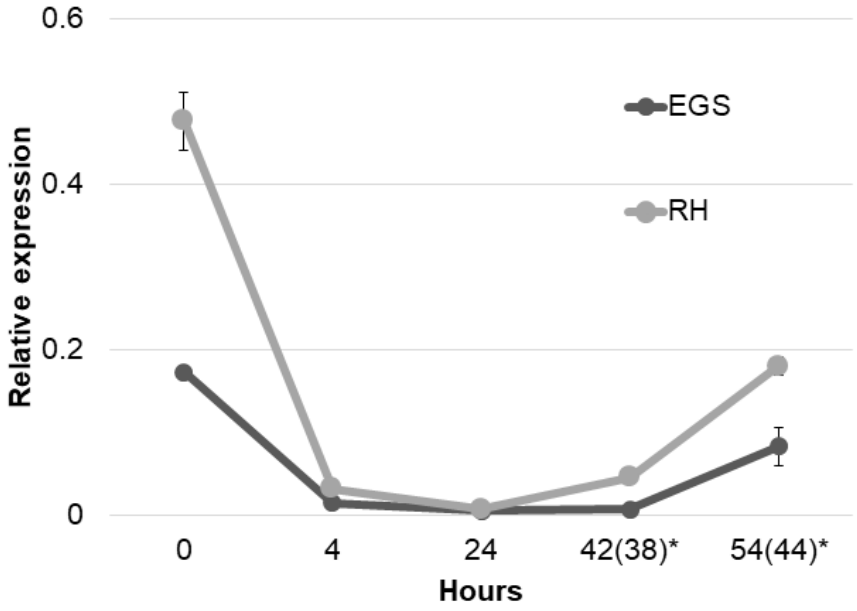

B

Relative expression coefficient (%)

Time point (hours)	0	4	24	42(38)*	54(44)*	Mean ± SE
EGS/RH	36.3	47.0	71.7	15.1	46.0	43.2 ± 8.2

Figure 52. *Mob1* transcripts of RH and EGS strains present different transcript levels but similar variation.

Comparison of *Mob1* transcript levels of RH and EGS tachyzoites. **A)** EGS tachyzoites present lower *Mob1* transcript levels compared to RH tachyzoites. However, *Mob1* transcript levels of RH and EGS strains vary in the same manner. Freshly egressed tachyzoites present higher levels of *Mob1* which dramatically lower after invasion and during active replication inside host cells. *Mob1* transcript levels become again higher in egressed tachyzoites. **B)** The coefficients between relative expression levels of *Mob1* EGS and RH transcripts at different time points remain constant, with mean ± SE of 43.2 ± 8.2%, indicating that both strains vary similarly over time. The last time points were sampled at different times to adjust for the difference in replication rate of type I RH and type II EGS strains (RH sampling at 38 and 44 hours correspond to EGS sampling at 42 and 54 hours). Data are presented as mean ± SE of three independent experiments. SE – standard error of the mean.

4.4.2. *Mob1* suffers extensive transcriptional and post-transcriptional regulation

After the incidental finding of *Mob1* alternative transcripts during the characterization of the Cko clonal lines, we initially hypothesized that this could be the result of a response mechanism triggered by the *Mob1* knockout. However, we verified that these events also occurred in the parental RH strain. Globally, we detected several types of alternative splicing events affecting *Mob1* transcripts, including partial intron retention, full exon deletion and partial exon deletion, alone or combined in the same transcript (Figure 53). These splicing events produce transcripts that could originate proteins similar to the canonical MOB1 protein but the more common observation for the transcripts detected in this analysis is a predicted protein with a premature stop. The cDNA synthesis was performed using oligodT as primer, therefore, the transcripts detected correspond to mature transcripts harboring a polyA tail. The great variety of *Mob1* transcripts, as well as the fact that many would probably not originate a functional protein due to the presence of premature Stop codons, raised the hypothesis that the *Mob1* locus could be transcribed from both genomic strands, the sense and antisense. In order to assess this, *Mob1* strand-specific cDNA was synthesized. Amplicons were successfully obtained from sense and antisense *Mob1* cDNAs and subsequently cloned (Figure 53). Sequencing showed that both amplicons corresponded to *Mob1* transcripts and confirmed that the *Mob1* locus is transcribed from both genomic strands. In the case of the *Mob1* sense cDNA, we were able to purify an amplicon although the amplification was very low and a band was barely visible after agarose-based electrophoresis. This contrasts with the very strong signal of the amplicon obtained from the *Mob1* antisense cDNA, similar in intensity to that obtained from the control oligodT cDNA. Further, sequence analysis identified alternatively spliced transcripts originating from both strands. The antisense transcripts detected did not code for a viable protein. In the sense and antisense amplicons, we did not detect the multitude of splicing events previously characterized from oligodT originated amplicons, therefore, we were not able to confirm the specific origin of the majority of the splicing events. However, it is most likely that most transcripts that do not produce a viable protein are antisense transcripts. Presumably, these transcripts play a role in the regulation of the level of sense transcripts available for translation, as sense and antisense transcripts present a very high degree of complementarity.

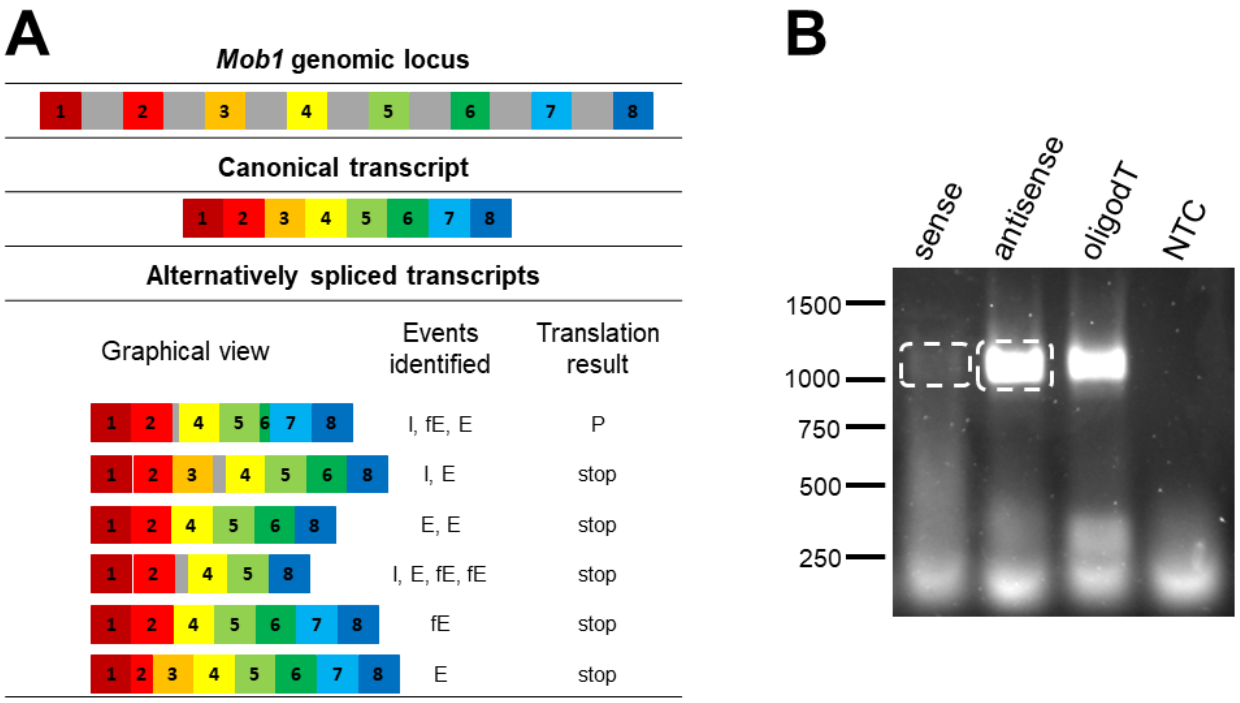

Figure 53. *Mob1* transcription produces variable mRNAs.

A) Colored segments represent numbered exons. Grey segments represent introns. I - partial intron retention; fE - full exon deletion; E - partial exon deletion; P - protein similar to canonical form; STOP - premature Stop codon. **B)** RNA was retro-transcribed using a *Mob1* specific primer for the sense strand (sense), a *Mob1* specific primer for the antisense strand (antisense) and the universal oligodT primer (oligodT). PCR confirmed that the *Mob1* locus is transcribed from both genomic strands. The dotted rectangles indicate the gel bands that were cut, purified and cloned for subsequent sequencing. Numbers on the left represent the molecular weight in bp. cDNA – complimentary DNA; NTC – non template control.

4.4.3. *Mob1* antisense transcripts are highly expressed in tachyzoites

We also analyzed *Mob1* sense and antisense specific transcripts in RH tachyzoites in comparison to overall RH transcript levels (Figure 54). The tendency for a much higher relative expression of antisense transcripts compared to sense transcripts was observed again and occurred in all the time points analyzed. This marked difference in sense and antisense transcript levels with a proportional variation throughout the infection. The coefficients between the relative expression values of sense, antisense and overall cDNAs are fairly constant throughout the infection, as can be observed by the similar coefficients at the various time points and the small values of SE. Relative expression coefficients present a mean ± SE of 6.9 ± 0.7% of sense transcripts compared to antisense transcripts, 3.0 ± 0.3% of sense transcripts compared to overall transcripts and 44.4 ± 2.1% of antisense transcripts compared to overall

transcripts. This is further evidence that *Mob1* sense, antisense and overall transcripts show the same tendency during host cell infection, with antisense transcripts highly surpassing sense transcripts. This presumed mechanism of post-transcriptional regulation appears to be constant in the tachyzoite stage. It is also visible that the sum of the relative expression of sense and antisense transcripts does not correspond to that of overall transcripts. Therefore, although our *Mob1* strand-specific cDNA assay is likely not suitable for absolute quantification, due to the use of different primers, it is still a useful tool to evaluate *Mob1* sense and antisense transcripts individually.

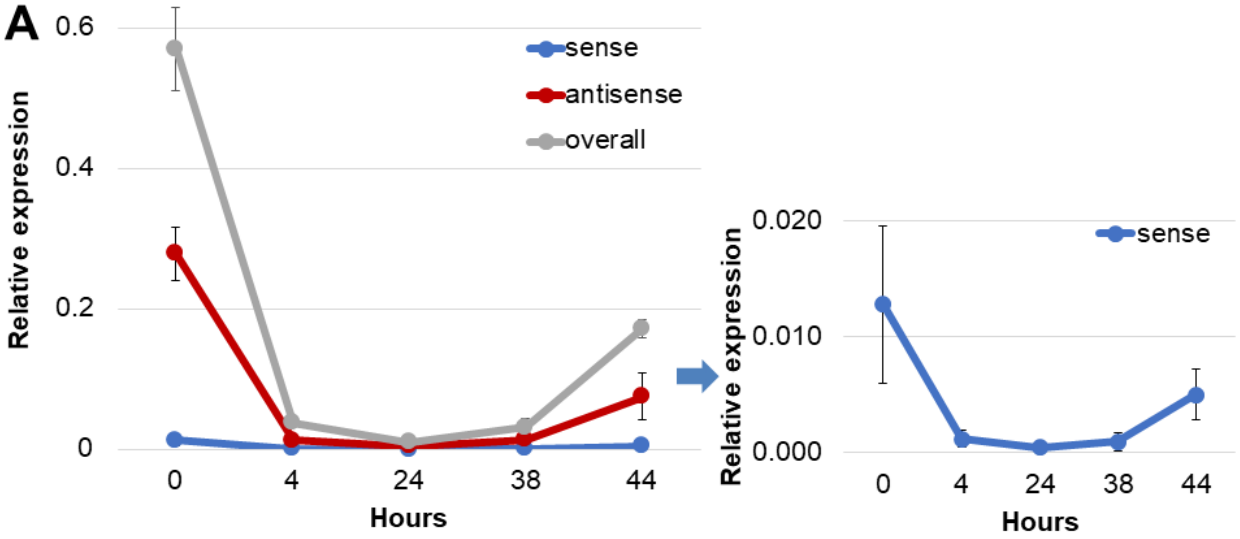

B

Relative expression coefficient (%)						
Time point (hours)	0	4	24	38	44	Mean ± SE
S / AS	4.6	8.6	8.3	6.4	6.7	6.9 ± 0.7
S / RH	2.2	3.1	4.0	2.9	2.9	3.0 ± 0.3
AS / RH	48.9	35.8	48.2	45.4	43.6	44.4 ± 2.1

Figure 54. *Mob1* sense and antisense transcripts present a similar variation pattern in tachyzoites. *Mob1* sense, antisense and overall transcript levels were analyzed in RH tachyzoites. **A)** *Mob1* sense, antisense and overall transcript levels vary proportionally in tachyzoites. *Mob1* sense transcripts present levels lower than antisense transcripts throughout the whole infection. The graph at the left shows simultaneously sense, antisense and overall transcripts of RH tachyzoites. The graph at the right shows only sense transcripts presented at a smaller scale. **B)** The table shows the coefficient between relative expression of sense, antisense and overall *Mob1* transcripts. There is very little variation in the coefficient value which indicates the three types of transcripts show proportional variations over time, although presenting very different values, particularly sense transcripts are present in much smaller amounts. Data are presented as mean ± SE of three independent experiments. S/AS – relative expression coefficient of sense over antisense transcripts; S/RH – relative expression coefficient of sense over overall transcripts of RH

tachyzoites; AS/RH – relative expression coefficient of antisense over overall transcripts; SE – standard error of the mean.

4.4.4. *Mob1* transcription is differentially regulated during the *Toxoplasma gondii* life cycle

RT-PCR amplification of the strand specific *Mob1* template cDNAs yielded a much higher amount of amplicon from the antisense cDNA compared to the sense cDNA, which was also observed in the qPCR analysis of RH vs *Mob1* overexpression strains, in the RH control strain. However, these data alone do not allow us to conclude on the relative quantities of *Mob1* sense and antisense transcripts as the *Mob1* sense and antisense cDNAs were synthesized using different specific primers. This prompted us to search for Mob1 strand specific data available at ToxoDB.org. Consulting strand specific NGS data on *Mob1* (TGME49_304730), we found data from nine strand specific transcriptomic analysis available (Table 19). Four tachyzoite time series of prototypic strains of *T. gondii* types I (RH and GT1), II (ME49) and III (VEG) show overall dominance of *Mob1* antisense transcript levels, excluding two time points (of a total of nineteen). Two bradyzoite analysis using ME49 and M4 strains show very similar *Mob1* sense and antisense transcript levels. Type II CZ strain tachyzoite and bradyzoite *Mob1* antisense transcript levels are higher than sense transcript levels in a 2019 analysis, although 2015 analysis of the same strain using tachyzoites and merozoites detected higher sense transcript levels. The 2019 CZ transcriptome also looked at feline enteroepithelial stages which showed higher *Mob1* sense transcript levels that increase steadily from time point one to five, while antisense transcript levels remain fairly unchanged. In an oocyst time series transcriptome beginning at sporulation using the type II M4 strain, *Mob1* sense transcript levels where higher than antisense transcript levels. Overall, most strand specific transcriptomic analysis detected higher *Mob1* antisense transcript levels compared to *Mob1* sense transcript levels, particularly regarding tachyzoite data. This pattern is also present in bradyzoite data, although not so consistently. The merozoite/enteroepithelial data show higher *Mob1* sense transcript levels. We also observed higher *Mob1* sense transcript levels in oocysts. These data validate our RT-PCR and qPCR results of higher *Mob1* antisense transcript levels in RH tachyzoites.

Table 19. Analysis of strand specific NGS *Mob1* data.

Name	Description	Reference	AS > S	S > AS	Comments
ME49 tachyzoite transcriptome time series	*T. gondii* ME49 tachyzoite mRNA Illumina sequences aligned to the ME49 genome, at 2, 4, 8, 16, 36 and 44 hpi.	Brian D. Gregory	X		At 44h, the S are slightly higher than AS.
VEG tachyzoite transcriptome time series	*T. gondii* VEG tachyzoite mRNA Illumina sequences aligned to the ME49 genome, at 2, 4, 8, 16, 36, and 44 hpi.	Brian D. Gregory	X		
RH tachyzoite transcriptome time series	*T. gondii* RH tachyzoite mRNA Illumina sequences aligned to the ME49 genome at 2, 22 and 36 hpi.	Brian D. Gregory	X		At 2h, S and AS are equal.
GT1 tachyzoite transcriptome time series	*T. gondii* GT1 tachyzoite mRNA Illumina sequences aligned to the ME49 genome at 2, 4, 8, and 16 hpi.	Brian D. Gregory	X		S only detected at 16 hours.
ME49 bradyzoite in vitro transcriptome	*T. gondii* ME49 bradyzoite mRNA Illumina sequences aligned to the ME49 genome.	David Sibley, Brian D. Gregory		X	S and AS are very similar.
Tachyzoite and merozoite transcriptomes	High-throughput RNA-Seq to compare the merozoite and tachyzoite transcriptomes from *T. gondii* CZ strain, aligned to the ME49 genome.	Hehl et al. 2015		X	Tachyzoite data conflicts with data from Ramakrishnan *et al.* 2019
M4 bradyzoite *in vivo* transcriptome	*T. gondii* M4 in vivo bradyzoite mRNA Illumina sequences aligned to the ME49 genome.	Buchholz et al. 2011	X		S and AS are very similar.
M4 oocyst time series	*T. gondii* M4 Oocyst mRNA Illumina sequences aligned to the ME49 genome, at several 0, 4 and 10 days post-sporulation.	H.M. Fritz et al. 2012		X	S decrease and AS increase through time.
Feline enterocyte stages transcriptome	Transcriptomes of *T. gondii* strain CZ clone H3 in feline enterocyte stages, aligned to the ME49 genome.	Ramakrishnan et al. 2019		X	Enter S increase from time 1 to 5.
Tachyzoite and bradyzoite stages transcriptome	Transcriptomes of *T. gondii* strain CZ clone H3 aligned to the ME49 genome.	Ramakrishnan et al. 2019	X		

Data extracted from ToxoDB.org, Transcriptomics section. The data refer to *Mob1*, TGME49_304730. AS – *Mob1* antisense transcript levels; S – *Mob1* sense transcript levels; Enter – feline enterocyte stages; hpi – hours *post* infection.

In contrast to tachyzoite and bradyzoite stages, *Mob1* sense transcripts seem to predominate over antisense transcripts in the enteroepithelial and oocyst stages, namely in the *T. gondii* sexual cycle (Figure 55). In the type II CZ strain, *Mob1* sense transcripts are upregulated in a time course of enteroepithelial stages reaching a maximum level of expression

in the latest stages. Total *Mob1* expression levels are much higher than those detected in tachyzoite and bradyzoite stages. Notably, the total levels of *Mob1* expression are much lower in tachyzoite and bradyzoite stages these still present a predominance of *Mob1* antisense transcripts as we detected for RH tachyzoites. Type II M4 oocysts also present a predominance of *Mob1* sense transcripts during a course of ten days. Total expression levels are comparable to those detected in the enteroepithelial stages of the CZ strain. These data suggest *Mob1* is regulated in a strand specific manner during the course of the *T. gondii* life cycle, presenting higher *Mob1* sense expression in *T. gondii* sexual cycle stages. Similarly to *Mob1*, the genes coding for the *T. gondii* NDR kinases TGME49_215670 and TGME49_272200, possible orthologs of ScDbf2/20p/ SpSid2p/ HsLATS1/2/ DmWarts and HsNDR1/2/ DmTricornered respectively, also present an mRNA expression that steadily increases in enteroepithelial staged during the course of the sexual cycle in the cat's intestinal epithelium and that is significantly higher compared to the mRNA levels in the *T. gondii* tachyzoite and bradyzoite asexual stages (Ramakrishnan 2019). These expression data point to a concerted biological function of the *T. gondii* genes *Mob1*, TGME49_215670, and TGME49_272200.

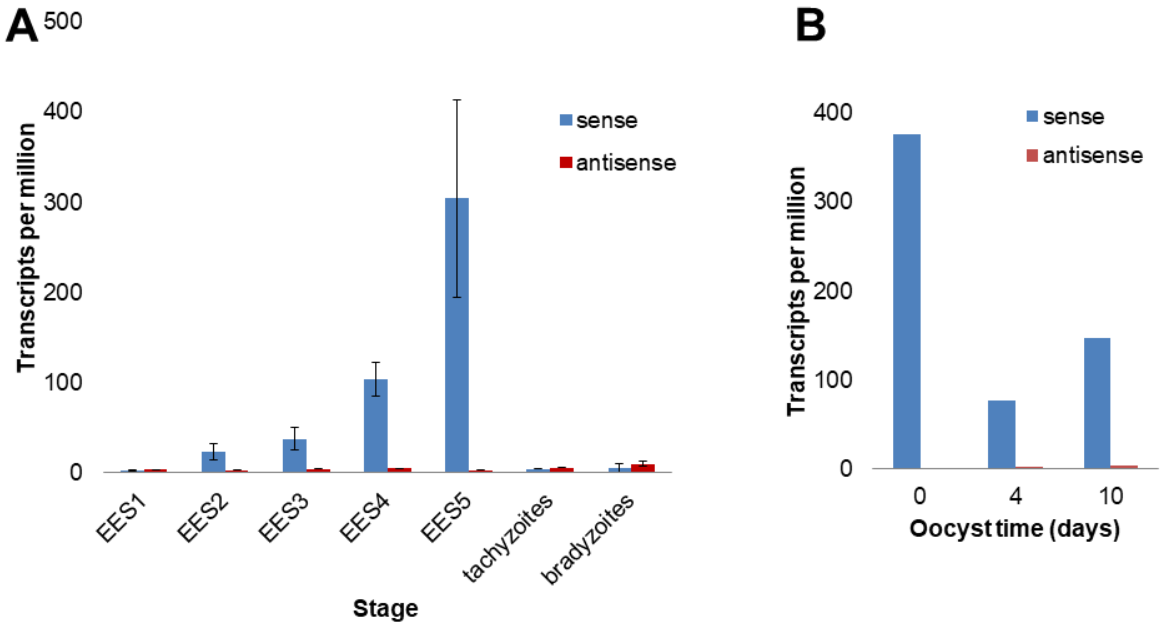

Figure 55. *Toxoplasma gondii* enteroepithelial and oocyst stages show a predominance of *Mob1* sense over antisense transcripts.

Data extracted from ToxoDB.org, Transcriptomics section, referring to *Mob1*, TGME49_304730. **A)** *Mob1* sense transcripts are upregulated in enteroepithelial stages reaching a maximum level of expression in the later stages. Tachyzoites and bradyzoites show the tendency we also detected of *Mob1* antisense transcripts predominance. Mob1 transcript levels are much higher in enteroepithelial stages compared to tachyzoite and bradyzoite stages. Data published by Ramakrishnan et al. (2019). EES – enteroepithelial stage. **B)** Oocysts also show a predominance of *Mob1* sense transcripts. Data published by H.M. Fritz et al. (2012).

5. Discussion

5.1. *Mob1* transcription indicates differential roles along the *Toxoplasma gondii* life cycle

The *Mob1* locus is transcribed from both genomic strands, originating sense transcripts (STs) and natural antisense transcripts (NATs), a type of long non-coding RNA. The *Mob1* NATs do not present any predicted open reading frame and overlap with the STs at least from start to stop codons. In tachyzoites, *Mob1* NATs were detected in levels much higher than STs. Still, we detected evidence of endogenous MOB1 in tachyzoites through nanoLC-MS/MS, in accordance with the detection of phenotypes associated with the knockout of *Mob1*. NATs are found in a wide variety of organisms and may regulate genes through various transcriptional or post-transcriptional mechanisms, namely transcriptional interference, RNA masking, double-stranded RNA-dependent mechanisms resulting in nuclear retention or chromatin modification, and antisense-induced methylation (Lavorgna 2004). The *Arabidopsis thaliana* vernalization response *gene AtMaf4* is regulated by NATs which promote *AtMaf4* transcription (Zhao et al. 2018). The *T. gondii Ulp1*, active in sumoylation and desumoylation pathways, is down-regulated by NATs and the micro-RNA Tg-miR-60 (Crater et al. 2018). A large-scale study confirmed conserved antisense transcription in *T. gondii,* with antisense transcripts representing an average of 21.5% of ST serial analysis of gene expression tags (Radke et al. 2005). The same study detected an inverse relationship between expression levels of sense and *cis*-antisense transcripts, coherent with our findings for *Mob1* in tachyzoites. The opposite position *Mob1* STs and NATs present in the genome would favor regulation through transcriptional interference. Also the *Mob1* STs and NATs are expected to be complementary in large extensions which would favor regulation through double-stranded RNA-dependent mechanisms and nuclear retention. Hence it is likely that NATs regulation of *Mob1* expression occurs through multiple mechanisms. Additionally, NGS data (available at ToxoDB.org) show that *Mob1* STs are much more frequent than NATs during the *T. gondii* sexual development in the definitive host's gut, implying a differentiated regulation of *Mob1* STs/NATs at various phases of the parasite's life cycle. There is a strong correlation between antisense transcription and alternative splicing in metazoans with antisense transcription likely functioning as a conserved regulation mechanism of alternative splicing (Morrissy et al. 2011). Both types of events have also been detected in *Plasmodium falciparum* (Gunasekera et al. 2004; Sorber et al. 2011). Therefore, the co-occurrence of *Mob1* NATs and alternatively spliced transcripts is also suggestive of antisense regulation of *Mob1* expression. *Mob1* transcripts were detected to harbor multiple alternative splicing events, namely partial intron retentions, full exon deletions,

and partial exon deletions. Although alternatively spliced *Mob1* transcripts were detected originating from both strands, it was not possible to attribute most of the detected alternative splicing events as occurring in STs or NATs. However, it is expected that most of the alternatively spliced transcripts detected represent NATs, as alternative splicing is often associated to antisense transcripts and it is unlikely that one gene originates high numbers of largely truncated protein isoforms. Alternative splicing events detected in *T. gondii* mirror what had been previously reported in other eukaryotes (Hassan et al. 2012). The *T. gondii* genes *Hxgprt*, *Pi1*, and *MyosinB/C* produce two protein isoforms with differing subcellular localizations, an alternative splicing event designated as cassette exon (Delbac et al. 2001; Chaudhary et al. 2005; Pszenny et al. 2011). The splicing factor *Sr3* regulates alternative splicing of over a thousand *T. gondii* genes (Yeoh et al. 2015). Regulation by alternative splicing in *T. gondii* has also been associated to different parasite stages which express distinct isoforms (Lunghi et al. 2016).

Mob1 transcripts are dramatically downregulated upon host cell invasion of tachyzoites. Transcript levels begin to increase briefly before egress and continue to grow in recently egressed tachyzoites. The same expression pattern was observed in RH and EGS tachyzoites, although with different levels of expression. The moment of *Mob1* downregulation within the *T. gondii* lytic cycle coincides with the period of tachyzoite active replication inside the host cell, indicating a necessity for regulation of *Mob1* during replication. Within the lytic cycle, *Mob1* is also regulated in a cell-cycle dependent manner. This is the case for more than a third of *T. gondii* tachyzoite transcripts which present a bi-modal organization with peak transcription occurring at S/M phase, for genes related to maturation of daughter cells and apicomplexan specific organelles, or at G1 phase, for genes involved in general cell functions (Behnke et al. 2010). Particularly, *Mob1* groups with the S/M phase peak transcription group (data available at ToxoDB.org) (Behnke et al. 2010). Conversely, *Drosophila melanogaster DmMob1* (*Mats*) expression is mostly constant throughout the cell cycle (Shimizu et al. 2008). Different *T. gondii* strains present distinct transcriptomes, independent of developmental stage (M.M.K. Croken et al. 2014). Notably, EGS tachyzoites presented consistently lower levels of *Mob1* expression compared to RH tachyzoites while maintaining the same expression pattern. This shows that the regulation of *Mob1* expression throughout the lytic cycle occurs in a conserved manner in different strains, even if the baseline transcriptome is distinct.

T. gondii transcription is regulated in a highly stage-specific manner (Radke et al. 2005). This is coherent with what has been observed for *Plasmodium* (Llinás and DeRisi 2004). Our analysis of strand specific NGS *Mob1* data (available at ToxoDB.org) indicates clear stage-

specific differences. In the *T. gondii* development in the intermediate host, involving tachyzoites and bradyzoites, *Mob1* NATs are more expressed compared to STs. In the *T. gondii* development in the definitive host's intestinal epithelium, involving merozoites, gamonts, gametes, and oocysts, STs present higher expression compared to NATs. *Mob1* ST levels are significantly higher during development in the felid's intestine compared to development of tachyzoites and bradyzoites. Also, *Mob1* ST levels steadily increase during the *T. gondii* development of the enteroepithelial stages, indicating *Mob1* expression is higher in later stages namely, gametocytes, gametes, and/or unsporulated oocysts. In general, *T. gondii* protein levels tend to correlate to mRNA levels, a characteristic also present in *P. falciparum* (Le Roch 2004; Radke et al. 2005). Therefore, considering *Mob1* expression levels detected in our study and in the available large-scale studies, we would expect very low MOB1 expression in tachyzoites, bradyzoites, and sporozoites, but comparatively high MOB1 expression in merozoites, gamonts, gametes, and oocysts, with highest expression in late gut stages and unsporulated oocysts, highlighting the relevance of MOB1 in these stages. In *Neospora caninum* tachyzoites of the more virulent Nc-Spain7 strain and the less virulent Nc-Spain1H strain, *Mob1* expression levels are low similarly to *T. gondii*'s and *Mob1* NATs present levels very close to the *Mob1* STs levels (data available at ToxoDB.org) (Horcajo et al. 2018). In *Eimeria tenella*, RNA-Seq data shows significantly higher levels of *Mob1* in gametocytes and unsporulated oocysts compared to sporulated oocysts, sporozoites and merozoites (data available at ToxoDB.org) (Reid et al. 2014; Walker et al. 2015). These observations point to a possible conserved regulation mechanism of *Mob1* expression.

Overall, there is evidence that *Mob1* expression is regulated at the cell cycle, lytic cycle, and life cycle levels. This regulation appears to occur at the transcriptional and post-transcriptional levels, through mechanisms involving natural antisense transcription and alternative splicing. The set of data generated in this work and collected from other publications points to a conserved and intricate regulation of *Mob1* transcription in coccidians, in coordination with its complex life cycles.

5.2. CRISPR/Cas9 is an efficient technology to produce transgenic strains in *Toxoplasma gondii*

CRISPR/Cas9 has been previously used to study gene function in *T. gondii* (Sidik et al. 2014; Shen et al. 2014). Most notably, Sidik et al. (2016) published a genome-wide loss-of-function screen using CRISPR/Cas9. We employed two CRISPR/Cas9 systems. In the splitCas9 system, used in the type I RH strain, Cas9 is constitutively expressed separated into

two subunits, the *Mob1* sgRNA is also constitutively expressed and nuclease activity is induced with rapamycin. The EGS strain was transiently transfected with a plasmid harboring the full Cas9 coding sequence along with another plasmid coding for the *Mob1* sgRNA.

With the splitCas9 system, we detected two concurrent phenotypes following nuclease activation. While part of the tachyzoite population continued to replicate normally, the other part presented an abnormal replication in what appeared as continuous replication without successful nuclear or cell division. This phenotype was present only in the first lytic cycle after splitCas9 activation of the iC strains and was observed with the three Mob1 *specific* sgRNAs. Continuous or subsequent splitCas9 activation, by rapamycin treatment, did not reproduce the abnormal replication phenotype. This phenotype is consistent with the cytotoxicity phenotype reported by Markus Meissner's Laboratory while using their splitCas9 system to knockout multiple *T. gondii* genes. Using two different systems to knockout the *Mec17* gene, the Meissner group detected the abnormal replication phenotype only using the splitCas9 system. The group also showed that this phenotype was present when using the splitCas9 system to knockout the *Sag1* gene, previously shown to be non-essential. Furthermore, using the splitCas9 system to knockout the *Sag1* gene in a RHΔku80 strain (ku80 is an essential component for the non-homologous end joining repair pathway), the frequency of abnormal parasites increased dramatically, suggesting that the repair of the Cas9 induced DSBs is involved in this cytotoxicity phenotype. The group proposed that the cytotoxicity phenotype could be the consequence of a failure to repair the DNA DSBs caused by the Cas9. It is still unclear why this repair failure affects only a subset of the clonal tachyzoites. These results of the Meissner group were presented at the Toxo14 – The 14th biennial conference of the *Toxoplasma gondii* research community by Stortz and colleagues (Stortz et al. 2017).

High-level expression of a heterologous protein can cause proteotoxic stress. Specifically, Cas9 expression may cause toxicity in cells, an issue that has been identified in prokaryote and eukaryote organisms, including *T. gondii* (Ryan et al. 2014; Cobb et al. 2015; Peng et al. 2015; Sidik et al. 2016). In the case of *T. gondii*, the co-expression of a sgRNA is an efficient strategy to reduce Cas9 toxicity (Sidik et al. 2016; Markus et al. 2019). The splitCas9 system does not constitutively express the active nuclease but an inactive Cas9 split into two subunits, therefore this should not be the cause of toxicity, although this type of system can present some leakage. Furthermore, the timing of the phenotype suggests the abnormal replication is caused when the splitCas9 system is specifically activated, which is congruent with the Meissner group's theory of cytotoxicity caused by failure to repair the DSBs caused by the nuclease. Cas9 has been shown to be toxic to human pluripotent stem cells through on-target

nuclease activity and not because of constitutive expression or off-target activity (Ihry et al. 2018). Cas9 activity can also cause off-target effects (Morgens et al. 2017; Tycko et al. 2019). However, we detected this phenotype with three *Mob1* specific gRNAs, indicating that this was the result of on-target nuclease activity rather than off-target effect due to unspecific DSBs.

Mob1 knockout in the EGS strain was obtained by co-transfection of plasmids harboring the full coding sequences for Cas9 and *Mob1* specific sgRNAs. Transfected tachyzoites were drug selected for the *pU6-gRNA1-Dhfr* vector. The simultaneous transfection of both plasmids resulted in the integration of the *pU6-gRNA1-Dhfr* vector at the site of DSB. This was widespread across the tested clonal lines. Drug selection for the plasmid vector's resistance cassette likely favored this integration. Although the insertions led to a *Mob1* knockout, it also likely caused chromatin remodeling to assimilate the multiple kb fragments. This recombination event invalidated one of the advantages of the CRISPR/Cas9 technology which is permitting genome editing with minimal structural changes to the genome. Our findings show that plasmid integration at the site of Cas9 mediated DSB is highly efficient even in the absence of homology arms. In fact, Cas9 has been used to increase the efficiency of homologous recombination allowing for the use of much shorter homology arms (Long et al. 2018). Long and colleagues reported 42 bp fragments while in our traditional homologous recombination strategy we used 2 kb fragments as homology arms. Vector integration at the site of Cas9 mediated DSB is common in mammalian cells (Chakraborty 2019; Hanlon et al. 2019). A strategy that is increasingly adopted to avoid this issue is the transfection of ready-to-use sgRNAs and Cas9 (ribonucleoprotein) instead of vectors (Kim et al. 2014; Vakulskas et al. 2018; Hoshijima et al. 2019). This strategy was recently employed in *T. gondii* and *B. besnoitia* (Winiger and Hehl 2020).

Overall, we obtained a high success rate for production of Cas9 mediated DSBs and isolation of *Mob1* functional knockout clonal lines in our experiments, with all of the tested clones having suffered a DSBs at the expected site. However, it proved essential to identify the DSBs that occurred to select clonal lines with appropriate indel repair. This is due to the occurrence of in-frame indels which may produce a wildtype-like MOB1 and confound the functional knockout phenotype.

5.3. Reverse genetics studies indicate *Mob1* is involved in the regulation of tachyzoite replication and tachyzoite to bradyzoite conversion

Contrary to what is described in other organisms and using two different technologies to generate *Mob1* knockout strains (CRISPR and homologous recombination), we showed that the

knockout of *Mob1* does not impede tachyzoite replication in type I or type I/III *T. gondii* strains. This is consistent with the results relative to *Mob1* of a genome-wide loss-of-function screen using CRISPR/Cas9 which indicate *Mob1* is not an essential gene in the lytic cycle of RH tachyzoites ("Phenotype" data available at ToxoDB.org) (Sidik et al. 2016). The *Mob1* knockout affected tachyzoite replication, parasitophorous vacuole (PV) regularity, and tissue cyst formation (Table 20). We did not detect any effect of *Mob1* knockout on tachyzoite invasion, similarly to the group's previous report that found no effect on invasion due to MOB1 overexpression (Tavares 2015).

Table 20. Summary of phenotypes detected in *Mob1* transgenic strains.

Strain	Genotype	P. strain	Type	Strategy	*In vitro* phenotype			Observations
					Replication	PV regularity	Tissue cysts	
Cko	*Mob1* KO	iC (RH)	I	CRISPR	↑	↓	NE	*Mob1* locus practically unchanged
GSko	*Mob1* KO	iGSoe (RH)	I	HR	↑	↓	↓	removal of full *Mob1* locus
Eko	*Mob1* KO	EGS	I/III	CRISPR	=	↓	↓	large insertion at *Mob1* locus
iGSoe	*Mob1* OE	diCre (RH)	I	HR	↓*	NE	↑*	removal of full *Mob1* locus
dMG MOB1	*Mob1* OE	RH	I	RI	↓	NE	NE	*Mob1* locus unchanged (Tavares 2015)
FB MOB1	*Mob1* OE	RH	I	RI	NE**	NE	NE	*Mob1* locus unchanged

P. strain – parental strain (baseline strain designated between brackets when pertinent); CRISPR - CRISPR/Cas9 mediated recombination; HR - homologous recombination; RI - random integration; Cko - *Mob1* splitCas9 functional knockout; iC - inducible *Mob1* splitCas9; GSko - *Mob1* gene-swap knockout; iGSoe - inducible *Mob1* gene-swap overexpressing MOB1; dMOMOB1 – dd-Myc-GFP-MOB1; FBMOB1 – FLAG-BirA-MOB1; KO – knockout; OE – overexpression; NE - not evaluated.* Phenotypes likely not solely to *Mob1* OE but also due to remodeling at the *Mob1* locus. ** The FBMOB1 strain was not tested in replication assays but observation during routine culture showed that the proliferation of FBMOB1 tachyzoites was not obviously different from its parental strain RH (contrary to iGSoe tachyzoites which presented a clearly slower proliferation during routine culture compared to its parental strain diCre).

Type I RH strain *Mob1* knockout tachyzoites showed an increase in replication. We observed this effect in Cko tachyzoites, using the splitCas9 strategy, and in GSko tachyzoites, using the gene-swap strategy. This is coherent with the group's previous findings which showed a decrease in replication of RH MOB1 overexpressing tachyzoites (Tavares 2015). The replication of type I/III EGS strain *Mob1* knockout tachyzoites was not affected. Different type strains typically present distinct proliferation rates *in vivo* which translate to different periods of the lytic cycle *in vitro*. This difference is mainly due to the length of the G1 phase which lasts 3-4 hours in RH (type I) *vs*. 6-8 hours in ME49 and VEG (type II and III respectively) (Radke et al. 2001). These differences could be readily observed during *in vitro* culturing in our laboratory, with RH tachyzoites presenting a significantly faster lytic cycle compared to EGS or ME49 tachyzoites. Strain-specific lytic cycle period is likely related to differential strain-specific transcriptional regulation (Radke et al. 2005; M.M.K. Croken et al. 2014). The fact that the increase in replication detected in RH *Mob1* knockout tachyzoites was not detected in Eko tachyzoites could be a consequence of the slower baseline replication rate, where the effect could have a lower magnitude and be harder to detect. It is possible that performing the replication assay using a longer time frame could help to detect an effect, similarly to what occurred with GSko tachyzoites, although the tendency of the data does not point to that.

The inducible gene-swap strategy was used to obtain MOB1 overexpressing iGSoe tachyzoites in which the *Mob1* endogenous locus was exchanged with a construct including the *Mob1* cDNA and a strong heterologous promotor. Tachyzoites of the iGSoe strain presented a prominent decrease in replication compared to its parental strain diCre. GSko tachyzoites, obtained through excision of the *Mob1* cDNA, maintained a rate of replication much closer to iGSoe than diCre tachyzoites, indicating that this phenotype could be not dependent, or solely dependent, on the overexpression of MOB1. MOB1 expression levels also indicate that the iGSoe phenotype is not solely due to MOB1 overexpression. FLAG-BirA-MOB1 tachyzoites consistently showed higher MOB1 expression when compared to iGSoe tachyzoites using multiple anti-MOB1 sera. But, FLAG-BirA-MOB1 tachyzoites present a typical RH proliferation rate, similar to that of diCre tachyzoites and significantly faster than iGSoe tachyzoites. So, the difference in the proliferation rate is not coherent with the levels of protein expression. These data led us to conclude that the iGSoe strain is not appropriate to analyze the phenotype of MOB1 overexpression and to analyze the phenotype of the GSko strain by comparison with the iGSoe strain rather than to the diCre strain. The phenotype of the iGSoe strain could be due to the lack of *Mob1* NATs, which are absent both in iGSoe and GSko tachyzoites in consequence of the gene-swap. Alternatively, this phenotype could be caused by changes in chromatin

structure due to the *Mob1* gene-swap. These structural changes could be interfering with chromatin remodeling, affecting the expected transcription pattern of one or more genes. The problems we faced to amplify the *Mob1* 3'UTR support the probable existence of a stable chromatin structure that was altered with the gene-swap. Chromatin remodeling is an important eukaryotic gene regulation mechanism, also described in *T. gondii.* Evidence indicates that this regulatory mechanism is involved in tachyzoite-bradyzoite differentiation. The *T. gondii* RSC8 (remodel the structure of chromatin complex subunit 8) regulates the transcription of bradyzoite-specific genes (Rooney et al. 2011). Histones are fundamental for assembly of the nucleosome, the fundamental structure of chromatin, and histone modifications are key events involved in gene regulation. Particularly, histone hyperacetylation (gene activation marker) of promoter regions of tachyzoite or bradyzoite specific genes is positively correlated with tachyzoite or bradyzoite stages, respectively (Sullivan and Hakimi 2006). Notably, iGSoe tachyzoites showed spontaneous *in vitro* tissue cyst formation. Although a low rate (2.8%), it is significant as its parental strain shows no spontaneous tissue cyst formation, a standard characteristic of the RH strain (Soete et al. 1994). The spontaneous cyst formation detected in iGSoe tachyzoites is also coherent with a phenotype caused by changes in chromatin structure. Still, this does not exclude the possibility that the phenotype of increased tachyzoite to bradyzoite differentiation is caused by MOB1 overexpression which would be in accordance with the decreased tachyzoite to bradyzoite differentiation observed with deletion of *Mob1*.

Mob1 deleted tachyzoites showed an increase in irregular PVs compared to the respective parental strains. The presence of PVs harboring a number of tachyzoites different than those expected in the classically described 2^n replication, where "n" indicates the number of divisions since invasion of the host cell, could have several explanations. This could be a consequence of a lack of synchronicity of tachyzoites replicating within the same PV. The knockout of the motor protein Myosin I or of the actin dynamics regulator formin 3 (FRM3) did not affect tachyzoite proliferation but caused disorganization and asynchronous replication inside the PV suggesting that these proteins, that localize to the residual body, allow tachyzoite connection and communication within the PV (Frénal, Jacot, et al. 2017; Tosetti et al. 2019a). Alternatively, the occurrence of irregular PVs could be a consequence of the occurrence of multiple daughter assembly inside one mother cell, with part of the tachyzoites undergoing division through schizogony rather than endodyogeny. Schizogony occurs in the asexual expansion phase of the *T. gondii* development in the definitive host's intestine, mostly in the form of endopolygeny, however is considered a rare phenomenon in tachyzoite proliferation. This relatively rare occurrence (0.5-10%) has been previously described in RH (type I) and P-

strain (type II) tachyzoites (Hu et al. 2002). An increase in occasional schizogony division in tachyzoites could justify the increase in replication detected in *Mob1* knockout tachyzoites. MOB1 could therefore regulate the commitment to the division mechanism chosen by *T. gondii* and its accordance with the stage that the parasite presents, directly related to its life cycle phase.

In addition to the increase in replication and irregular PVs, the *Mob1* knockout also led to a dramatic decrease in tachyzoite to bradyzoite differentiation and tissue cyst formation. This effect was observed in Eko and GSko tachyzoites, indicating this is not a strain specific effect. As explained previously, the iGSoe strain is not appropriate to study the effects of *Mob1* overexpression as it presents a difference in proliferation to its parental strain that is very dissimilar from that of other RH *Mob1* overexpression strains. So, without testing other *Mob1* overexpression strains, we are not able to attribute the formation of tissue cysts in iGSoe tachyzoites to MOB1 overexpression. But, it is interesting to note that the effect of *Mob1* knockout in tachyzoite to bradyzoite differentiation was detected in strains with different characteristics. The virulent type I RH strain does not normally form tissue cysts *in vivo* and is also resistant to spontaneous tissue cyst formation *in vitro* (Soete et al. 1994; Weiss and Kim 2000). In contrast, the EGS strain continues to show relatively high spontaneous formation of tissue cysts *in vitro*, despite having been isolated over two decades ago and being maintained in culture over prolonged periods (Paredes-Santos et al. 2013). Prolonged maintenance of Apicomplexa in the tachyzoite stage is linked to loss of stage differentiation aptitude. *T. gondii* and *Besnotia jellisoni* failed to produce oocysts and tissue cysts, respectively, after serial passage of the tachyzoite stage in mice through intraperitoneal inoculation (Frenkel et al. 1976). It is also frequently observed that avirulent strains, which show a greater aptitude to form tissue cysts, tend to decrease in its tissue cyst formation efficiency while usually presenting a faster proliferation rate after prolonged *in vitro* maintenance (Weiss and Kim 2000). Avirulent strains (e.g. types II and III) typically present slower proliferation rates compared to virulent strains (e.g. type I). This is frequently associated to a greater aptitude to form tissue cysts, including spontaneous tissue cyst formation *in vitro*. Prolonged tachyzoite maintenance *in vitro* frequently leads to a decrease in tissue forming aptitude concomitant with an increase in the proliferation rate. Therefore the two *in vitro* characteristics seem to be correlated. The knockout of *Mob1* in *T. gondii* led to an increase in replication and a decrease in spontaneous tissue cyst formation. *Mob1* deleted tachyzoites also presented an increase in irregular PVs, a possible consequence of increased tachyzoite replication through schizogony rather than endodyogeny, explaining the detected increase in replication. As a unicellular organism with a complex life cycle, the

T. gondii's replication mechanism is likely deeply connected with the stage it harbors and its ability to undergo stage differentiation. Furthermore, the control of cell number/density (proliferation *versus* apoptosis) may play a significant role in the *T. gondii* bradyzoite stage. Bradyzoites form tissue cysts, permanent structures including a glycoprotein rich tissue cyst wall that camouflages the parasite's presence in host's tissues and limits the space available for growth. The recent demonstration by Watts et al. (2015) that bradyzoites are not fully quiescent but actively replicate inside tissue cysts further highlight the necessity for parasite number control. The diameter of tissue cysts in the brains of mice varies but generally increases and tends to constant median and maximum sizes with the course of infection. Bradyzoites present both asynchronous and synchronous replication both also a wave replication pattern. Additionally, larger tissue cysts generally present lower bradyzoite densities indicating that the bradyzoite number is not the sole factor driving tissue cyst size. Tissue cysts may represent non-aggregative multicellular structures where mechanisms of parasite number/density (proliferation *versus* apoptosis) control are necessary for the biology of these structures and for the life cycle of *T. gondii*. MOB1 presents itself as a possible regulator of the intertwining processes of replication, differentiation and parasite number control.

MOB proteins are essential for accurate cell division, being required for ploidy maintenance, cell polarity definition, cytokinesis, or morphogenesis in unicellular organisms (Luca and Winey 1998; Luca et al. 2001; Hammarton et al. 2005; Slabodnick et al. 2014). Despite the conservation of MOB1 in *T. gondii*, which also occurs in other Apicomplexa, MOB1 is not essential for cell division in tachyzoites. In yeast, Mob1p has been characterized as a member of the core kinase module of the mitotic exit network (MEN)/ septation initiation network (SIN) (Hergovich and Hemmings 2012). The same core kinase module is largely conserved in Metazoa, participating in cell biology processes but also homeostasis, differentiation, and morphogenesis at the tissue/organ level (Bothos et al. 2005; Lai et al. 2005; Shimizu et al. 2008; Maerz et al. 2009; Hergovich et al. 2009; Galla et al. 2011; Tavares et al. 2012). Our findings show MOB1 regulates tachyzoite replication and is necessary for tachyzoite to bradyzoite differentiation and tissue cyst formation *in vitro*. MOB1's effect on replication could be related with *T. gondii*'s commitment to the division mechanism it undergoes and, ultimately, with the life cycle stage of the parasite. MOB proteins have been shown to regulate tissue differentiation in multicellular eukaryotes. *Mus musculus* MmMOB1 regulates the differentiation and maintenance of embryonic stem cells, bronchioalveolar stem cells, and liver cells (Mardin et al. 2010; Nishio et al. 2016; Otsubo et al. 2017). *D. melanogaster* DmMOB1 (Mats) is necessary for embryonic development (Shimizu et al. 2008). MOB proteins of filamentous fungi are documented to

control the development to key tissues. Notably, these organisms are able to multiply through sexual (e.g. fruiting body formation) and/or asexual (e.g. conidiation) reproduction. In *Neurospora crassa*, NcMOB1 is essential for fruiting body formation/ascosporogenesis and for conidiation, NcMOB2 influences conidiation while NcMOB4/Phocein is essential for fruiting body formation (Maerz et al. 2009). *Sordaria macrospora* SmMOB4/Phocein is also essential for the formation of fruiting bodies and reproductive spores (Bernhards and Pöggeler 2011). *Aspergillus nidulans An*MOB4/Phocein deletion caused increased conidiation and normal fruiting body formation but absence of ascosporogenesis (Elramli et al. 2019). *Colletotrichum higginsianum* ChMOB1 and ChMOB2 are necessary for conidiation while deletion of *Ch*MOB4/Phocein did not produce a phenotype (Schmidpeter et al. 2017). Interestingly, although *C. higginsianum* lacks a sexual cycle, its genome harbors an ortholog to *AnMob4/Phocein* and *SmMob4/Phocein* (Schmidpeter et al. 2017). Fungi MOB4/Phocein proteins are usually connected to sexual development, as is the case of *N. crassa*, *S. macrospora,* and *A. nidulans* (Maerz et al. 2009; Bernhards and Pöggeler 2011; Elramli et al. 2019). Plants can also go through sexual and asexual development, presenting multiple avenues for reproduction (Schmidt et al. 2015). *A. thaliana* AtMOB1 is essential for sporogenesis, gametogenesis and seed production (Galla et al. 2011; Cui et al. 2016). Overall, MOB proteins play important roles in tissue differentiation in multicellular organisms, particularly in the sexual and asexual development of plants and filamentous fungi. Additionally, MOB proteins are necessary for the formation of resistance forms, i.e. spores and seeds. The life cycles of plants and fungi present obvious parallels to the *T. gondii* life cycle, namely the ability of the organisms to proliferate through both sexual or asexual reproduction and the production of resistance forms which *T. gondii* is able to form in the environment and in the intermediate host. It is plausible that the conserved MOB proteins would take on similar functions in the context of these life cycles. In the case of *T. gondii*, a unicellular organism, stage conversion could be comparable to tissue differentiation.

Current efforts to identify the endogenous *T. gondii* MOB1 using indirect immunofluorescence and western blot techniques have not yielded results. Different *T. gondii* MOB1 recombinant proteins were frequently detected in a double band pattern using several anti-MOB1 sera and an anti-Myc monoclonal antibody. This indicates a MOB1 specific phenomenon that is causing a mobility shift in a fraction of the protein pool. MOB1 proteins are kinase adaptors that undergo phosphorylation for protein activation and this post-translational modification frequently causes small mobility shifts detected through western blot (Praskova et al. 2008; Hornbeck et al. 2015; Feng et al. 2019). Phosphorylation dependent double band patterns have been identified in endogenous MOB1 proteins of *Medicago sativa* and

M. musculus and in recombinant MOB1 proteins of *M. musculus* (Moreno et al. 2001; Citterio et al. 2006). This strongly indicates phosphorylation as the probable cause of the double band pattern we identified in the MOB1 recombinant proteins. The difficulties in the immune detection of the endogenous MOB1 may be due to characteristics of the sera used, which presented varying degrees of sensitivity and specificity in the detection of MOB1 recombinant proteins. Additionally, the endogenous MOB1 is likely expressed at low levels and/or only at specific times during the cell cycle of tachyzoites. This was observed with MOB1 recombinant proteins which accumulate between the daughter cell nuclei at a very specific and short time point of the tachyzoite cell cycle. This is also supported by the evidence indicating transcriptional and post-transcriptional regulation of *Mob1*, particularly the higher levels of *Mob1* NATs compared to STs in the tachyzoite. MOB1 proteins frequently present low expression levels, localizing at cell cycle associated organelles at specific time points in a cell cycle regulated manner. The *Trypanosoma brucei* TbMOB1 shows a punctate cytoplasmic localization, being necessary for cytokinesis(Hammarton et al. 2005). The *Tetrahymena thermophila* TtMob1 shows a highly polarized subcellular localization, accumulating mostly at the posterior pole basal bodies but also at the oral apparatus which is eccentrically located at the anterior pole of the cell (Tavares et al. 2012). TtMob1 is recruited to the division plane basal bodies and to the new oral apparatus during cell division (Tavares et al. 2012). In *D. melanogaster*, DmMOB1 (Mats) is expressed ubiquitously but at low levels in developing tissues (Shimizu et al. 2008). Yeast and human cells show a highly dynamic localization throughout the cell cycle. *Saccharomyces cerevisiae* ScMob1p is present in the cytoplasm but localizes to the spindle pole bodies in late mitosis and to the bud neck at cytokinesis (Luca et al. 2001). A similar distribution of SpMob1p occurs during the mitosis and cytokinesis of *Schizosaccharomyces pombe* (Salimova et al. 2000). The *Homo sapiens* HsMOB1 is cytoplasmic and localizes to the centrosome from late G2 phase until late cytokinesis, to the kinetochores in early mitosis, to the spindle midzone in late mitosis and to the midbody in late cytokinesis (Bothos et al. 2005; Hergovich et al. 2009; Wilmeth et al. 2010). In *M. sativa* root tip cells, MsMOB1 is present in grains and fibrillary structures in the cytoplasm during the cell cycle, being more prominent in the G_2 and mitosis phases (Citterio et al. 2006). MsMOB1 accumulates at the mid-plane between the daughter cells from late anaphase to cytokinesis and marks septum formation during cytokinesis. *T. gondii* MOB1 recombinant proteins present a cytoplasmic localization, excluded from the nucleus and from the apical pole, during most of the cell cycle. However, at the end of mitosis, MOB1 accumulates in a linear structure between the two daughter cell nuclei, starting immediately before daughter nuclei individualization and visible only a short period after the end

of mitosis. Notably, this time point coincides with the higher expression of *Mob1* transcripts at the S/M phase (data available at ToxoDB.org) (Behnke et al. 2010). Overall, the localization of recombinant MOB1 proteins in *T. gondii* is coherent with what has been described for MOB1 proteins of different organisms, pointing to conserved MOB1 localization and functions (Figure 56). The faint and diffuse punctate cytoplasmic pattern was abundantly described. The accumulation at the mid-plane between the two daughter cells was described in ciliates, yeast, and plants, organisms with different cell structures and consequently adapted cell division mechanisms. However the functional significance of this localization is not yet fully understood.

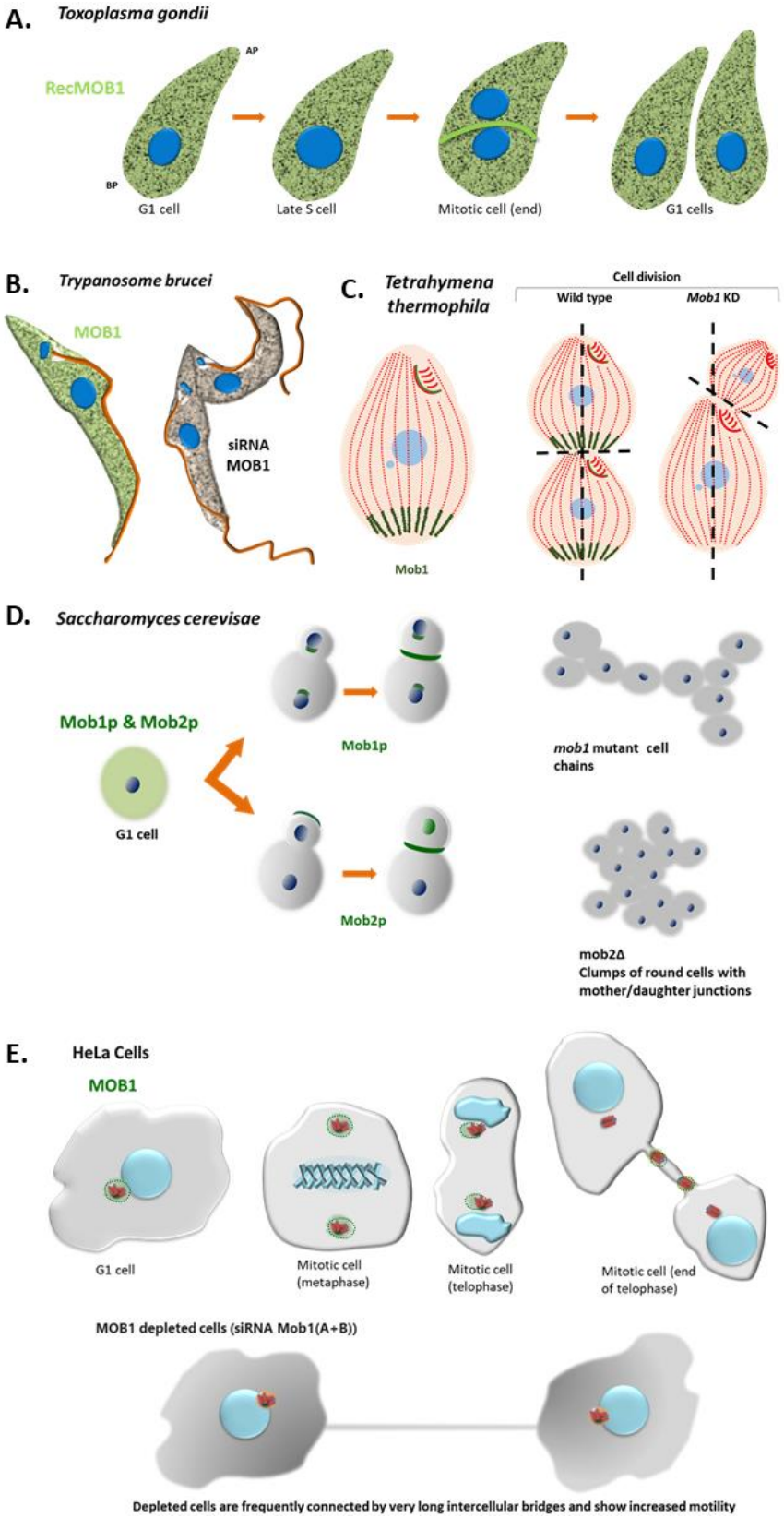

Figure 56. Localization of MOB proteins in different organisms.

A) In *Toxoplasma gondii*, recombinant MOB1 proteins (RecMOB1) show a punctate cytoplasmic localization that is excluded from the nucleus and the apical pole. At the end of mitosis, RecMOB1 accumulates in a midline between the two daughter nuclei, starting immediately before daughter nuclei individualization and visible only a short period after the end of mitosis. AP—apical pole; BP—basal pole. **B**) TbMOB1 in the bloodstream form of *T. brucei* presents a punctate distribution in the cytoplasm throughout the cell cycle. TbMOB1 was shown to be essential in both bloodstream and procyclic life cycle stages of the protozoan. Down-regulation of TbMOB1 in the bloodstream form results in a delay in cytokinesis and leads to a de-regulation of the cell cycle (not shown in the scheme) (Hammarton et al. 2005). In the procyclic form, it affects the accuracy of cytokinesis, presenting mispositioning of the cleavage furrow and incorrect cytokinesis. **C**) In the ciliate *Tetrahymena thermophila* Mob1 accumulates in basal bodies at the posterior pole of the cell forming a gradient through the anterior–posterior axis. During cell division Mob1 is recruited to the basal bodies at the equatorial zone where the cleavage furrow will be established (Tavares et al. 2012). Mob1 depletion causes the abnormal establishment of the cell division plane and cytokinesis is arrested. **D**) In budding yeast Mob1p localizes diffusely to the cytoplasm in G1, S, and G2 phases. In mitotic cells Mob1p first localizes to the spindle pole bodies during mid-anaphase and to a ring at the bud neck just before and during cytokinesis. Mob1p is required for cytokinesis in addition to mitotic exit (Luca et al. 2001). Cultures of mutant mob1 strains present cellular chains indicating the role of Mob1p in cytokinesis. In mitotic cells Mob2p first localizes to the growing bud tip and to the bud neck and the daughter nucleus in late mitosis. Mob2p is required for maintenance of polarized cell growth and for mother/daughter separation after cytokinesis. mob2Δ strains grow as clumps of round cells joined at certain regions (Colman-Lerner et al. 2001). (**E**) In human HeLa cells MOB1 localizes to the centrosome and this staining pattern remains until the centrioles duplicate and centrosomes separate (Bae et al. 2019). In late telophase cells with two separated centrioles, MOB1 is detected just in the stronger GFP-centrin signal (probably mother centriole), often the one closer to the midbody. Depletion of MOB1A and MOB1B by RNAi causes abscission failure and increases cell motility after cytokinesis inducing persistent centriole separation in G1 phase.

MOB1 proteins exhibit polarized localizations related to cell division and cytokinesis, being necessary for appropriate cell morphogenesis and polarity maintenance (Salimova et al. 2000; Luca et al. 2001; Tavares et al. 2012; Slabodnick et al. 2014; Schmidpeter et al. 2017). Ciliates studies showed that MOB1 is essential for appropriate cell polarity and morphogenesis which enable correct cytokinesis and maintenance of ploidy levels (Tavares et al. 2012; Slabodnick et al. 2014). In *M. sativa*, the marked accumulation of MsMOB1 indicates a role at the end of mitosis, cytokinesis and septation (Citterio et al. 2006). *C. higginsianum* and *S. pombe* also exhibit deficient septation associated to MOB1 depletion (Schmidpeter et al. 2017). In *S. cerevisiae* and *S. pombe*, Sc/SpMob1p localize at the bud neck/medial ring during cytokinesis (Salimova et al. 2000; Luca et al. 2001). ScMob1p is essential for mitosis completion, cytokinesis, and maintenance of ploidy levels (Luca and Winey 1998; Luca et al. 2001). SpMob1p localizes to the medial ring in late mitosis, flanking this structure during ring contraction (Salimova et al. 2000). Medial actomyosin ring contraction in *S. pombe* is dependent on SIN controlled septum formation (McCollum and Gould 2001). *S. cerevisiae* MEN is crucial for cytokinesis through actomyosin contractile ring formation (Lee et al. 2001). Myosin II is a

motor protein essential for actomyosin ring contraction in metazoans and fungi, but is absent from several taxa including Viridiplantae and Alveolata (Sebé-Pedrós et al. 2014). Plant cell abscission involves assembly of the phragmoplast, a structure localized at the mid-plane (Livanos and Müller 2019). The phragmoplast is rich in microtubules, F-actin, several motor proteins including kinesins and myosins, and scaffolds cell plate formation. Actomyosin is necessary for phragmoplast guidance and mid-plane cell plate positioning, where myosins also localize (Livanos and Müller 2019). The clathrin adaptor protein 1 complex (AP1) mediates the delivery of Golgi vesicles to the cleavage furrow of *S. pombe* or forming cell plate of *A. thaliana*, being essential for daughter cell abscission (Ma et al. 2009; Teh et al. 2013). *Ap1* deleted *T. gondii* tachyzoites showed decreased proliferation and side-to-side tethering, indicating a conserved mechanism of cell abscission in fungi, plants, and apicomplexans (Venugopal et al. 2017). Interestingly the *T. gondii* Myosins B and C, proteins involved in daughter cell budding and abscission, were identified as putative MOB1 interactors using proximity biotinylation. Myosins B and C, two proteins encoded by the same gene but the product of alternative splicing, localize to the periphery of tachyzoites and at the residual body, accumulating in what the authors describe as distinct structures or lamellae extending from the periphery between the daughter cells, strongly resembling the localization of MOB1 recombinant proteins (Delbac et al. 2001). These data strongly suggest a concerted action of MOB1 and Myosin B/C forming a scaffold between daughter cells that assists proper cell abscission, through a mechanism putatively conserved in fungi, plants, and apicomplexans. PV disorganization was detected in tachyzoites depleted for Myosin I, FRM3 and also in Myosin B overexpression, proteins that localize to the residual body, indicating myosin and actin related proteins support structure development in dividing tachyzoites (Delbac et al. 2001; Frénal, Jacot, et al. 2017; Tosetti et al. 2019b). Whereas MOB1 overexpression also led to a decrease in replication, no morphological alterations were detected in the PV structure (Tavares 2015). The phenotype observed in *Mob1* knockout tachyzoites appears to be more compatible with the occurrence of multiple daughter assembly, however we can not exclude the possibility that this phenotype is caused by an increase in PV disorganization. Multiple daughter assembly and PV disorganization could also be present simultaneously.

5.4. Bioinformatics analysis identified a hypothetical *Toxoplasma gondii* MEN/SIN/Hippo pathway closer to yeast MEN/SIN

Data mining, sequence similarity and STRING analyses allowed us to identify probable counterparts of several core components of MEN/SIN/Hippo beyond MOB1 as well as other

predicted MOB1 interactors (Table 21). The genes/proteins identified indicate a *T. gondii* MOB1 signaling more similar to what has been characterized in *S. cerevisiae* MEN and *S. pombe* SIN compared to what has been described in *H. sapiens* and *D. melanogaster* (Hippo).

Table 21. Summary of genes/proteins identified through sequence similarity and STRING analyses.

Gene[1]	Protein	Description	Seq. similarity		STRING
			MEN	Hippo	
TGME49_225960	S8FOU9	STE[2]	yes	yes	no
TGME49_215670	S8ESP0	NDR[3]	yes	yes	no
TGME49_272200	S8F1R4	NDR[3]	no	yes	yes
four genes	four proteins	14-3-3	no	yes	no
TGME49_314430	A0A125YZF0	CDC14	yes	no	yes
TGME49_218220	A0A125YRL7	CRK2	yes	no	no
TGME49_252500	S8F7N5	ROP kinase	no	no	yes
TGME49_256880	S8GBL3	Ser/Thr kinase	no	no	yes
TGME49_215670	S8ESP0	AGC kinase	no	no	yes
TGME49_205550	S8GN25	AGC kinase	no	no	yes
TGME49_261200	S8GLW6	Rab-GAP TBC protein	yes[4]	no	yes
TGME49_256070	A0A125YUD7	CMGC kinase	no	no	yes
TGME49_239910	S8FAP4	CRK-like	no	no	yes

The genes/proteins are identified with ToxoDB and Uniprot identifiers and a functional description is provided. 1 - TGME49_ gene ID number; 2 - no SARAH domain (similarly to ScCdc15p/SpCdc7p); 3 - expression similar to *Mob1* in cat intestine; 4 - same protein family as the MEN ScBub2p but not identified in sequence similarity analysis; Seq. – sequence; ROP – rhoptry; Ser – serine; Thr – threonine; AGC - kinases related to PKA, PKG, and PKC; NDR - nuclear dbf2-related; Rab GAP - Rab GTPase activating protein; TBC - Tre-2/Bub2/Cdc16; CRK - cyclin-dependent related kinase.

The STE protein family is largely reduced in Apicomplexa (Talevich et al. 2011). Piroplasms appear to completely lack this family and other apicomplexans frequently present one or very few STE proteins that have not been successfully classified into subfamilies. This contrasts with the generality of eukaryotes in which the family is highly conserved (Talevich et al. 2011). *N. caninum* harbors one STE7 and one STE20 proteins, with the STE20 presenting highest resemblance to the FRAY subfamily. The *T. gondii* STE protein presents highest sequence similarity to the *N. caninum* STE20. However, the Apicomplexa STE family is much

reduced and divergent which makes it challenging to classify these proteins into STE20 subfamilies. It is possible that the single or few STE apicomplexan proteins aggregate more than one subfamily functionality. Therefore, we considered the *T. gondii* STE protein a possible functional counterpart of the ScCdc15p/ SpCdc7p/ HsMST1/2/ DmHippo kinases (Figure 57). MST/Hippo kinase activity is not always necessary for LATS/Warts activation. YAP/Yorkie inhibition may be generated by the STE20 kinases MAP4K4/ Misshapen and MAP4K1/2/3/5/ Happyhour activate LATS1/2/ Warts, showing an activity redundant with MST1/2/ Hippo (Li et al. 2014; Zheng et al. 2015; Meng et al. 2015). LATS1/2 but not MST1/2 is regulated by G-protein coupled receptor (GPCR) signaling leading to YAP/TAZ activation or inhibition (Yu et al. 2012). The GPCR second messenger cyclic adenosine monophosphate (cAMP), acts through Rho GTPases and protein kinase A (PKA) to regulate LATS1/2 and YAP phosphorylation (Yu et al. 2013). These mechanisms are conserved in fly and mammal, indicating that alternative STE20 kinases and non STE kinases may substitute MST1/2/ Hippo in Hippo pathway activation. Cytoskeleton-mediated anoikis and E-cadherin–mediated contact inhibition of proliferation lead to YAP regulation through LATS1/2 modulation (Kim et al. 2011; Zhao et al. 2012). Notably, the *T. gondii* STE protein lacks a SARAH domain which is present in HsMST1/2/ DmHippo but absent in ScCdc15p/ SpCdc7p. Prosite identifies the SARAH domain in MST1/2, SAV, RASSF1-6, and CST1 proteins of metazoans and MST1 of the amebozoan *Dictyostelium discoideum* (slime mold). The SARAH domains of SAV and RASSF proteins form heterodimers with the SARAH domain of MST1/2 proteins regulating Hippo signaling (Hwang et al. 2007). No *T. gondii* counterparts to the STE20 kinases HsMAP4K4/6/7/ DmMisshapen and HsMAP4K1/2/3/5/ DmHappyhour were identified. Probable homologs to the *S. cerevisiae* and *S. pombe* effector proteins ScCdc14p/ SpCip1p and ScCdk1p were identified and the *T. gondii* CDC14 phosphatase was also predicted as a MOB1 interactor by STRING (Figure 57). The *T. gondii* CDC14 phosphatase had been previously identified as homologous to ScCdc14p/ SpCip1p/ HsCDC14A1 (Gubbels et al. 2008). CRK2 was also identified as the *T. gondii* homolog to CDK1 in a study of apicomplexan cell division checkpoints which identified ten CRK encoding genes in the *T. gondii* genome (Alvarez and Suvorova 2017) (Figure 57). A CRK-like protein not identified in this study was predicted as a MOB1 interactor by STRING (TGME49_239910; S8FAP4). Notably, this CRK-like protein is included in an OrthoMCL-DB ortholog group that appears to be exclusive of cyst-forming coccidia (OG6_489725). STRING also predicted a MOB1 interactor belonging to the TBC family (Tre-2/Bub2/Cdc16) and an *S. cerevisiae* member of this family, ScBub2p, acts upstream of ScCdc15p activating MEN signaling (Bardin and Amon 2001). The *T. gondii* genome also codes for an HsNDR1/2/

DmTricornered-like NDR kinase and four 14-3-3 proteins, components only characterized in Hippo signaling (Figure 57). These data point to additional signaling routes not characterized in *S. cerevisiae* MEN/ *S. pombe* SIN and coherent with the characterized Hippo signaling. It is noteworthy that the CDC14, CDK1, and 14-3-3 downstream proteins, highly conserved in eukaryotes mediating several signaling pathways, are not exclusive to MEN/SIN/Hippo signaling (van Heusden 2005; Talevich et al. 2011; Hergovich 2012). Thus the expression of these proteins in *T. gondii* indicates the possibility that MEN/SIN/Hippo-like signaling occurs in this organism in a conserved manner rather than specifically showing the presence of this pathway. No HsYAP/ DmYorkie or HsTAZ counterparts were identified. We detected an uncharacterized *T. gondii* protein (TGME49_306220; A0A125YQ80) harboring two WW domains in a pattern similar to HsYAP/ DmYorkie proteins, which could be a possible alternative effector protein in this organism. Interestingly, in *M. musculus* MmYAP/TEAD overexpression leads to an increase in MmCDK1 transcription, suggesting the prototypical Hippo and MEN/SIN effectors may be functionally related (Kapoor et al. 2014). However, this protein also harbors two FF domains which are not present in HsYAP/ DmYorkie. The presence of FF domains indicates that this *T. gondii* protein may act as a splicing factor rather than as a transcriptional regulator as HsYAP/ DmYorkie (Bedford and Leder 1999). Besides the CRK-like protein, another apicomplexan specific protein predicted as a MOB1 interactor was a ROP kinase (TGME49_252500; S8FAP4) pointing towards a possible apicomplexan specific MOB1 signaling.

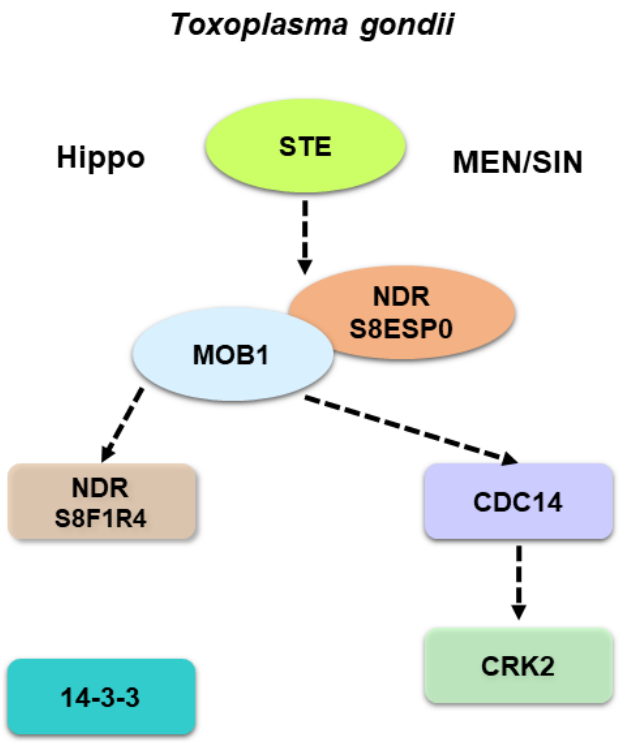

Figure 57. A Hypothetical *Toxoplasma gondii* MEN/SIN/Hippo-like pathway.

T. gondii predicted components of a hypothetical *T. gondii* MEN/SIN/Hippo pathway according to literature review and sequence analysis. The dotted arrows represented predicted interactions based on MEN/SIN/Hippo pathways. The Uniprot identifier is indicated for both *T. gondii* NDR kinases.

5.5. Proximity biotinylation experiments point to a multivalent role of MOB1, regulated by the ubiquitin-proteasome system

The MOB1 interactors and neighbors identified through proximity biotinylation include a varied group of proteins with distinct functional affinities, pointing to a multifunctional role of MOB1 in *T. gondii*, similarly to what has been described for MOB proteins in various organisms. This is also reflected by the various subcellular localizations that the MOB1 interactome is predicted to occupy. It is noteworthy that the proximity biotinylation experiments were performed using transgenes driven by the strong *Tub8* promoter which can favor overdetection, although this effect should be mostly controlled through the biotinylation detected in the FB control strain. Therefore, the functional categories and subcellular localizations identified may be slightly overestimated. None of the proteins predicted as possible *T. gondii* counterparts of MEN/SIN/Hippo components and as MOB1 interactors by STRING analysis were identified in the proximity biotinylation experiments. Most are kinases and/or cell cycle associated proteins as cyclins. These proteins frequently present high turnover rates which may impair its detection.

Alternatively, the hypothetical interaction of MOB1 with these proteins may be limited to a specific life cycle phase not analyzed in these experiments, making its detection more challenging or even not possible in the experimental conditions used. MOB1 recombinant proteins present a cell cycle-dependent subcellular localization, indicating that MOB1 interactions may occur in a very limited time frame when tachyzoites are intracellular, likely producing small amounts of biotinylated interactor and neighbor proteins, another possible limiting factor for detection. A possible approach to improve the detection of interactions that occur in a cell cycle-dependent manner would be to analyze protein extracts of different time points of the *T. gondii* cell cycle. This approach presents several technical challenges which prompted us to not use it as a starting method. Cell cycle synchronization is not easily achieved with high success rates. Using cultures at a more initial phase of the exponential growth, the yields of total protein will be substantially lower thus biotinylated protein yields as well. To reduce host cell contamination, parasites need to be isolated when still intracellular which also tends to reduce parasite yield. Integration of a cell cycle-dependent approach with our full lytic cycle approach will likely produce a more comprehensive database to understand the processes in which MOB1 is involved. Alternatively, using more recently developed proximity biotinylation methods such as TurboID that presents higher biotinylation activity could also improve sensibility. No prototypical MEN/SIN/Hippo components or known MOB1 interactors were identified in the *T. gondii* MOB1 proximity biotinylation interactome, obtained during the full *T. gondii* lytic cycle. Still, several of the identified proteins consist of probable *T. gondii* counterparts to proteins characterized as participating in MEN/Hippo signaling or as partners to MEN/Hippo components in other organisms. Of 15 MEN/Hippo related proteins, 14 were characterized in the context of Hippo signaling in multicellular eukaryotes while two were identified in the context of MEN signaling in yeast. However, this apparent higher similarity to multicellular eukaryote Hippo signaling is a possible consequence of a higher volume of studies focusing on these organisms.

Comparing our two BioID assays, none of the proteins identified in the first assay were confirmed in the second assay. However, similar proteins were identified in both assays, namely ribosomal proteins and secretory organelle proteins. This indicates that these proteins may more likely be detections based on neighboring positions rather than true interactions. Therefore, proteins categorized in the protein synthesis and fate and secretory system groups may represent MOB1 neighboring proteins. Notably, Hippo pathway signaling regulates skeletal muscle mass and protein synthesis in *M. musculus* (Watt et al. 2015).

Proteins related to the ubiquitine-proteasome system (UPS) make up an important share of the MOB1 interactome. In fact, we identified a comprehensive set of proteins essential for the functioning of the UPS including proteins involved in the ubiquitin conjugation cascade (E1, E2, and E3), three proteasome subunits, an ubiquitin family protein and an ubiquitin receptor protein. Regulation of MOB proteins by the UPS has been reported in mammals. In *H. sapiens*, HsMOB1 is ubiquitinated by the E3 ligase HsPraja2 mediated by HsFERMT2, inhibiting Hippo signaling through proteasome degradation of HsMOB1 (Lignitto et al. 2013; Song et al. 2019). HsMOB2 is also ubiquitinated at various lysine residues (Wagner et al. 2012; Akimov et al. 2018). HsMOB2 loss of function mutations are associated with increased nonsense mediated decay and proteasome degradation (O'Neill et al. 2018). In *M. musculus*, MmPTEN activates MsGSK3β which phosphorylates MmMOB1 at the serine 146 promoting its ubiquitination and degradation by the proteasome and controlling neurite outgrowth (Song et al. 2018). Of the UPS related proteins identified in the *T. gondii* MOB1 interactome, nine proteins are possible counterparts to proteins described as associated with MOB/MEN/Hippo components, namely E1, E2, and E3 enzymes, two PSMBs, SKP1, and RPN13. SKP1 integrates the Skp, Cullin, F-box (SCF) complex, a multi-protein E3 ubiquitin ligase complex that promotes ubiquitin-mediated proteolysis. The SCF complex promotes HsYAP ubiquitination following HsMST/HsLATS mediated HsYAP phosphorylation in *H. sapiens* (Liu et al. 2010; Zhao et al. 2010). In *S. cerevisiae*, ScSkp1p interacts with the MEN regulator ScBfa1p promoting mitotic exit and cytokinesis, an action that is proposed to be independent of the SCF complex (Kim et al. 2006). The expression of *MmPsmb5* is significantly increased in a mouse model of pancreatic ductal adenocarcinoma (PDAC) where tumor relapse is mediated by overexpression of the YAP/TEAD complex (Kapoor et al. 2014). In *S. cerevisiae*, ScRpn13p was identified in TurboID labeling experiments using ScCdc5p as bait, which contributes to regulate the targeting of ScDbf2p/Mob1p to the nucleolus (Zhou et al. 2021). We also identified a DA1-like protein in the *T. gondii* MOB1 interactome. DA1 proteins are ubiquitin receptors and, in *A. thaliana*, AtDA1 regulates cell proliferation, and seed and organ size determination (Dong et al. 2007; Li et al. 2018). The enrichment of the *T. gondii* MOB1 interactome in UPS related proteins strongly indicates that MOB1 post-translational regulation through ubiquitin-proteasome degradation is present in *T. gondii*, affecting the FBMOB1 recombinant protein.

Proteins involved in regulation of the cell cycle and DNA processing are also prominent among the MOB1 BioID interactome with 11 proteins being classified into this functional category. Of these, five proteins are probable counterparts to proteins described as associated with Hippo components. Three *T. gondii* RAD proteins were identified as possible MOB1

interactors, RAD25, RAD26, and RAD51. Mammalian LATS1 is necessary for establishing RAD51 nucleofilaments in genotoxic stress response (Pefani et al. 2014). In the PDAC mouse model, MmYAP/TEAD overexpression appears to drive *MmRad51* transcription (Kapoor et al. 2014). HsMOB2 interacts with HsRAD50 activating the DNA damage response and is involved in homologous recombination inhibition (Adamson et al. 2012; Gomez et al. 2015). Mammalian RAD25 and RAD26 are involved in nucleotide excision repair. RAD25 proteins present both helicase and transcriptional activity. A DYRK family protein and APC1 were also detected in the *T. gondii* MOB1 interactome. DYRK family proteins have been shown to regulate the Hippo pathway in *D. melanogaster* and interact with HsLATS2 in *H. sapiens* (Tschöp et al. 2011; Degoutin et al. 2013). APC1 integrates the anaphase-promoting complex/cyclosome (APC/C), an E3 ubiquitin ligase complex that controls cell cycle progression through adaptor proteins, namely cadherin 1, leading to ubiquitin-dependent proteolysis. This complex regulates Hippo signaling in a cell cycle-dependent manner namely through interaction of CDH1 with LATS leading to LATS degradation and YAP activation, in mammalian and fly (Kim 2019). APC/C interacts with and is regulated by the constitutive photomorphogenesis 9 signalosome (CSN), a proteasome/ubiquitin pathway regulator (Kob et al. 2009). Notably, CSN5 was also detected in the *T. gondii* MOB1 interactome. The CSN also regulates neddylation, a post-translational modification that is necessary for cardiac development in rodents and leads to MST1 degradation and Hippo signaling repression (Zou et al. 2018). Notably, the proteins CSN5, ubiquitin family protein, E1, E2, SKP1, RPN13, PSMB1, PSMB5, and APC1 integrated the STRING network analysis cluster 1 which was statistically significant. Therefore, there is strong evidence that cell cycle regulation of Hippo signaling is mediated by the UPS. It is possible that the cell cycle-dependent regulation of *T. gondii Mob1* expression is associated to the regulation of MOB1 levels through ubiquitin-dependent proteolysis.

MOB proteins were first described as kinase adaptors. Still the signal transduction functional category was not one of the most represented in the *T. gondii* MOB1 interactome pointing to a multivalent functionality, as has since been described in various organisms. *T. gondii* expresses three catalytic subunits and one regulatory cAMP-dependent protein kinase subunit (Sugi et al. 2016). PKAc1 and PKAc2 are localized at the periphery of the parasite while PKAc3 presents a cytoplasmic subcellular localization (Sugi et al. 2016). PKAR overexpression leads to decreased tachyzoite proliferation (Kurokawa et al. 2011). A decrease in proliferation was also observed upon inhibition of PKAc1 and deletion of *Pkac3* (Kurokawa et al. 2011). One catalytic (PKAc1) and the regulatory (PKAR) subunits were identified in the *T. gondii* MOB1 interactome. Both PKAc1 and PKAR seem to be necessary at appropriate levels for normal

tachyzoite proliferation (Kurokawa et al. 2011; Jia et al. 2017). In mammals and fly, PKA phosphorylates LATS leading to YAP inhibition (Kim et al. 2013; Yu et al. 2013; Zhang et al. 2019). This effect appears to be related to several upstream signals including actin cytoskeletal changes and G-protein coupled receptor signaling (Kim et al. 2013; Yu et al. 2013). The detection of PKAc1 and PKAR in the *T. gondii* MOB1 interactome suggests that this signaling pathway may also occur through interaction with MOB1 or with a yet unidentified MOB1-interacting kinase. Candidate MOB1 downstream kinases identified in the MOB1 interactome are CAMK1 and TKLK. Notably the coccidian specific PKAc3 is responsible for cAMP-dependent tachyzoite maintenance, inhibiting tachyzoite to bradyzoite differentiation (Sugi et al. 2016). Differential regulation of cAMP produces different biological responses in *T. gondii* with transient elevation of cAMP levels inducing differentiation to bradyzoites but sustained elevation resulting in inhibition of tachyzoite to bradyzoite differentiation (Kirkman et al. 2001; Hartmann et al. 2013). We hypothesize a cAMP-PKAc1-MOB1 signaling axis functioning in parallel to the cAMP-PKAc3 axis in the regulation of tachyzoite proliferation and tachyzoite to bradyzoite differentiation. This dual response mechanism would allow a finely regulated reaction of the parasite to extracellular signals conveyed through the cAMP second messenger. A phosphofructokinase (PFK) was also identified in the *T. gondii* MOB1 interactome. Notably, glucose metabolism-associated gene transcription regulation occurs through the YAP/TAZ/TEAD complex which is promoted by PFK stabilization of TEAD, a mechanism independent of LATS conserved in mammal and fly (Enzo et al. 2015).

Metabolism related proteins constitute a large proportion of the *T. gondii* MOB1 interactome. Particularly, hydrolases and proteins involved in amino acid metabolism are enriched in the MOB1 interactome. Amino acid metabolism enrichment is also patent in the STRING metabolism related cluster 2. Seven proteins with putative hydrolase activity were detected and bioinformatics based characterization identified two phospholipases, two peptidases, and one DNA glycosylase. This indicates a MOB1 interactome associated to intracellular signaling but also to proteolysis, likely mediated by the UPS. Among the metabolism related proteins identified in the MOB1 interactome, putative thioredoxin 1 is a possible counterpart of a protein described as associated with Hippo components. Studies have indicated that the Hippo pathway is regulated by oxidative stress signaling namely through thioredoxin-1 (Chae et al. 2012; Wu et al. 2013; López-Grueso et al. 2019). In mammals, thioredoxin-1 interacts with MST1 inhibiting Hippo signaling activation by MST1 in response to oxidative stress stimulation (Chae et al. 2012).

The detection of several transcription related proteins, including an ApiAP2 transcription factor, a polyadenylation factor subunit, and two mediator subunits, points to a MOB1 specific regulation of gene expression. This function that has been well characterized in several organisms in the context of MEN/SIN/Hippo signaling which lead to transcription of genes involved in the regulation of apoptosis and cell proliferation mediated by the CDK1 or YAP/TAZ effector proteins, as the genes *Sox4*, *c-myc*, *Ki67*, *Afp*, *Diap1*, *Birc2*, *Birc5*, and *Mcl1* (Huang et al. 2005; Dong et al. 2007; Zhang et al. 2008; Wu et al. 2013). ApiAP2 transcription factors have been characterized as important regulators of gene expression necessary for stage differentiation and life cycle progression in Apicomplexa (Jeninga et al. 2019). AP2VIIA4, detected in the *T. gondii* MOB1 interactome, may participate in a MOB1 associated regulation of stage differentiation, coherent with the phenotype of failure in tachyzoite to bradyzoite transition with MOB1 knockout.

Several proteins involved in cell transport were identified in the *T. gondii* MOB1 interactome, mostly involved in vesicle transport and ER protein translocation. SNARE proteins are components of the membrane trafficking and fusion machinery necessary for cell plate formation in *A. thaliana*, localizing to the forming cell plate during cytokinesis (Heese et al. 2001; Zheng et al. 2002; Zhang et al. 2011). AtSEC1 also contributes to cell plate formation interacting with the SNARE complex (Heese et al. 2001). In *T. gondii*, the SNAP/SNARE/Rab machinery regulates dense granule release using parasite protein through a mechanism conserved in *T. gondii* and mammalian (Chaturvedi et al. 1999). Actomyosin and vesicle transport proteins are essential for successful cytokinesis promoting cleavage furrow abscission or development of the phragmoplast which scaffolds cell plate assembly (Ma et al. 2009; Teh et al. 2013; Livanos and Müller 2019). The set of MyosinB/C, SEC61 and SNARE proteins identified in the MOB1 interactome and the lack of a cleavage furrow during *T. gondii* cytokinesis are highly suggestive of the presence of a conserved mechanism in tachyzoite cytokinesis where SNARE and SEC transport proteins contribute to the formation of a midline structure with a myosin scaffold between the two forming nuclei, where MOB1 also localizes, possibly contributing to appropriate cell polarity and morphogenesis, a role reported in various organisms (Salimova et al. 2000; Luca et al. 2001; Tavares et al. 2012; Slabodnick et al. 2014; Schmidpeter et al. 2017).

6. Concluding remarks and future perspectives

This work contributed to the elucidation of the mechanisms underlying parasite replication and parasite number regulation by analyzing the role of MOB1 in *T. gondii*.

Our results establish that the *Mob1* expression is regulated post-transcriptionally through alternative splicing and NATs. Our results combined with a comprehensive analysis of the information available at ToxoDB.org indicate that *Mob1* expression is regulated not only during the tachyzoite lytic cycle but also throughout the complex *T. gondii* life cycle. Significantly higher levels of *Mob1* detected during the *T. gondii* sexual development in the definitive host's intestinal epithelium indicate that MOB1 might be necessary at higher levels in these life cycle stages.

All the recombinant MOB1 proteins developed in this work present a cytoplasmic localization. However, accumulate in a linear pattern between the two daughter nuclei at the end of mitosis, presenting therefore a cell cycle dependent localization. In other organisms, MOB proteins are a hallmark of the cell division site and are frequently necessary for correct chromosome segregation and cytokinesis, namely through MEN/SIN signaling in yeast. The detection of Myosin B/C, SEC61, and SNARE proteins in the MOB1 proximity biotinylation interactome suggests that *T. gondii* may present a myosin and vesicle derived linear structure associated with mitosis/cytokinesis.

Still, *Mob1* is not an essential gene for the tachyzoite lytic cycle during *in vitro* culture. The deletion of *Mob1* causes a slight increase in the parasite replication rate, congruent with our previous observation of a delay in replication when MOB1 is overexpressed. The increase in the replication rate is coupled to a decrease in PV regularity. This led us to hypothesize that MOB1 is necessary for synchronous replication and/or to the commitment to the division mechanism chosen by the parasite. The regulation of *Mob1* expression throughout the *T. gondii* life cycle could be correlated with the replication and PV regularity phenotypes and with the different replication mechanisms that *T. gondii* presents during its life cycle.

Mob1 knockout also leads to a steep decrease in tachyzoite to bradyzoite differentiation, indicating that MOB1 may be necessary for the *T. gondii* stage differentiation process. Tachyzoites and bradyzoites present differing proliferation rates mostly due to different durations of the replicative phase. The regulation of the *T. gondii* replication rate is assumed to be correlated with tachyzoite and bradyzoite stage differentiation. At the same time bradyzoites, which replicate inside the tissue cyst at a slow rate, require a more stringent parasite number control when compared to tachyzoites, a stage that proliferates rapidly and promptly egresses from the PV. The need to control the cell number/density (proliferation *versus* apoptosis) is characteristic of multicellular organisms and is regulated by MOB proteins through Hippo

pathway signaling. Tissue cysts likely function as non-aggregative multicellular structures with controlled cell number/density and size. The control of cell number/density is intimately related to cell differentiation and self-renewal, processes in which MOB proteins also play important regulatory roles. Therefore, we propose that MOB1 mediated regulation of tachyzoite-bradyzoite differentiation consists of a conserved mechanism and that the regulation of *T. gondii* replication by MOB1 may be coupled to the control of stage differentiation, contributing to the control of parasite number homeostasis in tissue cysts. *T. gondii* PKAc1 and PKAr, which were detected in the MOB1 proximity biotinylation assays, contribute to appropriate tachyzoite proliferation. The *D. melanogaster* counterpart PKA participates in Hippo signaling regulation. This led us to suggest that a cAMP-PKAc1-MOB1 signaling axis may be involved in the *T. gondii* regulation of tachyzoite-bradyzoite stage conversion.

The *T. gondii* genome codes for probable counterparts to additional MEN/SIN/Hippo core components, namely a STE kinase, two NDR kinases, 14-3-3 Hippo signaling effector proteins, and the MEN/SIN effector proteins CDC14 and CRK2. Significantly, the NDR kinases present an expression pattern similar to *Mob1*'s during the *T. gondii* life cycle, suggesting a common functionality. The MOB1 proximity biotinylation interactome suggests that MOB1 regulation through the UPS is conserved in *T. gondii.* This interactome includes proteins that participate in a wide range of cellular functions, namely proteins related to metabolism, protein synthesis and fate, cell transport, cell cycle and DNA processing, transcription, signal transduction, secretory system and cell structure, indicating a possible multivalent role for MOB1 signaling. While we did not identify other probable counterparts to MEN/SIN/Hippo canonical signaling, we detected several proteins that are probable counterparts to proteins previously characterized as participating in MEN/Hippo signaling. We performed proximity biotinylation assays using the tachyzoite stage. Considering that MOB1 and the two *T. gondii* NDR kinases appear to present a differential regulation according to the *T. gondii* life cycle, we propose that MOB1 may participate in MEN/SIN/Hippo-like signaling with a life cycle dependent functionality. The proposed *T. gondii* MEN/SIN/Hippo-like pathway would act predominantly through non-canonical signaling in the tachyzoite and bradyzoite stages and through canonical signaling in the enteroepithelial and environmental stages. Therefore, *T. gondii* may consist of a key biological model to study both canonical and non-canonical signaling of MEN/SIN/Hippo-like pathways. Evolutionarily, at the level of sequence analysis, *T. gondii* presents gene candidates that are more related to the yeast pathways (MEN/SIN). Conversely, the phenotypes observed during the gain and loss of function of MOB1 together with the MOB1 interacting partners

identified through proximity biotinylation suggest that *T. gondii* presents a pathway functionally closer to Hippo (multicellular organisms).

This study contributed to a more comprehensive understanding of the *T. gondii* biological cycle and paved the way for the assembly of a MEN/SIN/Hippo-like signaling pathway in Apicomplexa. The CRISPR/Cas9 and BioID methodologies established during this work are available for application in future studies. Additionally, the results obtained comprise a foundation for the development of molecular and biochemical studies with the potential to define key biological pathways in apicomplexan organisms. Worthwhile efforts for future research building on this work will be directed towards: (i) studying the regulation of MOB1 by the UPS and through post-translational modifications, as phosphorylation, to understand the availability of this protein during the cell cycle, taking advantage of the *Mob1* gain-of-function *T. gondii* strains; (ii) distinguishing MOB1 interacting partners from proximity labeling among the identified MOB1 interactome to better define the molecular pathways in which MOB1 is involved; (iii) testing the hypothesis of MOB1 and Myosin B/C co-localization at the medial line during mitosis/cytokinesis and deciphering the role of this structure in cell division; (iv) clarifying the effect of *Mob1* knockout on PV regularity and its association with PV synchronicity and/or the commitment to the division mechanism chosen by the parasite, employing the *Mob1* loss-of function *T. gondii* strains; (v) studying the role of MOB1 during the rest of the *T. gondii* life cycle employing the gain and loss-of-function strains.

References

[ECDC]. 2021. Congenital toxoplasmosis. Stockholm. http://www.ncbi.nlm.nih.gov/pubmed/15865702

[WHO]. 2020. World malaria report 2020: 20 years of global progress and challenges. Geneva. https://www.jstor.org/stable/resrep27867

Adamson B, Smogorzewska A, Sigoillot FD, King RW, Elledge SJ. 2012. A genome-wide homologous recombination screen identifies the RNA-binding protein RBMX as a component of the DNA damage response. Nat Cell Biol. 14(3):318–328. https://doi.org/10.1038/ncb2426

Aguirre AA, Longcore T, Barbieri M, Dabritz H, Hill D, Klein PN, Lepczyk C, Lilly EL. 2019. The One Health Approach to Toxoplasmosis : Epidemiology , Control , and Prevention Strategies. Ecohealth . 16:378–390. https://doi.org/10.1007/s10393-019-01405-7

Akimov V, Barrio-hernandez I, Hansen SVF, Hallenborg P, Pedersen A, Bekker-jensen DB, Puglia M, Christensen SDK, Vanselow JT, Nielsen MM, et al. 2018. UbiSite approach for comprehensive mapping of. Nat Struct Mol Biol . 25:631–640. https://doi.org/10.1038/s41594-018-0084-y

Alexander DL, Mital J, Ward GE, Bradley P, Boothroyd JC. 2005. Identification of the moving junction complex of Toxoplasma gondii: A collaboration between distinct secretory organelles. PLoS Pathog. 1(2):0137–0149. https://doi.org/10.1371/journal.ppat.0010017

Álvarez-García G, García-Lunar P, Gutiérrez-Expósito D, Shkap V, Ortega-Mora LM. 2014. Dynamics of Besnoitia besnoiti infection in cattle. Parasitology. 141(11):1419–1435. https://doi.org/10.1017/S0031182014000729

Alvarez CA, Suvorova ES. 2017. Checkpoints of apicomplexan cell division identified in Toxoplasma gondii. PLoS Pathog. 13(7):1–28. https://doi.org/10.1371/journal.ppat.1006483

Alves BF, Oliveira S, Soares HS, Pena HFJ, Conte-Junior CA, Gennari SM. 2019. Isolation of viable Toxoplasma gondii from organs and Brazilian commercial meat cuts of experimentally infected pigs. Parasitol Res. 118(4):1331–1335. https://doi.org/10.1007/s00436-019-06229-6

Andenmatten N, Egarter S, Jackson AJ, Jullien N, Meissner M, Herman J-P, Meissner M. 2013. Conditional genome engineering in Toxoplasma gondii uncovers alternative invasion mechanisms. Nat Methods . 10(2):125–7. https://doi.org/10.1038/nmeth.2301

Anderson-White B, Beck JR, Chen C-T, Meissner M, Bradley PJ, Gubbels M-J. 2012. Cytoskeleton assembly in Toxoplasma gondii cell division. Int Rev Cell Mol Biol. 298:1–31. https://doi.org/10.1097/OPX.0b013e3182540562.The

Ankarklev J, Jerlström-Hultqvist J, Ringqvist E, Troell K, Svärd SG. 2010. Behind the smile: Cell biology and disease mechanisms of Giardia species. Nat Rev Microbiol . 8(6):413–422. https://doi.org/10.1038/nrmicro2317

Astamal RV, Maghoul A, Taefehshokr S, Bagheri T, Mikaeili E, Derakhshani A, Delashoub M, Taefehshokr N, Isazadeh A, Hajazimian S, et al. 2020. Regulatory role of microRNAs in cancer through Hippo signaling pathway. Pathol - Res Pract . 216(12):153241.

https://doi.org/10.1016/j.prp.2020.153241

Attias M, Teixeira DE, Benchimol M, Vommaro RC, Crepaldi PH, De Souza W. 2020. The life-cycle of Toxoplasma gondii reviewed using animations. Parasites and Vectors . 13(1):1–13. https://doi.org/10.1186/s13071-020-04445-z

Bae JS, Jeon Y, Kim SM, Jang JY, Park MK, Kim IH, Hwang DS, Lim DS, Lee H. 2018. Depletion of MOB1A/B causes intestinal epithelial degeneration by suppressing Wnt activity and activating BMP/TGF-β signaling. Cell Death Dis . 9(11). https://doi.org/10.1038/s41419-018-1138-0

Bae JS, Kim SM, Jeon Y, Sim J, Jang JY, Son J, Hong W, Park MK, Lee H. 2019. Loss of Mob1a/b impairs the differentiation of mouse embryonic stem cells into the three germ layer lineages. Exp Mol Med . 51(11). https://doi.org/10.1038/s12276-019-0342-z

Bardin a J, Amon a. 2001. Men and sin: what's the difference? Nat Rev Mol Cell Biol . 2(11):815–26. https://doi.org/10.1038/35099020

Barros M, Cabezón O, Dubey JP, Almería S, Ribas MP, Escobar LE, Ramos B, Medina-Vogel G. 2018. Toxoplasma gondii infection in wild mustelids and cats across an urban-rural gradient. PLoS One. 13(6):1–16. https://doi.org/10.1371/journal.pone.0199085

Barylyuk K, Koreny L, Ke H, Butterworth S, Crook OM, Lassadi I, Gupta V, Tromer E, Mourier T, Stevens TJ, et al. 2020. A Comprehensive Subcellular Atlas of the Toxoplasma Proteome via hyperLOPIT Provides Spatial Context for Protein Functions. Cell Host Microbe. 28(5):752-766.e9. https://doi.org/10.1016/j.chom.2020.09.011

Bedford MT, Leder P. 1999. The FF domain: A novel motif that often accompanies WW domains. Trends Biochem Sci. 24(7):264–265. https://doi.org/10.1016/S0968-0004(99)01417-6

Behnke MS, Wootton JC, Lehmann MM, Radke JB, Lucas O, Nawas J, Sibley LD, White MW. 2010. Coordinated progression through two subtranscriptomes underlies the tachyzoite cycle of toxoplasma gondii. PLoS One. 5(8). https://doi.org/10.1371/journal.pone.0012354

Berger F, Goulet V, Le Strat Y, Desenclos JC. 2009. Toxoplasmosis among pregnant women in France: Risk factors and change of prevalence between 1995 and 2003. Rev Epidemiol Sante Publique. 57(4):241–248. https://doi.org/10.1016/j.respe.2009.03.006

Bernhards Y, Pöggeler S. 2011. The phocein homologue SmMOB3 is essential for vegetative cell fusion and sexual development in the filamentous ascomycete Sordaria macrospora. Curr Genet. 57(2):133–149. https://doi.org/10.1007/s00294-010-0333-z

Beugnet F, Moreau Y. 2015. Babesiosis. OIE Rev Sci Tech. 34(2):627–639. https://doi.org/10.20506/rst.34.2.2385

Bidlingmaier S, Weiss EL, Seidel C, Drubin DG, Snyder M. 2001. The Cbk1p pathway is important for polarized cell growth and cell separation in Saccharomyces cerevisiae. Mol Cell Biol . 21(7):2449–2462. https://doi.org/10.1128/MCB.21.7.2449-2462.2001

Bisio H, Soldati-Favre D. 2019. Signaling cascades governing entry into and exit from host cells by Toxoplasma gondii. Annu Rev Microbiol. 73:579–599.

https://doi.org/10.1146/annurev-micro-020518-120235

Black MW, Boothroyd JC. 2000. Lytic Cycle of Toxoplasma gondii. 64(3):607–623.

Blaga R, Aubert D, Thébault A, Perret C, Geers R, Thomas M, Alliot A, Djokic V, Ortis N, Halos L, et al. 2019. Toxoplasma gondii in beef consumed in France: Regional variation in seroprevalence and parasite isolation. Parasite. 26. https://doi.org/10.1051/parasite/2019076

Bohne W, Heesemann J, Gross U. 1993. Induction of bradyzoite-specific Toxoplasma gondii antigens in gamma interferon-treated mouse macrophages. Infect Immun. 61(3):1141–1145. https://doi.org/10.1128/iai.61.3.1141-1145.1993

Bohne W, Heesemann J, Gross U. 1994. Reduced replication of Toxoplasma gondii is necessary for induction of bradyzoite-specific antigens: a possible role for nitric oxide in triggering stage conversion. Infect Immun . 62(5):1761–7. http://www.pubmedcentral.nih.gov/articlerender.fcgi?artid=186404&tool=pmcentrez&rendertype=abstract

Boothroyd JC, Black M, Bonnefoy S, Hehl A, Knoll LJ, Manger ID, Ortega-Barria E, Tomavo S. 1997. Genetic and biochemical analysis of development in Toxoplasma gondii. Philos Trans R Soc B Biol Sci. 352(1359):1347–1354. https://doi.org/10.1098/rstb.1997.0119

Bothos J, Tuttle RL, Ottey M, Luca FC, Halazonetis TD. 2005. Human LATS1 is a mitotic exit network kinase. Cancer Res. 65(15):6568–6575. https://doi.org/10.1158/0008-5472.CAN-05-0862

Bougdour A, Maubon D, Baldacci P, Ortet P, Bastien O, Bouillon A, Barale JC, Pelloux H, Ménard R, Hakimi MA. 2009. Drug inhibition of HDAC3 and epigenetic control of differentiation in Apicomplexa parasites. J Exp Med. 206(4):953–966. https://doi.org/10.1084/jem.20082826

Brandão GP, Melo MN, Caetano BC, Carneiro CM, Silva LA, Vitor RWA. 2011. Susceptibility to re-infection in C57BL/6 mice with recombinant strains of Toxoplasma gondii. Exp Parasitol. 128(4):433–437. https://doi.org/10.1016/j.exppara.2011.05.015

Brooks CF, Johnsen H, van Dooren GG, Muthalagi M, Lin SS, Bohne W, Fischer K, Striepen B. 2010. The Toxoplasma Apicoplast Phosphate Translocator Links Cytosolic and Apicoplast Metabolism and Is Essential for Parasite Survival. Cell Host Microbe . 7(1):62–73. https://doi.org/10.1016/j.chom.2009.12.002

Brossier F, Jewett TJ, Lovett JL, Sibley LD. 2003. C-terminal processing of the toxoplasma protein MIC2 is essential for invasion into host cells. J Biol Chem . 278(8):6229–6234. https://doi.org/10.1074/jbc.M209837200

Buchholz KR, Fritz HM, Chen X, Durbin-Johnson B, Rocke DM, Ferguson DJ, Conrad PA, Boothroyd JC. 2011. Identification of tissue cyst wall components by transcriptome analysis of in vivo and in vitro Toxoplasma gondii bradyzoites. Eukaryot Cell. 10(12):1637–1647. https://doi.org/10.1128/EC.05182-11

Bulman S, Siemens J, Ridgway HJ, Eady C, Conner AJ. 2006. Identification of genes from the obligate intracellular plant pathogen, Plasmodiophora brassicae. FEMS Microbiol Lett.

264(2):198–204. https://doi.org/10.1111/j.1574-6968.2006.00466.x

Caldas LA, Attias M, de Souza W. 2018. A structural analysis of the natural egress of Toxoplasma gondii. Microbes Infect . 20(1):57–62. https://doi.org/10.1016/j.micinf.2017.09.006

Calero-Berna R, Gennari SM. 2019. Clinical toxoplasmosis in dogs and cats: An update. Front Vet Sci. 6(54). https://doi.org/10.3389/fvets.2019.00054

Campbell M, Ganetzky B. 2013. Identification of Mob2, a novel regulator of larval neuromuscular junction morphology, in natural populations of Drosophila melanogaster. Genetics. 195(3):915–926. https://doi.org/10.1534/genetics.113.156562

Cappello S, Gray MJ, Badouel C, Lange S, Einsiedler M, Srour M, Chitayat D, Hamdan FF, Jenkins ZA, Morgan T, et al. 2013. Mutations in genes encoding the cadherin receptor-ligand pair DCHS1 and FAT4 disrupt cerebral cortical development. Nat Genet. 45(11):1300–1310. https://doi.org/10.1038/ng.2765

Cardoso R, Nolasco S, Goncalves J, Cortes HC, Leitao A, Soares H. 2014. Besnoitia besnoiti and Toxoplasma gondii: two apicomplexan strategies to manipulate the host cell centrosome and Golgi apparatus. Parasitology. 141:1436–1454. https://doi.org/10.1017/S0031182014000493

Carruthers V, Boothroyd JC. 2007. Pulling together: an integrated model of Toxoplasma cell invasion. Curr Opin Microbiol. 10(1):83–89. https://doi.org/10.1016/j.mib.2006.06.017

Carvalho CS, Melo EJT. 2006. Acidification of the parasitophorous vacuole containing Toxoplasma gondii in the presence of hydroxyurea. An Acad Bras Cienc. 78(3):475–484. https://doi.org/10.1590/s0001-37652006000300008

Cavalier-Smith T. 1991. Archamoebae: the ancestral eukaryotes? BioSystems. 25(1–2):25–38. https://doi.org/10.1016/0303-2647(91)90010-I

Cavalier-Smith T. 1993. Kingdom protozoa and its 18 phyla. [place unknown]. https://doi.org/10.1128/mmbr.57.4.953-994.1993

Cavalier-Smith T. 1998. A revised six-kingdom system of life. Biol Rev Camb Philos Soc. 73(3):203–266. https://doi.org/10.1017/s0006323198005167

Cérède O, Dubremetz JF, Soête M, Deslée D, Vial H, Bout D, Lebrun M. 2005. Synergistic role of micronemal proteins in Toxoplasma gondii virulence. J Exp Med. 201(3):453–463. https://doi.org/10.1084/jem.20041672

Chae JS, Gil Hwang S, Lim DS, Choi EJ. 2012. Thioredoxin-1 functions as a molecular switch regulating the oxidative stress-induced activation of MST1. Free Radic Biol Med . 53(12):2335–2343. https://doi.org/10.1016/j.freeradbiomed.2012.10.527

Chakraborty S. 2019. Sequencing data from Massachusetts General Hospital shows Cas9 integration into the genome, highlighting a serious hazard in gene-editing therapeutics. F1000Research. 8:1846. https://doi.org/10.12688/f1000research.20744.1

Chalker DL, Frankel J. 2014. Morphogenesis: A Mob Rules from the Rear. Curr Biol .

24(15):R700–R702. https://doi.org/10.1016/j.cub.2014.06.042

Charron AJ, Sibley LD. 2004. Molecular partitioning during host cell penetration by Toxoplasma gondii. Traffic. 5(11):855–867. https://doi.org/10.1111/j.1600-0854.2004.00228.x

Chaturvedi S, Qi H, Coleman D, Rodriguez A, Hanson PI, Striepen B, Roos DS, Joiner KA. 1999. Constitutive calcium-independent release of Toxoplasma gondii dense granules occurs through the NSF/SNAP/SNARE/Rab machinery. J Biol Chem . 274(4):2424–2431. https://doi.org/10.1074/jbc.274.4.2424

Chaudhary K, Donald RGK, Nishi M, Carter D, Ullman B, Roos DS. 2005. Differential Localization of Alternatively Spliced Hypoxanthine- Xanthine-Guanine Phosphoribosyltransferase Isoforms in Toxoplasma gondii *. J Biol Chem . 280(23):22053–22059. https://doi.org/10.1074/jbc.M503178200

Chen CT, Gubbels MJ. 2013. The Toxoplasma gondii centrosome is the platform for internal daughter budding as revealed by a Nek1 kinase mutant. J Cell Sci. 126(15):3344–3355. https://doi.org/10.1242/jcs.123364

Chen LF, Han XL, Li FX, Yao YY, Fang JP, Liu XJ, Li XC, Wu K, Liu M, Chen XG. 2018. Comparative studies of Toxoplasma gondii transcriptomes: Insights into stage conversion based on gene expression profiling and alternative splicing. Parasites and Vectors. 11(1):1–11. https://doi.org/10.1186/s13071-018-2983-5

Chen M, Wang M, Xu S, Guo X, Jiang J. 2015. Upregulation of miR-181c contributes to chemoresistance in pancreatic cancer by inactivating the Hippo signaling pathway. Oncotarget . 6(42):44466–79. https://doi.org/10.18632/oncotarget.6298

Chen M, Zhang H, Shi Z, Li Y, Zhang X, Gao Z, Zhou L, Ma J, Xu Q, Guan J, et al. 2018. The MST4-MOB4 complex disrupts the MST1-MOB1 complex in the Hippo-YAP pathway and plays a pro-oncogenic role in pancreatic cancer. [place unknown]. https://doi.org/10.1074/jbc.RA118.003279

Chen Y, Han H, Seo G, Vargas RE, Yang B, Chuc K, Zhao H, Wang W. 2020. Systematic analysis of the Hippo pathway organization and oncogenic alteration in evolution. Sci Rep . 10(1):3173. https://doi.org/10.1038/s41598-020-60120-4

Chiba S, Amagai Y, Homma Y, Fukuda M, Mizuno K. 2013. NDR2-mediated Rabin8 phosphorylation is crucial for ciliogenesis by switching binding specificity from phosphatidylserine to Sec15. EMBO J . 32(6):874–885. https://doi.org/10.1038/emboj.2013.32

Citterio S, Piatti S, Albertini E, Aina R, Varotto S, Barcaccia G. 2006. Alfalfa Mob1-like proteins are involved in cell proliferation and are localized in the cell division plane during cytokinesis. Exp Cell Res. 312(7):1050–1064. https://doi.org/10.1016/j.yexcr.2005.12.032

Citterio S, Piatti S, Albertini E, Aina R, Varotto S, Barcaccia G, Scienza P. 2005. Alfalfa Mob1-like proteins are involved in cell proliferation and are localized in the cell division plane during cytokinesis. 2. https://doi.org/10.1016/j.yexcr.2005.12.032

Cobb RE, Wang Y, Zhao H. 2015. High-Efficiency Multiplex Genome Editing of Streptomyces Species Using an Engineered CRISPR/Cas System. ACS Synth Biol. 4(6):723–

728. https://doi.org/10.1021/sb500351f

Colman-Lerner A, Chin TE, Brent R. 2001. Yeast Cbk1 and Mob2 activate daughter-specific genetic programs to induce asymmetric cell fates. Cell . 107(6):739–750. https://doi.org/10.1016/s0092-8674(01)00596-7

Cook AJ, Gilbert RE, Buffolano W, Zufferey J, Petersen E, Jenum PA, Foulon W, Semprini AE, Dunn DT. 2000. Sources of toxoplasma infection in pregnant women: European multicentre case-control study. European Research Network on Congenital Toxoplasmosis. BMJ . 321(7254):142–7. https://doi.org/10.1201/9781420092370

Coppens I, Dunn JD, Romano JD, Pypaert M, Zhang H, Boothroyd JC, Joiner KA. 2006. Toxoplasma gondii Sequesters Lysosomes from Mammalian Hosts in the Vacuolar Space. Cell. 125(2):261–274. https://doi.org/10.1016/j.cell.2006.01.056

Coppens I, Sinai AP, Joiner KA. 2000. Toxoplasma gondii exploits host low-density lipoprotein receptor- mediated endocytosis for cholesterol acquisition. J Cell Biol. 149(1):167–180. https://doi.org/10.1083/jcb.149.1.167

Cornils H, Kohler RS, Hergovich A, Hemmings BA. 2011. Human NDR kinases control G(1)/S cell cycle transition by directly regulating p21 stability. Mol Cell Biol . 31(7):1382–1395. https://doi.org/10.1128/MCB.01216-10

Corpet F. 1988. Multiple sequence alignment with hierarchical clustering. Nucleic Acids Res. 16(22):10881–10890. https://doi.org/10.1093/nar/16.22.10881

Coste A, Jager M, Chambon J-P, Manuel M. 2016. Comparative study of Hippo pathway genes in cellular conveyor belts of a ctenophore and a cnidarian. Evodevo . 7(4). https://doi.org/10.1186/s13227-016-0041-y

Couzens AL, Knight JDR, Kean MJ, Teo G, Weiss A, Dunham WH, Lin ZY, Bagshaw RD, Sicheri F, Pawson T, et al. 2013. Protein interaction network of the mammalian hippo pathway reveals mechanisms of kinase-phosphatase interactions. Sci Signal. 6(302). https://doi.org/10.1126/scisignal.2004712

Crater AK, Roscoe S, Fahim A, Ananvoranich S. 2018. Toxoplasma ubiquitin-like protease 1, a key enzyme in sumoylation and desumoylation pathways, is under the control of non-coding RNAs. Int J Parasitol . 48(11):867–880. https://doi.org/10.1016/j.ijpara.2018.05.001

Croken MM, Qiu W, White MW, Kim K. 2014. Gene Set Enrichment Analysis (GSEA) of Toxoplasma gondii expression datasets links cell cycle progression and the bradyzoite developmental program. BMC Genomics. 15(1):1–13. https://doi.org/10.1186/1471-2164-15-515

Croken MMK, Ma Y, Markillie LM, Taylor RC, Orr G, Weiss LM, Kim K. 2014. Distinct strains of Toxoplasma gondii feature divergent transcriptomes regardless of developmental stage. PLoS One. 9(11):1–10. https://doi.org/10.1371/journal.pone.0111297

Cui X, Guo Z, Song L, Wang Y, Cheng Y. 2016. NCP1/AtMOB1A Plays Key Roles in Auxin-Mediated Arabidopsis Development. PLoS Genet. 12(3):1–21. https://doi.org/10.1371/journal.pgen.1005923

Dabritz HA, Miller MA, Gardner IA, Packham AE, Atwill ER, Conrad PA. 2008. Risk factors for Toxoplasma gondii infection in wild rodents from Central Coastal California and a review of T. gondii prevalence in rodents. J Parasitol. 94(3):675–683. https://doi.org/10.1645/GE-1342R.1

Degoutin J, Milton CC, Yu E, Tipping M, Bosveld F, Bellaiche Y, Veraksa A, Harvey KF. 2013. Riquiqui and Minibrain, new regulators of the Hippo pathway downstream of Dachsous. Nat Cell Biol. 15(10):1176–1185. https://doi.org/10.1038/ncb2829.Riquiqui

Delbac F, Sänger A, Neuhaus EM, Stratmann R, Ajioka JW, Toursel C, Herm-Götz A, Tomavo S, Soldati T, Soldati D. 2001. Toxoplasma gondii myosins B/C: One gene, two tails, two localizations, and a role in parasite division. J Cell Biol. 155(4):613–623. https://doi.org/10.1083/jcb.200012116

Deol KK, Lorenz S, Strieter ER. 2019. Enzymatic Logic of Ubiquitin Chain Assembly. Front Physiol . 10:835. https://doi.org/10.3389/fphys.2019.00835

Desmonts G, Couvreur J, Alison F, Baudelot J, Gerbeaux J, Lelong M. 1965. Étude épidémiologique sur la toxoplasmose: de l'influence de la cuisson des viandes de boucherie sur la fréquence de l'infection humaine. Rev Fr Études Clin Biol. 10:952–958.

Dettmann A, Heilig Y, Ludwig S, Schmitt K, Illgen J, Fleißner A, Valerius O, Seiler S. 2013. HAM-2 and HAM-3 are central for the assembly of the NeurosporaSTRIPAK complex at the nuclear envelope and regulate nuclear accumulation of the MAP kinase MAK-1 in a MAK-2-dependent manner. Mol Microbiol. 90(4):796–812. https://doi.org/10.1111/mmi.12399

Dobrowolski JM, Carruthers VB, Sibley LD. 1997. Participation of myosin in gliding motility and host cell invasion by Toxoplasma gondii. Mol Microbiol. 26(1):163–173. https://doi.org/10.1046/j.1365-2958.1997.5671913.x

Dobrowolski JM, Sibley LD. 1996. Toxoplasma invasion of mammalian cells is powered by the actin cytoskeleton of the parasite. Cell. 84(6):933–939. https://doi.org/10.1016/S0092-8674(00)81071-5

Donald RGK, Carter D, Roos DS, Donald RGK, Carter D, Ullman B, Roos DS. 1996. Nucleic Acids , Protein Synthesis , and Molecular Genetics : Insertional Tagging , Cloning , and Expression of the Toxoplasma gondii Phosphoribosyltransferase Gene : USE AS A SELECTABLE MARKER FOR STABLE TRANSFORMATION Insertional Tagging , Cloning , and . https://doi.org/10.1074/jbc.271.24.14010

Dong J, Feldmann G, Huang J, Wu S, Zhang N, Comerford SA, Gayyed MFF, Anders RA, Maitra A, Pan D. 2007. Elucidation of a Universal Size-Control Mechanism in Drosophila and Mammals. Cell. 130(6):1120–1133. https://doi.org/10.1016/j.cell.2007.07.019

Dubey JP. 1995. Duration of Immunity to Shedding of Toxoplasma gondii Oocysts by Cats. J Parasitol . 81(3):410–415. https://doi.org/10.2307/3283823

Dubey JP. 1996. Pathogenicity and infectivity of Toxoplasma gondii oocysts for rats. J Parasitol. 82(6):951–956. https://doi.org/10.2307/3284205

Dubey JP. 1998. Advances in the life cycle of Toxoplasma gondii. Int J Parasitol .

28(7):1019–24. http://www.ncbi.nlm.nih.gov/pubmed/9724872

Dubey JP. 2001. Oocyst shedding by cats fed isolated bradyzoites and comparison of infectivity of bradyzoites of the VEG strain Toxoplasma gondii to cats and mice. J Parasitol. 87(1):215–219. https://doi.org/10.1645/0022-3395(2001)087[0215:osbcfi]2.0.co;2

Dubey JP. 2006. Comparative infectivity of oocysts and bradyzoites of Toxoplasma gondii for intermediate (mice) and definitive (cats) hosts. Vet Parasitol. 140(1–2):69–75. https://doi.org/10.1016/j.vetpar.2006.03.018

Dubey JP. 2009. Toxoplasmosis in sheep-The last 20 years. Vet Parasitol. 163(1–2):1–14. https://doi.org/10.1016/j.vetpar.2009.02.026

Dubey JP. 2010. Toxoplasma gondii infections in chickens (Gallus domesticus): Prevalence, clinical disease, diagnosis and public health significance. Zoonoses Public Health. 57(1):60–73. https://doi.org/10.1111/j.1863-2378.2009.01274.x

Dubey JP, Cerqueira-Cézar CK, Murata FHA, Kwok OCH, Hill D, Yang Y, Su C. 2020. All about Toxoplasma gondii infections in pigs: 2009–2020. Vet Parasitol. 288(July):109185. https://doi.org/10.1016/j.vetpar.2020.109185

Dubey JP, Frenkel JK. 1972. Cyst-Induced Toxoplasmosis in Cats. J Protozool. 19(1):155–177. https://doi.org/10.1111/j.1550-7408.1972.tb03431.x

Dubey JP, Frenkel JK. 1974. Immunity to Feline Toxoplasmosis: Modification by Administration of Corticosteroids. Vet Pathol. 11(4):350–379. https://doi.org/10.1177/030098587401100407

Dubey JP, Lindsay DS, Speer CA. 1998. Structures of Toxoplasma gondii tachyzoites, bradyzoites, and sporozoites and biology and development of tissue cysts. Clin Microbiol Rev. 11(2):267–299. https://doi.org/10.1128/cmr.11.2.267

Dubey JP, Murata FHA, Cerqueira-Cézar CK, Kwok OCH. 2020. Public health and economic importance of Toxoplasma gondii infections in goats: The last decade. Res Vet Sci . 132(May):292–307. https://doi.org/10.1016/j.rvsc.2020.06.014

Dubey JP, Murata FHA, Cerqueira-Cézar CK, Kwok OCH, Yang YR. 2020. Public Health Significance of Toxoplasma gondii Infections in Cattle: 2009-2020. J Parasitol. 106(6):772–788. https://doi.org/10.1645/20-82

Dubey JP, Verma SK, Ferreira LR, Oliveira S, Cassinelli AB, Ying Y, Kwok OCH, Tuo W, Chiesa OA, Jones JL. 2014. Detection and survival of Toxoplasma gondii in milk and cheese from experimentally infected goats. J Food Prot. 77(10):1747–1753. https://doi.org/10.4315/0362-028X.JFP-14-167

Dubey R, Harrison B, Dangoudoubiyam S, Bandini G, Cheng K, Kosber A, Agop-nersesian C, Howe DK, Samuelson J, Ferguson DJP, Gubbels M. 2017. Differential Roles for Inner Membrane Complex Proteins across Toxoplasma gondii and Sarcocystis neurona Development. mSphere. 2(5):1–19. https://doi.org/10.1128/mSphere .00409-17

Duhart JC, Raftery LA. 2020. Mob Family Proteins: Regulatory Partners in Hippo and

Hippo-Like Intracellular Signaling Pathways. Front Cell Dev Biol. 8(March):1–22. https://doi.org/10.3389/fcell.2020.00161

Eaton MS, Weiss LM, Kim K. 2006. Cyclic nucleotide kinases and tachyzoite-bradyzoite transition in Toxoplasma gondii. Int J Parasitol . 36(1):107–14. https://doi.org/10.1016/j.ijpara.2005.08.014

Elbediwy A, Thompson BJ. 2018. Evolution of mechanotransduction via YAP/TAZ in animal epithelia. Curr Opin Cell Biol . 51(February):117–123. https://doi.org/10.1016/j.ceb.2018.02.003

Elramli N, Karahoda B, Sarikaya-Bayram O, Frawley D, Ulas M, Oakley CE, Oakley BR, Seiler S, Bayram O. 2019. Assembly of a heptameric STRIPAK complex is required for coordination of light-dependent multicellular fungal development with secondary metabolism in aspergillus nidulans. PLoS Genet. 15(3):1–30. https://doi.org/10.1371/journal.pgen.1008053

Emery-Corbin SJ, Hamey JJ, Ansell BRE, Balan B, Tichkule S, Stroehlein AJ, Cooper C, McInerney B V, Hediyeh-Zadeh S, Vuong D, et al. 2020. Eukaryote-Conserved Methylarginine Is Absent in Diplomonads and Functionally Compensated in Giardia. Mol Biol Evol. 37(12):3525–3549. https://doi.org/10.1093/molbev/msaa186

Endo T, Sethi KK, Piekarski G. 1982. Toxoplasma gondii: Calcium lonophore A23187-mediated exit of trophozoites from infected murine macrophages. Exp Parasitol. 53(2):179–188. https://doi.org/10.1016/0014-4894(82)90059-5

Enzo E, Santinon G, Pocaterra A, Aragona M, Bresolin S, Forcato M, Grifoni D, Pession A, Zanconato F, Guzzo G, et al. 2015. Aerobic glycolysis tunes YAP / TAZ transcriptional activity. EMBO J. 34(10):1349–1370. https://doi.org/10.15252/embj.201490379

Farhat DC, Swale C, Dard C, Cannella D, Ortet P, Barakat M, Sindikubwabo F, Belmudes L, De Bock PJ, Couté Y, et al. 2020. A MORC-driven transcriptional switch controls Toxoplasma developmental trajectories and sexual commitment. Nat Microbiol. 5(4):570–583. https://doi.org/10.1038/s41564-020-0674-4

Feng X, Arang N, Rigiracciolo DC, Lee JS, Yeerna H, Wang Z, Lubrano S, Kishore A, Pachter JA, König GM, et al. 2019. A Platform of Synthetic Lethal Gene Interaction Networks Reveals that the GNAQ Uveal Melanoma Oncogene Controls the Hippo Pathway through FAK. Cancer Cell. 35(3):457-472.e5. https://doi.org/10.1016/j.ccell.2019.01.009

Ferguson DJP. 2002. Toxoplasma gondii and sex: Essential or optional extra? Trends Parasitol. 18(8):351–355. https://doi.org/10.1016/s1471-4922(02)02330-9

Ferguson DJP, Dubremetz J-F. 2014. The Ultrastructure of Toxoplasma gondii. In: Weiss LM, Kim K, editors. Toxoplasma Gondii . Second Edi. [place unknown]: Elsevier; p. 19–59. https://doi.org/10.1016/B978-0-12-396481-6.00002-7

Ferguson DJP, Hutchison WM. 1987. An ultrastructural study of the early development and tissue cyst formation of Toxoplasma gondii in the brains of mice. Parasitol Res. 73(6):483–491. https://doi.org/10.1007/BF00535321

Fernàndez-Sabé N, Cervera C, Fariñas MC, Bodro M, Muñoz P, Gurguí M, Torre-

Cisneros J, Martín-Dávila P, Noblejas A, Len Ó, et al. 2012. Risk factors, clinical features, and outcomes of toxoplasmosis in solid-organ transplant recipients: A matched case-control study. Clin Infect Dis. 54(3):355–361. https://doi.org/10.1093/cid/cir806

Flegr J, Prandota J, Sovičková M, Israili ZH. 2014. Toxoplasmosis - A global threat. Correlation of latent toxoplasmosis with specific disease burden in a set of 88 countries. PLoS One. 9(3):e90203. https://doi.org/10.1371/journal.pone.0090203

Florindo C, Perdigão J, Fesquet D, Schiebel E, Pines J, Tavares A a. 2012. Human Mob1 proteins are required for cytokinesis by controlling microtubule stability. J Cell Sci . 125(Pt 13):3085–90. https://doi.org/10.1242/jcs.097147

Fox BA, Gigley JP, Bzik DJ. 2004. Toxoplasma gondii lacks the enzymes required for de novo arginine biosynthesis and arginine starvation triggers cyst formation. Int J Parasitol. 34(3):323–331. https://doi.org/10.1016/j.ijpara.2003.12.001

Francia ME, Jordan CN, Patel JD, Sheiner L, Demerly JL, Fellows JD, de Leon JC, Morrissette NS, Dubremetz JF, Striepen B. 2012. Cell Division in Apicomplexan Parasites Is Organized by a Homolog of the Striated Rootlet Fiber of Algal Flagella. PLoS Biol. 10(12):e1001444. https://doi.org/10.1371/journal.pbio.1001444

Francia ME, Striepen B. 2014. Cell division in apicomplexan parasites. Nat Publ Gr . 12(2):125–136. https://doi.org/10.1038/nrmicro3184

Francisco S. 2019. Toxoplasma gondii Tubulin Cofactor B plays a key role in host cell invasion and replication. [place unknown]: Universidade de Lisboa.

Frankel J. 1999. Cell Biology of Tetrahymena thermophila. In: Methods Cell Biol . Vol. 62. [place unknown]: Methods Cell Biol; ; p. 27–125. https://doi.org/10.1016/S0091-679X(08)61528-9

Frankel J. 2008. What do genic mutations tell us about the structural patterning of a complex single-celled organism? Eukaryot Cell. 7(10):1617–1639. https://doi.org/10.1128/EC.00161-08

Frénal K, Dubremetz JF, Lebrun M, Soldati-Favre D. 2017. Gliding motility powers invasion and egress in Apicomplexa. Nat Rev Microbiol . 15(11):645–660. https://doi.org/10.1038/nrmicro.2017.86

Frénal K, Jacot D, Hammoudi PM, Graindorge A, MacO B, Soldati-Favre D. 2017. Myosin-dependent cell-cell communication controls synchronicity of division in acute and chronic stages of Toxoplasma gondii. Nat Commun. 8. https://doi.org/10.1038/ncomms15710

Frénal K, Marq JB, Jacot D, Polonais V, Soldati-Favre D. 2014. Plasticity between MyoC- and MyoA-Glideosomes: An Example of Functional Compensation in Toxoplasma gondii Invasion. PLoS Pathog. 10(11). https://doi.org/10.1371/journal.ppat.1004504

Frenkel JK, Dubey JP, R. L. Hoff. 1976. Loss of Stages after Continuous Passage of Toxoplasma gondii and Besnoitia jellisoni. J Protozool. 23(3):421–424. https://doi.org/10.1111/j.1550-7408.1976.tb03799.x

Frenz LM, Lee SE, Fesquet D, Johnston LH. 2000. The budding yeast Dbf2 protein kinase localises to the centrosome and moves to the bud neck in late mitosis. J Cell Sci . 113(19):3399–3408. https://jcs.biologists.org/content/joces/113/19/3399.full.pdf

Freppel W, Ferguson DJP, Shapiro K, Dubey JP, Puech PH, Dumètre A. 2019. Structure, composition, and roles of the Toxoplasma gondii oocyst and sporocyst walls. Cell Surf . 5(December 2018):100016. https://doi.org/10.1016/j.tcsw.2018.100016

Freyre A, Dubey JP, Smith DD, Frenkel JK. 1989. Gondii Oocyst-Induced Infections. J Parasitol . 75(5):750–755. https://doi.org/10.2307/3283060

Fritz H, Barr B, Packham A, Melli A, Conrad PA. 2012. Methods to produce and safely work with large numbers of Toxoplasma gondii oocysts and bradyzoite cysts. J Microbiol Methods . 88(1):47–52. https://doi.org/10.1016/j.mimet.2011.10.010

Fritz HM, Buchholz KR, Chen X, Durbin-Johnson B, Rocke DM, Conrad PA, Boothroyd JC. 2012. Transcriptomic analysis of toxoplasma development reveals many novel functions and structures specific to sporozoites and oocysts. PLoS One. 7(2). https://doi.org/10.1371/journal.pone.0029998

Fux B, Nawas J, Khan A, Gill DB, Su C, Sibley LD. 2007. Toxoplasma gondii strains defective in oral transmission are also defective in developmental stage differentiation. Infect Immun . 75(5):2580–90. https://doi.org/10.1128/IAI.00085-07

Galagan JE, Calvo SE, Borkovich KA, Selker EU, Read ND, Jaffe D, FitzHugh W, Ma L-J, Smirnov S, Purcell S, et al. 2003. The genome sequence of the filamentous fungus Neurospora crassa. Nature . 422(6934):859–68. https://doi.org/10.1038/nature01554

Galagan JE, Calvo SE, Cuomo C, Ma L-J, Wortman JR, Batzoglou S, Lee S-I, Baştürkmen M, Spevak CC, Clutterbuck J, et al. 2005. Sequencing of Aspergillus nidulans and comparative analysis with A. fumigatus and A. oryzae. Nature . 438(7071):1105–15. https://doi.org/10.1038/nature04341

Galla G, Zenoni S, Marconi G, Marino G, Botton A, Pinosa F, Citterio S, Ruperti B, Palme K, Albertini E, et al. 2011. Sporophytic and gametophytic functions of the cell cycle-associated Mob1 gene in Arabidopsis thaliana L . Gene . 484(1–2):1–12. https://doi.org/10.1016/j.gene.2011.05.009

García-Cortés JC, McCollum D. 2009. Proper timing of cytokinesis is regulated by Schizosaccharomyces pombe Etd1. J Cell Biol. 186(5):739–753. https://doi.org/10.1083/jcb.200902116

Gardiner KL, Downs L, Berta-Antalics AI, Santana E, Aguirre GD, Genini S. 2016. Photoreceptor proliferation and dysregulation of cell cycle genes in early onset inherited retinal degenerations. BMC Genomics . 17(1):1–18. https://doi.org/10.1186/s12864-016-2477-9

Di Genova BM, Wilson SK, Dubey JP, Knoll LJ. 2019. Intestinal delta-6-desaturase activity determines host range for Toxoplasma sexual reproduction. PLoS Biol. 17(8):1–19. https://doi.org/10.1371/journal.pbio.3000364

Gomez V, Gundogdu R, Gomez M, Hoa L, Panchal N, O'Driscoll M, Hergovich A. 2015.

Regulation of DNA damage responses and cell cycle progression by hMOB2. Cell Signal . 27(2):326–339. https://doi.org/10.1016/j.cellsig.2014.11.016

Gordon J, Hwang J, Carrier KJ, Jones CA, Kern QL, Moreno CS, Karas RH, Pallas DC. 2011. Protein phosphatase 2a (PP2A) binds within the oligomerization domain of striatin and regulates the phosphorylation and activation of the mammalian Ste20-Like kinase Mst3. BMC Biochem . 12(1):54. https://doi.org/10.1186/1471-2091-12-54

Graindorge A, Frénal K, Jacot D, Salamun J, Marq JB, Soldati-Favre D. 2016. The Conoid Associated Motor MyoH Is Indispensable for Toxoplasma gondii Entry and Exit from Host Cells. PLoS Pathog. 12(1):1–26. https://doi.org/10.1371/journal.ppat.1005388

Grallert A, Krapp A, Bagley S, Simanis V, Hagan IM. 2004. Recruitment of NIMA kinase shows that maturation of the S. pombe spindle-pole body occurs over consecutive cell cycles and reveals a role for NIMA in modulating SIN activity. Genes Dev . 18(9):1007–21. https://doi.org/10.1101/gad.296204

Gras S, Jackson A, Woods S, Pall G, Whitelaw J, Leung JM, Ward GE, Roberts CW, Meissner M. 2017. Parasites lacking the Micronemal protein MIC2 are deficient in surface attachment and host cell egress, but remain virulent in vivo. Wellcome Open Res. 2:1–26. https://doi.org/10.12688/wellcomeopenres.11594.1

Gras S, Jimenez-Ruiz E, Klinger CM, Schneider K, Klingl A, Lemgruber L, Meissner M. 2019. An endocytic-secretory cycle participates in Toxoplasma gondii in motility. PLoS Biol. 17(6):1–29. https://doi.org/10.1371/journal.pbio.3000060

Gray J, Zintl A, Hildebrandt A, Hunfeld KP, Weiss L. 2010. Zoonotic babesiosis: Overview of the disease and novel aspects of pathogen identity. Ticks Tick Borne Dis . 1(1):3–10. https://doi.org/10.1016/j.ttbdis.2009.11.003

Grewal JS, Lohia A. 2015. Mechanism of Cell Division in Entamoeba histolytica. In: Amebiasis . Tokyo: Springer Japan; p. 263–278. https://doi.org/10.1007/978-4-431-55200-0_16

Gubbels M-J, Vaishnava S, Boot N, Dubremetz J-F, Striepen B. 2006. A MORN-repeat protein is a dynamic component of the Toxoplasma gondii cell division apparatus. J Cell Sci . 119(Pt 11):2236–45. https://doi.org/10.1242/jcs.02949

Gubbels M-J, White M, Szatanek T. 2008. The cell cycle and Toxoplasma gondii cell division: tightly knit or loosely stitched? Int J Parasitol . 38(12):1343–58. https://doi.org/10.1016/j.ijpara.2008.06.004

Guertin DA, Chang L, Irshad F, Gould KL, McCollum D. 2000. The role of the Sid1p kinase and Cdc14p in regulating the onset of cytokinesis in fission yeast. EMBO J. 19(8):1803–1815. https://doi.org/10.1093/emboj/19.8.1803

Gunasekera AM, Patankar S, Schug J, Eisen G, Kissinger J, Roos D, Wirth DF. 2004. Widespread distribution of antisense transcripts in the Plasmodium falciparum genome. Mol Biochem Parasitol. 136(1):35–42. https://doi.org/10.1016/j.molbiopara.2004.02.007

Gundogdu, Hergovich. 2019. MOB (Mps one Binder) Proteins in the Hippo Pathway and Cancer. Cells . 8(6):569. https://doi.org/10.3390/cells8060569

Guo M, Dubey JP, Hill D, Buchanan RL, Ray Gamble H, Jones JL, Pradhan AK. 2015. Prevalence and risk factors for toxoplasma gondii infection in meat animals and meat products destined for human consumption. J Food Prot. 78(2):457–476. https://doi.org/10.4315/0362-028X.JFP-14-328

Guo Z, Yue X, Cui X, Song L, Cheng Y. 2020. AtMOB1 Genes Regulate Jasmonate Accumulation and Plant Development. Plant Physiol. 182(3):1481–1493. https://doi.org/10.1104/pp.19.01434

Håkansson S, Morisaki H, Heuser J, Sibley LD. 1999. Time-lapse video microscopy of gliding motility in Toxoplasma gondii reveals a novel, biphasic mechanism of cell locomotion. Mol Biol Cell. 10(11):3539–3547. https://doi.org/10.1091/mbc.10.11.3539

Haldrup C, Mundbjerg K, Vestergaard EM, Lamy P, Wild P, Schulz WA, Arsov C, Visakorpi T, Borre M, Høyer S, et al. 2013. DNA Methylation Signatures for Prediction ofBiochemical Recurrence After Radical Prostatectomy of Clinically Localized Prostate Cancer. J Clin Oncol. 31(26):3250–3259. https://doi.org/10.1200/JCO.2012.47.1847

Hall TA. 1999. BioEdit: a user friendly biological sequence alignment editor and analysis program for Windows 95/98/NT. Nucleic Acids Symp. 41:95–98.

Hammarton TC, Lillico SG, Welburn SC, Mottram JC. 2005. Trypanosoma brucei MOB1 is required for accurate and efficient cytokinesis but not for exit from mitosis. Mol Microbiol . 56(1):104–16. https://doi.org/10.1111/j.1365-2958.2005.04542.x

Hanlon KS, Kleinstiver BP, Garcia SP, Zaborowski MP, Volak A, Spirig SE, Muller A, Sousa AA, Tsai SQ, Bengtsson NE, et al. 2019. High levels of AAV vector integration into CRISPR-induced DNA breaks. Nat Commun. 10(1):1–11. https://doi.org/10.1038/s41467-019-12449-2

Harding CR, Frischknecht F. 2020. The Riveting Cellular Structures of Apicomplexan Parasites. Trends Parasitol . 36(12):979–991. https://doi.org/10.1016/j.pt.2020.09.001

Hartmann A, Arroyo-Olarte RD, Imkeller K, Hegemann P, Lucius R, Gupta N. 2013. Optogenetic modulation of an adenylate cyclase in toxoplasma gondii demonstrates a requirement of the parasite cAMP for host-cell invasion and stage differentiation. J Biol Chem. 288(19):13705–13717. https://doi.org/10.1074/jbc.M113.465583

Hartmann J, Hu K, He CY, Pelletier L, Roos DS, Warren G. 2006. Golgi and centrosome cycles in Toxoplasma gondii. Mol Biochem Parasitol. 145(1):125–127. https://doi.org/10.1016/j.molbiopara.2005.09.015

Hassan MA, Melo MB, Haas B, Jensen KDC, Saeij JPJ. 2012. De novo reconstruction of the Toxoplasma gondii transcriptome improves on the current genome annotation and reveals alternatively spliced transcripts and putative long non-coding RNAs. BMC Genomics. 13:696. https://doi.org/10.1186/1471-2164-13-696

He Y, Emoto K, Fang X, Ren N, Tian X, Jan Y-N, Adler PN. 2005. Tricornered (Trc) and Warts (Wts) Kinases. Mol Biol Cell . 16(9):4139–4152. https://doi.org/10.1091/mbc.e05-01-0018

Heaslip AT, Dzierszinski F, Stein B, Hu K. 2010. TgMORN1 is a key organizer for the

basal complex of Toxoplasma gondii. PLoS Pathog. 6(2):e1000754. https://doi.org/10.1371/journal.ppat.1000754

Heese M, Gansel X, Sticher L, Wick P, Grebe M, Granier F, Jürgens G. 2001. Functional characterization of the KNOLLE-interacting t-SNARE AtSNAP33 and its role in plant cytokinesis. J Cell Biol. 155(2):239–249. https://doi.org/10.1083/jcb.200107126

Hehl AB, Basso WU, Lippuner C, Ramakrishnan C, Okoniewski M, Walker RA, Grigg ME, Smith NC, Deplazes P. 2015. Asexual expansion of Toxoplasma gondii merozoites is distinct from tachyzoites and entails expression of non-overlapping gene families to attach, invade, and replicate within feline enterocytes. BMC Genomics. 16(1):1–16. https://doi.org/10.1186/s12864-015-1225-x

Heilig Y, Schmitt K, Seiler S. 2013. Phospho-Regulation of the Neurospora crassa Septation Initiation Network.Toda T, editor. PLoS One . 8(10):e79464. https://doi.org/10.1371/journal.pone.0079464

Hergovich A. 2011. MOB control: reviewing a conserved family of kinase regulators. Cell Signal . 23(9):1433–40. https://doi.org/10.1016/j.cellsig.2011.04.007

Hergovich A. 2012. MOB control : Reviewing a conserved family of kinase regulators. 23(9):1433–1440. https://doi.org/10.1016/j.cellsig.2011.04.007.MOB

Hergovich A. 2017. Hippo Signaling in Mitosis : An Updated View in Light. Monje-Casas F, Queralt E, editors. New York: Humana Press. https://doi.org/10.1007/978-1-4939-6502-1_19

Hergovich A, Bichsel SJ, Hemmings B a. 2005. Human NDR Kinases Are Rapidly Activated by MOB Proteins through Recruitment to the Plasma Membrane and Phosphorylation †. 25(18):8259–8272. https://doi.org/10.1128/MCB.25.18.8259

Hergovich A, Hemmings BA. 2012. Hippo signalling in the G2/M cell cycle phase: Lessons learned from the yeast MEN and SIN pathways. Semin Cell Dev Biol . 23(7):794–802. https://doi.org/10.1016/j.semcdb.2012.04.001

Hergovich A, Kohler RS, Schmitz D, Vichalkovski A, Cornils H, Hemmings B a. 2009. The MST1 and hMOB1 tumor suppressors control human centrosome duplication by regulating NDR kinase phosphorylation. Curr Biol . 19(20):1692–702. https://doi.org/10.1016/j.cub.2009.09.020

Herm-Götz A, Agop-Nersesian C, Münter S, Grimley JS, Wandless TJ, Frischknecht F, Meissner M. 2007. Rapid control of protein level in the apicomplexan Toxoplasma gondii. Nat Methods. 4(12):1003–1005. https://doi.org/10.1038/nmeth1134

van Heusden G. 2005. 14-3-3 Proteins: Regulators of numerous eukaryotic proteins. IUBMB Life (International Union Biochem Mol Biol Life) . 57(9):623–629. https://doi.org/10.1080/15216540500252666

Hill D, Coss C, Dubey JP, Wroblewski K, Sautter M, Hosten T, Muñoz-Zanzi C, Mui E, Withers S, Boyer K, et al. 2011. Identification of a Sporozoite-Specific Antigen from Toxoplasma gondii. J Parasitol . 97(2):328–337. https://doi.org/10.1645/GE-2782.1

Hilman D, Gat U. 2011. The Evolutionary History of YAP and the Hippo/YAP Pathway. Mol Biol Evol . 28(8):2403–2417. https://doi.org/10.1093/molbev/msr065

Hong D, Radke JB, White MW. 2017. Opposing Transcriptional Mechanisms Regulate Toxoplasma Development.Moreno SN, editor. mSphere . 2(1):1–15. https://doi.org/10.1128/mSphere.00347-16

Hong Y. 2018. aPKC: the Kinase that Phosphorylates Cell Polarity. F1000Research . 7(F1000 Faculty Rev):903. https://doi.org/10.12688/f1000research.14427.1

Horcajo P, Xia D, Randle N, Collantes-Fernández E, Wastling J, Ortega-Mora LM, Regidor-Cerrillo J. 2018. Integrative transcriptome and proteome analyses define marked differences between Neospora caninum isolates throughout the tachyzoite lytic cycle. J Proteomics . 180(October 2017):108–119. https://doi.org/10.1016/j.jprot.2017.11.007

Hornbeck P V, Zhang B, Murray B, Kornhauser JM, Latham V, Skrzypek E. 2015. PhosphoSitePlus, 2014: mutations, PTMs and recalibrations. Nucleic Acids Res . 43(Database issue):D512-20. https://doi.org/10.1093/nar/gku1267

Hoshijima K, Jurynec MJ, Shaw DK, Jacobi AM, Behlke MA, Grunwald DJ. 2019. Highly efficient methods for generating deletion mutations and F0 embryos that lack gene function in zebrafish. Dev Cell. 51(5):645–657. https://doi.org/10.1016/j.devcel.2019.10.004.Highly

Hotz M, Barral Y. 2014. The Mitotic Exit Network: new turns on old pathways. Trends Cell Biol . 24(3):145–152. https://doi.org/10.1016/j.tcb.2013.09.010

Hou M-C, Guertin DA, McCollum D. 2004. Initiation of cytokinesis is controlled through multiple modes of regulation of the Sid2p-Mob1p kinase complex. Mol Cell Biol . 24(8):3262–76. https://doi.org/10.1128/mcb.24.8.3262-3276.2004

Hou MC, Salek J, McCollum D. 2000. Mob1p interacts with the Sid2p kinase and is required for cytokinesis in fission yeast. Curr Biol . 10(10):619–22. https://doi.org/10.1016/s0960-9822(00)00492-9

Howe DK, Sibley LD. 1995. Toxoplasma gondii comprises three clonal lineages: Correlation of parasite genotype with human disease. J Infect Dis. 172(6):1561–1566. https://doi.org/10.1093/infdis/172.6.1561

Hu K. 2008. Organizational changes of the daughter basal complex during the parasite replication of Toxoplasma gondii. PLoS Pathog. 4(1):0108–0121. https://doi.org/10.1371/journal.ppat.0040010

Hu K, Johnson J, Florens L, Fraunholz M, Suravajjala S, DiLullo C, Yates J, Roos DS, Murray JM. 2006. Cytoskeletal components of an invasion machine - The apical complex of Toxoplasma gondii. PLoS Pathog. 2(2):0121–0138. https://doi.org/10.1371/journal.ppat.0020013

Hu K, Mann T, Striepen B, Beckers CJM, Roos DS, Murray JM. 2002. Daughter cell assembly in the protozoan parasite Toxoplasma gondii. Mol Biol Cell . 13(2):593–606. https://doi.org/10.1091/mbc.01-06-0309

Huang J, Wu S, Barrera J, Matthews K, Pan D. 2005. The Hippo signaling pathway coordinately regulates cell proliferation and apoptosis by inactivating Yorkie, the Drosophila homolog of YAP. Cell. 122(3):421–434. https://doi.org/10.1016/j.cell.2005.06.007

Huang S, Holmes MJ, Radke JB, Hong D-P, Liu T, White MW, Sullivan WJ. 2017. Toxoplasma gondii AP2IX-4 Regulates Gene Expression during Bradyzoite Development. Host-microbe Biol. 2(2):1–16.

Hwang E, Ryu KS, Pääkkönen K, Güntert P, Cheong HK, Lim DS, Lee JO, Young HJ, Cheong C. 2007. Structural insight into dimeric interaction of the SARAH domains from Mst1 and RASSF family proteins in the apoptosis pathway. Proc Natl Acad Sci U S A. 104(22):9236–9241. https://doi.org/10.1073/pnas.0610716104

Hwang J, Pallas DC. 2014. STRIPAK complexes: Structure, biological function, and involvement in human diseases. Int J Biochem Cell Biol . 47:118–148. https://doi.org/10.1016/j.biocel.2013.11.021

Iftode S, Cohen J, Ruiz F, Rueda AT, Chen-Shan L, Adoutte A, Beisson J. 1989. Development of surface pattern during division in Paramecium. II. Defective spatial control in the mutant kin241. Development. 105:191–211. https://doi.org/10.1242/dev.115.1.319

Ihara F, Nishikawa Y. 2014. Starvation of low-density lipoprotein-derived cholesterol induces bradyzoite conversion in Toxoplasma gondii. Parasites and Vectors. 7(1):1–5. https://doi.org/10.1186/1756-3305-7-248

Ihry RJ, Worringer KA, Salick MR, Frias E, Ho D, Theriault K, Kommineni S, Chen J, Sondey M, Ye C, et al. 2018. P53 inhibits CRISPR-Cas9 engineering in human pluripotent stem cells. Nat Med . 24(7):939–946. https://doi.org/10.1038/s41591-018-0050-6

Ikmi A, Gaertner B, Seidel C, Srivastava M, Zeitlinger J, Gibson MC. 2014. Molecular evolution of the Yap/Yorkie proto-oncogene and elucidation of its core transcriptional program. Mol Biol Evol . 31(6):1375–90. https://doi.org/10.1093/molbev/msu071

Ishino Y, Krupovic M, Forterre P. 2018. History of CRISPR-Cas from Encounter with a Mysterious Repeated Sequence to Genome Editing Technology. J Bacteriol. 200(7):e00580-17. https://doi.org/10.1128/JB.00580-17

Jacobs L, Remington JS, Melton ML. 1960. The Resistance of the Encysted Form of Toxoplasma gondii. J Parasitol . 46(1):11. https://doi.org/10.2307/3275325

Jacot D, Tosetti N, Pires I, Stock J, Graindorge A, Hung YF, Han H, Tewari R, Kursula I, Soldati-Favre D. 2016. An Apicomplexan Actin-Binding Protein Serves as a Connector and Lipid Sensor to Coordinate Motility and Invasion. Cell Host Microbe. 20(6):731–743. https://doi.org/10.1016/j.chom.2016.10.020

Jacquet A, Coulon L, De Nève J, Daminet V, Haumont M, Garcia L, Bollen A, Jurado M, Biemans R. 2001. The surface antigen SAG3 mediates the attachment of Toxoplasma gondii to cell-surface proteoglycans. Mol Biochem Parasitol. 116(1):35–44. https://doi.org/10.1016/S0166-6851(01)00297-3

Janouškovec J, Horák A, Oborník M, Lukeš J, Keeling PJ. 2010. A common red algal

origin of the apicomplexan, dinoflagellate, and heterokont plastids. Proc Natl Acad Sci U S A. 107(24):10949–10954. https://doi.org/10.1073/pnas.1003335107

Jaspersen SL, Winey M. 2004. The budding yeast spindle pole body: Structure, duplication, and function. Annu Rev Cell Dev Biol. 20:1–28. https://doi.org/10.1146/annurev.cellbio.20.022003.114106

Jeffers V, Tampaki Z, Kim K, Sullivan WJ. 2018. A latent ability to persist: differentiation in Toxoplasma gondii. Cell Mol Life Sci . 75(13):2355–2373. https://doi.org/10.1007/s00018-018-2808-x

Jeninga MD, Quinn JE, Petter M. 2019. Apiap2 transcription factors in apicomplexan parasites. Pathogens. 8(2):1–24. https://doi.org/10.3390/pathogens8020047

Jia Y, Marq J, Bisio H, Jacot D, Mueller C, Yu L, Choudhary J, Brochet M, Soldati-Favre D. 2017. Crosstalk between PKA and PKG controls pH -dependent host cell egress of Toxoplasma gondii. EMBO J. 36(21):3250–3267. https://doi.org/10.15252/embj.201796794

Jiang K, Yao G, Hu L, Yan Y, Liu J, Shi J, Chang Y, Zhang Y, Liang D, Shen D, et al. 2020. MOB2 suppresses GBM cell migration and invasion via regulation of FAK/Akt and cAMP/PKA signaling. Cell Death Dis . 11:230. https://doi.org/10.1038/s41419-020-2381-8

Jiang Y-Y, Maier W, Baumeister R, Joachimiak E, Ruan Z, Kannan N, Clarke D, Louka P, Guha M, Frankel J, Gaertig J. 2019. Two Antagonistic Hippo Signaling Circuits Set the Division Plane at the Medial Position in the Ciliate Tetrahymena. Genetics . 211(2):651–663. https://doi.org/10.1534/genetics.118.301889

Jiang Y-Y, Maier W, Baumeister R, Minevich G, Joachimiak E, Ruan Z, Kannan N, Clarke D, Frankel J, Gaertig J. 2017. The Hippo Pathway Maintains the Equatorial Division. Genetics. 206(June):873–888. https://doi.org/10.1093/genetics/206.2.NP

Jiménez-Ruiz E, Wong EH, Pall GS, Meissner M. 2014. Advantages and disadvantages of conditional systems for characterization of essential genes in Toxoplasma gondii. Parasitology . 141(11):1390-1398. https://doi.org/10.1017/S0031182014000559

Johnson AE, Mccollum D, Gould KL. 2012. Polar opposites: Fine-tuning cytokinesis through SIN asymmetry. Cytoskeleton. 69(10):686–699. https://doi.org/10.1002/cm.21044

Joiner KA, Roos DS. 2002. Secretory traffic in the eukaryotic parasite Toxoplasma gondii: Less is more. J Cell Biol. 157(4):557–563. https://doi.org/10.1083/jcb.200112144

Jones JL, Dargelas V, Roberts J, Press C, Remington JS, Montoya JG. 2009. Risk factors for Toxoplasma gondii infection in the United States. Clin Infect Dis. 49(6):878–884. https://doi.org/10.1086/605433

Jones TC, Hirsch JG. 1972. The interaction between toxoplasma gondii and mammalian cells: II. The absence of lysosomal fusion with phagocytic vacuoles containing living parasites. J Exp Med. 136(5):1173–1194. https://doi.org/10.1084/jem.136.5.1173

Juanes MA, Piatti S. 2016. The final cut: cell polarity meets cytokinesis at the bud neck in S. cerevisiae. Cell Mol Life Sci . 73(16):3115–36. https://doi.org/10.1007/s00018-016-2220-3

Jullien N. 2003. Regulation of Cre recombinase by ligand-induced complementation of inactive fragments. Nucleic Acids Res . 31(21):131e – 131. https://doi.org/10.1093/nar/gng131

Kafsack BFC, Pena JDO, Coppens I, Ravindran S, Boothroyd JC, Carruthers VB. 2009. Rapid membrane disruption by a perforin-like protein facilitates parasite exit from host cells. Science (80-). 323(5913):530–533. https://doi.org/10.1126/science.1165740

Kapoor A, Yao W, Ying H, Hua S, Liewen A, Wang Q, Zhong Y, Wu CJ, Sadanandam A, Hu B, et al. 2014. Yap1 activation enables bypass of oncogenic KRAS addiction in pancreatic cancer. Cell . 158(1):185–197. https://doi.org/10.1016/j.cell.2014.06.003

Kapperud G, Jenum PA, Stray-Pedersen B, Melby KK, Eskild A, Eng J. 1996. Risk factors for Toxoplasma gondii infection in pregnancy: Results of a prospective case-control study in Norway. Am J Epidemiol. 144(4):405–412. https://doi.org/10.1093/oxfordjournals.aje.a008942

Kato K. 2018. How does Toxoplama gondii invade host cells? J Vet Med Sci . 80(11):1702–1706. https://doi.org/10.1292/jvms.18-0344

Kato W, Nishio M, To Y, Togashi H, Mak TW, Takada H, Ohga S, Maehama T, Suzuki A. 2019. MOB1 regulates thymocyte egress and T-cell survival in mice in a YAP1-independent manner. Genes to Cells. 24(7):485–495. https://doi.org/10.1111/gtc.12704

Katris NJ, van Dooren GG, McMillan PJ, Hanssen E, Tilley L, Waller RF. 2014. The Apical Complex Provides a Regulated Gateway for Secretion of Invasion Factors in Toxoplasma.Sibley LD, editor. PLoS Pathog . 10(4):e1004074. https://doi.org/10.1371/journal.ppat.1004074

Kean BH, Kimball AC, Christenson WN. 1969. An epidemic of acute toxoplasmosis. JAMA . 208(6):1002–4. http://www.ncbi.nlm.nih.gov/pubmed/5818626

Khan A, Ajzenberg D, Mercier A, Demar M, Simon S, Dardé ML, Wang Q, Verma SK, Rosenthal BM, Dubey JP, Sibley LD. 2014. Geographic Separation of Domestic and Wild Strains of Toxoplasma gondii in French Guiana Correlates with a Monomorphic Version of Chromosome1a. PLoS Negl Trop Dis. 8(9):e3182. https://doi.org/10.1371/journal.pntd.0003182

Khan A, Fux B, Su C, Dubey JP, Darde ML, Ajioka JW, Rosenthal BM, Sibley LD. 2007. Recent transcontinental sweep of Toxoplasma gondii driven by a single monomorphic chromosome. Proc Natl Acad Sci U S A. 104(37):14872–14877. https://doi.org/10.1073/pnas.0702356104

Kim Minchul, Kim Miju, Lee Seunghee, Kuninaka S, Saya H, Lee H, Lee Sookyung, Lim DS. 2013. CAMP/PKA signalling reinforces the LATS-YAP pathway to fully suppress YAP in response to actin cytoskeletal changes. EMBO J . 32(11):1543–1555. https://doi.org/10.1038/emboj.2013.102

Kim N, Yoon H, Lee E, Song K. 2006. A New Function of Skp1 in the Mitotic Exit of Budding Yeast Saccharomyces cerevisiae. J Microbiol. 44(6):641–648.

Kim NG, Koh E, Chen X, Gumbiner BM. 2011. E-cadherin mediates contact inhibition of proliferation through Hippo signaling-pathway components. Proc Natl Acad Sci U S A.

108(29):11930–11935. https://doi.org/10.1073/pnas.1103345108

Kim S, Kim D, Cho SW, Kim J, Kim J-S. 2014. Highly efficient RNA-guided genome editing in human cells via delivery of purified Cas9 ribonucleoproteins. Genome Res . 24(6):1012–1019. https://doi.org/10.1101/gr.171322.113

King CA. 1988. Cell motility of sporozoan protozoa. Parasitol Today. 4(11):315–319. https://doi.org/10.1016/0169-4758(88)90113-5

Kirkman LA, Weiss LM, Kim K. 2001. Cyclic nucleotide signaling in Toxoplasma gondii bradyzoite differentiation. Infect Immun. 69(1):148–153. https://doi.org/10.1128/IAI.69.1.148-153.2001

Knoll LJ, Tomita T, Weiss LM. 2014. Bradyzoite Development. In: Weiss LM, Kim K, editors. Toxoplasma Gondii . [place unknown]: Academic Press; p. 521–549. https://doi.org/10.1016/B978-0-12-396481-6.00015-5

Kob R, Kelm J, Posorski N, Baniahmad A, Von Eggeling F, Melle C. 2009. Regulation of the anaphase-promoting complex by the COP9 signalosome. Cell Cycle. 8(13):2041–2049. https://doi.org/10.4161/cc.8.13.8850

Kohler RS, Schmitz D, Cornils H, Hemmings B a., Hergovich a. 2010. Differential NDR/LATS Interactions with the Human MOB Family Reveal a Negative Role for Human MOB2 in the Regulation of Human NDR Kinases. Mol Cell Biol . 30(18):4507–4520. https://doi.org/10.1128/MCB.00150-10

Komarnitsky SI, Chiang Y-C, Luca FC, Chen J, Toyn JH, Winey M, Johnston LH, Denis CL. 1998. DBF2 Protein Kinase Binds to and Acts through the Cell Cycle-Regulated MOB1 Protein. Mol Cell Biol . 18(4):2100–2107. https://doi.org/10.1128/MCB.18.4.2100

Koreny L, Zeeshan M, Barylyuk K, Tromer EC, van Hooff JJE, Brady D, Ke H, Chelaghma S, Ferguson DJP, Eme L, et al. 2021. Molecular characterization of the conoid complex in Toxoplasma reveals its conservation in all apicomplexans, including Plasmodium species. [place unknown]. https://doi.org/10.1371/journal.pbio.3001081

Kulaberoglu Y, Lin K, Holder M, Gai Z, Gomez M, Assefa Shifa B, Mavis M, Hoa L, Sharif AAD, Lujan C, et al. 2017. Stable MOB1 interaction with Hippo/MST is not essential for development and tissue growth control. Nat Commun . 8(1). https://doi.org/10.1038/s41467-017-00795-y

Kuravi VK, Kurischko C, Puri M, Luca FC. 2011. Cbk1 kinase and Bck2 control MAP kinase activation and inactivation during heat shock. Mol Biol Cell. 22(24):4892–4907. https://doi.org/10.1091/mbc.E11-04-0371

Kurokawa H, Kato K, Iwanaga T, Sugi T, Sudo A, Kobayashi K, Gong H, Takemae H, Recuenco FC, Horimoto T, Akashi H. 2011. Identification of Toxoplasma gondii cAMP dependent protein kinase and its role in the tachyzoite growth. PLoS One. 6(7):e22492. https://doi.org/10.1371/journal.pone.0022492

LaFavers KA, Márquez-Nogueras KM, Coppens I, Moreno SNJ, Arrizabalaga G. 2017. A novel dense granule protein, GRA41, regulates timing of egress and calcium sensitivity in

Toxoplasma gondii. Cell Microbiol. 19(9):1–20. https://doi.org/10.1111/cmi.12749

Lai Z-C, Wei X, Shimizu T, Ramos E, Rohrbaugh M, Nikolaidis N, Ho L-L, Li Y. 2005. Control of Cell Proliferation and Apoptosis by Mob as Tumor Suppressor, Mats. Cell . 120(5):675–685. https://doi.org/10.1016/j.cell.2004.12.036

Lane A, Soete M, Dubremetz JF, Smith JE. 1996. Toxoplasma gondii: Appearance of specific markers during the development of tissue cysts in vitro. Parasitol Res. 82(4):340–346. https://doi.org/10.1007/s004360050123

Lebrun M, Carruthers VB, Cesbron-Delauw M-F. 2014. Toxoplasma Secretory Proteins and Their Roles in Cell Invasion and Intracellular Survival. In: Toxoplasma Gondii . Second Edi. [place unknown]: Elsevier; p. 389–453. https://doi.org/10.1016/B978-0-12-396481-6.00012-X

Lee C, Levin A, Branton D. 1987. Copper staining: A five-minute protein stain for sodium dodecyl sulfate-polyacrylamide gels. Anal Biochem. 166(2):308–312. https://doi.org/10.1016/0003-2697(87)90579-3

Lee SE, Frenz LM, Wells NJ, Johnson AL, Johnston LH. 2001. Order of function of the budding-yeast mitotic exit-network proteins Tem1, Cdc15, Mob1, Dbf2, and Cdc5. Curr Biol . 11(10):784–788. https://doi.org/10.1016/S0960-9822(01)00228-7

Li D, Musante V, Zhou W, Picciotto MR, Nairn AC. 2018. Striatin-1 is a B subunit of protein phosphatase PP2A that regulates dendritic arborization and spine development in striatal neurons. J Biol Chem. 293(28):11179–11194. https://doi.org/10.1074/jbc.RA117.001519

Li Q, Li S, Mana-Capelli S, Roth Flach RJ, Danai L V., Amcheslavsky A, Nie Y, Kaneko S, Yao X, Chen X, et al. 2014. The Conserved Misshapen-Warts-Yorkie Pathway Acts in Enteroblasts to Regulate Intestinal Stem Cells in Drosophila. Dev Cell . 31(3):291–304. https://doi.org/10.1016/j.devcel.2014.09.012

Lignitto L, Arcella A, Sepe M, Rinaldi L, Delle Donne R, Gallo A, Stefan E, Bachmann VA, Oliva MA, Tiziana Storlazzi C, et al. 2013. Proteolysis of MOB1 by the ubiquitin ligase praja2 attenuates Hippo signalling and supports glioblastoma growth. Nat Commun . 4:1822. https://doi.org/10.1038/ncomms2791

Lin C-W, Chang Y-L, Chang Y-C, Lin J-C, Chen C-C, Pan S-H, Wu C-T, Chen H-Y, Yang S-C, Hong T-M, Yang P-C. 2013. MicroRNA-135b promotes lung cancer metastasis by regulating multiple targets in the Hippo pathway and LZTS1. Nat Commun . 4:1877. https://doi.org/10.1038/ncomms2876

Lin CH, Hsieh M, Fan SS. 2011. The promotion of neurite formation in Neuro2A cells by mouse Mob2 protein. FEBS Lett . 585(3):523–530. https://doi.org/10.1016/j.febslet.2011.01.003

Lindsay DS, Dubey JP. 2011. Toxoplasma gondii: The changing paradigm of congenital toxoplasmosis. Parasitology. 138(14):1829–1831. https://doi.org/10.1017/S0031182011001478

Liu C, Wu Y, Ma J. 2020. Interaction of non-coding RNAs and Hippo signaling: Implications for tumorigenesis. Cancer Lett . 493:207–216. https://doi.org/10.1016/j.canlet.2020.08.012

Liu CY, Zha ZY, Zhou X, Zhang H, Huang W, Zhao D, Li T, Chan SW, Lim CJ, Hong W, et al. 2010. The hippo tumor pathway promotes TAZ degradation by phosphorylating a phosphodegron and recruiting the SCFβ-TrCP E3 ligase. J Biol Chem . 285(48):37159–37169. https://doi.org/10.1074/jbc.M110.152942

Livanos P, Müller S. 2019. Division Plane Establishment and Cytokinesis. Annu Rev Plant Biol . 70(1):239–267. https://doi.org/10.1146/annurev-arplant-050718-100444

Llinás M, DeRisi JL. 2004. Pernicious plans revealed: Plasmodium falciparum genome wide expression analysis. Curr Opin Microbiol. 7(4):382–387. https://doi.org/10.1016/j.mib.2004.06.014

Long S, Brown K, Sibley L. 2018. CRISPR-mediated Tagging with BirA Allows Proximity Labeling in Toxoplasma gondii. BIO-PROTOCOL . 8(6):e2768. https://doi.org/10.21769/BioProtoc.2768

López-Grueso MJ, González R, Muntané J, Bárcena JA, Padilla CA. 2019. Thioredoxin downregulation enhances sorafenib effects in hepatocarcinoma cells. Antioxidants. 8(10):1–18. https://doi.org/10.3390/antiox8100501

Lorestani A, Ivey FD, Thirugnanam S, Busby MA, Marth GT, Cheeseman IM, Gubbels M-J. 2012. Targeted proteomic dissection of Toxoplasma cytoskeleton sub-compartments using MORN1. Cytoskeleton (Hoboken) . 69(12):1069–85. https://doi.org/10.1002/cm.21077

Lourido S, Tang K, David Sibley L. 2012. Distinct signalling pathways control Toxoplasma egress and host-cell invasion. EMBO J . 31(24):4524–4534. https://doi.org/10.1038/emboj.2012.299

Luca FC, Mody M, Kurischko C, Roof DM, Giddings TH, Winey M. 2001. Saccharomyces cerevisiae Mob1p Is Required for Cytokinesis and Mitotic Exit. Mol Cell Biol. 21(20):6972–6983. https://doi.org/10.1128/MCB.21.20.6972

Luca FC, Winey M. 1998. MOB1, an essential yeast gene required for completion of mitosis and maintenance of ploidy. Mol Biol Cell . 9:29–46. http://www.hubmed.org/display.cgi?uids=9436989

Lunghi M, Spano F, Magini A, Emiliani C, Carruthers VB, Di Cristina M. 2016. Alternative splicing mechanisms orchestrating post-transcriptional gene expression: intron retention and the intron-rich genome of apicomplexan parasites. Curr Genet . 62:31–38. https://doi.org/10.1007/s00294-015-0506-x

Lyu Z, Qin N, Tyasi TL, Zhu H, Liu D, Yuan S, Xu R. 2016. The Hippo/MST pathway member SAV1 plays a suppressive role in development of the prehierarchical follicles in hen ovary. PLoS One. 11(8):1–18. https://doi.org/10.1371/journal.pone.0160896

Ma S, Meng Z, Chen R, Guan K-L. 2019. The Hippo Pathway: Biology and Pathophysiology. Annu Rev Biochem . 88:577–604. https://doi.org/10.1146/annurev-biochem-013118-111829

Ma Y, Takeuchi M, Sugiura R, Sio SO, Kuno T. 2009. Deletion mutants of AP-1 adaptin subunits display distinct phenotypes in fission yeast. Genes to Cells. 14(8):1015–1028.

https://doi.org/10.1111/j.1365-2443.2009.01327.x

Maerz S, Dettmann A, Ziv C, Liu Y, Valerius O, Yarden O, Seiler S. 2009. Two NDR kinase-MOB complexes function as distinct modules during septum formation and tip extension in Neurospora crassa. Mol Microbiol . 74(3):707–723. https://doi.org/10.1111/j.1365-2958.2009.06896.x

Mah AS, Jang J, Deshaies RJ. 2001. Protein kinase Cdc15 activates the Dbf2-Mob1 kinase complex. Proc Natl Acad Sci . 98(13):7325–7330. https://doi.org/10.1073/pnas.141098998

Maleki B, Ahmadi N, Olfatifar M, Gorgipour M, Taghipour A, Abdoli A, Khorshidi A, Foroutan M, Mirzapour A. 2021. Toxoplasma oocysts in the soil of public places worldwide: a systematic review and meta-analysis . Trans R Soc Trop Med Hyg. 115(5):471–481. https://doi.org/10.1093/trstmh/traa133

Mann T, Beckers C. 2001. Characterization of the subpellicular network, a filamentous membrane skeletal component in the parasite Toxoplasma gondii. Mol Biochem Parasitol . 115(2):257–268. https://doi.org/10.1016/S0166-6851(01)00289-4

Mardin BR, Lange C, Baxter JE, Hardy T, Scholz SR, Fry AM, Schiebel E. 2010. Components of the Hippo pathway cooperate with Nek2 kinase to regulate centrosome disjunction. Nat Cell Biol. 12(12):1166–1176. https://doi.org/10.1038/ncb2120

Markova K, Uzlikova M, Tumova P, Jirakova K, Hagen G, Kulda J, Nohynkova E. 2016. Absence of a conventional spindle mitotic checkpoint in the binucleated single-celled parasite Giardia intestinalis. Eur J Cell Biol . 95(10):355–367. https://doi.org/10.1016/j.ejcb.2016.07.003

Markus BM, Bell GW, Lorenzi HA, Lourido S. 2019. Optimizing Systems for Cas9 Expression in Toxoplasma gondii . mSphere. 4(3):1–14. https://doi.org/10.1128/msphere.00386-19

McCollum D, Gould KL. 2001. Timing is everything: regulation of mitotic exit and cytokinesis by the MEN and SIN. Trends Cell Biol . 11(2):89–95. https://doi.org/10.1016/S0962-8924(00)01901-2

McFadden GI, Yeh E. 2017. The apicoplast: now you see it, now you don't. Int J Parasitol . 47(2–3):137–144. https://doi.org/10.1016/j.ijpara.2016.08.005

McLeod R, Van Tubbergen C, Montoya JG, Petersen E. 2014. Human Toxoplasma Infection. Second Edi. [place unknown]: Elsevier. https://doi.org/10.1016/B978-0-12-396481-6.00004-0

McPhillie MJ, Zhou Y, Hickman MR, Gordon JA, Weber CR, Li Q, Lee PJ, Amporndanai K, Johnson RM, Darby H, et al. 2020. Potent Tetrahydroquinolone Eliminates Apicomplexan Parasites. Front Cell Infect Microbiol. 10(June):1–27. https://doi.org/10.3389/fcimb.2020.00203

Medina-Aguilar R, Pérez-Plasencia C, Marchat LA, Gariglio P, García Mena J, Rodríguez Cuevas S, Ruíz-García E, Astudillo-de la Vega H, Hernández Juárez J, Flores-Pérez A, López-Camarillo C. 2016. Methylation Landscape of Human Breast Cancer Cells in Response to Dietary Compound Resveratrol.Castresana JS, editor. PLoS One .

11(6):e0157866. https://doi.org/10.1371/journal.pone.0157866

Meissner M, Schlüter D, Soldati D. 2002. Role of Toxoplasma gondii myosin a in powering parasite gliding and host cell invasion. Science (80-). 298(5594):837–840. https://doi.org/10.1126/science.1074553

Meitinger F, Palani S, Pereira G. 2012. The power of MEN in cytokinesis. Cell Cycle. 11(2):219–228. https://doi.org/10.4161/cc.11.2.18857

Melo EJL, Attias M, De Souza W. 2000. The single mitochondrion of tachyzoites of Toxoplasma gondii. J Struct Biol. 130(1):27–33. https://doi.org/10.1006/jsbi.2000.4228

Melo EJT, Carvalho TMU, de Souza W. 2001. Behaviour of Microtubules in Cells Infected with Toxoplasma gondii. Biocell. 25(1):53–59.

de Melo EJT, de Carvalho TU, de Souza W. 1992. Penetration of Toxoplasma gondii into Host Cells Induces Changes in the Distribution of the Mitochondria and the Endoplasmic Reticulum. Cell Struct Funct. 17(5):311–317. https://doi.org/10.1247/csf.17.311

Melo EJT, De Souza W. 1997. Relationship between the host cell endoplasmic reticulum and the parasitophorous vacuole containing Toxoplasma gondii. Cell Struct Funct. 22(3):317–323. https://doi.org/10.1247/csf.22.317

Meng Z, Moroishi T, Mottier-Pavie V, Plouffe SW, Hansen CG, Hong AW, Park HW, Mo J-S, Lu W, Lu S, et al. 2015. MAP4K family kinases act in parallel to MST1/2 to activate LATS1/2 in the Hippo pathway. Nat Commun . 6:8357. https://doi.org/10.1038/ncomms9357

Mercier A, Ajzenberg D, Devillard S, Demar MP, de Thoisy B, Bonnabau H, Collinet F, Boukhari R, Blanchet D, Simon S, et al. 2011. Human impact on genetic diversity of Toxoplasma gondii: Example of the anthropized environment from French Guiana. Infect Genet Evol. 11(6):1378–1387. https://doi.org/10.1016/j.meegid.2011.05.003

Mercier C, Dubremetz J-F, Rauscher B, Lecordier L, Sibley LD, Cesbron-Delauw M-F. 2002. Biogenesis of Nanotubular Network in Toxoplasma Parasitophorous Vacuole Induced by Parasite Proteins.Lippincott-Schwartz J, editor. Mol Biol Cell . 13(7):2397–2409. https://doi.org/10.1091/mbc.e02-01-0021

Milne G, Webster JP, Walker M. 2020. Toxoplasma gondii: An Underestimated Threat? Trends Parasitol . 36(12):959–969. https://doi.org/10.1016/j.pt.2020.08.005

Mineo JR, Kasper LH. 1994. Attachment of Toxoplasma gondii to Host Cells Involves Major Surface Protein, SAG-1 (P-30). Exp Parasitol. 79:11–20. https://doi.org/10.1006/expr.1994.1054

Mohl DA, Huddleston MJ, Collingwood TS, Annan RS, Deshaies RJ. 2009. Dbf2-Mob1 drives relocalization of protein phosphatase Cdc14 to the cytoplasm during exit from mitosis. J Cell Biol. 184(4):527–539. https://doi.org/10.1083/jcb.200812022

Monje-Casas F, Amon A. 2009. Cell Polarity Determinants Establish Asymmetry in MEN Signaling. Dev Cell . 16(1):132–145. https://doi.org/10.1016/j.devcel.2008.11.002

Montazeri M, Mikaeili Galeh T, Moosazadeh M, Sarvi S, Dodangeh S, Javidnia J, Sharif M, Daryani A. 2020. The global serological prevalence of Toxoplasma gondii in felids during the last five decades (1967-2017): A systematic review and meta-analysis. Parasites and Vectors . 13:82. https://doi.org/10.1186/s13071-020-3954-1

Montoya JG, Liesenfeld O. 2004. Toxoplasmosis. Lancet . 363(9425):1965–76. https://doi.org/10.1016/S0140-6736(04)16412-X

Mordue DG, Desai N, Dustin M, Sibley LD. 1999. Proteins on the Basis of Their Membrane Anchoring. J Exp Med. 190(12):1783–1792.

Moré G, Maksimov P, Pardini L, Herrmann DC, Bacigalupe D, Maksimov A, Basso W, Conraths FJ, Schares G, Venturini MC. 2012. Toxoplasma gondii infection in sentinel and free-range chickens from Argentina. Vet Parasitol . 184(2–4):116–121. https://doi.org/10.1016/j.vetpar.2011.09.012

Moreno CS, Lane WS, Pallas DC. 2001. A Mammalian Homolog of Yeast MOB1 is Both a Member and a Putative Substrate of Striatin Family-Protein Phosphatase 2A Complexes. J Biol Chem. 276(26):24253–24260. https://doi.org/10.1074/jbc.M102398200

Morgens DW, Wainberg M, Boyle EA, Ursu O, Araya CL, Kimberly Tsui C, Haney MS, Hess GT, Han K, Jeng EE, et al. 2017. Genome-scale measurement of off-target activity using Cas9 toxicity in high-throughput screens. Nat Commun . 8(May):1–8. https://doi.org/10.1038/ncomms15178

Morrissette NS, Sibley LD. 2002. Cytoskeleton of Apicomplexan Parasites. Microbiol Mol Biol Rev . 66(1):21–38. https://doi.org/10.1128/MMBR.66.1.21-38.2002

Morrissy AS, Griffith M, Marra MA. 2011. Extensive relationship between antisense transcription and alternative splicing in the human genome. Genome Res. 21(8):1203–1212. https://doi.org/10.1101/gr.113431.110

Mou F, Praskova M, Xia F, Van Buren D, Hock H, Avruch J, Zhou D. 2012. The Mst1 and Mst2 kinases control activation of rho family GTPases and thymic egress of mature thymocytes. J Exp Med. 209(4):741–759. https://doi.org/10.1084/jem.20111692

Nagini S, Sophia J, Mishra R. 2019. Glycogen synthase kinases: Moonlighting proteins with theranostic potential in cancer. Semin Cancer Biol . 56:25–36. https://doi.org/10.1016/j.semcancer.2017.12.010

Neisch AL, Neufeld TP, Hays TS. 2017. A STR IPAK complex mediates axonal transport of autophagosomes and dense core vesicles through PP2A regulation. J Cell Biol. 216(2):441–461. https://doi.org/10.1083/jcb.201606082

Nichols BA, Chiappino ML. 1987. Cytoskeleton of Toxoplasma gondii 1. J Protozool . 34(2):217–226. https://doi.org/10.1111/j.1550-7408.1987.tb03162.x

Nicolle C, Manceaux L. 1908. Sur une infection à corps de Leishman (ou organismes voisins) du gondi. Comptes Rendus des Séances l'Académie des Sci. 147:763–766.

Nicolle C, Manceaux L. 1909. Sur un protozoaire nouveau du gondi. Comptes Rendus

des Séances l'Académie des Sci. 148:369–372.

Nishi M, Hu K, Murray JM, Roos DS. 2008. Organellar dynamics during the cell cycle of Toxoplasma gondii. J Cell Sci . 121(9):1559–1568. https://doi.org/10.1242/jcs.021089

Nishio M, Hamada K, Kawahara K, Sasaki M, Noguchi F, Chiba S, Mizuno K, Suzuki SO, Dong Y, Tokuda M, et al. 2012. Cancer susceptibility and embryonic lethality in Mob1a/1b double-mutant mice. J Clin Invest. 122(12):4505–4518. https://doi.org/10.1172/JCI63735

Nishio M, Sugimachi K, Goto H, Wang J, Morikawa T, Miyachi Y, Takano Y, Hikasa H, Itoh T, Suzuki SO, et al. 2016. Dysregulated YAP1/TAZ and TGF-β signaling mediate hepatocarcinogenesis in Mob1a/1b-deficient mice. Proc Natl Acad Sci U S A. 113(1):E71–E80. https://doi.org/10.1073/pnas.1517188113

Nolan SJ, Romano JD, Coppens I. 2017. Host lipid droplets: An important source of lipids salvaged by the intracellular parasite Toxoplasma gondii. [place unknown]. https://doi.org/10.1371/journal.ppat.1006362

O'Donnell L, Panier S, Wildenhain J, Tkach JM, Al-Hakim A, Landry MC, Escribano-Diaz C, Szilard RK, Young JTF, Munro M, et al. 2010. The MMS22L-TONSL complex mediates recovery from replication stress and homologous recombination. Mol Cell . 40(4):619–631. https://doi.org/10.1016/j.molcel.2010.10.024

O'Neill AC, Kyrousi C, Einsiedler M, Burtscher I, Drukker M, Markie DM, Kirk EP, Götz M, Robertson SP, Cappello S. 2018. Mob2 insufficiency disrupts neuronal migration in the developing cortex. Front Cell Neurosci. 12(March):1–13. https://doi.org/10.3389/fncel.2018.00057

Okada T, Marmansari D, Li ZM, Adilbish A, Canko S, Ueno A, Shono H, Furuoka H, Igarashi M. 2013. A novel dense granule protein, GRA22, is involved in regulating parasite egress in Toxoplasma gondii. Mol Biochem Parasitol . 189(1–2):5–13. https://doi.org/10.1016/j.molbiopara.2013.04.005

de Oliveira AHC, Ruiz JC, Cruz AK, Greene LJ, Rosa JC, Ward RJ. 2006. Subproteomic analysis of soluble proteins of the microsomal fraction from two Leishmania species. Comp Biochem Physiol - Part D Genomics Proteomics. 1(3):300–308. https://doi.org/10.1016/j.cbd.2006.05.003

Opitz C, Soldati D. 2002. "The glideosome": A dynamic complex powering gliding motion and host cell invasion by Toxoplasma gondii. Mol Microbiol. 45(3):597–604. https://doi.org/10.1046/j.1365-2958.2002.03056.x

Otsubo K, Goto H, Nishio M, Kawamura K, Yanagi S, Nishie W, Sasaki T, Maehama T, Nishina H, Mimori K, et al. 2017. MOB1-YAP1/TAZ-NKX2.1 axis controls bronchioalveolar cell differentiation, adhesion and tumour formation. Oncogene . 36(29):4201–4211. https://doi.org/10.1038/onc.2017.58

Paredes-Santos TC, Martins-Duarte ES, Vitor RWA, de Souza W, Attias M, Vommaro RC. 2013. Spontaneous cystogenesis in vitro of a Brazilian strain of Toxoplasma gondii. Parasitol Int . 62(2):181–188. https://doi.org/10.1016/j.parint.2012.12.003

Parise ME, Hotez PJ, Slutsker L. 2014. Neglected parasitic infections in the United States: Needs and opportunities. Am J Trop Med Hyg. 90(5):783–785. https://doi.org/10.4269/ajtmh.13-0727

Paulsen RD, Soni D V, Wollman R, Hahn AT, Yee M, Hesley JA, Miller SC, Cromwell EF, Solow-cordero DE, Meyer T, Cimprich KA. 2009. Processes and Pathways that Mediate Genome Stability. Mol Cell. 35(2):228–239. https://doi.org/10.1016/j.molcel.2009.06.021.A

Pefani DE, Latusek R, Pires I, Grawenda AM, Yee KS, Hamilton G, Van Der Weyden L, Esashi F, Hammond EM, O'Neill E. 2014. RASSF1A-LATS1 signalling stabilizes replication forks by restricting CDK2-mediated phosphorylation of BRCA2. Nat Cell Biol. 16(10):962–971. https://doi.org/10.1038/ncb3035

Peixoto L, Chen F, Harb OS, Davis PH, Beiting DP, Brownback CS, Ouloguem D, Roos DS. 2010. Integrative genomic approaches highlight a family of parasite-specific kinases that regulate host responses. Cell Host Microbe. 8(2):208–218. https://doi.org/10.1016/j.chom.2010.07.004

Pena HFJ, Marvulo MFV, Horta MC, Silva MA, Silva JCR, Siqueira DB, Lima PACP, Vitaliano SN, Gennari SM. 2011. Isolation and genetic characterisation of Toxoplasma gondii from a red-handed howler monkey (Alouatta belzebul), a jaguarundi (Puma yagouaroundi), and a black-eared opossum (Didelphis aurita) from Brazil. Vet Parasitol . 175(3–4):377–381. https://doi.org/10.1016/j.vetpar.2010.10.015

Peng D, Kurup SP, Yao PY, Minning TA, Tarleton RL. 2015. CRISPR-Cas9-Mediated Single-Gene and Gene Family Disruption in Trypanosoma cruzi.Johnson PJ, editor. MBio . 6(1):e02097-14. https://doi.org/10.1128/mBio.02097-14

Peng D, Tarleton R. 2015. EuPaGDT: a web tool tailored to design CRISPR guide RNAs for eukaryotic pathogens. Microb Genomics. 1(4):1–7. https://doi.org/10.1099/mgen.0.000033

Pereira G, Tanaka TU, Nasmyth K, Schiebel E. 2001. Modes of spindle pole body inheritance and segregation of the Bfa1p-Bub2p checkpoint protein complex. EMBO J . 20(22):6359–70. https://doi.org/10.1093/emboj/20.22.6359

Piel M, Tran PT. 2009. Cell Shape and Cell Division in Fission Yeast. Curr Biol . 19(17):R823–R827. https://doi.org/10.1016/j.cub.2009.08.012

Popiel I, Gold MC, Booth KS. 1996. Quantification of Toxoplasma gondii bradyzoites. J Parasitol. 82(2):330–332. https://doi.org/10.2307/3284172

Praskova M, Xia F, Avruch J. 2008. MOBKL1A/MOBKL1B Phosphorylation by MST1 and MST2 Inhibits Cell Proliferation. Curr Biol. 18(5):311–321. https://doi.org/10.1016/j.cub.2008.02.006

Prestes EB, Stoco PH, de Moraes MH, Moura H, Grisard EC. 2019. Messenger RNA levels of the Polo-like kinase gene (PLK) correlate with cytokinesis in the Trypanosoma rangeli cell cycle. Exp Parasitol . 204(March):107727. https://doi.org/10.1016/j.exppara.2019.107727

Pszenny V, Davis PH, Zhou XW, Hunter CA, Carruthers VB, Roos DS. 2011. Targeted Disruption of Toxoplasma gondii Serine Protease Inhibitor 1 Increases Bradyzoite Cyst

Formation In Vitro and Parasite Tissue Burden in Mice. Infect Immun. 8(3):1156–1165. https://doi.org/10.1128/IAI.06167-11

Putyrski M, Schultz C. 2012. Protein translocation as a tool: The current rapamycin story. FEBS Lett . 586(15):2097–2105. https://doi.org/10.1016/j.febslet.2012.04.061

Quan M, Chen Z, Jiao F, Xiao X, Xia Q, Chen J, Chao Q, Li Y, Gao Y, Yang H, et al. 2020. Lysine demethylase 2 (KDM2B) regulates hippo pathway via MOB1 to promote pancreatic ductal adenocarcinoma (PDAC) progression. J Exp Clin Cancer Res . 39(1):13. https://doi.org/10.1186/s13046-019-1489-0

R_Core_Team. 2017. R: A language and environment for statistical computing . https://www.r-project.org/

Rabenau KE, Sohrabi A, Tripathy A, Reitter C, Ajioka JW, Tomley FM, Carruthers VB. 2001. TgM2AP participates in toxoplasma gondii invasion of host cells and is tightly associated with the adhesive protein TgMIC2. Mol Microbiol. 41(3):537–547. https://doi.org/10.1046/j.1365-2958.2001.02513.x

Radke JB, Worth D, Hong D, Huang S, Sullivan WJ, Wilson EH, White MW. 2018. Transcriptional repression by ApiAP2 factors is central to chronic toxoplasmosis. PLoS Pathog. 14(5):1–26. https://doi.org/10.1371/journal.ppat.1007035

Radke JR, Behnke MS, Mackey AJ, Radke JB, Roos DS, White MW. 2005. The transcriptome of Toxoplasma gondii. BMC Biol . 3:26. https://doi.org/10.1186/1741-7007-3-26

Radke JR, Guerini MN, Jerome M, White MW. 2003. A change in the premitotic period of the cell cycle is associated with bradyzoite differentiation in Toxoplasma gondii. Mol Biochem Parasitol. 131(2):119–127. https://doi.org/10.1016/S0166-6851(03)00198-1

Radke JR, Striepen B, Guerini MN, Jerome ME, Roos DS, White MW. 2001. Defining the cell cycle for the tachyzoite stage of Toxoplasma gondii. Mol Biochem Parasitol. 115(2):165–175. https://doi.org/10.1016/S0166-6851(01)00284-5

Ramakrishnan C, Maier S, Walker RA, Rehrauer H, Joekel DE, Winiger RR, Basso WU, Grigg ME, Hehl AB, Deplazes P, Smith NC. 2019. An experimental genetically attenuated live vaccine to prevent transmission of Toxoplasma gondii by cats. (December 2018):1–14. https://doi.org/10.1038/s41598-018-37671-8

Rausch V, Hansen CG. 2020. The Hippo Pathway, YAP/TAZ, and the Plasma Membrane. Trends Cell Biol . 30(1):32–48. https://doi.org/10.1016/j.tcb.2019.10.005

Rees T, Vandepitte L, Vanhoorne B, Decock W. 2020. All genera of the world: an overview and estimates based on the March 2020 release of the Interim Register of Marine and Nonmarine Genera (IRMNG). Megataxa . 1(2):123–140. https://doi.org/10.11646/megataxa.1.2.3

Reichel MP, Alejandra Ayanegui-Alcérreca M, Gondim LFP, Ellis JT. 2013. What is the global economic impact of Neospora caninum in cattle - The billion dollar question. Int J Parasitol . 43(2):133–142. https://doi.org/10.1016/j.ijpara.2012.10.022

Reid AJ, Blake DP, Ansari HR, Billington K, Browne HP, Bryant J, Dunn M, Hung SS, Kawahara F, Miranda-Saavedra D, et al. 2014. Genomic analysis of the causative agents of coccidiosis in domestic chickens. Genome Res. 24(10):1676–1685. https://doi.org/10.1101/gr.168955.113

Robert-Gangneux F, Dardé ML. 2012. Epidemiology of and diagnostic strategies for toxoplasmosis. Clin Microbiol Rev. 25(2):264–296. https://doi.org/10.1128/CMR.05013-11

Le Roch KG. 2004. Global analysis of transcript and protein levels across the Plasmodium falciparum life cycle. Genome Res . 14(11):2308–2318. https://doi.org/10.1101/gr.2523904

Romano JD, Nolan SJ, Porter C, Ehrenman K, Hartman EJ, Hsia R ching, Coppens I. 2017. The parasite Toxoplasma sequesters diverse Rab host vesicles within an intravacuolar network. J Cell Biol. 216(12):4235–4254. https://doi.org/10.1083/jcb.201701108

Romano JD, Sonda S, Bergbower E, Smith ME, Coppens I. 2013. Toxoplasma gondii salvages sphingolipids from the host Golgi through the rerouting of selected Rab vesicles to the parasitophorous vacuole. Mol Biol Cell. 24(12):1974–1995. https://doi.org/10.1091/mbc.E12-11-0827

Rooney PJ, Neal LM, Knoll LJ. 2011. Involvement of a toxoplasma gondii chromatin remodeling complex ortholog in developmental regulation. PLoS One. 6(5):e19570. https://doi.org/10.1371/journal.pone.0019570

Roux KJ, Kim DI, Raida M, Burke B. 2012. A promiscuous biotin ligase fusion protein identifies proximal and interacting proteins in mammalian cells. J Cell Biol . 196(6):801–10. https://doi.org/10.1083/jcb.201112098

Ruehle MD, Stemm-Wolf AJ, Pearson CG. 2020. Sas4 links basal bodies to cell division via Hippo signaling. J Cell Biol . 219(8):e201906183. https://doi.org/10.1083/jcb.201906183

Ruepp A, Zollner A, Maier D, Albermann K, Hani J, Mokrejs M, Tetko I, Güldener U, Mannhaupt G, Münsterkötter M, Mewes HW. 2004. The FunCat, a functional annotation scheme for systematic classification of proteins from whole genomes. Nucleic Acids Res. 32(18):5539–5545. https://doi.org/10.1093/nar/gkh894

Ruggiero MA, Gordon DP, Orrell TM, Bailly N, Bourgoin T, Brusca RC, Cavalier-Smith T, Guiry MD, Kirk PM. 2015. A Higher Level Classification of All Living Organisms.Thuesen E V., editor. PLoS One . 10(4):e0119248. https://doi.org/10.1371/journal.pone.0119248

Russell DG, Burns RG. 1984. The polar ring of coccidian sporozoites: a unique microtubule-organizing centre. J Cell Sci. 65:193–207. https://doi.org/10.1242/jcs.65.1.193

Ryan OW, Skerker JM, Maurer MJ, Li X, Tsai JC, Poddar S, Lee ME, DeLoache W, Dueber JE, Arkin AP, Cate JHD. 2014. Selection of chromosomal DNA libraries using a multiplex CRISPR system. Elife. 3:e03703. https://doi.org/10.7554/eLife.03703

Ryning FW, McLeod R, Maddox JC, Hunt S, Remington JS. 1979. Probable transmission of Toxoplasma gondii by organ transplantation. Ann Intern Med. 90(1):47–49. https://doi.org/10.7326/0003-4819-90-1-47

Sacks JJ, Roberto RR, Brooks NF. 1982. Toxoplasmosis Infection Associated With Raw Goat's Milk. JAMA J Am Med Assoc. 248(14):1728–1732. https://doi.org/10.1001/jama.1982.03330140038029

Salimova E, Sohrmann M, Fournier N, Simanis V. 2000. The S. pombe orthologue of the S. cerevisiae mob1 gene is essential and functions in signalling the onset of septum formation. J Cell Sci . 113(10):1695–1704. https://jcs.biologists.org/content/joces/113/10/1695.full.pdf

Saputo S, Chabrier-Rosello Y, Luca FC, Kumar A, Krysan DJ. 2012. The RAM Network in Pathogenic Fungi. Eukaryot Cell . 11(6):708–717. https://doi.org/10.1128/EC.00044-12

Schmidpeter J, Dahl M, Hofmann J, Koch C. 2017. ChMob2 binds to ChCbk1 and promotes virulence and conidiation of the fungal pathogen Colletotrichum higginsianum. BMC Microbiol . 17:22. https://doi.org/10.1186/s12866-017-0932-7

Schmidt A, Schmid MW, Grossniklaus U. 2015. Plant germline formation: common concepts and developmental flexibility in sexual and asexual reproduction. Development. 142(2):229–241. https://doi.org/10.1242/dev.102103

Schmidt S, Sohrmann M, Hofmann K, Woollard A, Simanis V. 1997. The Spg1p GTPase is an essential, dosage-dependent inducer of septum formation in Schizosaccharomyces pombe. Genes Dev. 11(12):1519–1534. https://doi.org/10.1101/gad.11.12.1519

Schulte J, Sepp KJ, Jorquera RA, Wu C, Song Y, Hong P, Troy Littleton J. 2010. DMob4/Phocein regulates synapse formation, axonal transport, and microtubule organization. J Neurosci. 30(15):5189–5203. https://doi.org/10.1523/JNEUROSCI.5823-09.2010

Schultz AJ, Carruthers VB. 2018. Toxoplasma gondii LCAT Primarily Contributes to Tachyzoite Egress.Blader IJ, editor. mSphere . 3(1):1–10. https://doi.org/10.1128/mSphereDirect.00073-18

Schumacher FR, Al Olama AA, Berndt SI, Benlloch S, Ahmed M, Saunders EJ, Dadaev T, Leongamornlert D, Anokian E, Cieza-Borrella C, et al. 2018. Association analyses of more than 140,000 men identify 63 new prostate cancer susceptibility loci. Nat Genet. 50(7):928–936. https://doi.org/10.1038/s41588-018-0142-8

Sebé-Pedrós A, Grau-Bové X, Richards TA, Ruiz-Trillo I. 2014. Evolution and classification of myosins, a paneukaryotic whole-genome approach. Genome Biol Evol. 6(2):290–305. https://doi.org/10.1093/gbe/evu013

Sebé-Pedrós A, Zheng Y, Ruiz-Trillo I, Pan D. 2012. Premetazoan origin of the Hippo signaling pathway. Cell Rep . 1(1):13–20. https://doi.org/10.1016/j.celrep.2011.11.004

Sehgal A, Bettiol S, Pypaert M, Wenk MR, Kaasch A, Blader IJ, Joiner KA, Coppens I. 2005. Peculiarities of host cholesterol transport to the unique intracellular vacuole containing Toxoplasma. Traffic. 6(12):1125–1141. https://doi.org/10.1111/j.1600-0854.2005.00348.x

Seybold C, Schiebel E. 2013. Spindle pole bodies. Curr Biol . 23(19):R858–R860. https://doi.org/10.1016/j.cub.2013.07.024

Shapiro K, Bahia-Oliveira L, Dixon B, Dumètre A, de Wit LA, VanWormer E, Villena I.

2019. Environmental transmission of Toxoplasma gondii: Oocysts in water, soil and food. Food Waterborne Parasitol . 15:e00049. https://doi.org/10.1016/j.fawpar.2019.e00049

Sheffield HG, Melton ML. 1968. The Fine Structure and Reproduction of Toxoplasma gondii. J Parasitol . 54(2):209–226. https://doi.org/10.2307/3276925

Shen B, Brown KM, Lee TD, Sibley LD. 2014. Efficient Gene Disruption in Diverse Strains of Toxoplasma gondii Using CRISPR/CAS9.Weiss LM, editor. MBio . 5(3):1–11. https://doi.org/10.1128/mBio.01114-14

Shimizu T, Ho L-L, Lai Z-C. 2008. The mob as tumor suppressor gene is essential for early development and regulates tissue growth in Drosophila. Genetics . 178(2):957–65. https://doi.org/10.1534/genetics.107.081570

Shimobayashi M, Hall MN. 2014. Making new contacts: The mTOR network in metabolism and signalling crosstalk. Nat Rev Mol Cell Biol. 15(3):155–162. https://doi.org/10.1038/nrm3757

Sibley LD, Niesman IR, Parmley SF, Cesbron-Delauw MF. 1995. Regulated secretion of multi-lamellar vesicles leads to formation of a tubulovesicular network in host-cell vacuoles occupied by Toxoplasma gondii. J Cell Sci. 108(4):1669–1677. https://doi.org/10.1242/jcs.108.4.1669

Sidik SM, Hackett CG, Tran F, Westwood NJ, Lourido S. 2014. Efficient genome engineering of Toxoplasma gondii using CRISPR/Cas9. PLoS One. 9(6):e100450. https://doi.org/10.1371/journal.pone.0100450

Sidik SM, Huet D, Ganesan SM, Huynh M-H, Wang T, Nasamu AS, Thiru P, Saeij JPJ, Carruthers VB, Niles JC, Lourido S. 2016. A Genome-wide CRISPR Screen in Toxoplasma Identifies Essential Apicomplexan Genes. Cell . 166(6):1423-1435.e12. https://doi.org/10.1016/j.cell.2016.08.019

Simanis V. 2015. Pombe's thirteen - control of fission yeast cell division by the septation initiation network. J Cell Sci . 128(8):1465–74. https://doi.org/10.1242/jcs.094821

Sinai AP, Webster P, Joiner KA. 1997. Association of host cell endoplasmic reticulum and mitochondria with the Toxoplasma gondii parasitophorous vacuole membrane: a high affinity interaction. J Cell Sci . 110(17):2117–2128. https://doi.org/10.1242/jcs.110.17.2117

Slabodnick MM, Ruby JG, Dunn JG, Feldman JL, DeRisi JL, Marshall WF. 2014. The Kinase Regulator Mob1 Acts as a Patterning Protein for Stentor Morphogenesis. PLoS Biol. 12(5):e1001861. https://doi.org/10.1371/journal.pbio.1001861

Šlapeta J, Morin-Adeline V. 2011. Apicomplexa Levine 1970, Sporozoa Leucart 1879. Tree Life Web Proj [Internet]. [accessed 2020 Oct 25] http://tolweb.org/Apicomplexa/2446/2011.05.18

Smith DD, Frenkel JK. 1995. PREVALENCE OF ANTIBODIES TO TOXOPLASMA GONDII IN WILD MAMMALS OF MISSOURI AND EAST CENTRAL KANSAS: BIOLOGIC AND ECOLOGIC CONSIDERATIONS OF TRANSMISSION. J Wildl Dis . 31(1):15–21. https://doi.org/10.7589/0090-3558-31.1.15

Soete M, Camus D, Dubrametz JF. 1994. Experimental Induction of Bradyzoite-Specific Antigen Expression and Cyst Formation by the RH Strain of Toxoplasma gondii in Vitro. Exp Parasitol . 78(4):361–370. https://doi.org/10.1006/expr.1994.1039

Soete M, Fortier B, Camus D, Dubremetz JF. 1993. Toxoplasma gondii : Kinetics of Bradyzoite-Tachyzoite Interconversion in vitro. Exp Parasitol . 76(3):259–264. https://doi.org/10.1006/expr.1993.1031

Sohrmann M, Schmidt S, Hagan I, Simanis V. 1998. Asymmetric segregation on spindle poles of the Schizosaccharomyces pombe septum-inducing protein kinase Cdc7p. Genes Dev . 12(1):84–94. https://doi.org/10.1101/gad.12.1.84

Soldati D, Meissner M. 2004. Toxoplasma as a novel system for motility. Curr Opin Cell Biol. 16:32–40. https://doi.org/10.1016/j.ceb.2003.11.013

Song J, Wang T, Chi X, Wei X, Xu S, Yu M, He H, Ma J, Li X, Du J, et al. 2019. Kindlin-2 Inhibits the Hippo Signaling Pathway by Promoting Degradation of MOB1. Cell Rep. 29(11):3664–3677. https://doi.org/10.1016/j.celrep.2019.11.035

Song X, Lin M, Li M, Yang X, Liu J, Liu Q. 2020. Toxoplasma gondii metacaspase 2 is an important factor that influences bradyzoite formation in the Pru strain. Parasitol Res. 119(7):2287–2298. https://doi.org/10.1007/s00436-020-06722-3

Song Z, Han X, Zou H, Zhang B, Ding Y, Xu X, Zeng J, Liu J, Gong A. 2018. PTEN–GSK3β–MOB1 axis controls neurite outgrowth in vitro and in vivo. Cell Mol Life Sci. 75(23):4445–4464. https://doi.org/10.1007/s00018-018-2890-0

Sorber K, Dimon MT, Derisi JL. 2011. RNA-Seq analysis of splicing in Plasmodium falciparum uncovers new splice junctions, alternative splicing and splicing of antisense transcripts. Nucleic Acids Res. 39(9):3820–3835. https://doi.org/10.1093/nar/gkq1223

Sparks CA, Morphew M, McCollum D. 1999. Sid2p, a Spindle Pole Body Kinase That Regulates the Onset of Cytokinesis. J Cell Biol . 146(4):777–790. https://doi.org/10.1083/jcb.146.4.777

Speer CA, Dubey JP. 2005. Ultrastructural differentiation of Toxoplasma gondii schizonts (types B to E) and gamonts in the intestines of cats fed bradyzoites. Int J Parasitol. 35(2):193–206. https://doi.org/10.1016/j.ijpara.2004.11.005

Splendore A. 1908. Un nuovo protozoa parassita de' conigli. Rev Soc Sci. 3:109–112.

Stelzer S, Basso W, Benavides Silván J, Ortega-Mora LM, Maksimov P, Gethmann J, Conraths FJ, Schares G. 2019. Toxoplasma gondii infection and toxoplasmosis in farm animals: Risk factors and economic impact. Food Waterborne Parasitol . 15:e00037. https://doi.org/10.1016/j.fawpar.2019.e00037

Stephens R, Lim K, Portela M, Kvansakul M, Humbert PO, Richardson HE. 2018. The Scribble Cell Polarity Module in the Regulation of Cell Signaling in Tissue Development and Tumorigenesis. J Mol Biol . 430(19):3585–3612. https://doi.org/10.1016/j.jmb.2018.01.011

Stortz JF, Jimenez-Ruiz E, Gow M, Meissner M. 2017. Cas9 activity compromises

nuclear integrity and cellular morphology in T. gondii. In: Toxo14 – 14th Bienn Conf Toxoplasma gondii Res community. [place unknown]; p. 313.

Striepen B, Crawford MJ, Shaw MK, Tilney LG, Seeber F, Roos DS. 2000. The plastid of Toxoplasma gondii is divided by association with the centrosomes. J Cell Biol. 151(7):1423–1434. https://doi.org/10.1083/jcb.151.7.1423

Su C, Evans D, Cole RH, Kissinger JC, Ajioka JW, Sibley LD. 2003. Recent expansion of Toxoplasma through enhanced oral transmission. Science. 299(5605):414–416. https://doi.org/10.1126/science.1078035

Sugi T, Ma YF, Tomita T, Murakoshi F, Eaton MS, Yakubu R, Han B, Tu V, Kato K, Kawazu S-I, et al. 2016. Toxoplasma gondii Cyclic AMP-Dependent Protein Kinase Subunit 3 Is Involved in the Switch from Tachyzoite to Bradyzoite Development.Sibley LD, editor. MBio . 7(3):e00755-16. https://doi.org/10.1128/mBio.00755-16

Sullivan WJ, Hakimi MA. 2006. Histone mediated gene activation in Toxoplasma gondii. Mol Biochem Parasitol. 148(2):109–116. https://doi.org/10.1016/j.molbiopara.2006.03.010

Sullivan WJ, Narasimhan J, Bhatti MM, Wek RC. 2004. Parasite-specific eIF2 (eukaryotic initiation factor-2) kinase required for stress-induced translation control. Biochem J. 380(2):523–531. https://doi.org/10.1042/BJ20040262

Sweeney KR, Morrissette NS, Lachapelle S, Blader IJ. 2010. Host cell invasion by Toxoplasma gondii is temporally regulated by the host microtubule cytoskeleton. Eukaryot Cell. 9(11):1680–1689. https://doi.org/10.1128/EC.00079-10

Szklarczyk D, Gable AL, Lyon D, Junge A, Wyder S, Huerta-Cepas J, Simonovic M, Doncheva NT, Morris JH, Bork P, et al. 2019. STRING v11: Protein-protein association networks with increased coverage, supporting functional discovery in genome-wide experimental datasets. Nucleic Acids Res. 47(D1):D607–D613. https://doi.org/10.1093/nar/gky1131

Talevich E, Mirza A, Kannan N. 2011. Structural and evolutionary divergence of eukaryotic protein kinases in Apicomplexa. BMC Evol Biol . 11:321. https://doi.org/10.1186/1471-2148-11-321

Tang F, Zhang L, Xue G, Hynx D, Wang Y, Cron PD, Hundsrucker C, Hergovich A, Frank S, Hemmings BA, Schmitz-Rohmer D. 2014. hMOB3 modulates MST1 apoptotic signaling and supports tumor growth in glioblastoma multiforme. Cancer Res. 74(14):3779–3789. https://doi.org/10.1158/0008-5472.CAN-13-3430

Tavares AJ. 2015. The Role of Mob Proteins in Protozoan Cell Cycle Regulation. [place unknown]: Universidade de Lisboa.

Tavares Alexandra, Gonçalves J, Florindo C, Tavares Alvaro a, Soares H. 2012. Mob1: defining cell polarity for proper cell division. J Cell Sci . 125(Pt 2):516–27. https://doi.org/10.1242/jcs.096610

Taylor MA, Coop RL, Wall RL. 2016. Veterinary Parasitology. Oxford: Wiley-Blackwell.

Teh OK, Shimono Y, Shirakawa M, Fukao Y, Tamura K, Shimada T, Hara-Nishimura I. 2013. The AP-1 μ adaptin is required for KNOLLE localization at the cell plate to mediate cytokinesis in arabidopsis. Plant Cell Physiol. 54(6):838–847. https://doi.org/10.1093/pcp/pct048

de Thoisy B, Demar M, Aznar C, Carme B. 2003. Ecological correlates of Toxoplasma gondii exposure in free-ranging neotropical mammals. J Wildl Dis. 39(2):456–459. https://doi.org/10.7589/0090-3558-39.2.456

Tomasina R, Francia ME. 2020. The Structural and Molecular Underpinnings of Gametogenesis in Toxoplasma gondii. Front Cell Infect Microbiol. 10(December):1–8. https://doi.org/10.3389/fcimb.2020.608291

Tomavo S, Boothroyd JC. 1995. Interconnection between organellar functions, development and drug resistance in the protozoan parasite, Toxoplasma gondii. Int J Parasitol. 25(11):1293–1299. https://doi.org/10.1016/0020-7519(95)00066-B

Tosetti N, Dos Santos Pacheco N, Soldati-Favre D, Jacot D. 2019a. Three F-actin assembly centers regulate organelle inheritance, cell-cell communication and motility in Toxoplasma gondii. Elife . 8:1–32. https://doi.org/10.7554/eLife.42669

Tosetti N, Dos Santos Pacheco N, Soldati-Favre D, Jacot D. 2019b. Three F-actin assembly centers regulate organelle inheritance, cell-cell communication and motility in Toxoplasma gondii. Elife . 8:e42669. https://doi.org/10.7554/eLife.42669

Trammell MA, Mahoney NM, Agard DA, Vale RD. 2008. Mob4 plays a role in spindle focusing in Drosophila S2 cells. J Cell Sci. 121(8):1284–1292. https://doi.org/10.1242/jcs.017210

Tschöp K, Conery AR, Litovchick L, DeCaprio JA, Settleman J, Harlow E, Dyson N. 2011. A kinase shRNA screen links LATS2 and the pRB tumor suppressor. Genes Dev. 25(8):814–830. https://doi.org/10.1101/gad.2000211

Tycko J, Wainberg M, Marinov GK, Ursu O, Hess GT, Ego BK, Aradhana, Li A, Truong A, Trevino AE, et al. 2019. Mitigation of off-target toxicity in CRISPR-Cas9 screens for essential non-coding elements. Nat Commun . 10:4063. https://doi.org/10.1038/s41467-019-11955-7

Tzipori S, Ward H. 2002. Cryptosporidiosis: Biology, pathogenesis and disease. Microbes Infect. 4(10):1047–1058. https://doi.org/10.1016/S1286-4579(02)01629-5

Vakulskas CA, Dever DP, Rettig GR, Turk R, Jacobi AM, Collingwood MA, Bode NM, McNeill MS, Yan S, Camarena J, et al. 2018. A high-fidelity Cas9 mutant delivered as a ribonucleoprotein complex enables efficient gene editing in human hematopoietic stem and progenitor cells. Nat Med . 24(8):1216–1224. https://doi.org/10.1038/s41591-018-0137-0

Venugopal K, Werkmeister E, Barois N, Saliou J, Poncet A, Huot L, Sindikubwabo F, Hakimi MA, Langsley G, Lafont F, Marion S. 2017. Dual role of the Toxoplasma gondii clathrin adaptor AP1 in the sorting of rhoptry and microneme proteins and in parasite division.Coppens I, editor. PLOS Pathog . 13(4):e1006331. https://doi.org/10.1371/journal.ppat.1006331

Vichalkovski A, Gresko E, Cornils H, Hergovich A, Schmitz D, Hemmings BA. 2008. NDR Kinase Is Activated by RASSF1A/MST1 in Response to Fas Receptor Stimulation and

Promotes Apoptosis. Curr Biol . 18(23):1889–1895. https://doi.org/10.1016/j.cub.2008.10.060

Vrabioiu AM, Struhl G. 2015. Fat/Dachsous Signaling Promotes Drosophila Wing Growth by Regulating the Conformational State of the NDR Kinase Warts. Dev Cell . 35(6):737–749. https://doi.org/10.1016/j.devcel.2015.11.027

Wagner SA, Beli P, Weinert BT, Schölz C, Kelstrup CD, Young C, Nielsen ML, Olsen J V, Brakebusch C, Choudhary C. 2012. Proteomic analyses reveal divergent ubiquitylation site patterns in murine tissues. Mol Cell Proteomics . 11(12):1578–85. https://doi.org/10.1074/mcp.M112.017905

Waldman BS, Schwarz D, Wadsworth MH, Saeij JP, Shalek AK, Lourido S. 2020. Identification of a Master Regulator of Differentiation in Toxoplasma. Cell . 180(2):359-372.e16. https://doi.org/10.1016/j.cell.2019.12.013

Walker G, Dorrell RG, Schlacht A, Dacks JB. 2011. Eukaryotic systematics: A user's guide for cell biologists and parasitologists. Parasitology. 138(13):1638–1663. https://doi.org/10.1017/S0031182010001708

Walker ME, Hjort EE, Smith SS, Tripathi A, Hornick JE, Hinchcliffe EH, Archer W, Hager KM. 2008. Toxoplasma gondii actively remodels the microtubule network in host cells. Microbes Infect . 10(14–15):1440–1449. https://doi.org/10.1016/j.micinf.2008.08.014

Walker RA, Sharman PA, Miller CM, Lippuner C, Okoniewski M, Eichenberger RM, Ramakrishnan C, Brossier F, Deplazes P, Hehl AB, Smith NC. 2015. RNA Seq analysis of the Eimeria tenella gametocyte transcriptome reveals clues about the molecular basis for sexual reproduction and oocyst biogenesis. BMC Genomics . 16:94. https://doi.org/10.1186/s12864-015-1298-6

Wang J-L, Zhang N-Z, Li T-T, He J-J, Elsheikha HM, Zhu X-Q. 2019. Advances in the Development of Anti-Toxoplasma gondii Vaccines: Challenges, Opportunities, and Perspectives. Trends Parasitol . 35(3):239–253. https://doi.org/10.1016/j.pt.2019.01.005

Wang L, Li B, Zhang L, Li Qing, He Z, Zhang X, Huang X, Xu Zhipeng, Xia Y, Zhang Q, et al. 2019. miR - 664a - 3p functions as an oncogene by targeting Hippo pathway in the development of gastric cancer. (November 2018):1–14. https://doi.org/10.1111/cpr.12567

Wang SE, Amir AS, Nguyen T, Poole AM, Simoes-Barbosa A. 2018. Spliceosomal introns in Trichomonas vaginalis revisited. Parasit Vectors . 11:607. https://doi.org/10.1186/s13071-018-3196-7

Watt KI, Turner BJ, Hagg A, Zhang X, Davey JR, Qian H, Beyer C, Winbanks CE, Harvey KF, Gregorevic P. 2015. The Hippo pathway effector YAP is a critical regulator of skeletal muscle fibre size. Nat Commun . 6:6048. https://doi.org/10.1038/ncomms7048

Watts E, Zhao Y, Dhara A, Eller B, Patwardhan A, Sinai P. 2015. Novel Approaches Reveal that Toxoplasma gondii Bradyzoites within Tissue Cysts Are Dynamic and Replicating Entities In Vivo. 6(5):1–24. https://doi.org/10.1128/mBio.01155-15.Editor

Weiss EL, Kurischko C, Zhang C, Shokat K, Drubin DG, Luca FC. 2002. The Saccharomyces cerevisiae Mob2p-Cbk1p kinase complex promotes polarized growth and acts

with the mitotic exit network to facilitate daughter cell-specific localization of Ace2p transcription factor. J Cell Biol. 158(5):885–900. https://doi.org/10.1083/jcb.200203094

Weiss LM, Kim K. 2000. The development and biology of bradyzoites of toxoplasma gondii. Front Biosci . 5(3):391–405. https://doi.org/10.2741/Weiss

Weiss LM, Laplace D, Takvorian PM, Tanowitz HB, Cali A, Wittner M. 1995. A Cell Culture System for Study of the Development of Toxoplasma gondii Bradyzoites. J Eukaryot Microbiol. 42(2):150–157. https://doi.org/10.1111/j.1550-7408.1995.tb01556.x

Whitelaw JA, Latorre-Barragan F, Gras S, Pall GS, Leung JM, Heaslip A, Egarter S, Andenmatten N, Nelson SR, Warshaw DM, et al. 2017. Surface attachment, promoted by the actomyosin system of Toxoplasma gondii is important for efficient gliding motility and invasion. BMC Biol . 15(1):1–23. https://doi.org/10.1186/s12915-016-0343-5

Wilmeth LJ, Shrestha S, Montaño G, Rashe J, Shuster CB. 2010. Mutual Dependence of Mob1 and the Chromosomal Passenger Complex for Localization during Mitosis.Wang Y-L, editor. Mol Biol Cell . 21(3):380–392. https://doi.org/10.1091/mbc.e09-06-0471

Winiger RR, Hehl AB. 2020. A streamlined CRISPR/Cas9 approach for fast genome editing in Toxoplasma gondii and Besnoitia besnoiti. J Biol Methods . 7(4):e140. https://doi.org/10.14440/jbm.2020.343

Wloga D, Frankel J. 2012. From Molecules to Morphology: Cellular Organization of Tetrahymena thermophila. In: Methods Cell Biol . Vol. 109. [place unknown]: Methods Cell Biol; ; p. 83–140. https://doi.org/10.1016/B978-0-12-385967-9.00005-0

Wong Y-H, Lee T-Y, Liang H-K, Huang C-M, Wang T-Y, Yang Y-H, Chu C-H, Huang H-D, Ko M-T, Hwang J-K. 2007. KinasePhos 2.0: a web server for identifying protein kinase-specific phosphorylation sites based on sequences and coupling patterns. Nucleic Acids Res . 35(Web Server issue):W588-94. https://doi.org/10.1093/nar/gkm322

Wu H, Xiao Y, Zhang S, Ji S, Wei L, Fan F, Geng J, Tian J, Sun X, Qin F, et al. 2013. The Ets Transcription Factor GABP Is a Component of the Hippo Pathway Essential for Growth and Antioxidant Defense. Cell Rep . 3(5):1663–1677. https://doi.org/10.1016/j.celrep.2013.04.020

Xiong J, Cui X, Yuan X, Yu X, Sun J, Gong Q. 2016. The Hippo/STE20 homolog SIK1 interacts with MOB1 to regulate cell proliferation and cell expansion in Arabidopsis. J Exp Bot. 67(5):1461–1475. https://doi.org/10.1093/jxb/erv538

Xiong S, Couzens AL, Kean MJ, Mao DY, Guettler S, Kurinov I, Gingras AC, Sicheri F. 2017. Regulation of protein interactions by Mps one binder (MOB1) phosphorylation. Mol Cell Proteomics. 16(6):1111–1125. https://doi.org/10.1074/mcp.M117.068130

Yan M, Chu L, Qin B, Wang Z, Liu X, Jin C, Zhang G, Gomez M, Hergovich A, Chen Z, et al. 2015. Regulation of NDR1 activity by PLK1 ensures proper spindle orientation in mitosis. Sci Rep . 5:10449. https://doi.org/10.1038/srep10449

Yang B, Kuang M, Kang J, Zhao J, Ma J, Ma X. 2020. Human umbilical cord mesenchymal stem cell-derived exosomes act via the miR-1263 / Mob1 / Hippo signaling

pathway to prevent apoptosis in disuse osteoporosis. Biochem Biophys Res Commun. 524:883–889. https://doi.org/10.1016/j.bbrc.2020.02.001

Yeoh LM, Goodman CD, Hall NE, Dooren GG Van, Mcfadden I, Ralph SA. 2015. A serine – arginine-rich (SR) splicing factor modulates alternative splicing of over a thousand genes in Toxoplasma gondii. 43(9):4661–4675. https://doi.org/10.1093/nar/gkv311

Yu F, Zhao B, Panupinthu N, Jewell JL, Lian I, Wang LH, Zhao J, Yuan H, Tumaneng K, Li H, et al. 2012. Regulation of the Hippo-YAP Pathway by G-Protein-Coupled Receptor Signaling. Cell . 150(4):780–791. https://doi.org/10.1016/j.cell.2012.06.037

Yu FX, Zhang Y, Park HW, Jewell JL, Chen Q, Deng Y, Pan D, Taylor SS, Lai ZC, Guan KL. 2013. Protein kinase A activates the Hippo pathway to modulate cell proliferation and differentiation. Genes Dev. 27(11):1223–1232. https://doi.org/10.1101/gad.219402.113

Zhang J, Smolen GA, Haber DA. 2008. Negative regulation of YAP by LATS1 underscores evolutionary conservation of the Drosophila Hippo pathway. Cancer Res. 68(8):2789–2794. https://doi.org/10.1158/0008-5472.CAN-07-6205

Zhang L, Noguchi Y taro, Nakayama H, Kaji T, Tsujikawa K, Ikemoto-Uezumi M, Uezumi A, Okada Y, Doi T, Watanabe S, et al. 2019. The CalcR-PKA-Yap1 Axis Is Critical for Maintaining Quiescence in Muscle Stem Cells. Cell Rep . 29(8):2154-2163.e5. https://doi.org/10.1016/j.celrep.2019.10.057

Zhang L, Zhang H, Liu P, Hao H, Jin JB, Lin J. 2011. Arabidopsis R-SNARE proteins VAMP721 and VAMP722 are required for cell plate formation. PLoS One. 6(10). https://doi.org/10.1371/journal.pone.0026129

Zhang S, Zhu H. 2018. Cytokinesis and the Hippo Pathway: New Molecular Links Between Intimate Partners. Gastroenterology .:119–121. https://doi.org/10.1053/j.gastro.2018.09.006

Zhao B, Li L, Tumaneng K, Wang C-Y, Guan K-L. 2010. A coordinated phosphorylation by Lats and CK1 regulates YAP stability through SCF -TRCP. Genes Dev . 24:72–85. https://doi.org/10.1101/gad.1843810

Zhao B, Li L, Wang L, Wang C-Y, Yu J, Guan K-L. 2012. Cell detachment activates the Hippo pathway via cytoskeleton reorganization to induce anoikis. Genes Dev . 26:54–68. https://doi.org/10.1101/gad.173435.111

Zhao X, Li J, Lian B, Gu H, Li Y, Qi Y. 2018. Global identification of Arabidopsis lncRNAs reveals the regulation of MAF4 by a natural antisense RNA. Nat Commun . 9:5056. https://doi.org/10.1038/s41467-018-07500-7

Zheng H, Bednarek SY, Sanderfoot AA, Alonso J, Ecker JR, Raikhel N V. 2002. NPSN11 is a cell plate-associated SNARE protein that interacts with the syntaxin KNOLLE. Plant Physiol. 129(2):530–539. https://doi.org/10.1104/pp.003970

Zheng Y, Wang W, Liu B, Deng H, Uster E, Pan D. 2015. Identification of Happyhour/MAP4K as Alternative Hpo/Mst-like Kinases in the Hippo Kinase Cascade. Dev Cell . 34(6):642–655. https://doi.org/10.1016/j.devcel.2015.08.014

Zhou D, Conrad C, Xia F, Park J-S, Payer B, Yin Y, Lauwers GY, Thasler W, Lee JT, Avruch J, Bardeesy N. 2009. Mst1 and Mst2 Maintain Hepatocyte Quiescence and Suppress Hepatocellular Carcinoma Development through Inactivation of the Yap1 Oncogene. Cancer Cell . 16(5):425–438. https://doi.org/10.1016/j.ccr.2009.09.026

Zhou X, Li W, Liu Y, Amon A. 2021. Cross-compartment signal propagation in the mitotic exit network. Elife . 10:e63645. https://doi.org/10.7554/eLife.63645

Zhu Henan, Zhou Z, Wang D, Liu W, Zhu Hao. 2013. Hippo pathway genes developed varied exon numbers and coevolved functional domains in metazoans for species specific growth control. BMC Evol Biol . 13:76. https://doi.org/10.1186/1471-2148-13-76

Zou J, Ma W, Li J, Littlejohn R, Zhou H, Kim I man, Fulton DJR, Chen W, Weintraub NL, Zhou J, Su H. 2018. Neddylation mediates ventricular chamber maturation through repression of Hippo signaling. Proc Natl Acad Sci U S A. 115(17):E4101–E4110. https://doi.org/10.1073/pnas.1719309115

Zulpo DL, Sammi AS, dos Santos JR, Sasse JP, Martins TA, Minutti AF, Cardim ST, de Barros LD, Navarro IT, Garcia JL. 2018. Toxoplasma gondii: A study of oocyst re-shedding in domestic cats. Vet Parasitol . 249(51):17–20. https://doi.org/10.1016/j.vetpar.2017.10.021

Annexes

Annex I

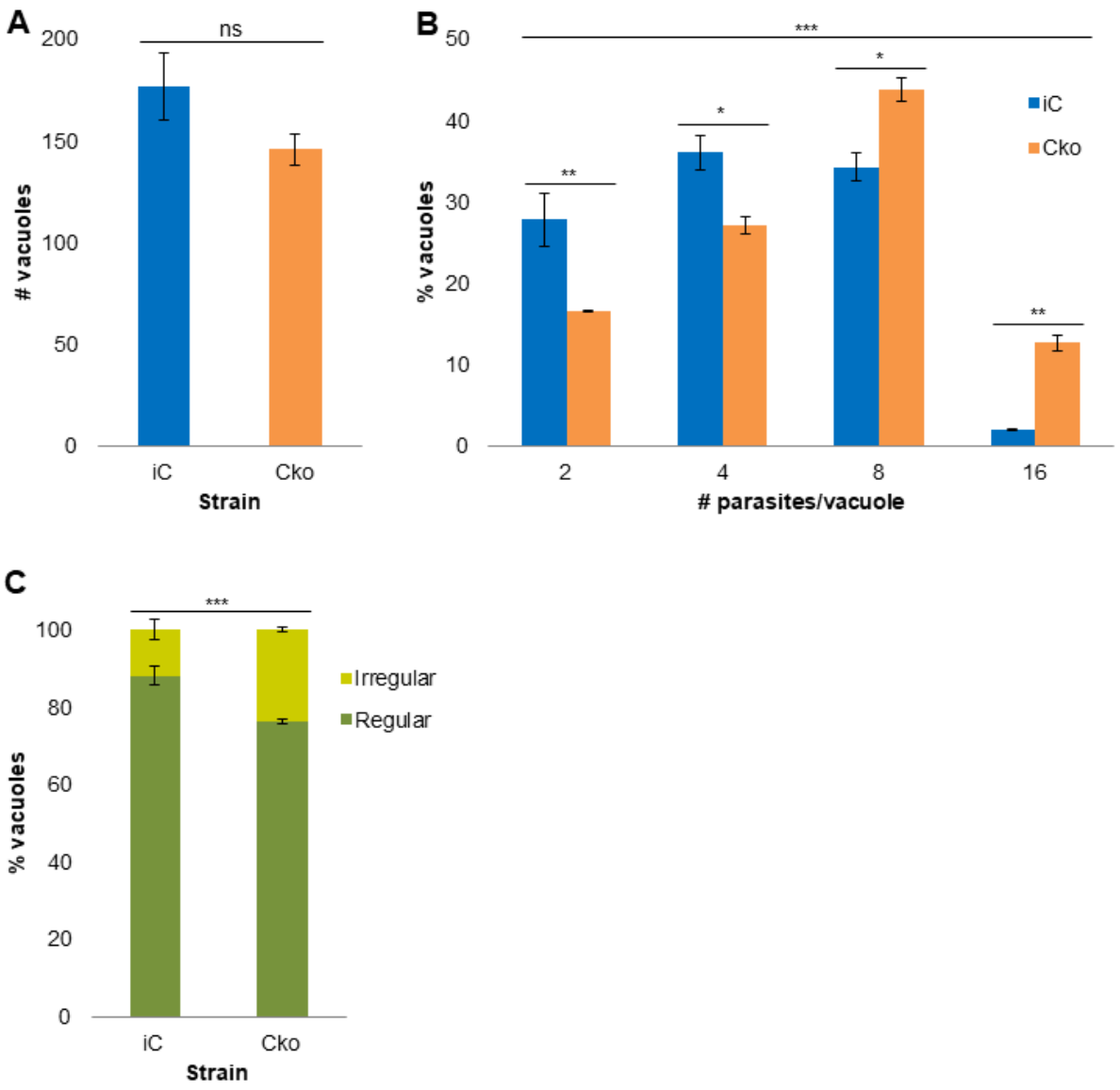

Figure 1. Analysis of *in vitro* phenotypes of Cko tachyzoites expressing the *Mob1* sgRNA2.

Cko tachyzoites expressing the *Mob1* sgRNA2 were analyzed for its invasion efficiency, replication efficiency, and PV regularity in comparison to the respective control iC tachyzoites. **A)** Invasion assays did not detect significant differences between iC and Cko tachyzoites (p= 0.1661). **B)** Replication assays detected significant differences between iC and Cko tachyzoites (p<0.0001). Cko tachyzoites present a higher replication rate compared to iC tachyzoites. Data are presented as mean ± SE of three independent experiments. **C)** PV regularity assays detected significantly higher irregular vacuoles in Cko tachyzoites compared to iC tachyzoites (p=0.0001). Data are presented as mean ± SE of three independent experiments. iC – inducible *Mob1* splitCas9; Cko – *Mob1* functional knockout; Irregular – vacuoles with a number of tachyzoites different from 4, 8, 16 or 32; Regular – vacuoles with a number of tachyzoites equal to 4, 8, 16 or 32.

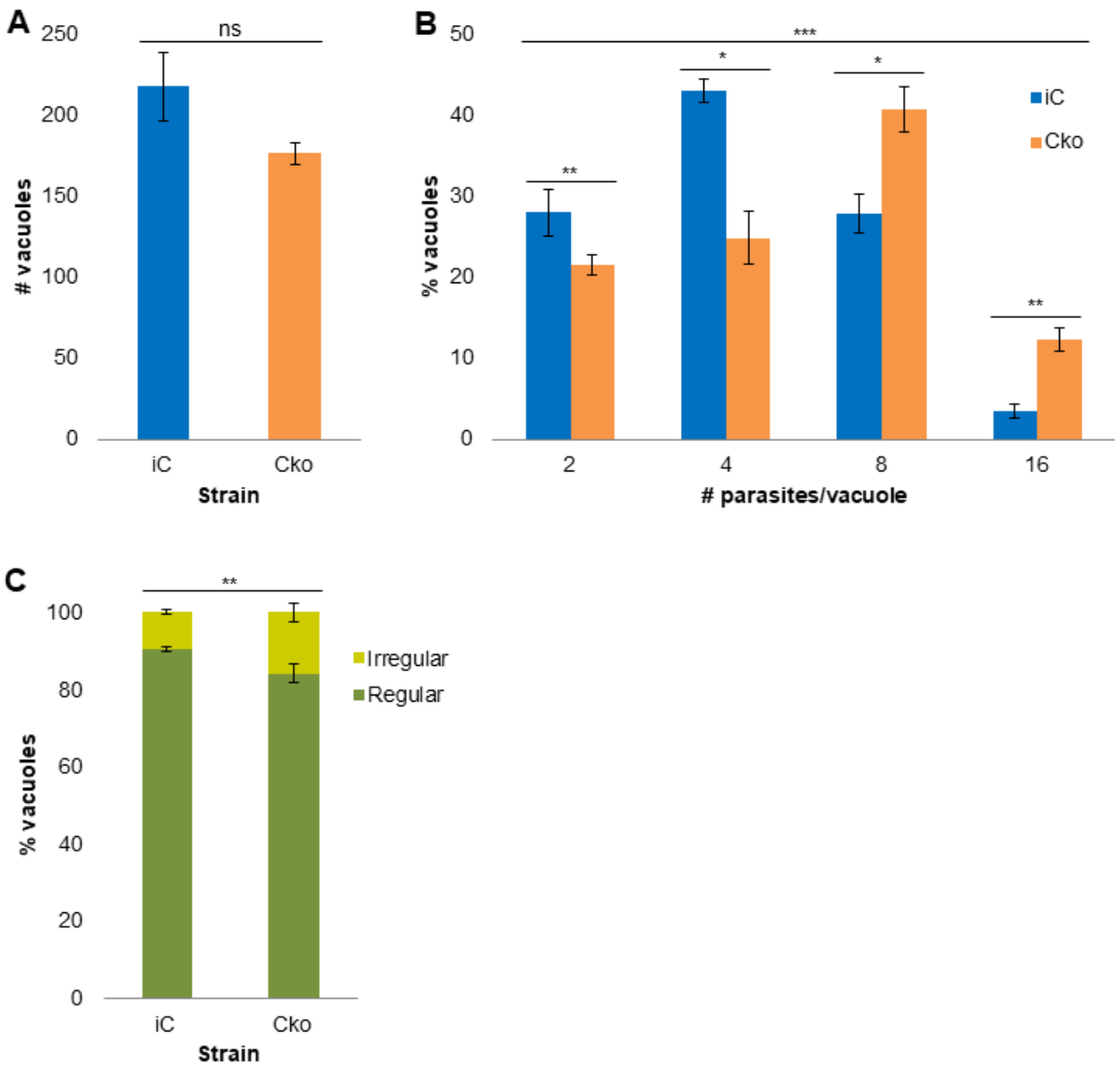

Figure 2. Analysis of *in vitro* phenotypes of Cko tachyzoites expressing the *Mob1* sgRNA3.

Cko tachyzoites expressing the *Mob1* sgRNA3 were analyzed for its invasion efficiency, replication efficiency, and PV regularity in comparison to the respective control iC tachyzoites. **A)** Invasion assays did not detect significant differences between iC and Cko tachyzoites (p= 0.1350). **B)** Replication assays detected significant differences between iC and Cko tachyzoites (p<0.0001). Cko tachyzoites present a higher replication rate compared to iC tachyzoites. Data are presented as mean ± SE of three independent experiments. **C)** PV regularity assays detected significantly higher irregular vacuoles in Cko tachyzoites compared to iC tachyzoites (p=0.0062). Data are presented as mean ± SE of three independent experiments. iC – inducible *Mob1* splitCas9; Cko – *Mob1* functional knockout; Irregular – vacuoles with a number of tachyzoites different from 4, 8, 16 or 32; Regular – vacuoles with a number of tachyzoites equal to 4, 8, 16 or 32.

Annex II

Table 1. Differentially biotinylated FLAG-BirA-MOB1 proteins.

ToxoDB[a]	Description	Symbol	Predicted sub. localization	Functional category	Counterpart/ related to			STRING cluster	Unique peptides
					Mo	Me	Hi		
204160	Translation initiation factor 2A		ribosome	Protein synthesis and fate				3	60
228150	Uncharacterized protein		nucleus						39
281400	Phosphofructokinase		cytosol	Signal transduction			yes		30
305610	Uncharacterized protein								29
242070	cAMP-dependent protein kinase regulatory subunit	PKAR	IMC	Signal transduction			yes	9	26
290290	Ubiquitin-activating enzyme E1	E1	cytosol	Ubiquitin-proteasome system			yes	1	22
258390	DnaJ protein		apicoplast	Protein synthesis and fate					21
212260	Uncharacterized protein		nucleus						20
234190	Serine hydroxymethyltransferase		cytosol	Metabolism				2	15
209950	Thioredoxin		apicoplast	Metabolism			yes		13
226030	cAMP-dependent protein kinase catalytic subunit 1	PKAc1	IMC	Signal transduction			yes	9	13
228630	Mir domain-containing protein		apicoplast	Protein synthesis and fate					11
214790	Mitochondrial glycoprotein		mitochondrion	Protein synthesis and fate					9
290005	proteasome subunit beta type 1	PSMB1	proteasome	Ubiquitin-proteasome system			yes	1	7
299080	VTC domain-containing protein		ER	Transport					4
239330	Ribosomal protein L37	RPL37	ribosome	Protein synthesis and fate				4	4
219120	E3 ligase RING-type domain-containing protein	E3	nucleus	Ubiquitin-proteasome system	yes		yes		4
203630	Ribosomal protein L44	RPL44	ribosome	Protein synthesis and fate				4	4
310790	Uncharacterized protein		ER						4
218920	proteasome subunit beta type 5	PSMB5	proteasome	Ubiquitin-proteasome system			yes	1	4
265390	E3 ligase Gid-type RING domain-containing protein	E3	cytosol	Ubiquitin-proteasome system	yes		yes		4
312960	Ribosome biogenesis protein Nop16		nucleus	Protein synthesis and fate					3
234560	Uncharacterized protein		PM						3
264030	Aminotransferase		nucleus	Metabolism				2	3

221360	Autophagy related 6 homolog/Beclin1	ATG6/ BECN1		Transport			3
260140	Phosphomannose isomerase type I		cytosol	Metabolism		2	3
255410	Uncharacterized protein		Golgi	Metabolism			3
213660	Zinc finger motif-containing protein						2
313600	phospholipase DDHD1	DDHD1	cytosol	Metabolism			2
210345	Alpha/beta hydrolase			Metabolism			2
252380	Alkaline phosphatase D family protein	PhoD	ER	Signal transduction			2
309590	Rhoptry protein ROP1	ROP1	rhoptries	Secretion system			2
243290	Uncharacterized protein		ER				2
255190	Myosin B/C		IMC	Cell structure			2
237260	coiled-coil domain containing protein 124	Ccdc124	nucleus	Cell cycle and DNA processing			2
202750	exosome complex component/rRNA-processing protein 42	RRP42	nucleus	Transcription			2
262780	FHA domain-containing protein		nucleus	Cell cycle and DNA processing			2
309050	Alpha/gamma-adaptin-binding protein p34			Transport			2
260680	DNA primase small subunit			Cell cycle and DNA processing		7	2
202820	Ubiquitin-conjugating enzyme E2	E2	proteasome	Ubiquitin-proteasome system	yes	1	2
258490	Uncharacterized protein		nucleus				2
227990	Uncharacterized protein		mitochondrion				2
265010	Glutamate 5-kinase		cytosol	Metabolism		2	2
226900	Uncharacterized protein		nucleus				2
293050	Trafficking protein particle complex subunit		Golgi	Transport			2
261220	Supressor of Ty 4	SPT4	nucleus	Cell cycle and DNA processing		6	2
215990	ATP-dependent RNA helicase		nucleus	Cell cycle and DNA processing		8	2
321340	Uncharacterized protein		ER				2
276100	Uncharacterized protein		nucleus				2
210778	Protein OS9-like	OS9	ER	Ubiquitin-proteasome system			2
294690	Rhomboid protease ROM5	ROM5	PM	Secretion system			2
269660	XPB DNA repair helicase RAD25	RAD25	nucleus	Cell cycle and DNA processing		6	2
247690	Phospholipid-transporting P-type ATPase		PM	Transport			2
213010	Uncharacterized protein		apicoplast				2

254210	Cleavage stimulation factor	CSTF	nucleus	Transcription			10	2
279330	ATP-dependent RNA helicase DDX49		nucleus	Protein synthesis and fate			8	2
207680	S-phase kinase-associated protein 1	SKP1	nucleus	Ubiquitin-proteasome system	yes	yes	1	2
263190	Adenylosuccinate lyase	ASL	proteasome	Metabolism			2	1
239130	Tyrosine kinase-like kinase	TKLK		Signal transduction				1
265830	Alkaline phosphatase D family protein	PhoD	ER	Signal transduction				1
308590	COP9 signalosome complex subunit 5	CSN5		Protein synthesis and fate		yes	1	1
222200	Limb development membrane 1 family protein	LMBR1	Golgi	Signal transduction				1
309890	Uncharacterized protein			Metabolism				1
271600	alpha/beta hydrolase		nucleus					1
214480	Replication factor a protein 3 protein		nucleus	Cell cycle and DNA processing				1
297970	Aspartyl aminopeptidase	DNPEP	cytosol	Metabolism			3	1
260650	Uncharacterized protein							1
284590	Mediator complex subunit 10	MED10		Transcription				1
270750	DNA glycosylase		nucleus	Metabolism				1
231150	MBL fold metallo-hydrolase		mitochondrion	Metabolism				1
229500	Uncharacterized rhoptry protein		rhoptries	Secretion system				1
263330	Adaptin ear-binding coat-associated protein 2	NECAP2		Transport				1
223510	Alpha/beta hydrolase-1 domain-containing protein		Golgi	Metabolism				1
260450	DEAD/DEAH box helicase		apicoplast	Transcription				1
263140	SWI2/SNF2-containing protein RAD26	RAD26	nucleus	Cell cycle and DNA processing			6	1
264740	Phospholipase C-like phosphodiesterase	PLC	Golgi	Metabolism				1
201120	ELMO family protein		cytoskeleton	Cell structure				1
312410	Methyltransferase			Metabolism				1
243680	Dihydrodipicolinate reductase	DHDPR		Metabolism			2	1
291320	Uncharacterized protein		Golgi					1
230110	Uncharacterized protein		PM					1
202120	Pleckstrin homology domain-containing protein		PM	Metabolism				1
246990	Uncharacterized protein		apical					1
272230	ATP-dependent protease HslV subunit		proteasome	Ubiquitin-proteasome system			5	1

272900	DNA repair protein RAD51	RAD51	nucleus	Cell cycle and DNA processing	yes	7	1
203400	Uncharacterized protein		PM				1
238995	calcium-activated potassium channel alpha chain		PM	Transport			1
242320	Zinc finger protein constans-like 9		apical				1
254600	Ubiquitin family protein		nucleus	Ubiquitin-proteasome system	yes	1	1
206540	Uncharacterized protein		PM				1
268250	Polyadenylation factor subunit		nucleus	Transcription		10	1
216820	major facilitator family transporter protein	MFS	micronemes	Transport			1
204880	Uncharacterized protein		apical				1
243590	2',5'-phosphodiesterase	PDE	mitochondrion	Transcription			1
215420	SNAP receptor (synaptobrevin homolog)	SNARE	nucleus	Transport			1
278600	Uncharacterized protein						1
203710	AP2 domain transcription factor AP2VIIa-4	AP2VIIa-4	nucleus	Transcription			1
209060	Thrombospondin type 1 domain-containing protein	TSP	end. vesicles	Transport			1
213520	Peptidase M20D amidohydrolase		apicoplast	Metabolism		2	1
215250	Thiamin pyrophosphokinase	TPK	mitochondrion	Metabolism		2	1
216720	Uncharacterized protein		extracellular				1
216920	Mediator complex subunit 8	MED8		Transcription			1
222090	Rab5-interacting protein		ER	Transport			1
237250	GOLD domain-containing protein		Golgi	Transport			1
297510	Farnesyltransferase			Protein synthesis and fate			1
295370	Uncharacterized protein		mitochondrion				1
310600	Heat shock factor binding 1	HSBP1	nucleus	Transcription			1
225120	Uncharacterized protein		dense granules				1
295090	Oligosaccharyl transferase		ER	Protein synthesis and fate			1
216630	Trigger factor protein		apicoplast	Protein synthesis and fate		2	1
229390	Ubiquitin receptor protein DA1-like	DA1	dense granules	Ubiquitin-proteasome system			1
224110	proteasome regulatory subunit RPN13	RPN13	proteasome	Ubiquitin-proteasome system	yes	1	1
272670	M3 peptidase		mitochondrion	Protein synthesis and fate		5	1
304730	Monopolar spindle one binder 1	MOB1	cytosol				1
213415	Uncharacterized protein						1

254150	Uncharacterized protein						1
281480	Uncharacterized protein						1
230380	Protein translocation complex SEC61 gamma subunit	SEC61	ER	Transport		4	1
275410	Anaphase-promoting complex subunit 1	APC1	nucleus	Cell cycle and DNA processing	yes	1	1
204280	Dual specificity tyrosine phosphorylation regulated kinase	DYRK	nucleus	Cell cycle and DNA processing	yes	9	1
214870	Ribosomal protein L9	RPL9	mitochondrion	Protein synthesis and fate			1
268320	Uncharacterized protein						1
292190	rRNA-processing protein Fcf1/Utp23		ribosome	Protein synthesis and fate		8	1
226500	Uncharacterized protein		mitochondrion				1
309780	Ribosomal RNA-processing protein 15	RRP15	ribosome	Protein synthesis and fate			1
235750	calcium/calmodulin dependent protein kinase 1	CAMK1	Golgi	Signal transduction			1
316750	rRNA-processing arch domain containing protein			Protein synthesis and fate		8	1

a - TGME49 gene ID; sub. - subellular; end. - endomembrane; Mo – MOB; Me – MEN; H – Hippo.